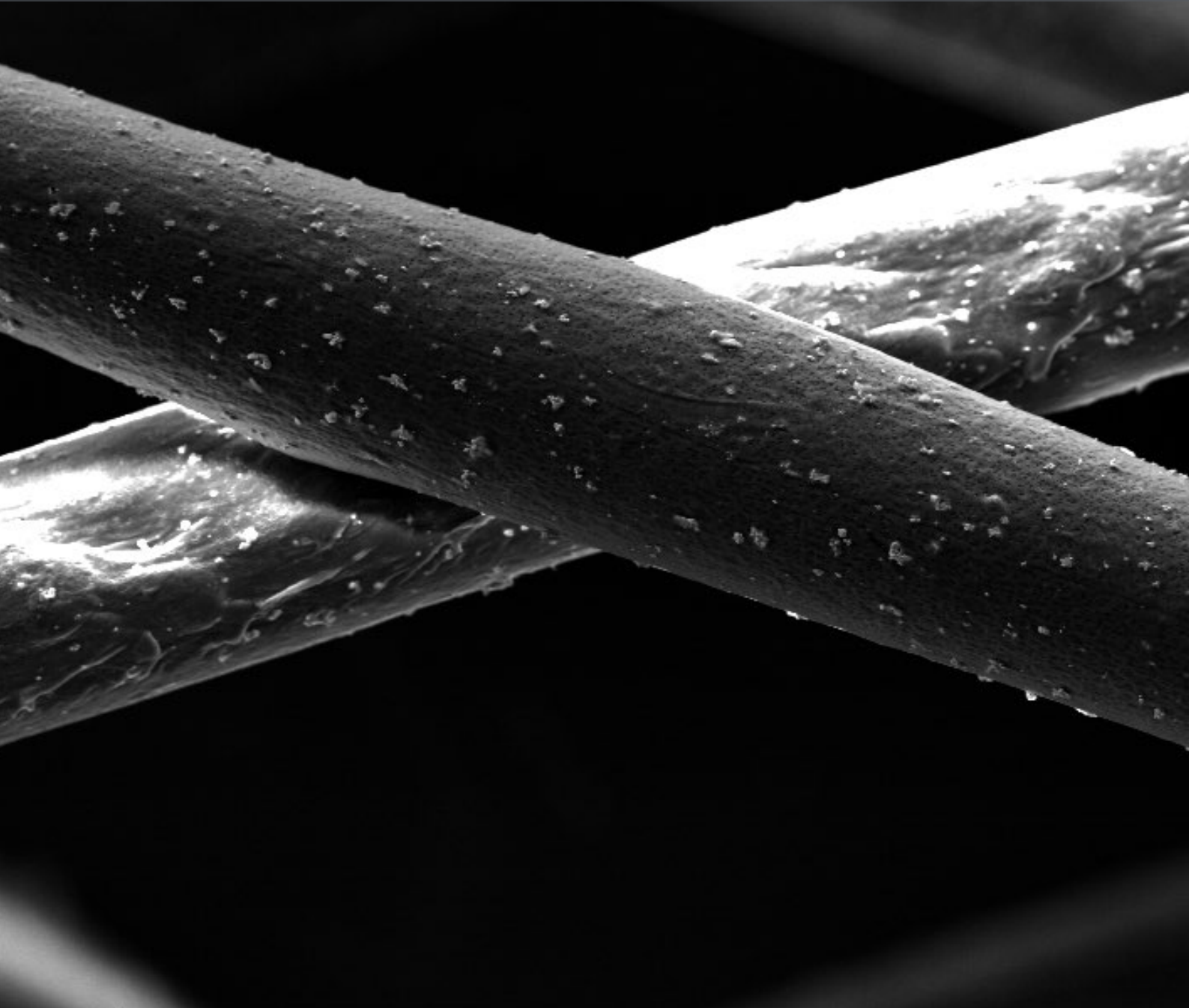


3D-printed Polymeric Bioresorbable Stents for Cardiovascular Applications

Victor Chausse Calbet



Doctoral Program in Materials Science and Engineering

Universitat Politècnica de Catalunya

Doctoral Program in Materials Science and Engineering

PhD Thesis

3D-printed Polymeric Bioresorbable Stents for Cardiovascular Applications

Victor Chausse Calbet

Supervisor: Marta Pegueroles Neyra

Biomaterials, Biomechanics and Tissue Engineering Group

Materials Science and Engineering Department

Universitat Politècnica de Catalunya



March 31st, 2023

Victor Chausse Calbet

3D-printed Polymeric Bioresorbable Stents for Cardiovascular Applications

Doctoral Program in Materials Science and Engineering

Supervisor: Marta Pegueroles Neyra

March 31st, 2023

Universitat Politècnica de Catalunya

Biomaterials, Biomechanics and Tissue Engineering Group

Materials Science and Engineering Department

Barcelona

Abstract

Bioresorbable stents (BRS) have been envisioned as a revolution in the treatment of coronary heart disease. Ideally, stents would initially retain sufficient radial strength after implantation to prevent vessel recoil while degrading and ultimately being resorbed, thus leaving the vessel with a healthy endothelium. Still, the use of polymeric BRS has limitations of its own, such as the need for large strut thickness to achieve enough radial strength or the inherent lack of radiopacity and bioactivity of polymers. Therefore, the main challenge of BRS lies in simultaneously providing enough mechanical support to prevent recoil in the first months while controlling the degradation rate, minimizing strut thickness and improving BRS hemocompatibility and tissue integration.

The main aim of the present PhD Thesis is the design and development of tunable novel polymeric bioresorbable stents manufactured by means of solvent-cast direct-writing (SC-DW) with reinforced mechanical properties, radiopacity, suitable degradation timeframe, drug release capability and enhanced biointegration.

First, a novel versatile additive manufacturing fabrication strategy for BRS production by using polymeric inks and SC-DW onto a rotating cylinder is presented. Initially, poly-L-lactic acid (PLLA) was used to manufacture and characterize a variety of designs with different mesh patterns. Expansion assays showed that stents withstood pressures of at least 16 atm and the indirect cytotoxicity test indicated that stents were biocompatible. In a second step, poly(L-lactic-co- ϵ -caprolactone) (PLCL) was introduced, and inks were further modified with the addition of iodine, triiodobenzoic acid (TIBA) and barium sulfate (BaSO_4) in order to produce radiopaque BRS. Microcomputed tomography was used to assess stents' radiopacity, showing that TIBA and BaSO_4 -containing stents presented high X-Ray attenuation values, maintained over 3 months incubation time.

With the aim to gain further insight into PLLA and PLCL stents degradation, a complete study was performed by comparing chemical vs thermal accelerated degradation assays. The results showed that under alkaline conditions, stents underwent surface erosion, whereas stents immersed at 50 °C experienced bulk degradation. Molecular weight decrease was accurately described by the autocatalyzed kinetic model, with PLCL showing a degradation rate 1.5 times higher than PLLA. Additionally, stents were subjected to γ -irradiation and ethylene oxide (EtO) sterilization. Whereas EtO-sterilized stents

remained structurally unaltered, γ -irradiated stents presented severe deterioration as a result of extensive chain scission.

Fabricated 3D-printed stents lacked bioactivity, thus further ink and surface modifications were developed in order to control hemocompatibility and tissue integration. In that sense, a combination of SC-DW and electrospinning (ES) was proposed as a new approach to generate everolimus-eluting BRS for cardiovascular applications. A Design of Experiment was conducted to determine the parameters necessary for optimal homogeneous coating with high specific surface. Drug loading was achieved either encapsulated in the struts of the stent or in an electrospun PLCL membrane covering the stent. When encapsulated, everolimus release was found to be insufficient, whereas release from PLCL-coated 3D-printed stents would match the dose and timeframe required for *in vivo* applications.

Finally, functionalization of 3D-printed PLLA and PLCL BRS with endothelial cell (EC) adhesive peptides was explored. Solid phase peptide synthesis was used to synthesize linear RGDS and YIGSR sequences, as well as a dual peptidic platform (PF) containing both motifs in a single biomolecule. Successful functionalization of films and stents was confirmed upon water angle measurements and confocal fluorescence microscopy. Endothelial cell adhesion assays evidenced significantly increased cell number and spreading onto functionalized films with respect to control samples. Stents' hemocompatibility was evaluated upon a blood perfusion assay, with PLCL showing pronouncedly diminished platelet adhesion with reference to PLLA. In addition, functionalization with RGDS, YIGSR and the PF rendered BRS stents displaying even further reduced platelet adhesion.

In summary, this PhD Thesis has contributed to the development and optimization of a novel 3D Printing technique for polymeric BRS manufacturing. Moreover, printed stents have been further modified in order to display radiopacity or release anti-proliferative drug. Additionally, biofunctionalization of stents with EC-adhesive peptides has proven to be an effective strategy to prevent platelet activation. Globally, it has been demonstrated that PLCL presented reinforced mechanical properties while presenting a more suitable degradation timeframe than PLLA. Furthermore, PLCL ink modification renders radiopaque or drug-eluting stents, and functionalization strategies result in improved hemocompatibility.

Resum

Els *stents* bioabsorbibles (BRS, *Bioresorbable Stents*) s'han plantejat com una revolució en el tractament de la malaltia de les artèries coronàries. Idealment, els *stents* conservarien inicialment la força radial després de la implantació per evitar el retrocés del vas sanguini mentre es degraden i finalment es reabsorbeixen, deixant així l'artèria amb un endoteli sa. Tot i així, l'ús de BRS polimèrics té limitacions pròpies, com ara la necessitat d'un gran gruix de filament per aconseguir una força radial suficient o la manca inherent de radiopacitat i bioactivitat dels polímers. Per tant, el principal repte dels BRS rau a proporcionar simultàniament prou suport mecànic per evitar el retrocés durant els primers mesos, alhora que es minimitza el gruix de filament per millorar-ne l'hemocompatibilitat i la integració en el teixit.

L'objectiu principal de la present tesi doctoral és el disseny i desenvolupament d'*stents* bioabsorbibles polimèrics fabricats mitjançant escriptura directa amb dissolvent (SC-DW, *solvent-cast direct-writing*) amb propietats mecàniques reforçades, període de degradació adequat, capacitat d'alliberament de fàrmac i biointegració millorada.

En primer lloc, es presenta una nova estratègia versàtil de fabricació additiva per a la producció de BRS mitjançant l'ús de tintes polimèriques i SC-DW en un cilindre giratori. Inicialment, l'àcid poli-L-làctic (PLLA) s'ha utilitzat per fabricar i caracteritzar una varietat de dissenys amb diferents patrons de malla. Els assajos d'expansió han demostrat que els *stents* resisteixen pressions d'almenys 16 atm i la prova de citotoxicitat indirecta ha indicat que els *stents* són biocompatibles. En un segon pas, s'ha introduït el copolímer poli(L-làctic-co- ϵ -caprolactona) (PLCL) i s'han modificat les tintes amb l'addició de iode, àcid triiodobenzoic (TIBA) i sulfat de bari (BaSO_4) per tal de produir BRS radiopacs. S'ha utilitzat la microtomografia computada per avaluar la radiopacitat dels *stents*, mostrant que els *stents* que contenen TIBA i BaSO_4 presenten valors alts d'atenuació de raigs X, mantinguts durant 3 mesos de temps d'incubació.

Amb l'objectiu d'obtenir més informació sobre la degradació dels *stents* de PLLA i PLCL, s'ha realitzat un estudi complet tot comparant assaigs de degradació accelerada química i tèrmica. Els resultats han mostrat que en condicions alcalines els *stents* van patir erosió superficial, mentre que els *stents* immersos a 50 °C van experimentar una degradació en massa. La disminució del pes molecular ha estat descrita amb precisió pel model cinètic autocatalitzat, amb el copolímer PLCL mostrant una taxa de degradació 1,5 vegades

superior a la del PLLA. A més, els stents han estat sotmesos a irradiació γ i esterilització per òxid d'etilè (EtO). Mentre que els stents esterilitzats amb EtO no han presentat canvis estructurals, els stents irradiats amb γ han sofert un greu deteriorament com a resultat d'escissió de la cadena generalitzada.

Els stents impresos en 3D manquen de bioactivitat, per la qual cosa s'han desenvolupat modificacions de tinta i superfície per controlar l'hemocompatibilitat i la integració en els teixits. En aquest sentit, es proposa una combinació de SC-DW i electrofilat (ES, *electrospinning*) com a nou enfocament per generar BRS amb everolimus per a aplicacions cardiovasculars. S'ha dut a terme un disseny d'experiment per determinar els paràmetres necessaris per a un recobriment homogeni òptim amb una superfície específica elevada. La càrrega de fàrmacs s'ha aconseguit o bé encapsulada en els filaments de l'*stent* o en una membrana electrofilada de PLCL que recobreix l'*stent*. En el cas encapsulat, s'ha trobat que l'alliberament d'everolimus és insuficient, mentre que l'alliberament dels *stents* impresos en 3D recoberts de PLCL coincidiria amb la dosi i el període de temps necessaris per a aplicacions *in vivo*.

Finalment, s'ha explorat la funcionalització d'*stents* de PLLA i PLCL impresos en 3D amb pèptids adhesius de cèl·lules endotelials (ECs, *endothelial cells*). La síntesi de pèptids en fase sòlida s'ha utilitzat per sintetitzar les seqüències lineals RGDS i YIGSR, així com una plataforma peptídica dual (PF) que conté tots dos motius en una sola biomolècula. La funcionalització de pel·lícules i stents s'ha confirmat mitjançant mesures d'angle de contacte i microscòpia de fluorescència confocal. Els assajos d'adhesió de cèl·lules endotelials han evidenciat un augment significatiu del nombre i extensió de cèl·lules en mostres funcionalitzades respecte el control. L'hemocompatibilitat dels *stents* s'ha avaluat mitjançant un assaig de perfusió de sang, obtenint una disminució marcada en termes d'adhesió plaquetària en *stents* de PLCL respecte als de PLLA. A més, la funcionalització amb RGDS, YIGSR i la PF ha fet que els *stents* mostrin una adhesió plaquetària encara més reduïda.

En resum, aquesta tesi doctoral ha contribuït al desenvolupament i optimització d'una nova tècnica d'impressió 3D per a la fabricació de BRS polimèrics. Els stents impresos s'han modificat per mostrar radioopacitat o alliberar fàrmacs antiproliferatius. Alhora, la biofuncionalització de stents amb pèptids adhesius per a ECs ha demostrat ser una estratègia eficaç per prevenir l'activació plaquetària. Globalment, s'ha vist que el PLCL presenta propietats mecàniques reforçades mentre que presenta un període de degradació més adequat que el PLLA. A més, amb la modificació de la tinta de PLCL s'obtenen *stents* radiopacs o alliberadors de fàrmacs, i les estratègies de funcionalització donen lloc a una hemocompatibilitat millorada.

Agraïments

Escriure els agraïments és la part més maca d'aquest final de tesi. Ja fa dies que hi anava donant tombs, però mitja hora en bici ha estat suficient per donar-hi forma i començar a deixar-los per escrit tan bon punt he arribat a casa. Potser no estaran gaire endreçats ni reflexionats, però és tal com ragen.

Si comencem pel començament, com a les bones històries, el 30 de maig del 2018 vaig enviar un correu a una tal Noelia presentant-me i demanant per quines opcions hi havia de fer el doctorat al BBT. L'endemà, vaig rebre un correu de la Marta, i al cap de pocs dies ens vam reunir per parlar de possibles projectes en l'àmbit dels *stents* cardiovasculars. **Marta**, vas aconseguir transmetre'm la teva passió per la recerca i em vas engrescar a fer el doctorat. Anys més tard, mirant enrere va ser la millor decisió, però en aquell moment m'ho vas posar tan i tan fàcil que només vaig poder dir que sí. Han estat uns anys fantàstics, així que tot el meu agraïment per haver-me convençut. És evident que hi ha hagut un aprenentatge des del punt de vista professional, però allò que m'emportaré amb més carinyo és la relació personal. Has estat un pilar fonamental des del primer moment. Moltes gràcies per tot.

Seguim, i ja que ha aparegut el nom de la **Noelia**, us la presentaré. A banda de ser una peça indispensable en l'engranatge del BBT i de fer-nos la vida més fàcil a tots, la Noelia té un cor enorme, encara que de vegades no l'ensenyi a tothom. Gràcies per deixar-me'l veure. A la vora de la Noelia hi tenim la **Txell**, la segona part de l'engranatge, la general directora dels laboratoris amb mà de ferro però guant de seda. No ha de ser gens fàcil gestionar-ho tot amb tanta eficiència, només per això ja tens tota la meva admiració. Sempre disposada a donar un cop de mà si algú ho necessita, ets un sol de persona. Ha estat un plaer aprendre de tu tots aquests anys al laboratori. Trobaré a faltar baixar al vostre despatx (no sempre a l'horari que tocava) i quedar-nos xerrant com tres tietes. Només ens faltava la manteta a la falda i les agulles de ganxet.

Si ens posem una mica més seriosos, hi ha hagut molta gent que en algun moment o altre d'aquests anys han aportat el seu granet de sorra. Sense ànim de ser exhaustiu, no voldria deixar-me l'**Araceli**, per la seva ajuda a l'hora d'interpretar i processar les dades de microCT; la **Ina**, per tenir la paciència d'explicar-me un cop i un altre com integrar els espectres de NMR; el **Kim**, per ajudar-me amb qualsevol problema mecànic; el **Jordi** i l'**Elisabet**, per fer les anàlisis de GPC; el **Trifon** i l'**Isaac**, per les formacions i sessions

de SEM; la **Judit**, per la formació de confocal i per donar-me un cop de mà sempre que t'ho he demanat; i el **Javier**, per ajudar-me a purificar els pèptids a la Pompeu, en el que probablement fos el dia més estressant del meu doctorat.

Parlant de pèptids, l'**Helena** mereix una menció especial: moltes gràcies per la docència i la paciència, al teu costat vaig entrar al fabulós món dels pèptids i els aminoàcids. Ets una investigadora de deu. L'altre premi a la paciència és per la **Meri**: la formació de cèl·lules va ser aclaparadora. Hi havia moments que amb la Claudia teníem la sensació de no poder assumir més informació. Tot i això, vas aconseguir que m'arribés a sentir còmode en una cabina de cultius descongelant, pipetejant, sembrant, tripsinitzant, bloquejant, centrifugant, comptant, passant, congelant i sobretot, rentant-me les mans compulsivament. Un món nou amb un vocabulari nou, intens però gratificant. Gràcies per fer funcionar cultius com un rellotge.

Del BBT només en puc dir bones paraules. **Cristina**, la quantificació del fàrmac va tirar endavant gràcies als teus consells, moltes gràcies per haver-t'hi implicat. **Carles**, la ment pensant rere la síntesi dels pèptids i la plataforma, moltes gràcies per trobar un moment sempre que he tingut algun dubte. Faig extensiu l'agraïment a la resta de membres del grup, passats i presents, companys de despatx, postdocs i participants als seminaris de metalls. **Pau**, crec que té molt mèrit que un grup com el BBT funcioni, i funcioni tan bé en aquest país on a la recerca se li dóna la importància que se li dóna. Enlloc hauria treballat més a gust, ni m'hauria sentit tan acompanyat. Us desitjo a tots molts èxits, tant professionals com personals.

Des del principi del doctorat que vaig saber que no faria cap estada fora, i potser per això les meves visites al Parc Científic i Tecnològic de Girona han sigut especials. Moltes gràcies, **Enric**, per introduir-me en el món de l'*electrospinning*, per la feineda i la perseverança en tirar el projecte endavant. Una bona part del tercer capítol d'aquesta tesi és obra teva, tenies el meu agraiement en privat però des d'aquí també t'ho vull agrair públicament. De l'Hospital Clínic també en tinc molt bons records. Per una banda, el **Manel** i el **Salvatore** ens van permetre seguir en directe una intervenció de cateterisme. Per l'altra, la **Maribel** i el **Ginés** ens van obrir les portes del laboratori per fer-hi els assajos de trombogenicitat. Espero, **Marc**, no haver-te espantat gaire, ni a tu ni a l'infermera que va ser testimoni de l'espectacle.

No em voldria deixar els meus estudiants. Brian, Clàudia i David, ha estat un plaer dirigir-vos a tots tres, espero no haver estat massa sever i que el vostre pas pel BBT hagi estat profitós. **Brian**, et vas fer teu el projecte i vam dissenyar junts l'estratègia per modificar els stents amb agents radiopacs. Crec que tots dos en vam aprendre molt. **Clàudia**, des del principi vaig tenir claríssim que ens entendríem, gràcies per posar les bases dels assajos de degradació i per implicar-te en tot el que et vaig anar proposant. Quan vas marxar ho vas deixar tot tan endreçat que només vaig haver de

seguir les teves instruccions. **David**, vam començar havent de replantejar el teu TFG, i vam haver d'aprendre que de vegades les coses no surten com volem i que hem de ser prou flexibles per poder canviar el guió. Encara que la teva contribució no formi part estrictament d'aquest manuscrit, també en formes part. Per últim, **Francisco**, no he pogut estar per tu tant com hauria volgut. Espero que el teu temps a Barcelona t'hagi provat i que puguis tornar a Alemanya amb energies renovades.

A tots els qui aquests darrers anys heu anat seguint els progressos amb la típica pregunta de "*I què, com va el doctorat?*". Sabíeu perfectament que després us arriscàveu a que parlés durant mitja hora de cèl·lules ("*no sé per què però no fan el que haurien de fer*"), de síntesi de pèptids ("*és com si ajuntessis peces de LEGO, però si t'equivoques no pots tirar enrere i has de tornar a començar*"), de la impressora 3D ("*no sé ben bé per què però avui els stents no s'han imprès bé, em sembla que és cosa de l'electricitat estàtica*"), de l'últim paper rebutjat ("*crec que se l'han llegit en diagonal*"), de degradació hidrolítica ("*és superinteressant, a 50 °C els stents es degraden seguint un mecanisme diferent que en solució alcalina*") o d'assajos de perfusió ("*sí sí, amb la meva sang i a costa de la meva salut, el que s'arriba a fer per la ciència*"). **Marc, Irene, Folch, Saumell, Marta i Anna**, i d'altres amics i familiars que segur que em deixo, espero no haver-vos avorrit gaire tots aquests anys amb les meves batalletes.

D'amics, també n'hi ha que han marxat fora, i que aquests darrers anys no ens hem pogut veure tant. **Joan**, al final sembla que acabarem el doctorat prou alhora. Moltes gràcies per haver estat el proveïdor oficial de formatges de Suïssa cada cop que venies – encara hem de fer moltes *fondues* a la teva salut. I **Pere**, perquè per molt temps que passi, quan ens retrobem és com si no n'hagués passat gens. Una abraçada de les teves no es pot expressar amb paraules.

I dels amics de tota la vida, als amics per tota la vida. Gent que vas coneixent poc a poc, que t'hi vas avenint i que acaben sent imprescindibles. **Claudia**, he tingut el privilegi de compartir aquests anys amb tu. Hi ha hagut moments de tot, algunes llàgrimes, però sobretot rialles i mirades còmplices. Sempre seràs algú molt especial per mi. **Yago**, gràcies per compartir el teu coneixement i fer que les coses complexes semblin fàcils. **Lluís**, què he de dir, ets amor incondicional, sigues una ànima lliure i no canviïs mai. **Joanna**, ets única i irrepetible i si no existissis t'haurien d'inventar. **Miguel**, tens un cor que no et cap al pit. **Mar**, sort que vas tornar de Maastricht i que vas posar una mica d'ordre, no sé on seríem sense tu. **Xavi**, tan sèrio que semblés i ets el més pallasso de tots, has omplert d'alegria molt moments. **Laura**, amb qui he compartit més hores de laboratori, i penes i glòries d'impressió 3D. **Linh**, sempre disposada a donar un cop de mà sense esperar res a canvi. I **David**, l'últim en arribar però un més de la família des del primer dia. Tot i que no mostri gaire sovint les meves emocions i no parli gaire de mi, quan ho he necessitat hi heu sigut. Sempre us estaré agraït i se'm farà molt estrany

deixar-nos de veure cada dia. Sapigueu que no us lliurareu de fer una calçotada cada any per allà baix.

Ja arribem a la família. **Iaia**, sempre que enraonem em fas la pregunta de "*Què, com va això que fas, lo doctorat?*". Ara ja et podré dir que l'he acabat, que tot ha anat bé i que no t'hauràs d'amoïnar més per mi. **Xixu**, gràcies per ser-hi sempre encara que només ens puguem veure de tant en tant. Fàtima i Albert, sabeu el que significa una tesi doctoral. **Fàtima**, no podria haver tingut una millor directora a l'ombra, sort que m'has lligat curt. **Albert**, has estat amb molta diferència el públic més agraït quan explico algun nou projecte de la tesi. **Albertet**, ets el germà que sempre havia volgut tenir, no puc demanar més. Gràcies a tots tres per haver-me adoptat als Bonyiga.

Comencem a tocar os. Papà, mamà, és gràcies a vosaltres que sóc qui sóc. **Papà**, mai hem estat de dir-nos que ens estimem, però últimament la vida ens hi ha portat. **Mamà**, des del dia que vas llegir que la intel·ligència s'heretava per via materna no perdies ocasió en anar-ho recordant. Potser sigui cert, però em quedo amb totes les altres coses que vaig aprendre de tu. No recordo qui va ser, però fa uns mesos algú em va dir que només jo podria dir que havies estat la meva mare. Espero, també, que tu poguessis dir amb un punt d'orgull que jo era el teu fill.

Last but not least, que diuen. **Maria**, bitxo, a aquestes alçades de la pel·lícula crec que ja ens ho hem dit tot. I com que és difícil posar-hi paraules, agafaré prestats els versos de l'Enric Casasses:

*No haver-te conegut
seria terrible.
Però terrible terrible.
I no ho sabia.
A sobre, no ho sabia.*

Que tot allò que ha de vindre ho puguem veure i ho puguem viure junts. T'estimo.

Barcelona, 18 de febrer de 2023

Abbreviations

ACN	Acetonitrile
AM	Additive Manufacturing
ATR	Attenuated Total Reflection
BaSO₄	Barium sulfate
BMS	Bare Metal Stent(s)
BRS	Bioresorbable Stent(s)
BSA	Bovine Serum Albumin
BVS	Bioresorbable Vascular Scaffold
CABG	Coronary Artery Bypass Graft
CAD	Computer-Aided Design
CE	<i>Conformité Européene</i>
CF	Carboxyfluorescein
CHCl₃	Chloroform
CH₂I₂	Diiodomethane
CHD	Coronary Heart Disease
CoCr	Cobalt-Chromium
CT	Computed Tomography
CVD	Cardiovascular Disease
DAPI	4',6-diamidino-2-phenylidole
DAPT	Dual Anti-Platelet Therapy
DCM	Dichloromethane
DES	Drug Eluting Stent(s)
DIC	N,N-diisopropylcarbodiimide
DIW	Direct Ink Writing
DMF	N,N-dimethylformamide
DoE	Design of Experiment
DSC	Differential Scanning Calorimetry
EC	Endothelial Cell(s)
ECM	Extra Cellular Matrix
EDS	1-ethyl-3-(3-dimethylaminopropyl) carbodiimide
EPC	Endothelial Progenitor Cell(s)
ES	Electrospinning
EtO	Ethylene Oxide

EU	European Union
FBS	Fetal Bovine Serum
FDA	Food & Drug Administration
FDM	Fused Deposition Modeling
FTIR	Fourier Transform Infrared Spectroscopy
GPC	Gel Permeation Chromatography
¹H-NMR	Nuclear Magnetic Resonance
HAZ	Heat Affected Zone
HEM	Hemoglobin
HPLC	High Performance Liquid Chromatography
HU	Houndsfield Units
HUVEC	Human Umbilical Vein Endothelial Cell(s)
ISR	In-Stent Restenosis
IUPAC	International Union of Pure and Applied Chemistry
IV	Inherent Viscosity
I₂	Iodine
LC-MS	Liquid Chromatography – Mass Spectrometry
LDH	Lactate Dehydrogenase
LST	Late Stent Thrombosis
MALDI-TOF	Matrix-Assisted Laser Desorption/Ionization Time-Of-Flight
M_w	Weight average Molecular weight
M_n	Number average Molecular weight
NaOH	Sodium Hydroxide
NHS	N-hydroxysuccinimide
NO	Nitric Oxide
PB	Presto Blue
PBS	Phosphate-Buffered Saline
PC	Polycarbonate
PCI	Percutaneous Coronary Intervention
PCL	Poly(ϵ -caprolactone)
PDI	Polydispersity Index
PDLA	Poly-D-lactic acid
PDLLA	Poly-D,L-lactide
PDLLGA	Poly-D,L-lactico-glycolic acid
PEG	Polyethylene glycol
PF	Platform
PFA	Paraformaldehyde
PGA	Poly-glycolic acid
PLA	Poly-lactic acid
PLCL	Poly(L-lactic-co- ϵ -caprolactone)
PLGA	Poly(lactide-co-glycolide)
PLLA	Poly-L-lactic acid
PPDO	Poly(p-dioxanone)

PTCA	Percutaneous Transluminal Coronary Angioplasty
QCM-D	Quartz Crystal Microbalance with Dissipation
RBP	Rated Burst Pressure
RT	Room Temperature
SA	Salicylic acid
SC-DW	Solvent-Cast Direct-Writing
SD	Standard Deviation
SEM	Scanning Electron Microscopy
SLA	Stereolithography
SLS	Selective Laser Sintering
SMC	Smooth Muscle Cell(s)
SPPS	Solid Phase Peptide Synthesis
TFA	Trifluoroacetic acid
T_g	Glass transition temperature
T_m	Melting temperature
TIBA	2,3,5-triiodobenzoic acid
TT	Thermal Treatment
UV	Ultraviolet
3D	Three-dimensional

Symbols

d	stent diameter
d_{tip}	capillary tip inner diameter
E_a	activation energy
f	flow
k	degradation constant
l	stent length
l_{tip}	capillary tip length
n_p	number of peaks
n_r	number of revolutions
R	universal gas constant
s	rotation speed
s_t	strut thickness
t	time
t_R	retention time
T	temperature
v	velocity
X_{PLLA}	PLLA fraction

γ	total surface free energy
γ^d	surface free energy (dispersive component)
γ^p	surface free energy (polar component)
$\dot{\gamma}_{\text{New}}$	Newtonian shear rate
$\dot{\gamma}_w$	process-related shear rate
δ	chemical shift
ΔH_c	crystallization enthalpy
ΔH_m	fusion enthalpy
ΔH_m^0	theoretical fusion enthalpy of a 100% crystalline sample
Δy	advance in the y axis
η_{app}	process-related apparent viscosity
θ	mesh angle
$\theta_{\text{CH}_2\text{I}_2}$	static diiodomethane contact angle
$\theta_{\text{H}_2\text{O}}$	static water contact angle
τ_w	process-related shear stress
χ_c	percentage of the polymer in crystalline form

Amino Acids

Name	3 letter code	1 letter code
Alanine	Ala	A
Arginine	Arg	R
Aspartic acid	Asp	D
Glutamic acid	Glu	E
Glycine	Gly	G
Isoleucine	Ile	I
Lysine	Lys	K
Methionine	Met	M
Serine	Ser	S
Tryptophan	Trp	W
Tyrosine	Tyr	Y
Valine	Val	V

List of Figures

1.1	Causes of death in the EU	1
1.2	Coronary vessels and arteries structure	2
1.3	Atherosclerosis	3
1.4	PTCA procedure	4
1.5	Stent deployment scheme	5
1.6	BRS degradation under operating conditions	9
1.7	PLLA degradation mechanism	10
1.8	BRS stents overview	11
1.9	Polymer stents manufacturing	19
1.10	Additive manufacturing techniques	20
1.11	Drug loading approaches	23
3.1	Design scheme of a stent with n_p peaks and printing setup	39
3.2	PLLA and PLCL inks rheological characterization	44
3.3	3D-printed PLLA stents	44
3.4	PLLA stents characterization: SEM	45
3.5	PLLA stents characterization: mechanical properties	46
3.6	PLLA stents characterization: thrombogenicity assay	47
3.7	Radiopaque stents 3D printing	47
3.8	Radiopaque stents characterization: SEM	49
3.9	Radiopaque stents characterization: mechanical properties	50
3.10	Radiopaque stents characterization: microCT	51
3.11	Radiopaque stents characterization: mechanical properties after incubation	52
3.12	Radiopaque stents characterization: cytotoxicity test	52
3.S1	Thrombogenicity test setup	58
3.S2	Stents surface area	58
3.S3	Radiopaque stents characterization: heat flow curves	59
3.S4	PLLA stents characterization: expansion test	60
3.S5	PLLA stents characterization: cytotoxicity assay	60
3.S6	Radiopaque stents overview	60
3.S7	Radiopaque stents characterization: expansion test	61
4.1	Accelerated alkaline degradation: mechanical characterization	73
4.2	Accelerated alkaline degradation: appearance	74
4.3	Accelerated alkaline degradation: $^1\text{H-NMR}$ spectra	76

4.4	Accelerated temperature degradation: mechanical characterization	77
4.5	Accelerated temperature degradation: appearance	77
4.6	Accelerated temperature degradation: ¹ H-NMR spectra	80
4.7	Effects of sterilization: mechanical characterization and FTIR spectra	81
4.8	Degradation models	86
4.S1	Accelerated alkaline degradation: heat flow curves	88
4.S2	Accelerated alkaline degradation: molecular weight distribution curves	88
4.S3	Accelerated temperature degradation: heat flow curves	89
4.S4	Accelerated temperature degradation: molecular weight distribution curves	89
4.S5	Effects of sterilization: heat flow and molecular weight distribution curves	90
5.1	Drug-loading techniques scheme	99
5.2	Everolimus-loaded PLLA and PLCL stents: appearance	102
5.3	Everolimus-loaded PLLA and PLCL stents: surface morphology and mechanical properties	103
5.4	Everolimus-loaded PLLA and PLCL stents: everolimus release	103
5.5	Everolimus-loaded PLLA and PLCL stents: degradation analysis	104
5.6	PLLA stents with PLCL ES coating	105
5.7	ES coating optimization through Design of Experiment	107
5.8	Everolimus-loaded PLCL-coated PLLA stents	108
5.9	Everolimus-loaded PLCL-coated PLLA stents: everolimus release	109
5.S1	Release medium and everolimus chromatograms	113
5.S2	Fiber orientation as a function of design parameters	114
6.1	Chemical structure of the linear peptides and platform, and functionalization scheme	126
6.2	Blood perfusion assay scheme	129
6.3	Dual platform synthesis steps	131
6.4	PLLA and PLCL films functionalization: confocal fluorescence microscopy	133
6.5	PLLA and PLCL stents functionalization: confocal fluorescence microscopy	133
6.6	HUVECs cell adhesion on functionalized PLLA and PLCL films	136
6.7	Platelet adhesion on control and functionalized PLLA and PLCL stents	138

List of Tables

1.1	Material properties of biodegradable polymers and metallic alloys	8
1.2	BRS classification and characteristics	13
3.1	Summary of tested inks	39
3.2	Radiopaque stents strut thickness and crystallinity	48
4.1	Accelerated alkaline degradation: DSC results	75
4.2	Accelerated alkaline degradation: GPC results	75
4.3	Accelerated temperature degradation: DSC results	78
4.4	Accelerated temperature degradation: GPC results	79
4.5	Effects of sterilization: DSC and GPC results	81
4.6	Degradation rate constants	86
5.1	Design of Experiment for ES-coated samples	100
5.2	PLCL-coated PLLA stents characterization	106
5.3	Everolimus-loaded PLCL-coated PLLA stents characterization	108
6.1	PLLA and PLCL films functionalization: physicochemical characterization .	132
6.2	PLLA and PLCL films functionalization: biomolecule quantification	134

Table of Contents

Abstract	iii
Resum	v
Agraïments	vii
Abbreviations	xi
List of Figures	xvi
List of Tables	xvii
Outline of the Thesis	xxiii
1 Introduction	1
1.1 Introduction to cardiovascular stents	1
1.1.1 Artery structure	2
1.1.2 Coronary Heart Disease	2
1.1.3 Percutaneous transluminal coronary angioplasty	4
1.1.4 Bare metal stents	4
1.1.5 Drug eluting stents	6
1.2 Bioresorbable stents	7
1.2.1 Materials selection for BRS	8
1.2.2 Current polymeric BRS technology	11
1.2.3 Biodegradable metallic stents	15
1.2.4 BRS clinical performance	16
1.2.5 Future perspectives of BRS	17
1.3 Stent manufacturing technologies	18
1.3.1 Current metal and polymer stents manufacturing	18
1.3.2 Additive Manufacturing	19
1.4 Bioactive cardiovascular stents	22
1.4.1 Drug delivery	22
1.4.2 Functionalization of cardiovascular stents	25
References	26
2 Scope and aims of the Thesis	33

3 Solvent-cast direct-writing as a fabrication strategy for radiopaque stents	35
3.1 Introduction	36
3.2 Materials and methods	38
3.2.1 Chemicals and materials	38
3.2.2 Polymer-based ink preparation and characterization	38
3.2.3 3D Printing of stents	38
3.2.4 Stents characterization	40
3.2.5 Statistical analysis	43
3.3 Results	43
3.3.1 PLLA ink preparation and characterization	43
3.3.2 PLLA stents production and characterization	43
3.3.3 Radiopaque stents production and characterization	46
3.4 Discussion	52
3.5 Conclusions	57
3.6 Supplementary information	58
References	61
4 Chemical vs thermal accelerated hydrolytic degradation of 3D-printed PLLA/PLCL bioresorbable stents: characterization and influence of sterilization	67
4.1 Introduction	68
4.2 Materials and methods	70
4.2.1 Chemicals and materials	70
4.2.2 3D Printing of stents	70
4.2.3 Accelerated <i>in vitro</i> degradation	70
4.2.4 Stents characterization	71
4.2.5 Sterilization methods	72
4.2.6 Statistical analysis	72
4.3 Results	73
4.3.1 Accelerated alkaline degradation	73
4.3.2 Accelerated temperature degradation	76
4.3.3 Effects of γ -irradiation and EtO sterilization	80
4.4 Discussion	81
4.5 Conclusions	87
4.6 Supplementary information	88
References	89
5 Solvent-cast direct-writing and electrospinning as a dual fabrication strategy for drug-eluting polymeric bioresorbable stents	95
5.1 Introduction	96
5.2 Materials and methods	98
5.2.1 Chemicals and materials	98

5.2.2	3D Printing of stents	98
5.2.3	ES coating of stents	99
5.2.4	Stents characterization	100
5.2.5	In vitro accelerated everolimus release study	101
5.2.6	Statistical analysis	101
5.3	Results	101
5.3.1	Everolimus-loaded PLLA and PLCL stents	101
5.3.2	ES coating of stents	104
5.3.3	Everolimus/PLCL-coated 3D-printed stents	107
5.4	Discussion	109
5.5	Conclusions	112
5.6	Supplementary information	113
	References	115
6	Functionalization of 3D-printed polymeric bioresorbable stents with a dual cell-adhesive peptidic platform combining RGDS and YIGSR sequences	121
6.1	Introduction	122
6.2	Materials and methods	124
6.2.1	Chemicals and materials	124
6.2.2	Solvent casting of films	124
6.2.3	3D Printing of stents	124
6.2.4	Solid-phase peptide synthesis	125
6.2.5	Surface functionalization	127
6.2.6	Surface physicochemical characterization	127
6.2.7	Biological characterization	128
6.2.8	Statistical analysis	130
6.3	Results and discussion	130
6.3.1	Biomolecules design and synthesis	130
6.3.2	Peptide immobilization on films and stents	131
6.3.3	Cell adhesion	134
6.3.4	Platelet adhesion	136
6.4	Conclusions	139
	References	140
7	Concluding remarks	147
7.1	General conclusions	147
7.2	Future perspectives	150
	Outcomes of the Thesis	151

Outline of the Thesis

Chapter 1 reviews the historical evolution in the field of cardiovascular stents, from bare metal stents (BMS) and drug-eluting stents (DES) to bioresorbable stents (BRS). The potential benefits of BRS in the long term are discussed, as well as the limitations associated to polymeric stents, with an overview of polymeric BRS under development. Current stent manufacturing technologies are reviewed, followed by novel Additive Manufacturing (AM) techniques that may be applied for BRS production. Finally, drug loading approaches and corresponding release kinetics are discussed in the field of BRS, as well as functionalization strategies regarding improved BRS biointegration and hemocompatibility.

Chapter 2 states the aims of the thesis, followed by 4 experimental chapters.

Chapter 3 presents a novel versatile AM fabrication strategy for BRS production by using polymeric inks and solvent-cast direct-writing (SC-DW) onto a rotating cylinder. Initially, poly-L-lactic acid (PLLA) was used to manufacture and characterize a variety of designs with different mesh patterns. In a second step, poly(L-lactic-co- ϵ -caprolactone) (PLCL) was introduced, and inks were further modified with the addition of iodine, triiodobenzoic acid (TIBA) and barium sulfate (BaSO_4) in order to produce radiopaque BRS.

Chapter 4 reports a complete study on the hydrolytic degradation of SC-DW PLLA and PLCL stents comparing chemical vs thermal accelerated degradation assays. The aim was to study the structural degradation mechanism that stents undergo in both conditions as well as their degradation rate. In addition, stents were subjected to gamma irradiation and EtO sterilization in order to evaluate effects of sterilization on PLLA and PLCL structure and mechanical properties.

Chapter 5 proposes a combination of solvent-cast direct-writing (SC-DW) and electrospinning (ES) using PLLA and PLCL as a new approach to generate everolimus-eluting BRS for cardiovascular applications. A Design of Experiment (DoE) was conducted to determine the parameters necessary for optimal homogeneous coating. Drug loading was achieved either encapsulated in the struts of the stent or in an electrospun PLCL membrane covering the stent.

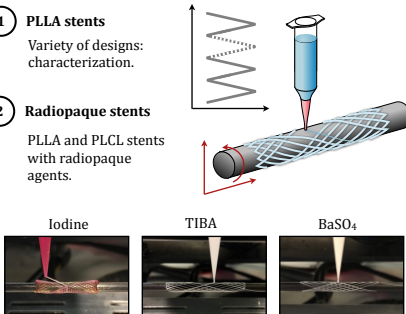
Chapter 6 explores the functionalization of 3D-printed PLLA and PLCL BRS with endothelial cell (EC) adhesive peptides. Solid phase peptide synthesis was used to synthesize linear RGDS and YIGSR sequences, as well as a dual peptidic platform containing both motifs in a single biomolecule. Biological evaluation comprised a cell adhesion test on functionalized films with endothelial cells (ECs) and a blood perfusion assay on functionalized stents to assess ECs response and device hemocompatibility, respectively.

Chapter 7 summarizes the general conclusions of the PhD Thesis, followed by future perspectives and the outcomes of the Thesis regarding publications and contributions to conferences.


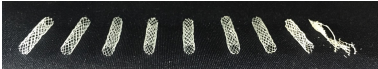
Introduction

Scope and aims of the Thesis

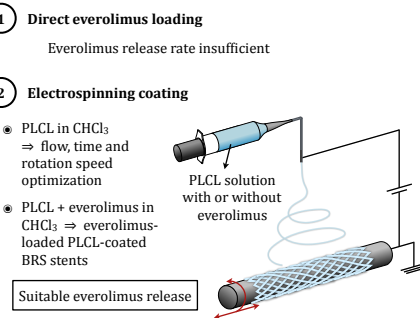
Chapter 3. Solvent-cast direct-writing as a fabrication strategy for radiopaque stents

- 1 **PLLA stents**
Variety of designs: characterization.
 - 2 **Radiopaque stents**
PLLA and PLCL stents with radiopaque agents.
- 
- Iodine TIBA BaSO₄

Chapter 4. Chemical vs thermal accelerated hydrolytic degradation of 3D-printed PLLA/PLCL bioresorbable stents: characterization and influence of sterilization

- 1 **Alkaline (0.1 M NaOH at 37 °C)**
 Surface erosion
- 2 **Thermal (PBS at 50 °C)**
 Bulk degradation
- 3 **Sterilization: EtO vs γ -irradiation**


Chapter 5. Solvent-cast direct-writing and electrospinning as a dual fabrication strategy for drug-eluting polymeric bioresorbable stents

- 1 **Direct everolimus loading**
Everolimus release rate insufficient
- 2 **Electrospinning coating**
 - PLCL in CHCl₃ \Rightarrow flow, time and rotation speed optimization
 - PLCL + everolimus in CHCl₃ \Rightarrow everolimus-loaded PLCL-coated BRS stents

PLCL solution with or without everolimus

Suitable everolimus release

Chapter 4. Functionalization of 3D printed polymeric bioresorbable stents with a dual cell-adhesive peptidic platform combining RGDS and YIGSR sequences

- 1 **Solid phase peptide synthesis**
 Cell adhesive peptides Dual platform (PF)
- 2 **Surface functionalization**


O₂ plasma activation EDC/NHS treatment Funct. samples
- 3 **Biological evaluation**
 - ECs adhesion assay
 - Blood perfusion assay

Functionalized samples presented higher ECs adhesion and spreading and lower platelet activation

Concluding remarks

Outcomes of the Thesis

Introduction

1.1 Introduction to cardiovascular stents

The World Health Organization reported in the latest *Global Health Estimates* that the leading global causes of death were predominantly associated to cardiovascular, respiratory and neonatal conditions [1]. Cardiovascular diseases (CVDs) accounted for 32.2% of global deaths in 2019, showing a 5 point increase over the last two decades. Among them, coronary heart disease (CHD) was responsible for 16% of the world's total deaths, rising to 8.9 million deaths in 2019 [1]. According to the latest available data gathered by the *European Heart Network* in 2017 [2], CVDs are also the main cause of death in the European Union (EU) accounting for 1.8 million deaths each year. Thirty-seven percent of all deaths in the EU (40% of deaths in women and 34% of deaths in men) are from CVD, as shown in Figure 1.1. CHD is also the single most common cause of death in the EU, accounting for over 630,000 deaths in the EU each year: 14% of deaths among men, and 12% of deaths among women.

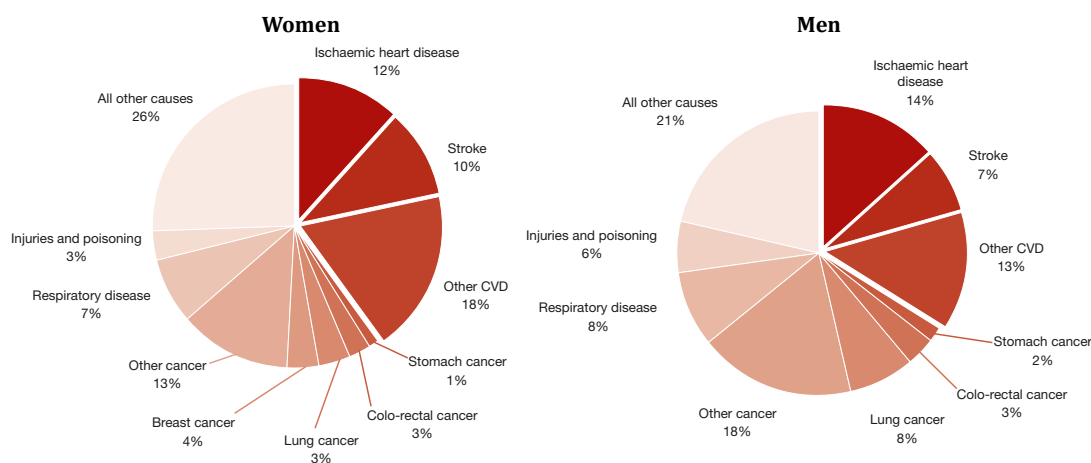


Fig. 1.1 Deaths by cause, women (left) and men (right), latest available year, EU. Adapted from [2].

Overall, CVD is estimated to cost the EU economy almost €210 billion a year, with around 53% due to direct health care costs, 26% to productivity losses due to mortality and morbidity and 21% to the informal care of people with CVD. In turn, CHD is estimated to cost the EU economy €59 billion a year: 28% of the overall cost of CVD [2].

1.1.1 Artery structure

CHD is a condition of the coronary arteries, that is, vessels that branch from the aorta and supply the heart muscle with oxygen-rich blood (Figure 1.2a) [3]. Arteries are composed of three major layers [4], as it can be seen in Figure 1.2b.

- ▷ **Tunica externa.** The outermost coat, also known as tunica adventitia, is a tough layer consisting mainly of fibroblasts and collagen fibers that act as a supportive element.
- ▷ **Tunica media.** The middle coat is made up principally of smooth muscle cells (SMCs) and elastic fibers arranged in spiral layers.
- ▷ **Tunica intima.** The innermost layer of the artery is composed of three layers:
 - (i) An elastic layer which consists of a membrane containing a network of elastic fibers in the longitudinal direction.
 - (ii) A subendothelial layer with connective tissue formed by collagen and proteoglycans.
 - (iii) A monolayer of endothelial cells (ECs) in contact with the internal cavity in which the blood flows (lumen), known as endothelium. As the cellular interface between the circulating blood and the vessel wall, it inhibits blood coagulation under healthy conditions.

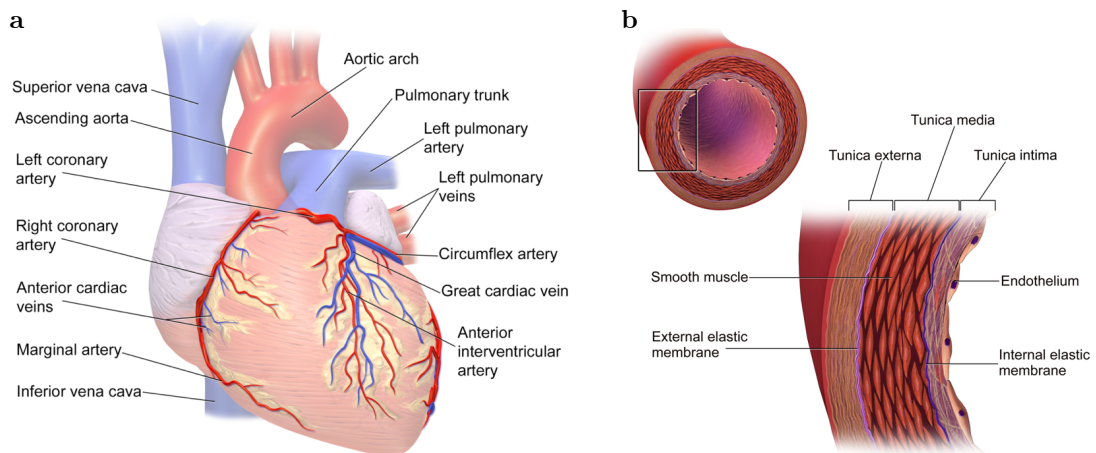


Fig. 1.2 (a) Coronary vessels and (b) structure of an artery. Adapted from [5].

1.1.2 Coronary Heart Disease

Coronary heart disease (CHD) is triggered by atherosclerosis, a disease of the arteries characterized by a thickening of the arterial walls due to the deposition and accumula-

tion of fatty deposits like cholesterol between the endothelium and the tunica media, as shown in Figure 1.3.

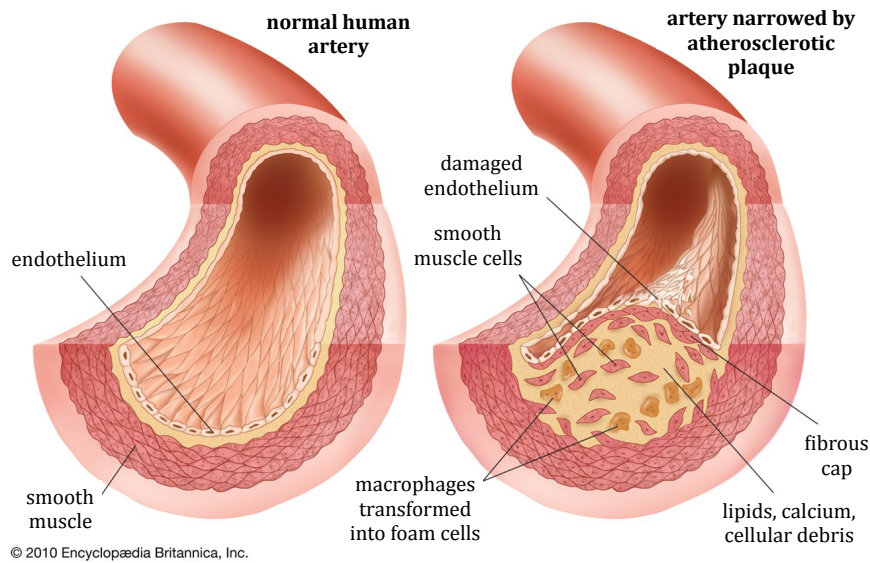


Fig. 1.3 Atherosclerosis in an artery. Adapted from [6].

Adhesion of circulating monocytes to the surface of the endothelium appears to be an early event in the development of atherosclerotic lesions. Next, they transfer through the endothelium and transform into macrophages, which ingest lipids and form a fatty deposit [7]. Meanwhile, a number of molecular factors, like platelets adhesion, generate proliferation of SMCs in the tunica intima. Monocytes, lipids, platelets, SMCs and fibrous connective tissues form an inflammatory plaque called atheroma. The formation of the atheroma plaque leads to a progressive long-term narrowing (stenosis) of the artery lumen, thus obstructing blood flow with the consequent risk of ischemia in the surrounding tissue [8]. If no treatment is applied, the plaque can become unstable and vulnerable to rupture, followed by acute vessel occlusion leading to myocardial infarction or potentially stroke.

In early stages of atherosclerosis development, the condition may be managed with conventional drug treatments, designed to lower the risk of myocardial infarction through improved control of blood pressure and cholesterol levels. However, when the vessel is damaged, thrombosis may occur, that is, the formation of a blood clot inside the vessel. In this cases it is necessary to perform a revascularization procedure in order to fully restore blood flow [8]. Depending on the severity and extent of the disease, surgeons decide between performing a coronary artery bypass graft (CABG) operation or a percutaneous coronary intervention (PCI). CABG consists in diverting blood flow around a section of a blocked or partially blocked artery in the heart by using a blood vessel from another part of the body. This technique remains the standard for patients with complex multivessel disease, whereas in patients with less complex disease PCI is a reasonable alternative treatment to CABG [9].

1.1.3 Percutaneous transluminal coronary angioplasty

In the 1970s, Andreas Gruentzig pioneered the use of a balloon for percutaneous transluminal coronary angioplasty (PTCA). This technique involves the use of a catheter inserted through a peripheral artery, most commonly the femoral or radial artery, to deliver a balloon at the site of the vessel narrowing. The balloon is then inflated under pressure, thus compressing the atherosclerotic plaque against the artery wall and expanding the vessel to improve blood flow [8]. Figure 1.4 illustrates the procedure. In 1979, Gruentzig performed the first PTCA with an expandable balloon on an awake human [10], and in the following years various technical advances in catheter design and materials were reported, making this technique increasingly widespread [11].

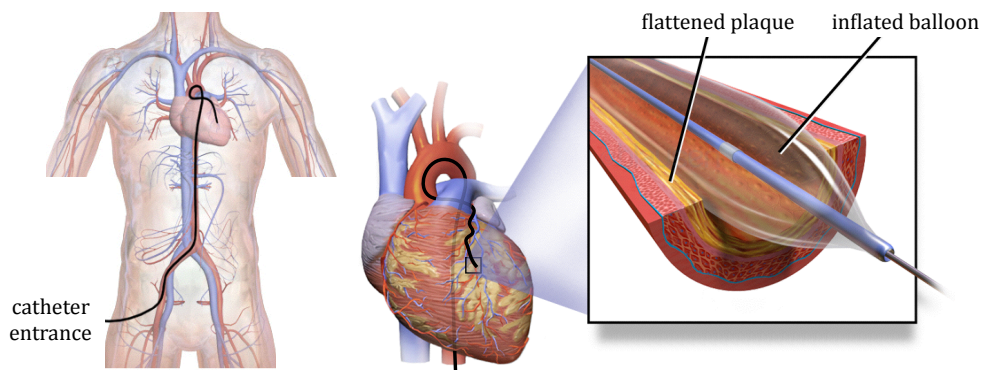


Fig. 1.4 PTCA procedure. Adapted from [5].

However, despite the effectiveness of the procedure, it presented limitations, such as acute vessel closure and elastic recoil in the short term, and restenosis in the long term. The process of restenosis was thought to be triggered by the severe injury to the artery endothelium caused by the expansion of the balloon. This damage induces SMCs proliferation and extracellular matrix deposition, which progressively narrows again the lumen of the artery. This effect was found in around one third of the patients [12].

1.1.4 Bare metal stents

In order to prevent acute vessel occlusion and restenosis after PTCA, the implantation of a mechanical support device, known as stent, was proposed. This technique was first performed by Sigwart and Puel in 1986 using a self-expandable stainless steel stent [8]. Alternatively, another deployment mechanism was developed, by placing the compressed (crimped) stent on a balloon-mounted catheter until reaching the stenosed region, where the balloon is inflated (8 to 20 atm) to plastically deform the stent against the artery walls, and left as a permanent implant. Figure 1.5 shows a scheme of the deployment procedure.

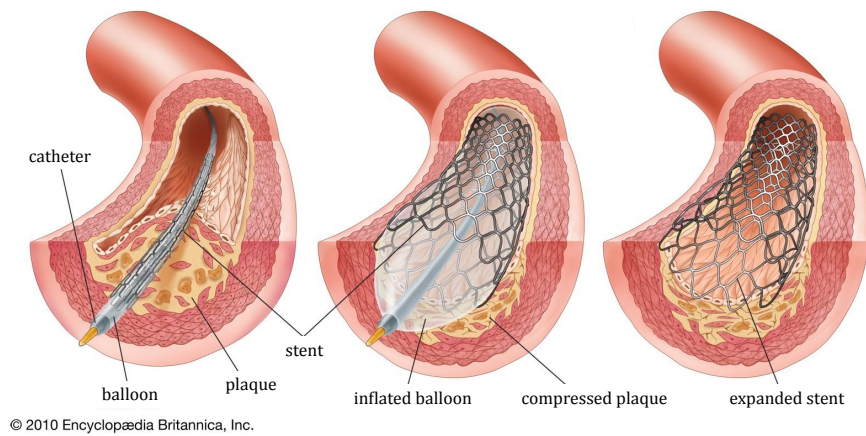


Fig. 1.5 Stent deployment scheme. Adapted from [13].

The first-generation stents, which are called bare metal stents (BMS) to distinguish them from more sophisticated modern designs, were initially associated with somewhat high incidence of subacute thrombosis, although this was successfully overcome with more aggressive antiplatelet therapy [14]. Overall, the placement of stents significantly reduced restenosis rates in comparison to balloon angioplasty alone, from 32% to 22% ($p = .02$) [15]. However, while such reductions in restenosis were welcome, stents did not completely remove this problem. In fact, it became clear that the use of these devices gave rise to a new healing response, so-called in-stent restenosis (ISR) [8].

Although the mechanisms underlying ISR are still not completely understood, it has generally been viewed as a distortion of the natural healing response to the injury caused on the endothelium due to stent placement. Endothelial denudation results in platelet adhesion and activation of neutrophils, monocytes and macrophages. This acute response releases cytokines and growth factors which in turn trigger SMCs to proliferate and migrate towards the lumen, together with the deposition of extracellular matrix, in a process known as neointimal hyperplasia [16].

In general, strategies to overcome ISR aimed at improving stent design in order to reduce the extent of vessel injury. Some design criteria had to be met, such as [8]:

- (i) Mechanical properties: high radial strength to prevent stent recoil, flexibility and excellent fatigue properties.
- (ii) Geometry and strut thickness: thinner struts cause lower rates of restenosis.
- (iii) Material properties: hemo- and biocompatibility, radiopacity and corrosion resistance.

In spite of the contributions to minimize the contact area between stent and vessel wall, the key technology that contributed the most in reducing ISR was the use of a local pharmacological therapy.

1.1.5 Drug eluting stents

The development of drug eluting stents (DES) constituted a revolution in stent design, with the combination of a metallic scaffold, a layer of drug carrier substance and an antiproliferative agent. The aim of this design is to avoid the overproliferation of SMCs by providing localised drug delivery directly to the affected lesion in high concentrations. Although some DES use direct bonding of drug to the metal, most manufacturers use a matrix polymer to better control the release profile of the drug [14].

Initially, two antirestenotic drugs showed significant efficacy in clinical trials: sirolimus and paclitaxel. Sirolimus is an antibiotic which causes an inhibition of the immune response through inhibition of T-lymphocyte activation, and also has an antiproliferative effect on SMCs [17]. Paclitaxel is an antineoplastic drug with an effect on stabilising the microtubules during mitosis, therefore inhibiting cell cycle and the proliferation of SMCs [18].

Preliminary feasibility studies of DES showed good clinical results. Soon, a large, randomised trial compared the local effects of the implantation of a sirolimus-eluting stent compared with an uncoated stent, showing a reduction in major adverse cardiac events for the sirolimus-eluting stent (5.8% vs 28.8% for BMS $p < .001$) at 1-year follow-up [19].

Although DES significantly reduce ISR, this comes with a negative effect on delayed arterial healing and increased risk of late stent thrombosis (LST). LST occurs more than one year after stent implantation, with a rate as high as 9.4% [20]. This late thrombosis suggests that the endothelium has not completely recovered after dual anti-platelet therapy (DAPT) is removed, because both sirolimus and paclitaxel inhibit ECs proliferation at the same concentration required to inhibit SMCs proliferation [21]. Therefore, several strategies were developed in order to overcome this limitation of DES, such as (i) prolongation of DAPT after 1 year of stent implantation, (ii) search for alternative drugs that could inhibit SMCs proliferation while having no detrimental effect on recovery of a functional endothelium, or (iii) development of bioresorbable stents (BRS).

1.2 Bioresorbable stents

Bioresorbable stents were envisaged to have the potential to revolutionize cardiology in a manner similar to that seen with the original BMS and then DES [22]. In the literature, they are sometimes referred to as bioresorbable scaffolds (BRS), with the term *scaffold* highlighting the temporary nature of BRS, in contrast with stents associated to a permanent implant [23]. The theory of using a BRS is to provide a transient support to the vessel allowing it to heal while the structure slowly degrades until completely resorbed [24].

The idea of dissolvable scaffolds is not novel, as it dates to the description of Tamai *et al.* [25] of the first successful use of a fully degradable stent in the early 1990s. However, this concept was nearly forgotten and set aside due to the success of BMS and, later, DES. With long-term data and the revelation of the risks of permanent metal stents, BRS development was reinitiated, resulting in a variety of devices [23].

The fact that the stent should disappear once its main function has been served is the main idea regarding BRS. Ideally, stents would retain sufficient radial strength after implantation to prevent acute vessel recoil and to release the antiproliferative drug. After the healing period, they would degrade and be resorbed completely, leaving the vessel with a healthy endothelium [24]. This approach would come with the following potential clinical benefits [26]:

- ▷ Potential reductions in adverse clinical events associated with the permanent presence of polymeric or metallic implants within the artery wall. Due to BRS degradation, no foreign body remains in the vessel in the long term, thus late stent thrombosis risks are potentially reduced or eliminated [23].
- ▷ The absence of any residual foreign material and restoration of the endothelium would also reduce the need for long-term DAPT, therefore decreasing the risk of bleeding, especially in older patients.
- ▷ The possibility that the vessel recovers its natural state of vasomotion to control blood flow and blood pressure.
- ▷ Treated patients may undergo further diagnostic investigations involving magnetic resonance imaging or coronary computed tomography angiography without concern.
- ▷ Stented vessels would remain suitable for the full range of revascularization strategies should this be required in the future, which is particularly important for younger adult patients and children.

1.2.1 Materials selection for BRS

Despite the numerous advantages regarding the use of BRS, they also present a few limitations which must be taken into account. Since the implantation of the first Igaki-Tamai BRS in human in 1999, made of poly-L-lactic acid (PLLA) [25], efforts have been mainly dedicated to the improvement of mechanical properties and making the device radiopaque.

Currently, the majority of BRS are manufactured with polymers, being PLLA the most used in the field. On the other hand, corrodible metals such as magnesium (Mg) have also been examined as a promising material [27]. In general, polymers present poorer mechanical properties than metals. Table 1.1 shows the gap between the mechanical properties of different biodegradable materials used presently for biomedical devices fabrication compared to cobalt chromium, a metal used for conventional DES.

Tab. 1.1 Material properties of biodegradable polymers and metallic alloys: poly-L-lactic acid (PLLA), poly-D-lactic acid (PDLA), poly(ϵ -caprolactone) (PCL), poly(lactic-co- ϵ -caprolactone) (PLCL) (90:10), polycarbonate (PC) and cobalt-chromium (CoCr). Adapted from [24], [28] and [29]

Material	Tensile modulus [GPa]	Tensile strength [MPa]	Elongation at break [%]	Glass transition temperature [°C]	Melting point [°C]	Degradation [months]
PLLA	2–4	60–70	2–6	60–65	173–178	18–36
PDLA	1–3.5	40–55	2–6	55–60	Amorphous	12–16
PCL	0.2–0.4	25–35	> 300	–60	58–63	24–36
PLCL	1.2–1.5	24–29	≈ 300	45–57	155–173	24–36
PC	2–2.4	55–75	80–150	147	Amorphous	> 14
CoCr	210–235	1449	40	–	1330	Biostable

The strength to weight ratio of polymers is lower than that of metals, thus making it a challenge to manufacture a degradable device with sufficient radial strength. For instance, PLLA exhibits approximately 100-fold lower tensile modulus than conventional metallic DES materials such as cobalt-chromium alloys. As the tensile modulus is directly proportional to radial stiffness, stents fabricated from bioresorbable materials require thicker struts in order to match up with the current DES performance [24]. Whereas most DES display strut thickness $< 100 \mu\text{m}$, BRS in development present strut thickness around $150 \mu\text{m}$. Moreover, the design of the stents has to take into account the degradability of the material, as radial strength needs to be maintained for at least 4 to 6 months [28]. Figure 1.6 shows a scheme of the degradation process that polymeric BRS undergo in operating conditions. Initially, a decrease in molecular weight (M_w) is found, followed by a decrease in radial strength until the polymer is completely resorbed [26].

Mechanical properties of PLLA depend on its crystallinity and M_w . Semi-crystalline PLLA is composed of crystalline lamellae linked with amorphous tie chains. With

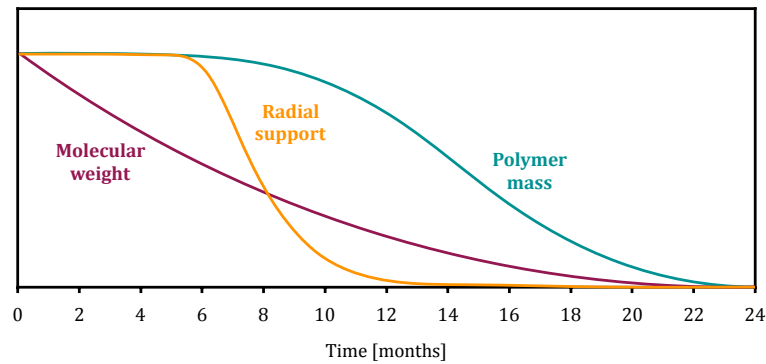


Fig. 1.6 BRS degradation under operating conditions. Adapted from [26].

increasing M_w , lamellae are more close-packed [30], resulting in increased crystallinity and improved mechanical properties [31].

Alternatively, PLLA mechanical properties may be enhanced when blending it with other polymers such as poly(ϵ -caprolactone) (PCL) or the copolymer poly(lactic-co- ϵ -caprolactone) (PLCL). PCL is a semi-crystalline biodegradable polyester susceptible to undergo autocatalyzed bulk hydrolysis and slow degradation, and shows low tensile modulus and high elongation at break while PLLA shows high modulus and low elongation at break [32]. Therefore, PCL can be used as a plasticizer to improve the flexibility and the processability of PLLA [33].

On the other hand, PLCL copolymers' main application is found in structural devices with the aim to add flexibility to PLLA through the incorporation of caprolactone monomers [34]. In general, the introduction of increasing amounts of caprolactone results in a decrease in Young's Modulus, a decrease in tensile strength and an increase in elongation at break [29]. Therefore, PLCL copolymers present different mechanical properties depending on the ratio lactide-to-caprolactone and the chemical structure.

Polyester degradation mechanism

Degradation of polyesters such as PLLA plays a significant role in the performance of the stent while implanted. PLLA degrades *in vivo* via hydrolysis, as shown in Figure 1.7. The reaction usually takes place at an ester bond, where a H_2O molecule breaks the PLLA chain into shorter chains. In the first stage, hydrolysis of the amorphous tie chains that are binding the crystal lamellae occurs, leading to a decrease in M_w with little effect on the mechanical properties. In the second stage, the polymer starts to fragment into segments of low-weight oligomers as radial strength starts to decrease as a result of the scission of amorphous tie chains connecting the crystalline regions. The third stage comprises the dissolution of the monomers by phagocytes, then metabolized into L-lactate and pyruvate, which enters the Krebs cycle and is further converted into CO_2 and H_2O [24], resulting in the complete resorption of the polymer. The degradation time of PLLA depends on its molecular weight, but it usually needs 2 to 3 years [28].

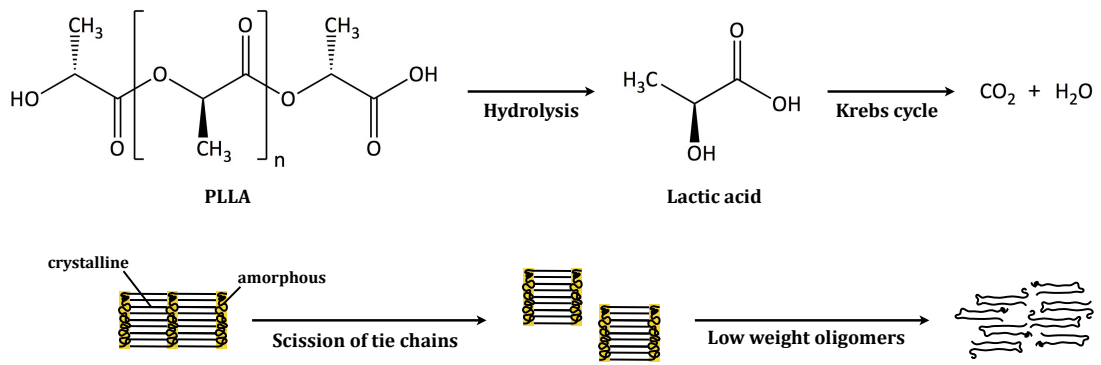


Fig. 1.7 PLLA degradation mechanism. Adapted from [24].

The degradation rate of PLLA also depends on its M_w and crystallinity, as hydrolysis initially occurs in amorphous regions [34]. Besides, the degradation rate may also be tuned when blending it with other polymers, such as PCL or PLCL (Table 1.1).

BRS limitations

The profile and deliverability of BRS is affected by their large strut thickness [35]. Thicker struts can also result in more flow disturbance, which can potentially increase incidence of acute thrombotic events. Additionally, PLLA devices have inherent limit of expansion (low ductility) and can fracture due to overdilatation. As a consequence, BRS implantation requires more steps than that of current DES [22]:

1. **Lesion preparation with predilatation.** It is mandatory to obtain a stent-like dilatation before scaffolding, which should minimize the risk of thrombosis.
2. **Sizing, stepwise deployment, and balloon inflation.** Careful BRS sizing is of great importance in order to match artery diameter. Scaffold deployment should be performed in a stepwise fashion (2 atm every 5 s). Finally, balloon inflation should be maintained for 30 seconds to achieve optimal expansion.
3. **Postdilatation with a noncompliant balloon.** Use of a noncompliant balloon inflated at high pressure, with a nominal diameter larger than the nominal scaffold diameter. This step is very important during BRS implantation, given that a low percentage of postdilatation is associated with a high rate of scaffold thrombosis.

Deliverability of BRS is also affected by their lack of radiopacity. Cardiologists track the delivery catheter through the patient's vasculature and accurately place the stent at the site of a lesion, which is achieved by fluoroscopy or similar X-ray visualization procedures. Stents should be more absorptive of X-rays than the surrounding tissue to be visible. However, the X-ray attenuation coefficient of most polymeric materials is low, thus polymeric BRS suffer from a lack of radiopacity as compared to traditional metallic stents. In order to overcome this limitation, most of the current

BRS have radiopaque metallic markers in the device for visibility under X-ray. Although markers can aid in accurate positioning of the scaffold, assessment of scaffold expansion and lesion coverage remains a challenge [24].

1.2.2 Current polymeric BRS technology

BRS are mainly made of biodegradable polymeric materials, including polymers synthesised from lactic acid, glycolic and caprolactone, such as poly-L-lactic acid (PLLA), poly(lactide-co-glycolide) (PLGA), poly-glycolic acid (PGA), poly(D,L-lactic-co-glycolic acid) copolymer (PDLLGA), poly-D,L-lactide (PDLLA), poly(ϵ -caprolactone) (PCL) and poly(lactic-co- ϵ -caprolactone) copolymer (PLCL) [28, 36].

Currently, there are more than 15 polymeric BRS available. Most are still either under preclinical evaluation or being examined in clinical trials. Five of them have already acquired *Conformité Européenne* (CE) mark approval: the Igaki-Tamai stent for the treatment of peripheral vascular disease, and the Absorb BVS, the DESolve, the Fantom and the ART Pure for CHD [28]. Table 1.2 summarizes the characteristics of the different BRS, which are shown in Figure 1.8, regarding structural material, coating, antiproliferative drugs, strut thickness, resorption time, radiopacity and development status.

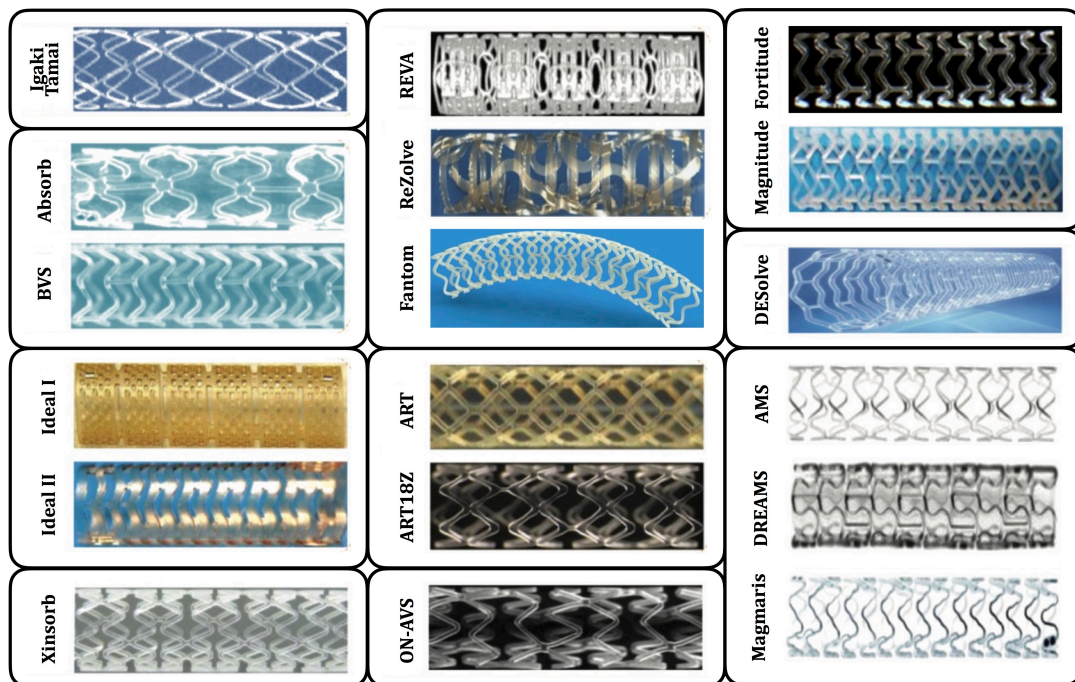


Fig. 1.8 BRS stents overview. Adapted from [26, 37, 38].

Igaki-Tamai (KYOTO MEDICAL PLANNING CO.)

The Igaki-Tamai scaffold was the first fully bioresorbable stent implanted in humans and was made of PLLA. The first revision of the scaffold had a helical zigzag design, was mounted on a standard angioplasty balloon, and was both thermal self-expanding and balloon expandable. Scaffold expansion was performed with the use of heated contrast (up to 70 °C). The device continued expanding after its implantation over a 20–30 minute period, until it reached its final dimensions [37]. The Igaki-Tamai stent obtained CE marking for use in peripheral arteries in November 2007, becoming the world's first certified bioresorbable stent [34]. Although the short- and long-term follow-up results were encouraging, this device failed to progress, mainly due to the large guide catheters required for implantation, and the concerns that the heated contrast used for device deployment may cause vessel wall injury [37].

ABSORB Bioresorbable Vascular Scaffold BVS (ABBOTT VASCULAR)

ABSORB was the world's first clinically available BRS for CHD. It was given CE mark in 2011 and Food & Drug Administration (FDA) clearance in 2016 [34]. The first version of the stent (ABSORB 1.0) consisted of (i) a platform made of semi-crystalline PLLA with an out-of-phase zigzag design and strut thickness of 150 μm , (ii) a 2-4 μm coating of PDLLA containing antiproliferative drug everolimus and (iii) a pair of radiopaque platinum markers at both ends to allow visualization. However, there were several issues with the first generation, namely scaffold recoil and area shrinkage at 6 months. A few changes were made for the second generation (ABSORB BVS), such as a different in-phase zigzag design and a blow moulding manufacturing process to provide it with prolonged radial support. Nevertheless, the ABSORB BVS was voluntarily and permanently withdrawn from sale by Abbott Vascular in September 2017 (see Section 1.2.4). Abbott Vascular are currently working on the clinical development of a newer generation device with thinner struts referred to as *Falcon*, with strut diameter < 100 μm in order to improve deliverability and acute performance [39].

DESolve (ELIXIR MEDICAL CORP.)

DESolve stents (CE mark) consist of a PLLA-based polymer, with the first generation (DESolve 150) presenting a strut thickness of 150 μm and myolimus as antiproliferative drug. The second generation (DESolve 100) was granted CE mark in 2014, used novolimus instead of myolimus and reduced the strut profile to 100 μm . Two others stents are currently under development or evaluated in clinical trials: DESolve Cx, with 120 μm strut diameter, and DESolve NTx, with contoured struts and improved radiographic visibility [34]. The differentiating features of DESolve from the other BRS are: (i) inherent self-correcting properties of the device in case of minor strut malapposition, which is due to the proprietary processing technique and (ii) its relative ductility that allows DESolve a wide range of expansion without risk of strut fracture [24].

Tab. 1.2 BRS classification and characteristics. Adapted from [24, 28, 34]

Manufacturer	Stent	Materials	Elution drugs	Strut thickness [μm]	Resorption time [months]	Radiopacity	Development status
Kyoto Med. Plan.	Igaki-Tamai	PLLA	-	170	24	Gold markers	CE mark
Abbott Vascular	Absorb 1.0	PLLA	Everolimus	150	24	Platinum markers	Discontinued
	Absorb BVS	PLLA	Everolimus	150	24	Platinum markers	CE mark
Elixir Medical	DESolve 150	PLLA	Myolimus	150	24-36	Platinum markers	CE mark
	DESolve 100	PLLA	Novolimus	100	24-36	Platinum markers	CE mark
REVA Medical Inc.	REVA	Tyrosine polycarbonate	-	200	24	Radiopaque scaffold	-
	ReZolve	Tyrosine polycarbonate	Sirolimus	115-230	6	Radiopaque scaffold	-
	ReZolve2	Tyrosine polycarbonate	Sirolimus	100	48	Radiopaque scaffold	Clinical trials
	Fantom	Tyrosine polycarbonate	Sirolimus	125	36	Radiopaque scaffold	CE mark
Amaranth Medical Inc.	Fortitude	PLLA	Sirolimus	150-200	3-6	-	Clinical trials
	Aptitude	PLLA	Sirolimus	115	3-6	-	Clinical trials
	Magnitude	PLLA	Sirolimus	<100	-	-	Clinical trials
Huaan Biotech. Co.	XINSORB	PLLA	Sirolimus	160	24-36	Radiopaque markers	Clinical trials
Bioabsorbable Therapeutics Inc.	Ideal I	polylactide anhydride	Sirolimus	200	9-12	-	Clinical trials
	Ideal II	polylactide anhydride	Sirolimus	175	>12	-	Preclinical trials
Arterial Remodelling Technologies Inc.	ART Pure	PLLA	-	170	18	-	CE mark
	ART18Z	PDLLA	-	170	18-24	-	Clinical trials
OrbusNeich	ON-AVS	PLLA/PDLA/PLCL	Sirolimus CD34+	150	>6	Radiopaque markers	Preclinical trials
Biotronik	AMS	Mg alloy	-	165	<4	-	Discontinued
	DREAMS 1	Mg alloy / PLGA	Paclitaxel	125	9	-	Clinical trials
	Magmaris	Mg alloy / PLLA	Sirolimus	150	9	Tantalum markers	CE mark

REVA, ReZolve, Fantom (REVA MEDICAL INC.)

Stents manufactured by REVA are made of a tyrosine-derived polycarbonate (PC) polymer and show radiopacity because of iodine covalently bound to the polymer backbone [39]. The first generation (REVA) had a strut thickness of 200 μm without any drug, whereas the second generation (ReZolve) introduced a sirolimus coating. The third generation (ReZolve2) included a stiffer, fully radiopaque polymer with sirolimus. Finally, the fourth generation (Fantom), which gained CE marking in April 2017, is a sirolimus-eluting BRS with a strut thickness of 125 μm [34] and high radial strength, which protects against early elastic recoil [22].

FORTITUDE, APTITUDE, MAGNITUDE (AMARANTH MEDICAL INC.)

The Amaranth scaffold family is made of sirolimus-eluting BRS with peculiar polymer production features: in contraposition with the crystalline frame of other PLLA scaffolds, these scaffolds are made of ultra high molecular weight PLLA with an amorphous structure, which increases its elongation at break with respect to typical polymer capabilities [39]. FORTITUDE (150–200 μm), APTITUDE (115 μm) and MAGNITUDE (90 μm) are currently undergoing clinical evaluation [34].

XINSORB (HUAAN BIOTECHNOLOGY GROUP CO.)

This sirolimus-eluting scaffold made of PLLA has a strut thickness of 160 μm . The device is balloon expandable and has radiopaque markers to facilitate its deployment [37]. Preclinical studies comparing Xinsorb BRS and the Excel DES found no significant difference in restenosis rates at 6 months [39].

IDEAL (BIOABSORBABLE THERAPEUTICS INC.)

The IDEAL BRS consists of 2 components: (i) polylactide anhydride mixed with a polymer of salicylic acid as core and (ii) a salicylate layer containing sirolimus. Salicylate is an anti-inflammatory drug that has shown to confer anti-inflammatory and antiplatelet properties to the scaffold, thereby reducing restenosis [24]. This first-generation stent had a strut thickness of 200 μm , which was reduced for the second generation down to 175 μm with higher dose of sirolimus. The scaffold has not yet achieved CE marking or regulatory approval from the FDA in the US [34]. The 2nd IDEAL is now entering preclinical studies [39].

ART Pure (ARTERIAL REMODELLING TECHNOLOGIES INC.)

The first generation ART is based on amorphous PLLA [37], without drug eluting capability and CE marking as of May 2015 [34]. The second generation (ART18Z) is made of a mixed PDLLA polymer with a strut thickness of 170 μm [24]. Another generation of the device with thinner struts and sirolimus-eluting design is currently under preclinical evaluation [24].

ON-AVS (ORBUSNEICH)

The ON-AVS BRS is fabricated from a polymeric blend of PLLA/PDLA/PLCL and presents a strut thickness of 150 μm [34] with sirolimus on the abluminal surface and CD34+ antibodies on the luminal surface for endothelial progenitor cell (EPC) capture. The antibodies draw circulating EPCs to the stent with the aim to achieve faster endothelialisation [24].

1.2.3 Biodegradable metallic stents

Stents made of biodegradable metals were developed in parallel to PLLA polymeric scaffolds. Potential advantages of metal over polymer include (i) good radial strength, (ii) negligible early elastic recoil and (iii) single-step inflation [22]. Therefore, bioresorbable stent made from biocorrosible metals are able to have thinner struts compared to polymeric BRS [24]. Metallic alloys used for BRS are Mg, Fe and Zn with a combination of some rare metals [27].

Biotronik is the main company involved in the development of biodegradable metallic stents, starting from the original Absorbable Mg Scaffold (AMS) series, then improved with the first generation of the DREAMS stent. This stent was made of a Mg alloy with slower resorption, reduced strut thickness and paclitaxel-eluting polymeric coating. The second generation DREAMS stent, renamed as Magmaris, received its CE mark in 2016. The device has an improved design with 150 μm strut thickness [40], a sirolimus-eluting coating [41] based on PLA, radiopaque markers and a resorption time of 9 months [40].

Nevertheless, Mg-based alloys present limitation, such as (i) a high corrosion rate, thus failing to provide sufficient support before arterial remodeling, and (ii) release of degradation products such as hydrogen, which may cause damage to the host tissue.

On the other hand, iron's mechanical properties are similar to traditional stainless steel, it is radiopaque and less brittle than Mg, making it possible to achieve thinner struts. However, superior corrosion resistance of Fe-based stents leads to long-term retention in the vessel. Therefore, research is focused on accelerating the corrosion rate. Finally, Zn-based stents have appeared as a new alternative, as Zn shows intermediate corrosion resistance between Mg and Fe, and excellent biocompatibility. Nevertheless, pure Zn has poor mechanical properties, which limits its further application [24].

1.2.4 BRS clinical performance

Among all polymeric BRS, the ABSORB Bioresorbable Vascular Scaffold (BVS) has been the most implanted worldwide, with more than 125,000 devices [22]. Therefore, it has been the most clinically studied BRS, and commonly compared with Xience, a cobalt-chromium DES. Preliminary studies showed that the Xience performed better with larger acute gain, larger minimal luminal diameter as well as lower percentage diameter stenosis compared to the BVS. This outcome was likely attributed to the greater strut thickness of the BVS as well as its inability to overexpand without the risk of stent fracturing compared to Xience [42].

Later, a meta-analysis involving everolimus-eluting BVS and metallic everolimus-eluting stents reported an increased rate of device-oriented adverse events and device thrombosis cumulatively at 2 years and between 1 and 2 years of follow-up compared with metallic DES [43]. Results from the ABSORB III trial after 2 years follow-up revealed an increase in major adverse cardiac events for BVS compared to the Xience group (target lesion failure: 11.0% vs 7.9% ($p = .03$)) [44].

This outcome prompted the FDA to investigate the increased 2-year rate of major adverse cardiac events observed with the BVS. EU regulatory authority and Abbott Vascular also decided to restrict commercial availability of the device in Europe from May 2017 onwards [24]. The ABSORB BVS was voluntarily and permanently withdrawn from sale by Abbott Vascular in September 2017 [34] due to low sales [45].

A systematic review concerning critical evaluation of stents in coronary angioplasty was presented in 2021 [46]. Stevens *et al.* reported that performance of BRS was found to be equivalent to that shown by DES regarding in-stent thrombosis. Nevertheless, despite promising early research, it is still unclear whether BRS are superior to DES in terms of effectiveness or safety. Similar conclusions were drawn by Zong *et al.*, as the incidence of clinical events for patients treated with BRS was similar to those treated with DES, according to the clinical trials that have been completed thus far [47]. However, polymeric BRS present inferior mechanical properties than DES, which in turn implies thicker struts to compensate for the insufficient radial strength, with the associated risks in terms of malapposition and thrombotic events. In conclusion, further research is needed to obtain bioresorbable polymeric stents with thinner struts in order to achieve the envisaged benefits in the long term.

1.2.5 Future perspectives of BRS

The main challenge of BRS development is to find a way of fine tuning the mechanical properties between providing enough vessel support to prevent recoil in the first months after implantation while minimizing the resorption time in order to reduce late undesirable events and maximizing stent endothelialization [39]. The following aspects need to be properly addressed:

- ▷ **Strut thickness, width and design.** Mechanical properties of bioresorbable materials is inferior to the metallic alloys used for DES. The scaffold footprint (defined as the percentage of vascular circumference occupied by struts) should be minimized in order to improve the integration of the stent in the surrounding tissue and the endothelialization process.
- ▷ **Low visibility.** The polymeric structure makes the struts radiolucent, while the radiopaque markers may be difficult to identify especially in calcific lesions or in obese patients.
- ▷ **Limited over-expansion capability.** This may lead to an increased risk of strut fracture upon deployment, and therefore to late thrombotic events.
- ▷ **Mandatory postdilatation.** Current devices are limited by the fact of being crimped on a very compliant balloon in order to minimize crossing profile and to have better deliverability. This hampers the possibility to implant BRS at high pressure, thus making postdilatation mandatory in order to achieve optimal results.
- ▷ **Duration of dual antiplatelet therapy (DAPT).** Thicker and wider struts may lead to a higher risk of thrombosis and may take more time to be completely endothelialized. While current guidelines do not suggest prolonged DAPT, it may be considered in patients without high bleeding risk.

Should these points be successfully addressed, BRS have the potential to revolutionize interventional cardiology as originally envisaged and display the numerous clinical benefits that were foreseen.

1.3 Stent manufacturing technologies

1.3.1 Current metal and polymer stents manufacturing

Over the last 30 years, stents have been fabricated using different techniques. These techniques can be divided in two groups, depending on the material in which the stents are fabricated [48].

Metal stents manufacturing

Although metal stents can be manufactured by photochemical machining, electroforming, wire bending or powder metallurgy, the majority are produced from metallic ingots fabricated by casting followed by thermomechanical treatments. Next, minitubes are fabricated by tube drawing, from which stents will be laser cut. Lasers allow precise cutting and offer a wide flexibility in terms of stent design [49]. Different laser types may be used for this process, such as solid state lasers, diode-pumped solid state lasers, optical fibre lasers or ultrashort pulse lasers [50]. After laser cutting, annealing is performed in order to relieve the residual stress produced during tube drawing and laser cutting and to improve the mechanical properties of the stent. Finally, annealed cut tubes are acid pickled to remove debris and electropolished [49]. For instance, stents made of stainless steel, nitinol, CoCr or magnesium can be processed with this technique.

Polymer stents manufacturing

Commercial polymer stents are commonly fabricated by a method comprising mold injection and laser machining.

- 1. Mold injection.** The polymer is heated to a molten state, extruded and injected into a mold with the shape of a tube [34]. The injection process presents two challenges: (i) the maintenance of the concentricity in the mold when filling it, and (ii) the thermal degradation of the polymer during the injection.
- 2. Laser machining.** The tubes are machined by laser cutting. The type of laser must be chosen carefully regarding power, pulse time and beam width. For instance, ultrashort pulse lasers directly evaporate the material from solid to vapor, without generating a heat affected zone (HAZ) which would compromise the mechanical properties of the stent [51]. Other lasers are being studied as a more economical alternative, like CO₂ lasers, although they create large HAZs which may lead to stent damage [52]. Figure 1.9 shows a typical laser-machined stent with an ultrashort pulse laser.

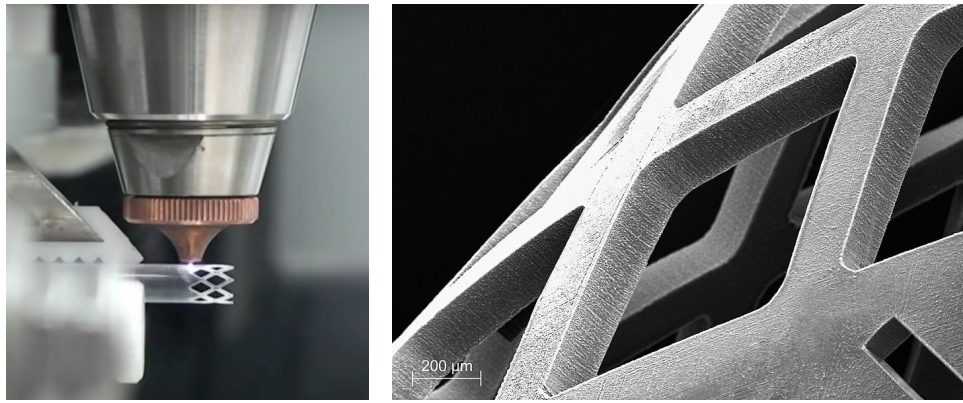


Fig. 1.9 (Left) Laser machining of a polymeric stent. (Right) Structure detail. Extracted from [53, 54].

Mechanical properties of polymeric stents are highly tunable by using different processing approaches. Several techniques are known to improve the performance of PLLA stents. Among others, manufacturers use extrusion drawing, blow moulding, solid die-drawing or solvent-based polymer spraying. Finally, annealing is performed to remove residual stresses and to improve the properties of the polymer by increasing its crystallinity [34].

1.3.2 Additive Manufacturing

Current stent fabrication techniques do not allow performing customisable stents addressed to patients with special needs such as diabetes or small vessel diameter. Alternatively, additive manufacturing (AM) has the ability to manufacture personalised medical solutions. Unique parts are usually costly and time consuming to produce, but when printers are combined with the 3D imaging techniques already being used by the health industry, this approach becomes viable regarding the potential benefits for the patient [55].

Three-dimensional printing (3D Printing) includes a wide variety of manufacturing techniques, which are all based on digitally-controlled deposition of materials layer-by-layer to create freeform geometries [56]. These techniques may be broadly classified in 3 groups: light-based, inkjet-based or nozzle-based printing methods. Figure 1.10a presents an overview of selected 3D Printing techniques.

Light-based 3D Printing

The use of light to fabricate objects was first applied in the stereolithography (SLA) of photocurable resins [58]. In SLA, the liquid photopolymer is exposed to light, either through the projection of a photopattern or using a scanning laser. As the liquid resin is polymerized, the object is translated and a new layer of liquid resin is introduced and subsequently photoirradiated in selected regions until crosslinking is complete

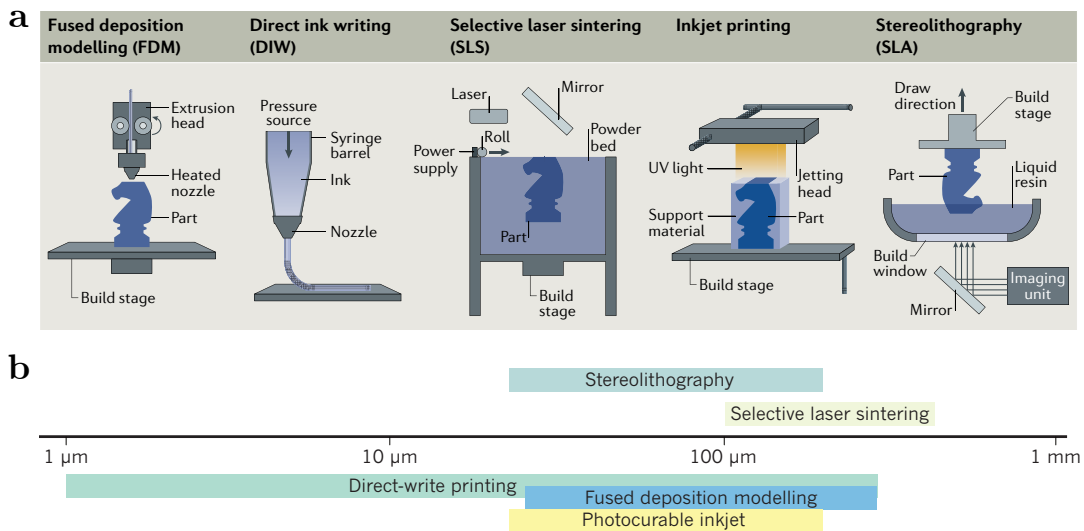


Fig. 1.10 (a) Additive manufacturing techniques overview. Extracted from [57]. (b) Resolution range for several light-, inkjet- and nozzle-based printing methods. Adapted from [58].

[57]. The process is repeated in a layer-by-layer fashion until the desired 3D object is complete.

In a similar way, selective laser sintering (SLS) uses the power of light to locally heat and fuse together thermoplastic powders. Once the first layer has been printed, powder is cast again across the bed and locally sintered to the previous layer [57]. As the 3D object is printed layer by layer, the remaining non-fused powder serves as support. Typically, powders used for SLS present a diameter between 10 and 100 μm , and thus the maximum achievable resolution is around 100 μm [58].

Inkjet-based 3D Printing

Inkjet printing is an overall term to describe systems based on the placement of small liquid drops onto a substrate using a pattern-generating device. Depending on the substrate, one can distinguish between Drop-on-Powder or Drop-on-Drop.

The former uses a combination of a powder bed and a binder ink in solvent to build a solid structure in a layer-wise manner. The machine is composed of a pair of horizontal $x - y$ axes suspended over a vertical z -piston. The process starts by spreading a thin layer of powder onto the top of the piston plate. The binder ink is passed through a nozzle, which moves in 2D following the desired pattern over the powder bed to print droplets that bind the powder particles together. Then, the powder bed is lowered and a new layer of fresh powder is applied on top. The process is repeated until completion of the structure. The last step generally consists in thermal sintering, which allows the removal of residual volatile solvents [56].

On the other hand, drop-on-drop uses a combination of a dissolved polymer as ink and a heated bed. The ink is passed through a nozzle using a piezoelectric element, and deposited onto the heated bed, where the solvent will evaporate and the polymer will solidify. Subsequent layers are printed on top of already dry drops until completion of the structure. The critical parameter in order to optimize this technique is polymer viscosity, as it has to be in the range where it allows ejection through the nozzle but without uncontrollable spreading [56]. It has been reported that a suitable viscosity is ranged between 3 and 20 mPa·s [59].

Nozzle-based 3D Printing

Nozzle-based deposition consists in the continuous and direct application of the ink through a nozzle to create a 3D pattern layer-by-layer [56]. The ink may be obtained by polymer melting, known as fused-deposition modeling (FDM), or by dissolving the polymer in a solvent and extruding it through pressure-assisted microsyringes, known as direct ink writing (DIW) or solvent-cast direct-writing (SC-DW). The width of the extruded filament will depend on the nozzle diameter, although DIW presents a broader resolution range than FDM (Figure 1.10b).

In FDM, a molten thermoplastic polymer filament is extruded by two rollers through a high temperature nozzle and thereafter solidifies onto a build plate. Generally, the print head can move within the $x - y$ plane whereas the platform, which can be thermostated, can move vertically on the z axis, but in other configurations the print head moves in the z axis whereas the platform moves in the $x - y$ plane [56]. The requirement of a thermoplastic material for this technology limits its application and versatility, where the most commonly used material is acrylonitrile butadiene styrene [60]. On top of that, high temperature conditions hamper the addition of drugs to the polymer as they may degrade.

On the other hand, SC-DW consists in the direct writing of a dissolved polymer through a nozzle by means of pressure. This technique requires specific ink rheological and viscoelastic properties. First, the ink viscosity should be low to facilitate its extrusion through a capillary micronozzle under applied pressure. Second, the rigidity of the filament after extrusion must quickly increase due to solvent evaporation in order to achieve shape retention [61]. This approach allows the loading of drugs to the polymeric ink without the limitations of FDM, as the procedure can be performed at room temperature. On top of that, SC-DW allows for the printing of practically any material, from polymers to ceramics to metals, provided that the ink presents the required rheological behavior. As a consequence, the versatility of SC-DW permits its application in a plethora of different fields, such as electronics or biomedical engineering [62].

Electrospinning

Although electrospinning (ES) is not regarded as an AM technique, its combination with 3D Printing provides an effective and powerful platform to fabricate novel structural biomaterials. ES uses a polymeric ink together with high voltage to generate micro- or nanofibers with very high specific surface area. Moreover, it is the most efficient and straightforward method to align nanofibers in order to mimic the native extracellular matrix (ECM), thus providing a suitable platform for cell adhesion, migration and proliferation. Additionally, drugs, peptides and other bioactive factors may be encapsulated in electrospun fibers or surface immobilized. Nevertheless, membranes composed of electrospun fibers lack mechanical strength, and therefore their combination with 3D Printing techniques may suppose an effective strategy to obtain biomaterials with controllable shape, high porosity with interconnected structure, appropriate strength and ECM-like surface with cell bioactive cues [63].

1.4 Bioactive cardiovascular stents

Materials used for stent manufacturing present the appropriate bulk properties regarding their main function, that is, to keep the vessel open for restored blood flow. Nevertheless, as medical devices, stents must also be biocompatible, that is, "*able to be in contact with a living system without producing an adverse effect*", as defined by the International Union of Pure and Applied Chemistry (IUPAC) [64]. Biocompatibility of stents may be achieved by surface modification in order to avoid detrimental interactions between the stent surface and blood [65]. Still, stent functionalization aims at not only providing biocompatibility, but also to confer bioactivity. According to the IUPAC, a substance is bioactive when it "*provokes a response from a living system*", usually reflecting a beneficial change [64].

The main strategies towards bioactive cardiovascular stents include the use of drugs, coatings and biomolecules in order to enhance stents hemocompatibility and the endothelialization process [66].

1.4.1 Drug delivery

As mentioned in Section 1.1.5, the development of DES constituted a revolution in stent design. DES loaded with antiproliferative drugs to avoid the overproliferation of SMCs provided localized drug delivery directly to the affected lesion in high concentrations. Although some DES directly bind the drug to the metal, most manufacturers use a matrix polymer to better control the release profile of the drug [14]. In the following, different drug loading techniques are discussed.

Drug loading approaches and release kinetics

In general, therapeutic molecules may be incorporated into the material matrix or adsorbed on the external biomaterial surface. Figure 1.11 shows the different mechanisms for loading drugs into/on implant materials.

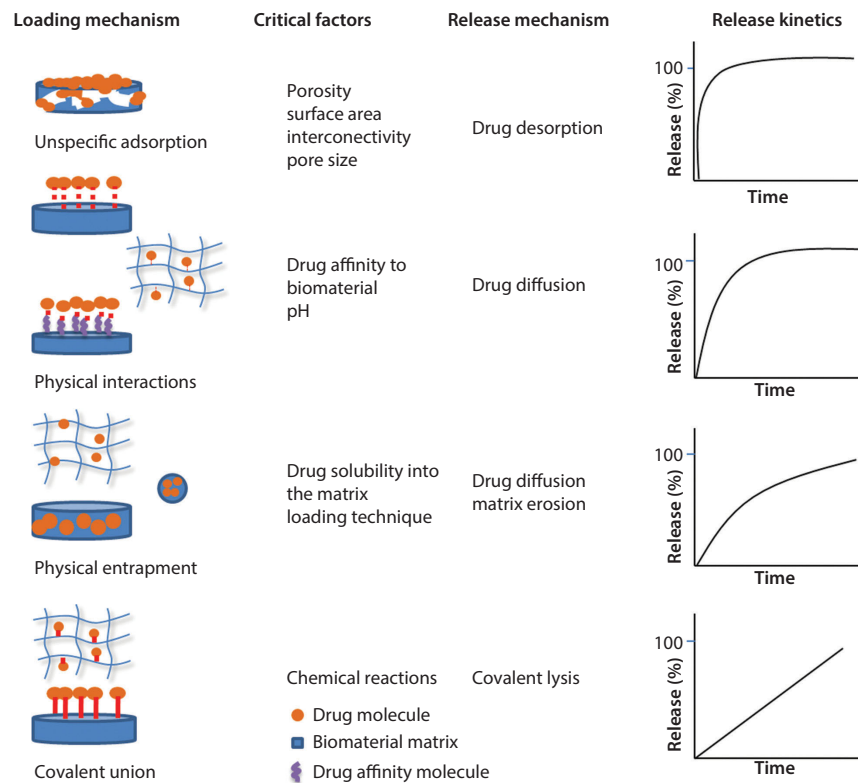


Fig. 1.11 Drug loading approaches, associated release mechanisms and release kinetics. Adapted from [67].

In general, drugs can be included during the material synthesis process (physical entrapment loading) or on the surface of the final biomaterial. In the latter case, drugs can be unspecifically adsorbed on the material surface, covalently linked to the surface or attached by physical interactions to the internal or external surface of the matrices or polymeric gel networks [67].

Unspecific adsorption. The most common method is the immersion of porous materials into high concentration drug solutions, allowing for unspecific adsorption, which mainly depends on structural parameters of the biomaterial such as specific surface, total porosity and pore size distribution [67]. Once implanted, these loaded systems undergo drug desorption, with release profiles characterised by an initial burst effect due to the fast dissolution of the drug molecules adsorbed on the surface followed by a release highly dependent on drug solubility and pore structure.

Physical interactions. Physical interactions such as hydrogen bonding, van der Waals' forces, electrostatic or hydrophobic interactions are used to load drugs in biomaterials

and achieve desirable controlled release profiles [67]. Many of these interactions are highly dependent on pH. The release profile is not as steep as for unspecific adsorption, and no burst release is observed.

Physical entrapment. Drugs can be physically entrapped into polymers during their synthesis or production processes. In general, more prolonged release profiles than for drug-adsorbed systems are achieved, driven by diffusion and matrix erosion. The entrapment of drugs is possible through different approaches, such as added to the liquid phase of a polymer solution or mixed with the polymer powder. The drug release profile will depend on material composition, molecular weight of polymers, polymer concentration and cross-linking conditions [67].

Chemical immobilisation. This process relies on the formation of a covalent bond between the drug and the surface of the biomaterial. For instance, the covalent union of peptides or proteins is a common mechanism for loading drugs in polymeric materials, and the factors controlling release are the degradation of covalent unions as well as the diffusion through the polymeric system to the medium [67].

Drug loading design of BRS

BRS without drugs such as AMS and REVA were associated with neointimal hyperplasia, therefore suggesting the indispensability of drug loading to enable clinical application. BRS can be loaded with anti-coagulant, anti-inflammatory or anti-proliferative drugs [28]. Sirolimus is the most used drug in BRS, as the ReSolve2, Fantom, Aptitude, Xinsorb, Ideal, ON-Avs and Magmaris stents are loaded with it, among others. Alternatively, the Absorb BVS was loaded with Everolimus, and the DESolve stents with myolimus and novolimus [34].

Release kinetics have a significant role in the revascularization of the artery wall, and rapid vs slow drug release offer advantages and drawbacks. Short release times may reduce the time period when DAPT is necessary. On the other hand, in some cases, the restenotic process is still active several months after implantation and only stents with long drug release timeframe could prevent this phenomenon. Slow rate kinetics also has its drawbacks, as it leaves stent struts unendothelized for longer time and late stent thrombosis may occur [14]. Overall, a drug release time of about 3 months seems a good compromise [34]. Therefore, the release profile must be stable in time, and that is why physical entrapment is the preferred drug loading technique, as the drug diffuses through matrix erosion [67].

Nevertheless, drug-loaded BRS may present altered mechanical properties with respect to the polymeric material alone, and also different degradation mechanisms. This is the reason why drugs are sometimes loaded in a polymeric coating, different from the core of the stent. For instance, the Absorb consisted of a platform made of semi-crystalline

PLLA with a 2-4 μm coating of PDLLA containing everolimus [34]. However, this coating may also affect the degradation timeline of the stent [28].

1.4.2 Functionalization of cardiovascular stents

All stents present some degree of thrombogenicity in contact with blood as a consequence of endothelium disruption when deployed [65]. Metals surface electrical charge and wettability influence protein adsorption behavior in such a way that protein denaturation may occur, which in turn eventually leads to coagulation and thrombosis. Polymer-coated stents are mainly hydrophobic and delaminate as they degrade, leaving the underlying metal exposed [68]. Moreover, antiproliferative drugs cause endothelial dysfunction [21, 69] and newly developed biodegradable stents have high strut profiles, causing increased blood flow disturbance, also contributing to thrombotic potential of stents [26, 70]. For these reasons, improving the clinical performance of stents requires an approach that can simultaneously increase the hemocompatibility of the device while differentially regulating the behavior of vascular endothelial and smooth muscles cells [68].

Therefore, stents should have surface properties which reduce thrombogenicity, prevent denaturation of adsorbed proteins and ideally accelerate re-endothelialisation [65].

Coatings and surface modification

Surface modification of stents for improved biocompatibility can be done by several means. Some designs introduce a layer of material on the stent surface in order to prohibit or reduce undesirable protein adhesion [65]. One of these proteins, fibrinogen, leads to activation of platelets when desaturated, then triggers a cascade reaction eventually leading to blood coagulation and thrombosis.

Various types of polymer coatings have shown to reduce platelet adhesion and protein adsorption. These coatings can be deposited by means of nonthermal plasma, an extensively used technique for surface activation and/or modification [71]. For instance, antifouling coatings based on polyethylene glycol (PEG) show significant results in preventing nonspecific protein adsorption [72, 73]. Other plasma-based polymeric coatings have been tested, such as heparin and chitosan. The former is a highly sulfated, linear polysaccharide clinically used as an anticoagulant drug, and the latter is a good candidate for antimicrobial films. Meng *et al.* [74] coated chitosan and heparin onto a coronary stent to accelerate re-endothelialization and healing processes after coronary stent deployment and tested both *in vitro* and *in vivo*. Results verified that the modification process could substantially enhance re-endothelialization compared with unmodified stents.

Biofunctionalization strategies

Another approach to achieving hemocompatibility of stents is to functionalize their surface with active biological agents such as nitric oxide (NO) donors, antibodies, growth factors or proteins [69, 75–77]. The preferred immobilization method is covalent binding, as biomolecules must be able to withstand stent crimping and expansion as well as exposure to long-term pulsatile blood flow [68].

NO plays a key role in vascular biology, as it inhibits the adhesion of platelets and leukocytes, reduces SMCs proliferation and their synthesis of collagen [78–80]. Antibodies have particular potential to accelerate re-endothelialization by capturing circulating endothelial progenitor cells (EPCs) to immobilize them on the stent surface [81]. However, although CD34-binding antibodies capture EPCs from the circulation, no surface marker is unique for EPCs or ECs identification and capture. Regarding the use of growth factors, Lee *et al.* reported a bilayered PCL scaffold functionalized with vascular endothelial growth factor to increase ECs proliferation [82].

A range of proteins have been shown to play critical roles in local regulation of thrombosis, endothelialization, and SMCs proliferation. On the one hand, collagen and fibronectin are two extracellular matrix (ECM) proteins known to enhance ECs attachment and proliferation. However, despite having favorable endothelial cell interactions, both collagen and fibronectin are known to be prothrombogenic and also promote SMCs migration [68]. On the other hand, tropoelastin has shown to have favorable interactions with ECs, low thrombogenicity and growth inhibition of SMCs [68]. Nevertheless, the use of proteins is associated to problems such as enzymatic instability, immunogenicity, inflammation risk and high costs [83].

In this regard, the use of custom-made bioadhesive peptides, which are derived from ECM proteins but encompass only defined cell adhesive motifs, overcome these limitations and efficiently enhance cell adhesion and improve biointegration *in vitro* and *in vivo* [83]. Peptides can be covalently immobilized on polymeric substrates following a plasma treatment to activate carboxylic groups [68]. Regarding peptide sequences, RGDS (Arg-Gly-Asp-Ser) is a universal cell adhesive recognition motif from fibronectin, but REDV (Arg-Glu-Asp-Val, from fibronectin) and YIGSR (Tyr-Ile-Gly-Ser-Arg, from laminin) sequences specifically mediate adhesion and migration of ECs while preventing SMCs and platelet adhesion [72, 84]. Moreover, distinct bioactive peptides can be combined to exert synergistic or complementary effects on the surface of an implant [85]. Interestingly, it has been recently shown that the combination of RGDS with REDV & YIGSR enhances the endothelialization of metallic stents [86] and vascular grafts [87].

References

- [1] World Health Organization, *Global health estimates 2020: deaths by cause, age, sex, by country and by region, 2000-2019*. Geneva, 2020.
- [2] E. Wilkins, L. Wilson, K. Wickramasinghe, P. Bhatnagar, J. Leal, R. Luengo-Fernandez, R. Burns, M. Rayner, and N. Townsend, “European cardiovascular disease statistics 2017”, 2017.
- [3] Enciclopaedia Britannica, “Coronary artery”, 2019.
- [4] —, “Artery”, 2019.
- [5] Blausen.com, “Medical gallery of blausen medical 2014”, *WikiJournal of Medicine*, vol. 1, no. 2, 2014.
- [6] Enciclopaedia Britannica, “Atherosclerosis”, 2023.
- [7] A. Ghattas, H. R. Griffiths, A. Devitt, G. Y. Lip, and E. Shantsila, “Monocytes in coronary artery disease and atherosclerosis: where are we now?”, *Journal of the American College of Cardiology*, vol. 62, no. 17, pp. 1541–1551, 2013.
- [8] C. McCormick, “Overview of cardiovascular stent designs”, in *Functionalised Cardiovascular Stents*, Elsevier, 2018, pp. 3–26.
- [9] F. W. Mohr, M.-C. Morice, A. P. Kappetein, T. E. Feldman, E. Stähle, A. Colombo, M. J. Mack, D. R. Holmes Jr, M.-a. Morel, N. Van Dyck, *et al.*, “Coronary artery bypass graft surgery versus percutaneous coronary intervention in patients with three-vessel disease and left main coronary disease: 5-year follow-up of the randomised, clinical SYNTAX trial”, *The Lancet*, vol. 381, no. 9867, pp. 629–638, 2013.
- [10] A. Gruentzig, R. Myler, E. Hanna, and M. Turina, “Transluminal angioplasty of coronary artery stenoses”, *Circulation*, vol. 84, pp. 56–66, 1977.
- [11] R. L. Mueller and T. A. Sanborn, “The history of interventional cardiology: cardiac catheterization, angioplasty, and related interventions”, *American Heart Journal*, vol. 129, no. 1, pp. 146–172, 1995.
- [12] M. Hamon, C. Bauters, E. McFadden, N. Wernert, J. Lablanche, B. Dupuis, and M. Bertrand, “Restenosis after coronary angioplasty”, *European Heart Journal*, vol. 16, pp. 33–48, 1995.
- [13] Enciclopaedia Britannica, “Angioplasty”, 2023.
- [14] M. Wawrzyńska, J. Arkowski, A. Włodarczak, M. Kopaczyńska, and D. Biały, “Development of drug-eluting stents (DES)”, in *Functionalised Cardiovascular Stents*, Elsevier, 2018, pp. 45–56.
- [15] P. W. Serruys, P. De Jaegere, F. Kiemeneij, C. Macaya, W. Rutsch, G. Heyndrickx, H. Emanuelsson, J. Marco, V. Legrand, P. Materne, *et al.*, “A comparison of balloon-expandable-stent implantation with balloon angioplasty in patients with coronary artery disease”, *New England Journal of Medicine*, vol. 331, no. 8, pp. 489–495, 1994.
- [16] P. H. Grewe, T. Deneke, A. Machraoui, J. Barmeyer, and K.-M. Müller, “Acute and chronic tissue response to coronary stent implantation: pathologic findings in human specimen”, *Journal of the American College of Cardiology*, vol. 35, no. 1, pp. 157–163, 2000.

- [17] S. O. Marx and A. R. Marks, *Bench to bedside: the development of rapamycin and its application to stent restenosis*, 2001.
- [18] S. J. Sollott, L. Cheng, R. R. Pauly, G. M. Jenkins, R. E. Monticone, M. Kuzuya, J. P. Froehlich, M. T. Crow, E. G. Lakatta, and E. K. Rowinsky, “Taxol inhibits neointimal smooth muscle cell accumulation after angioplasty in the rat”, *The Journal of clinical investigation*, vol. 95, no. 4, pp. 1869–1876, 1995.
- [19] P. W. Serruys, M. Degertekin, K. Tanabe, A. Abizaid, J. E. Sousa, A. Colombo, G. Guagliumi, W. Wijns, W. K. Lindeboom, J. Ligthart, *et al.*, “Intravascular ultrasound findings in the multicenter, randomized, double-blind ravel (randomized study with the sirolimus-eluting velocity balloon-expandable stent in the treatment of patients with de novo native coronary artery lesions) trial”, *Circulation*, vol. 106, no. 7, pp. 798–803, 2002.
- [20] P. W. Serruys, Y. Onuma, S. Garg, P. Vranckx, B. De Bruyne, M.-C. Morice, A. Colombo, C. Macaya, G. Richardt, J. Fajadet, *et al.*, “5-year clinical outcomes of the ARTS II (arterial revascularization therapies study II) of the sirolimus-eluting stent in the treatment of patients with multivessel de novo coronary artery lesions”, *Journal of the American College of Cardiology*, vol. 55, no. 11, pp. 1093–1101, 2010.
- [21] T. J. Parry, R. Brosius, R. Thyagarajan, D. Carter, D. Argentieri, R. Falotico, and J. Siekierka, “Drug-eluting stents: sirolimus and paclitaxel differentially affect cultured cells and injured arteries”, *European journal of pharmacology*, vol. 524, no. 1-3, pp. 19–29, 2005.
- [22] C. Indolfi, S. De Rosa, and A. Colombo, “Bioresorbable vascular scaffolds—basic concepts and clinical outcome”, *Nature Reviews Cardiology*, vol. 13, no. 12, p. 719, 2016.
- [23] J. Wiebe, H. M. Nef, and C. W. Hamm, “Current status of bioresorbable scaffolds in the treatment of coronary artery disease”, *Journal of the American College of Cardiology*, vol. 64, no. 23, pp. 2541–2551, 2014.
- [24] H. Ang, J. Ng, H. Bulluck, P. Wong, S. Venkatraman, Y. Huang, and N. Foin, “Fundamentals of bioresorbable stents”, in *Functionalised Cardiovascular Stents*, Elsevier, 2018, pp. 75–97.
- [25] H. Tamai, K. Igaki, E. Kyo, K. Kosuga, A. Kawashima, S. Matsui, H. Komori, T. Tsuji, S. Motohara, and H. Uehata, “Initial and 6-month results of biodegradable poly-L-lactic acid coronary stents in humans”, *Circulation*, vol. 102, no. 4, pp. 399–404, 2000.
- [26] Y. Sotomi, Y. Onuma, C. Collet, E. Tenekecioglu, R. Virmani, N. S. Kleiman, and P. W. Serruys, “Bioresorbable scaffold: the emerging reality and future directions”, *Circulation research*, vol. 120, no. 8, pp. 1341–1352, 2017.
- [27] I. Cockerill, C. W. See, M. L. Young, Y. Wang, and D. Zhu, “Designing better cardiovascular stent materials: a learning curve”, *Advanced functional materials*, vol. 31, no. 1, p. 2005361, 2021.
- [28] T. Hu, C. Yang, S. Lin, Q. Yu, and G. Wang, “Biodegradable stents for coronary artery disease treatment: recent advances and future perspectives”, *Materials Science and Engineering: C*, vol. 91, pp. 163–178, 2018.
- [29] J. Fernandez, A. Etxeberria, and J.-R. Sarasua, “Synthesis, structure and properties of poly (L-lactide-co- ϵ -caprolactone) statistical copolymers”, *Journal of the Mechanical Behavior of biomedical Materials*, vol. 9, pp. 100–112, 2012.
- [30] T. R. Welch, R. C. Eberhart, J. Reisch, and C.-J. Chuong, “Influence of thermal annealing on the mechanical properties of PLLA coiled stents”, *Cardiovascular Engineering and Technology*, vol. 5, no. 3, pp. 270–280, 2014.

- [31] G. Perego, G. D. Cella, and C. Bastioli, “Effect of molecular weight and crystallinity on poly (lactic acid) mechanical properties”, *Journal of Applied Polymer Science*, vol. 59, no. 1, pp. 37–43, 1996.
- [32] T. Patrício and P. Bártolo, “Thermal stability of PCL/PLA blends produced by physical blending process”, *Procedia Engineering*, vol. 59, pp. 292–297, 2013.
- [33] P. Menčík, R. Příklad, I. Stehnová, V. Melčová, S. Kontárová, S. Figalla, P. Alexy, and J. Bočkaj, “Effect of selected commercial plasticizers on mechanical, thermal, and morphological properties of poly (3-hydroxybutyrate)/poly (lactic acid)/plasticizer biodegradable blends for three-dimensional (3D) print”, *Materials*, vol. 11, no. 10, p. 1893, 2018.
- [34] S. McMahon, N. Bertollo, E. D. O. Cearbhaill, J. Salber, L. Pierucci, P. Duffy, T. Dürig, V. Bi, and W. Wang, “Bio-resorbable polymer stents: a review of material progress and prospects”, *Progress in Polymer Science*, vol. 83, pp. 79–96, 2018.
- [35] N. Foin, R. D. Lee, R. Torii, J. L. Guitierrez-Chico, A. Mattesini, S. Nijjer, S. Sen, R. Petraco, J. E. Davies, C. Di Mario, *et al.*, “Impact of stent strut design in metallic stents and biodegradable scaffolds”, *International journal of cardiology*, vol. 177, no. 3, pp. 800–808, 2014.
- [36] N. Bink, V. B. Mohan, and S. Fakirov, “Recent advances in plastic stents: a comprehensive review”, *International Journal of Polymeric Materials and Polymeric Biomaterials*, vol. 70, no. 1, pp. 54–74, 2021.
- [37] Y. Zhang, C. V. Bourantas, V. Farooq, T. Muramatsu, R. Diletti, Y. Onuma, H. M. Garcia-Garcia, and P. W. Serruys, “Bioresorbable scaffolds in the treatment of coronary artery disease”, *Medical Devices (Auckland, NZ)*, vol. 6, p. 37, 2013.
- [38] A. Abizaid and J. Ribamar Costa Jr, “The unmet needs: how future technologies will address current limitations of bioresorbable scaffold technology”, *Catheterization and Cardiovascular Interventions*, vol. 88, no. S1, pp. 54–59, 2016.
- [39] D. Regazzoli, P. P. Leone, A. Colombo, and A. Latib, “New generation bioresorbable scaffold technologies: an update on novel devices and clinical results”, *Journal of thoracic disease*, vol. 9, no. Suppl 9, S979, 2017.
- [40] S. Garg, C. Bourantas, and P. W. Serruys, “New concepts in the design of drug-eluting coronary stents”, *Nature Reviews Cardiology*, vol. 10, no. 5, p. 248, 2013.
- [41] R. Colleran and A. Kastrati, “Percutaneous coronary intervention: balloons, stents and scaffolds”, *Clinical Research in Cardiology*, vol. 107, no. 2, pp. 55–63, 2018.
- [42] S. Cassese, R. A. Byrne, G. Ndrepepa, S. Kufner, J. Wiebe, J. Repp, H. Schunkert, M. Fusaro, T. Kimura, and A. Kastrati, “Everolimus-eluting bioresorbable vascular scaffolds versus everolimus-eluting metallic stents: a meta-analysis of randomised controlled trials”, *The Lancet*, vol. 387, no. 10018, pp. 537–544, 2016.
- [43] Z. A. Ali, P. W. Serruys, T. Kimura, R. Gao, S. G. Ellis, D. J. Kereiakes, Y. Onuma, C. Simonton, Z. Zhang, and G. W. Stone, “2-year outcomes with the absorb bioresorbable scaffold for treatment of coronary artery disease: a systematic review and meta-analysis of seven randomised trials with an individual patient data substudy”, *The Lancet*, vol. 390, no. 10096, pp. 760–772, 2017.
- [44] S. G. Ellis, D. J. Kereiakes, G. W. Stone, *et al.*, “Everolimus-eluting bioresorbable vascular scaffolds in patients with coronary artery disease: ABSORB III trial 2-year results”, in *Annual Meeting of the American College of Cardiology*, vol. 18, 2017.

- [45] D. Capodanno, “Bioresorbable scaffolds in coronary intervention: unmet needs and evolution”, *Korean circulation journal*, vol. 48, no. 1, pp. 24–35, 2018.
- [46] J. R. Stevens, A. Zamani, J. I. A. Osborne, R. Zamani, and M. Akrami, “Critical evaluation of stents in coronary angioplasty: a systematic review”, *BioMedical Engineering OnLine*, vol. 20, no. 1, p. 46, 2021.
- [47] J. Zong, Q. He, Y. Liu, M. Qiu, J. Wu, and B. Hu, “Advances in the development of biodegradable coronary stents: a translational perspective”, *Materials Today Bio*, p. 100368, 2022.
- [48] B. Polanec, J. Kramberger, and S. Glodež, “A review of production technologies and materials for manufacturing of cardiovascular stents.”, *Advances in Production Engineering & Management*, vol. 15, no. 4, 2020.
- [49] M. Moravej and D. Mantovani, “Biodegradable metals for cardiovascular stent application: interests and new opportunities”, *International journal of molecular sciences*, vol. 12, no. 7, pp. 4250–4270, 2011.
- [50] A. Schuesseler *et al.*, “Manufacturing of stents: optimize the stent with new manufacturing technologies”, *New technologies in vascular biomaterials: fundamentals about stent II*, pp. 93–106, 2007.
- [51] “Athermal laser machining for medical implants”, *Norman Noble, Inc.*, 2015.
- [52] B. Stępak, A. Antończak, M. Bartkowiak-Jowska, J. Filipiak, C. Pezowicz, and K. Abramski, “Fabrication of a polymer-based biodegradable stent using a CO₂ laser”, *archives of civil and mechanical engineering*, vol. 14, no. 2, pp. 317–326, 2014.
- [53] “Ultrashort pulse lasers applications”, *Rofin*, May 2013.
- [54] “Reduced costs of tube processing with lasers”, *Rofin*, Aug. 2013.
- [55] A. B. AlAli, M. F. Griffin, and P. E. Butler, “Three-dimensional printing surgical applications”, *Eplasty*, vol. 15, 2015.
- [56] J. Goole and K. Amighi, “3D printing in pharmaceuticals: a new tool for designing customized drug delivery systems”, *International journal of pharmaceuticals*, vol. 499, no. 1-2, pp. 376–394, 2016.
- [57] T. Wallin, J. Pikul, and R. F. Shepherd, “3D printing of soft robotic systems”, *Nature Reviews Materials*, vol. 3, no. 6, pp. 84–100, 2018.
- [58] R. L. Truby and J. A. Lewis, “Printing soft matter in three dimensions”, *Nature*, vol. 540, no. 7633, pp. 371–378, 2016.
- [59] J. Sumerel, J. Lewis, A. Doraiswamy, L. F. Deravi, S. L. Sewell, A. E. Gerdon, D. W. Wright, and R. J. Narayan, “Piezoelectric ink jet processing of materials for medical and biological applications”, *Biotechnology Journal: Healthcare Nutrition Technology*, vol. 1, no. 9, pp. 976–987, 2006.
- [60] A.-V. Do, B. Khorsand, S. M. Geary, and A. K. Salem, “3D printing of scaffolds for tissue regeneration applications”, *Advanced healthcare materials*, vol. 4, no. 12, pp. 1742–1762, 2015.
- [61] S.-Z. Guo, F. Gosselin, N. Guerin, A.-M. Lanouette, M.-C. Heuzey, and D. Therriault, “Solvent-cast three-dimensional printing of multifunctional microsystems”, *Small*, vol. 9, no. 24, pp. 4118–4122, 2013.

- [62] M. Saadi, A. Maguire, N. T. Pottackal, M. S. H. Thakur, M. M. Ikram, A. J. Hart, P. M. Ajayan, and M. M. Rahman, “Direct ink writing: a 3D printing technology for diverse materials”, *Advanced Materials*, vol. 34, no. 28, p. 2108855, 2022.
- [63] D.-L. Yang, F. Faraz, J.-X. Wang, and N. Radacsi, “Combination of 3D printing and electrospinning techniques for biofabrication”, *Advanced Materials Technologies*, vol. 7, no. 7, p. 2101309, 2022.
- [64] M. Vert, Y. Doi, K.-H. Hellwich, M. Hess, P. Hodge, P. Kubisa, M. Rinaudo, and F. Schué, “Terminology for biorelated polymers and applications (iupac recommendations 2012)”, *Pure and Applied Chemistry*, vol. 84, no. 2, pp. 377–410, 2012.
- [65] A. Foerster, M. Duda, H. Kraśkiewicz, M. Wawrzyńska, H. Podbielska, and M. Kopczyńska, “Physico-chemical stent surface modifications”, in *Functionalised Cardiovascular Stents*, Elsevier, 2018, pp. 137–148.
- [66] A. Srivastava, “Chemistry of targeted immobilization of biomediators”, in *Functionalised Cardiovascular Stents*, Elsevier, 2018, pp. 231–250.
- [67] P. Díaz-Rodríguez and M. Landin, “Implantable materials for local drug delivery in bone regeneration”, *Advanced Materials Interfaces*, pp. 325–378, 2016.
- [68] M. Santos, A. Waterhouse, B. Lee, A. Chan, R. Tan, P. Michael, E. Filipe, J. Hung, S. Wise, and M. Bilek, “Simple one-step covalent immobilization of bioactive agents without use of chemicals on plasma-activated low thrombogenic stent coatings”, in *Functionalised Cardiovascular Stents*, Elsevier, 2018, pp. 211–228.
- [69] P. Qi, S. Chen, T. Liu, J. Chen, Z. Yang, Y. Weng, J. Chen, J. Wang, M. F. Maitz, and N. Huang, “New strategies for developing cardiovascular stent surfaces with novel functions”, *Biointerphases*, vol. 9, no. 2, p. 029017, 2014.
- [70] K. Kolandaivelu, R. Swaminathan, W. J. Gibson, V. B. Kolachalama, K.-L. Nguyen-Ehrenreich, V. L. Giddings, L. Coleman, G. K. Wong, and E. R. Edelman, “Stent thrombogenicity early in high-risk interventional settings is driven by stent design and deployment and protected by polymer-drug coatings”, *Circulation*, vol. 123, no. 13, pp. 1400–1409, 2011.
- [71] M. Ramkumar, P. Cools, A. Arunkumar, N. De Geyter, R. Morent, V. Kumar, S. Udaykumar, P. Gopinath, S. Jaganathan, and K. Pandiyaraj, “Polymer coatings for biocompatibility and reduced nonspecific adsorption”, in *Functionalised Cardiovascular Stents*, Elsevier, 2018, pp. 155–198.
- [72] H.-W. Jun and J. L. West, “Modification of polyurethaneurea with PEG and YIGSR peptide to enhance endothelialization without platelet adhesion”, *Journal of Biomedical Materials Research Part B: Applied Biomaterials*, vol. 72, no. 1, pp. 131–139, 2005.
- [73] J.-k. Park, D.-G. Kim, I. H. Bae, K. S. Lim, M. H. Jeong, C. Choi, S.-K. Choi, S. C. Kim, and J.-W. Nah, “Blood-compatible and biodegradable polymer-coated drug-eluting stent”, *Macromolecular Research*, vol. 23, no. 3, pp. 237–244, 2015.
- [74] S. Meng, Z. Liu, L. Shen, Z. Guo, L. L. Chou, W. Zhong, Q. Du, and J. Ge, “The effect of a layer-by-layer chitosan–heparin coating on the endothelialization and coagulation properties of a coronary stent system”, *Biomaterials*, vol. 30, no. 12, pp. 2276–2283, 2009.
- [75] K. Zhang, T. Liu, J.-A. Li, J.-Y. Chen, J. Wang, and N. Huang, “Surface modification of implanted cardiovascular metal stents: from antithrombosis and antirestenosis to endothelialization”, *Journal of Biomedical Materials Research Part A*, vol. 102, no. 2, pp. 588–609, 2014.

- [76] P. Mulinti, J. Brooks, B. Lervick, J. Pullan, and A. Brooks, “Strategies to improve the hemocompatibility of biodegradable biomaterials”, in *Hemocompatibility of Biomaterials for Clinical Applications*, Elsevier, 2018, pp. 253–278.
- [77] J. Zhao and Y. Feng, “Surface engineering of cardiovascular devices for improved hemocompatibility and rapid endothelialization”, *Advanced Healthcare Materials*, vol. 9, no. 18, p. 2000920, 2020.
- [78] L. J. Taitte, P. Yang, H.-W. Jun, and J. L. West, “Nitric oxide-releasing polyurethane–PEG copolymer containing the YIGSR peptide promotes endothelialization with decreased platelet adhesion”, *Journal of Biomedical Materials Research Part B: Applied Biomaterials*, vol. 84, no. 1, pp. 108–116, 2008.
- [79] S. Omar and A. de Belder, “Nitric oxide donor delivery”, in *Functionalised Cardiovascular Stents*, Elsevier, 2018, pp. 291–304.
- [80] N. Beshchasna, M. Saqib, H. Kraskiewicz, Ł. Wasyluk, O. Kuzmin, O. C. Duta, D. Ficai, Z. Ghizdavet, A. Marin, A. Ficai, *et al.*, “Recent advances in manufacturing innovative stents”, *Pharmaceutics*, vol. 12, no. 4, p. 349, 2020.
- [81] F. Boccafoschi, L. Fusaro, and M. Cannas, “Immobilization of peptides on cardiovascular stent”, in *Functionalised Cardiovascular Stents*, Elsevier, 2018, pp. 305–318.
- [82] S. J. Lee, M. E. Kim, H. Nah, J. M. Seok, M. H. Jeong, K. Park, I. K. Kwon, J. S. Lee, and S. A. Park, “Vascular endothelial growth factor immobilized on mussel-inspired three-dimensional bilayered scaffold for artificial vascular graft application: in vitro and in vivo evaluations”, *Journal of colloid and interface science*, vol. 537, pp. 333–344, 2019.
- [83] M. López-García and H. Kessler, “Stimulation of bone growth on implants by integrin ligands”, *Handbook of Biomineralization: Biological Aspects and Structure Formation*, pp. 109–126, 2007.
- [84] J. A. Hubbell, S. P. Massia, N. P. Desai, and P. D. Drumheller, “Endothelial cell-selective materials for tissue engineering in the vascular graft via a new receptor”, *Bio/technology*, vol. 9, no. 6, p. 568, 1991.
- [85] C. Mas-Moruno, R. Fraioli, F. Albericio, J. M. Manero, and F. J. Gil, “Novel peptide-based platform for the dual presentation of biologically active peptide motifs on biomaterials”, *ACS applied materials & interfaces*, vol. 6, no. 9, pp. 6525–6536, 2014.
- [86] M. I. Castellanos, C. Mas-Moruno, A. Grau, X. Serra-Picamal, X. Trepal, F. Albericio, M. Joner, F. J. Gil, M. P. Ginebra, J. M. Manero, *et al.*, “Functionalization of CoCr surfaces with cell adhesive peptides to promote huvecs adhesion and proliferation”, *Applied Surface Science*, vol. 393, pp. 82–92, 2017.
- [87] H. Aubin, C. Mas-Moruno, M. Iijima, N. Schütterle, M. Steinbrink, A. Assmann, F. J. Gil, A. Lichtenberg, M. Pegueroles, and P. Akhyari, “Customized interface biofunctionalization of decellularized extracellular matrix: toward enhanced endothelialization”, *Tissue Engineering Part C: Methods*, vol. 22, no. 5, pp. 496–508, 2016.

Scope and aims of the Thesis

Bioresorbable stents (BRS) have been envisioned as a revolution in the treatment of coronary heart disease. Since the stent resorbs, the cause of potential inflammation that can lead to late stent thrombosis and restenosis may be avoided. Nevertheless, although BRS have shown equivalent or improved performance with respect to current drug-eluting stents (DES) in the long term, it is unclear whether BRS are superior to DES in terms of effectiveness or safety in the short term. Still, as polymeric BRS display inferior mechanical properties than metallic DES, the need for thicker struts is associated to increased risk of platelet activation and thrombosis rate. Therefore, the main challenge of BRS lies in simultaneously providing enough mechanical support to prevent recoil in the first months while minimizing strut thickness and resorption time in order to reduce late undesirable biological events and favor biointegration to the artery.

The main aim of the present PhD Thesis is the design and development of tunable polymeric bioresorbable stents manufactured by means of solvent-cast direct-writing (SC-DW) with reinforced mechanical properties, suitable degradation timeframe and enhanced biointegration.

To accomplish the general goal, several specific objectives are defined as follows:

Objective 1. To develop and optimize the SC-DW technique in order to obtain polymeric stents with enhanced mechanical properties and reduced strut thickness. The following subgoals were considered:

- ▷ To fabricate 3D-printed biodegradable polymeric stents by SC-DW technique using a modified commercial FDM 3D printer. Two different bioresorbable polymers will be tested: poly-L-lactic acid (PLLA) and poly(L-lactic-co- ϵ -caprolactone) (PLCL). Different designs and extrusion nozzle dimensions will be evaluated to optimize the mechanical properties with respect to strut thickness.
- ▷ To adjust the polymeric inks with radiopaque agents in order to confer radiopacity to 3D-printed stents.

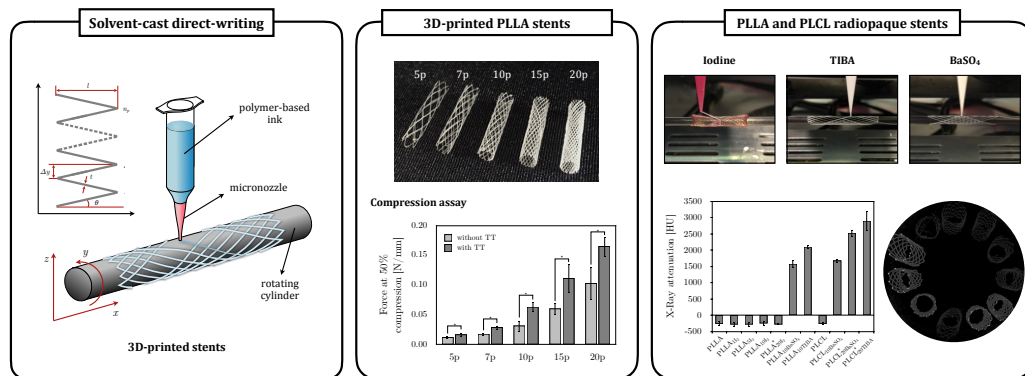
- ▷ To study the degradation of 3D-printed stents under accelerated hydrolytic conditions, chemical vs thermal, in terms of degradation mechanism and rate.
- ▷ To study the effects of ethylene oxide sterilization and γ -irradiation on PLLA and PLCL stents.

Objective 2. To modify the fabricated stents in order to control the biological response and assess device hemocompatibility and endothelialization. The following sub-goals were considered:

- ▷ To develop drug-eluting 3D-printed BRS stents with an antiproliferative drug following two strategies: (i) by encapsulation in the stent struts or (ii) by loading the drug in a customized electrospun PLCL membrane covering the stent.
- ▷ To synthesize linear cell-adhesive peptides as well as a dual peptidic platform and to functionalize 3D-printed PLLA and PLCL BRS with the aim to investigate the effects on endothelial cell and platelet adhesion.

Solvent-cast direct-writing as a fabrication strategy for radiopaque stents

Bioresorbable stents (BRS) potential in treating coronary heart disease is still to be further developed. Current trends include research with new polymeric materials, the need for thinner struts combined with appropriate mechanical properties, radiopacity and optimized local drug delivery. This work presents a novel solvent-cast direct-write (SC-DW) printing system to manufacture BRS onto a rotating cylinder with poly-L-lactic acid (PLLA) and poly(L-lactic-co- ϵ -caprolactone) (PLCL) inks. Printed stents were characterized in terms of mechanical, thermal and biological properties with human umbilical vein endothelial cells (HUVECs). Expansion assays showed that stents withstood pressures of at least 16 atm and the indirect cytotoxicity test indicated that stents were biocompatible. Polymeric inks were further modified with the addition of 3 radiopaque agents, namely iodine, triiodobenzoic acid (TIBA) and barium sulfate (BaSO_4) to render stents radiopaque. Subsequent characterization showed a general increase in strut thickness with respect to control PLLA or PLCL stents, which in turn resulted in higher resistance to compression. Microcomputed tomography was used to assess stents' radiopacity, showing that TIBA and BaSO_4 -containing stents presented high X-Ray attenuation values and maintained their radiopacity after 3 months incubation time.



V. Chausse, R. Schieber, Y. Raymond, B. Ségry, R. Sabaté, K. Kolandaivelu, M.-P. Ginebra, M. Pegueroles, *Solvent-cast direct-writing as a fabrication strategy for radiopaque stents*, Additive Manufacturing (2021) 102392.

3.1 Introduction

Bioresorbable stents (BRS) are designed to solve current permanent stents diseases such as restenosis and late stent thrombosis (LST). BRS should provide a transient support to the vessel allowing it to heal while the structure slowly degrades until completely resorbed [1].

In BRS clinical studies, although Abbott Vascular's Absorb BVS has shown non-inferiority regarding short-term efficacy on post-procedural angiographic results compared to Xience™, a cobalt-chromium drug eluting stent (DES) [2], an increase in stent thrombosis rate was reported in a meta-analysis compiling six trials [3]. Follow-up results after 2 years revealed an increase in major adverse cardiac events [4] and the Absorb was finally withdrawn from the market. The main challenge of BRS development is to find a way of fine tuning the mechanical properties between providing enough vessel support to prevent recoil in the first months after implantation and minimizing the resorption time in order to reduce late undesirable events [5]. The majority of BRS are manufactured with polymers, being poly-L-lactic acid (PLLA) the most used in the field. Despite the potential advantages regarding the use of BRS, they also present a few limitations, such as the need for thicker stent struts in order to achieve sufficient radial strength. Thicker struts might result in more flow disturbance, thus potentially increasing acute thrombotic events [1]. PLLA mechanical properties may be tailored when blending it with other polymers such as poly(ϵ -caprolactone) (PCL) or the copolymer poly(L-lactic-co- ϵ -caprolactone) (PLCL). In general, the introduction of increasing amounts of caprolactone results in a decrease in Young's Modulus, a decrease in tensile strength and an increase in elongation at break [6, 7]. Nevertheless, the optimal polymer combination to obtain stents with thin struts and enhanced mechanical properties has not yet been elucidated.

In contrast to metallic stents, which are inherently visible under X-ray imaging, BRS lack radiopacity. Consequently, most of the current BRS include radiopaque metallic markers in the device for visibility under X-ray. Although markers can aid in accurate positioning of the scaffold, assessment of scaffold expansion and lesion coverage remains a challenge [1]. Alternatively, radiopaque polymers have been developed, such as an iodinated tyrosine-derived polymer used for the Fantom stents by REVA [8]. Iodine has been used as a radiopaque agent for PCL [9, 10], chitosan [11], polymeric nanoparticles [12], electrospun PCL/PLLA fibers [13], injectable poly(ethylene glycol)/polyester thermogel [14, 15], α -tocopherol nano-emulsions [16] and degradable poly(vinyl alcohol) hydrogels [17]. Other strategies involve the use of 2,3,5-triiodobenzoic acid (TIBA), an organic-solvent soluble, iodine-based contrast agent, used for PCL modification [18], infused into poly(p-dioxanone) (PPDO) [19] or melt-blended with PPDO and implanted in swine for *in vivo* evaluation [20]. Alternatively, the use of barium sulfate

has been reported *in vivo* as a radiopaque agent for PLA urethral stents in rabbits [21], PLA pancreatic stents in rats [22], and PLA biliary stents in pigs [23], showing good biocompatibility. Despite recent advances in radiopaque polymers research, its application to bioresorbable stents is still under development.

Current stent fabrication technologies such as stent braiding or laser machining [24, 25] are continuously making progress to develop stents addressed to patients with special needs such as small vessel diameter or diabetes [26, 27]. Still, three-dimensional printing (3D Printing) appears as an alternative when personalized medical solutions are required [28]. Unique parts are usually costly and time consuming to produce, but when printers are combined with the 3D imaging techniques already being used by the health industry, this approach becomes viable regarding the potential benefits for the patient [29]. Among 3D Printing techniques, nozzle-based deposition is widely used as a continuous and direct application of the ink through a nozzle to create a 3D pattern layer-by-layer [30]. The ink may be obtained by polymer melting, known as fused-deposition modelling (FDM), or by dissolving the polymer in a solvent and extruding it through pressure-assisted microsyringes, known as solvent-cast direct-writing (SC-DW). SC-DW broadens the range of possibilities regarding stent design and allows for modifications in order to render stents with supplementary features, such as radiopaque BRS.

Recently, there have been advances regarding BRS fabrication by means of different additive manufacturing (AM) approaches such as stereolithography and photopolimerization by exposure to UV light [31], FDM [32–35] or a combination of FDM and post-print crosslinking to develop a biliary stent with BaSO₄ coating for X-Ray imaging purposes [36]. However, previous approaches involve the use of high temperatures, which may induce polymer degradation and prevent the use of thermally-degradable additives, whereas SC-DW appears as a more flexible technique in terms of ink design. As a proof of concept, Schieber *et al.* [37] fabricated PLLA bioresorbable stents by SC-DW to assess its feasibility. To the best of our knowledge, a complete characterization of such type of stents has never been reported.

This work presents a versatile AM fabrication strategy for stents by using polymeric inks and direct-writing onto a rotating cylinder. The rheological properties of the PLLA ink in chloroform have been analyzed, and stents with varying geometries have been printed and mechanically tested under compression and expansion tests. Stents were characterized by means of scanning electron microscopy (SEM), differential scanning calorimetry (DSC), thrombogenicity and cytotoxicity assays with human umbilical vein endothelial cells (HUVECs). PLLA and PLCL inks were further modified with the addition of 3 radiopaque agents: (i) iodine, (ii) TIBA and (iii) BaSO₄. Radiopaque stents were characterized by means of SEM, DSC and a degradation analysis. Stents' radiopacity

was assessed using micro-computed tomography imaging and stents' biocompatibility was evaluated by means of a cytotoxicity assay with HUVECs.

3.2 Materials and methods

3.2.1 Chemicals and materials

Medical grade PLLA (Purasorb[®] PL 65; inherent viscosity 6.5 dl/g, $M_w = 1675000$ g/mol) and PLCL (Purasorb[®] PLC 9538, 95:5 lactic-to-caprolactone molar ratio, $IV = 3.8$ dl/g, $M_w = 700000$ g/mol) were purchased from Corbion (Netherlands). Iodine (>99.99%), TIBA (2,3,5-triiodobenzoic acid, 98%), barium sulfate (99.99%) and chloroform ($\geq 99.5\%$) were obtained from Sigma-Aldrich (USA).

3.2.2 Polymer-based ink preparation and characterization

Printable ink was prepared by dissolution of PLLA or PLCL pellets in chloroform at a 10% or 12.5% ratio (w/v), respectively. Polymer dissolution was ensured by means of a Dual Asymmetric Centrifuge (SpeedMixer[™], AC 150.1 FVZ, FlackTek, Germany). Obtained ink was introduced in 3cc cartridges (Optimum[®], Nordson, USA).

Radiopaque inks consisted of a polymeric solution in chloroform with the addition of a radiopaque agent. Table 3.1 summarizes all conditions tested, using two polymers as base (PLLA and PLCL), with iodine, TIBA or BaSO₄, at different concentrations. BaSO₄ was chosen as a positive control for radiopacity assessment. As BaSO₄ is not soluble in chloroform, prior to mixing in the centrifuge, sonication in CHCl₃ was performed in order to break agglomerates and ensure proper dispersion. Two types of tips (Optimum[®] SmoothFlow[™], Nordson, USA) were used, with internal diameters of 250 μm or 200 μm . Stents printed with the latter are labeled with an asterisk (*).

The viscosity of the PLLA and PLCL solutions was evaluated by means of a capillary flow analysis as described in [38, 39]. The study consisted in placing the ink in a cartridge with a capillary tip (Nordson, with inner diameter $d_{\text{tip}} = 410 \mu\text{m}$ and length $l_{\text{tip}} = 12.7$ mm), which was extruded at different velocities ($v = 1 - 60$ mm/s) using a compression setup (Bionix 858 Test System, MTS, USA). The required extrusion force corresponding to each velocity was recorded after reaching steady state.

3.2.3 3D Printing of stents

Stents were fabricated by means of SC-DW technique. A commercial FDM 3D printer (BCN 3D+, BCN 3D technologies, Spain) was modified in order to extrude the polymeric

Tab. 3.1 Overview of inks preparation regarding base polymer, polymer to chloroform ratio, radiopaque agent and its concentration, and printer nozzle diameter. Inks labeled with an asterisk (*) were printed with 200 μm nozzle.

Ink	Polymer	Polymer to chloroform ratio [% w/v]	Radiopaque agent	Concentration [wt.%]	Nozzle diameter [μm]
PLLA	PLLA	10	–	–	250
PLLA _{1I₂}	PLLA	10	Iodine	1	250
PLLA _{5I₂}	PLLA	10	Iodine	5	250
PLLA _{10I₂}	PLLA	10	Iodine	10	250
PLLA _{20I₂} *	PLLA	10	Iodine	20	200
PLLA _{10BaSO₄}	PLLA	10	BaSO ₄	10	250
PLLA _{10TIBA}	PLLA	10	TIBA	10	250
PLCL	PLCL	12.5	–	–	250
PLCL _{10BaSO₄}	PLCL	12.5	BaSO ₄	10	250
PLLA _{20BaSO₄} *	PLCL	12.5	BaSO ₄	20	200
PLCL _{20TIBA} *	PLCL	12.5	TIBA	20	200

solution in chloroform. The printer's y axis was substituted by introducing a rotating mandrel of variable diameter, thus allowing to print cylindrical monolayer structures.

Stents were designed with a structure composed of rhombic cells using Computer-Aided Design (CAD) programme Fusion 360™ (Autodesk, USA). Design parameters were stent length (l), stent diameter (d), strut thickness (s_t), number of peaks (n_p) and number of revolutions (n_r). The parameters n_p and n_r determine mesh density, therefore influencing mechanical properties.

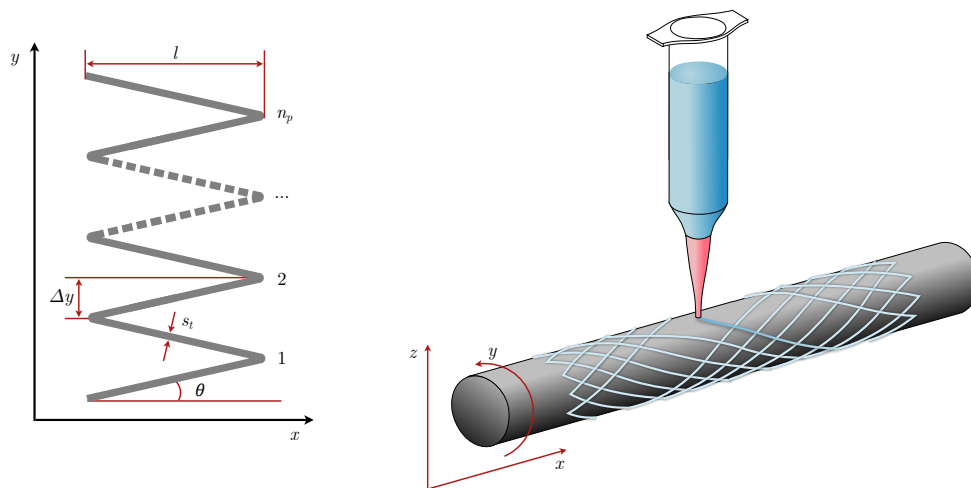


Fig. 3.1 Design scheme of a stent with n_p peaks and printing setup. The design in the plane xy was printed as a monolayer onto the rotating cylinder's surface.

Figure 3.1 shows the design scheme of a stent with n_p peaks. The xy plane represents the unfolded cylinder surface, where the x axis corresponds to the longitudinal axis and the y axis unfolds in the rotation direction. Δy stands for the advance in the y axis for

a single trajectory in the x axis with length l , and can be calculated from the number of peaks, the number of revolutions and the stent diameter as

$$\Delta y = n_r \pi d + \frac{\pi d}{2n_p} \quad (3.1)$$

where the first term accounts for the number of revolutions of the rotating cylinder for a single trajectory in the x axis, parametrized by n_r , and the second one for the incremental distance due to the number of peaks, parametrized by n_p . The angle θ can be calculated as

$$\theta = \arctan\left(\frac{\Delta y}{l}\right) \quad (3.2)$$

Stent length was set to 30 mm, n_r was set to 1, stent diameter was determined by the mandrel diameter (3 or 5 mm) and stents were printed with 5, 7, 10, 15 and 20 peaks (labeled as 5p, 7p, 10p, 15p and 20p, respectively). Alternative geometries with varying n_r and n_p values were also obtained. Stents were printed at a velocity of 4 mm/s. Radiopaque stents were fabricated with a fixed design of $n_r = 1$, $n_p = 10$ and 3 mm in diameter. Stents underwent a thermal treatment (TT) after production at 80 °C for 12 hours, thus ensuring complete chloroform evaporation [37].

3.2.4 Stents characterization

Microscopy

Stents were visually examined under optical microscopes Olympus SZX16 and BX51 (Olympus, Japan) and strut thickness was measured using AnalySIS Docu (Olympus, Japan). Results in strut thickness are given as mean \pm standard deviation. PLLA stents were coated with platinum-palladium (80:20) and examined under SEM (JEOL JSM-7001F, Jeol, Japan) at 2 kV acceleration voltage. Radiopaque stents were coated with carbon and examined using Phenom XL (PhenomWorld, USA) at an operating voltage between 5 and 15 kV.

Differential scanning calorimetry (DSC)

PLLA pellets and stents with and without TT were analyzed by means of a DSC assay (DSC2920, TA instruments, USA). Under a controlled nitrogen atmosphere, samples were heated from room temperature to 250 °C at a rate of 10 °C/min, and maintained at the final temperature for 1 minute. From the obtained heat scans, by measuring the

area of the melting peak and crystallization peak (if present), one can calculate the crystallinity as

$$\chi_c(\%) = \frac{\Delta H_m + \Delta H_c}{\Delta H_m^0 \times X_{\text{PLLA}}} \times 100 \quad (3.3)$$

where χ_c is the percentage of the polymer in crystalline form, ΔH_m is the fusion enthalpy of the polymer, ΔH_c is its crystallization enthalpy, X_{PLLA} is the fraction of PLLA in the sample (in mass) and ΔH_m^0 is the theoretical fusion enthalpy of a 100% crystalline PLLA sample, namely 93 J/g [40]. For PLCL stents, crystallinity was calculated with the assumption that lactide units were the only ones to crystallize [7].

Mechanical tests

Radial strength of printed stents was assessed by means of a compression resistance parallel plate test performed with a rheometer (Discovery HR-2, TA instruments, USA). Stents with 3 mm in diameter and $n_p = 5, 7, 10, 15$ and 20 were tested, before and after undergoing thermal treatment. Stents were compressed up to 50% reduction in diameter between two flat plates, with the upper plate advancing towards the lower one at 1 mm/min, according to ISO 25539-2 [41]. Radial force was measured and normalized by the respective stent length and given in N/mm. Stent elastic recovery was calculated as the ratio between final and initial diameter, in percentage.

Stents were crimped onto a balloon with 3 mm in nominal diameter (MSI HH100/200, Machine Solutions Inc., USA) and deployed into a silicone tube with 3.17 mm in diameter, which corresponds to the average diameter of the aortic artery [42]. Stents' expansion behaviour and average breaking pressure were evaluated using mounted stents onto a balloon filled with blue-stained water, in order to facilitate the visualization of broken struts. The balloon was inflated at a rate of 1 atm per 20 s up to 16 atm, which corresponded to the balloon's rated burst pressure (RBP). The pressure at which strut fracture or detachment became visible was noted.

Ex vivo flow setup to evaluate thrombogenicity

To evaluate stent thrombosis with donors' human blood a modified Chandler loop was used, where motor-controlled rotors accelerate blood-filled silicone loops generating pulsatile flow simulating coronary-like hemodynamics (peak flow, 200 mL/min) at 37 °C [43, 44]. To model wall injury, loop segments were made reactive through a 24-hour incubation with 10% bovine type I collagen solution (Beckton Dickinson, USA) and subsequently rinsed with PBS, pH 7.4. The reactive site was composed of three concentric silicone tubes of 3.17 mm, 6.37 mm, and 9.52 mm to generate higher pressure at the place where the stent was deployed (Figure 3.S1). The non-reactive part of the loop was loaded with a solution of 2.5% (w/v) bovine serum albumin (Beckton

Dickinson, USA) 1-hour prior to the assay and subsequently rinsed with PBS. 3D printed PLLA stents (labeled as PLLA, printed with 250 μm diameter nozzle, and PLLA^{*}, printed with 200 μm diameter nozzle), and a commercial polymeric stent Absorb GT1 stent (Abbott Vascular, USA) were crimped into a 3.0 mm diameter balloon (Abbott Vascular, USA) and balloon expanded up to 16 atm into the reactive segments. Blood was collected from two human healthy donors in 10% acid-citrate-dextrose solution (85 mM trisodium citrate, 69 mM citric acid, 111 mM glucose; pH 4.6). Before use, blood was replenished with a 100 mM CaCl₂/75 mM MgCl₂ solution with 62.5 μL calcium/magnesium solution per 1 mL blood. Loops were filled, rotor mounted, and run for 4 minutes to allow in-stent thrombus formation. Free blood was emptied, and reactive segments were isolated and flushed with 120 mL Tyrode solution supplemented with HEPES buffer and magnesium (0.01 mol/L HEPES, 0.75 mM MgCl₂). After visual assessment, stented segments were excised and filled with 1% Triton-X solution for 20 minutes. Equivolume lysates were collected and lactate dehydrogenase (LDH) and hemoglobin (HEM) levels were determined to provide a quantitative measure of total cell/red-cell reflecting thrombogenicity (Cyto-Tox 96 Non-Radioactive Cytotoxicity Assay, Promega Corp; Hemoglobin Colorimetric Detection Kit, Invitrogen, USA) [43, 44].

Micro-computed tomography imaging

Stents were scanned in a micro-CT scanner (Skyscan 1272, Bruker, USA). Scans were taken with the following parameters: X-ray tube voltage of 65 kV; anode current of 153 mA; 1 mm Al filter; spatial resolution of pixel size 13 μm ; 0.6° rotation step over 180° and scan average $n = 3$. The reconstruction software NRecon (Skyscan, version 1.7.0.4) was used to transform raw micro-CT data into tomographic images in 3D in 8-bit BMP format, with grey level ranging from 0 to 255. Subsequent analysis was performed using CTAn software (Skyscan, version 1.16.9) by segmentation and thresholding to differentiate the sample from the background. Radiopacity was expressed as X-Ray attenuation in Hounsfield Units (HU), calculated as the average HU value for each voxel within the sample. HU values were calibrated against a water sample.

Degradation analysis

Among all printed stents, 5 of them were selected to undergo a degradation test: PLLA₁₁₂, PLLA₅₁₂, PLLA₁₀₁₂, PLLA_{10TIBA} and PLLA_{10BaSO₄}. Stents were placed in 20 mL of PBS, and were incubated at 37 °C for 3 months. Afterwards, stents were air dried and stored in a desiccator until further analysis. Radial strength and stents' radiopacity was measured and compared to non-degraded stents.

Cytotoxicity test

The effect of the thermal treatment on PLLA stents was evaluated by means of an indirect cytotoxicity assay following ISO 10993-5 and ISO 10993-12 [45, 46] via lactate dehydrogenase (LDH) quantification (Cytotoxicity Detection Kit PLUS, Roche Diagnostic

GmbH, Germany). Radiopaque stents' cytotoxicity was assessed via colorimetric Presto Blue (PB) assay (PrestoBlue HS Cell Viability, Invitrogen, Life Technologies). Stents were UV-sterilized, HUVECs were purchased at PromoCell (Germany) and all the experiments were conducted at passages 8 to 10. To calculate cell viability, LDH quantification was performed on a MicroPlate Reader (Synergy HTX multi-mode microplate reader, BioTek Instruments, USA) in absorbance mode, whereas PB was quantified in fluorescence mode.

3.2.5 Statistical analysis

Each assay condition was tested in triplicate unless stated otherwise and all data are represented as mean values \pm standard deviation (SD). Non-parametric Mann-Whitney U-test were used to determine statistically significant differences (p -value $<$ 0.05 between the different groups) and 95% confidence interval (95% CI). Statistical analysis was performed using Minitab software (Minitab Inc., USA).

3.3 Results

3.3.1 PLLA ink preparation and characterization

PLLA dissolution in chloroform rendered a transparent, gel-like ink with high viscosity, which was further characterized by means of capillary flow analysis (Figure 3.2). The value for n was determined as the slope of the log-log plot of τ_w versus $\dot{\gamma}_{New}$, and found to be 0.2991, as shown in Figure 3.2a. The coefficient of determination (R) was very close to 1, therefore ensuring the suitability of the Rabinowitch-Mooney correction in order to account for Non-Newtonian effects [38]. Figures 3.2b and 3.2c present shear stress and viscosity versus shear rate, respectively. A shear-thinning behaviour can be observed in the investigated range of printing speeds, as the viscosity decreases for increasing shear rate (Figure 3.2d).

3.3.2 PLLA stents production and characterization

Stents were successfully manufactured onto a rotating cylinder with varying n_r and n_p values, as shown in Figure 3.3. Mean strut thickness was found to be $131 \pm 9 \mu\text{m}$ among 3-mm in diameter stents. Struts' area coverage ranged from 16% for 5p stents up to 57% for 20p samples, as shown in Figure 3.S2a.

SEM allowed for stents' surface analysis, showing that printed filaments were not completely cylindrical. Filaments were deposited onto the mandrel as solvent evaporation occurred, and therefore they presented a flattened contact face as an unavoidable

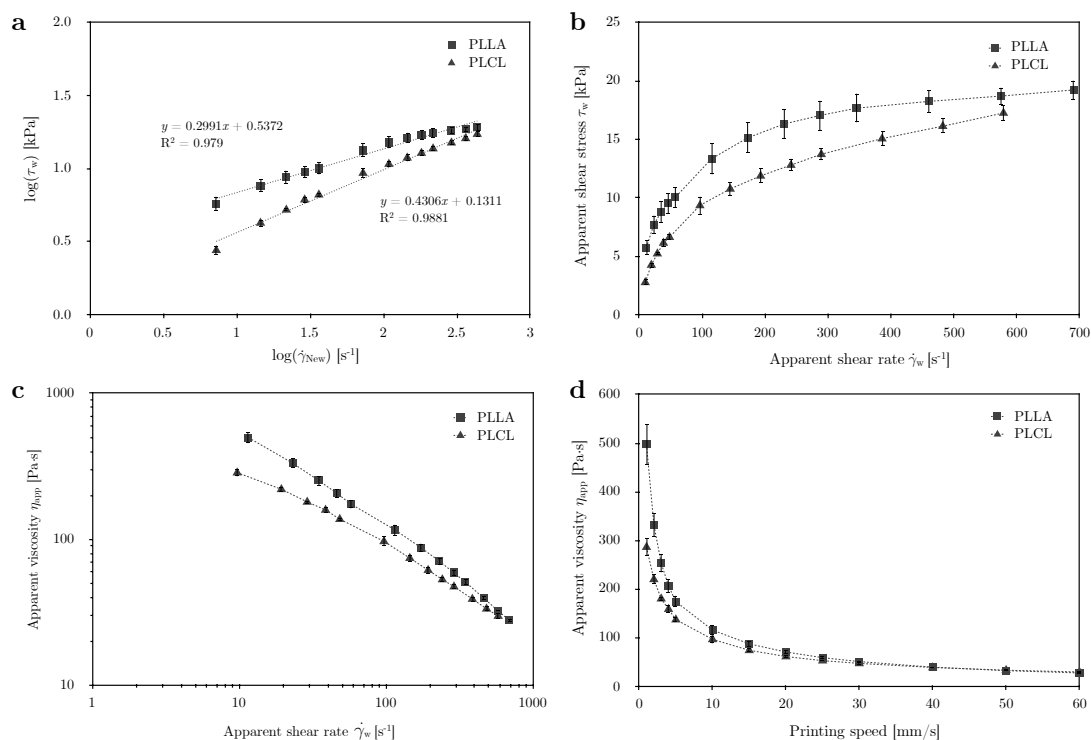


Fig. 3.2 Rheological curves for PLLA and PLCL inks. (a) Log-log plot of the process-related shear stress (τ_w) versus the Newtonian shear rate ($\dot{\gamma}_{New}$). (b) Process-related shear stress (τ_w) versus the process-related shear rate ($\dot{\gamma}_w$). (c) Process-related apparent viscosity (η_{app}) plotted as a function of the process-related shear rate ($\dot{\gamma}_w$). (d) Process-related apparent viscosity (η_{app}) as a function of printing speed.

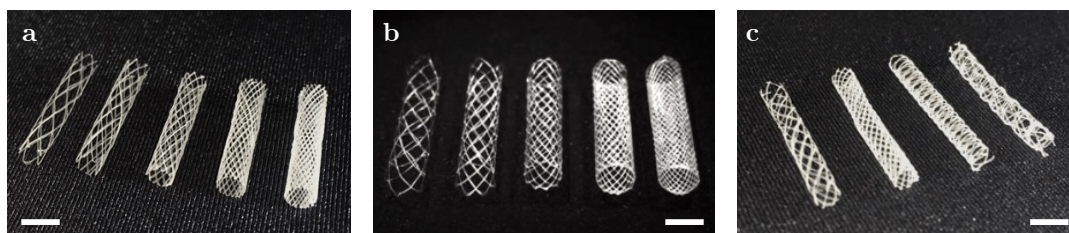


Fig. 3.3 3D-printed PLLA stents. (a) Stents with 3 mm in diameter. From left to right, with $n_p = 5, 7, 10, 15$ and 20 . (b) Stents with 5 mm in diameter. From left to right, with $n_p = 5, 7, 10, 15$ and 20 . (c) Other stent geometries achievable with the experimental setup, with different n_r and n_p values. Scale bar corresponds to 5 mm.

characteristic of the SC-DW fabrication method. Junctions between two overlapping filaments were welded as shown in Figure 3.4a and Figure 3.4b, thus ensuring a strong union through extensive contact surface. In contrast to the inner flattened face, stents' outer face presented micropores due to fast solvent evaporation after PLLA filament extrusion (Figure 3.4c). A cross-section cut showed no inner porosity (Figure 3.4d). Chloroform evaporation resulted in material retraction and surface micropore formation as an inherent feature of the fabrication process. No relevant morphological differences were found when comparing stents before and after thermal treatment, as micropore size and orientation were found to be unaltered.

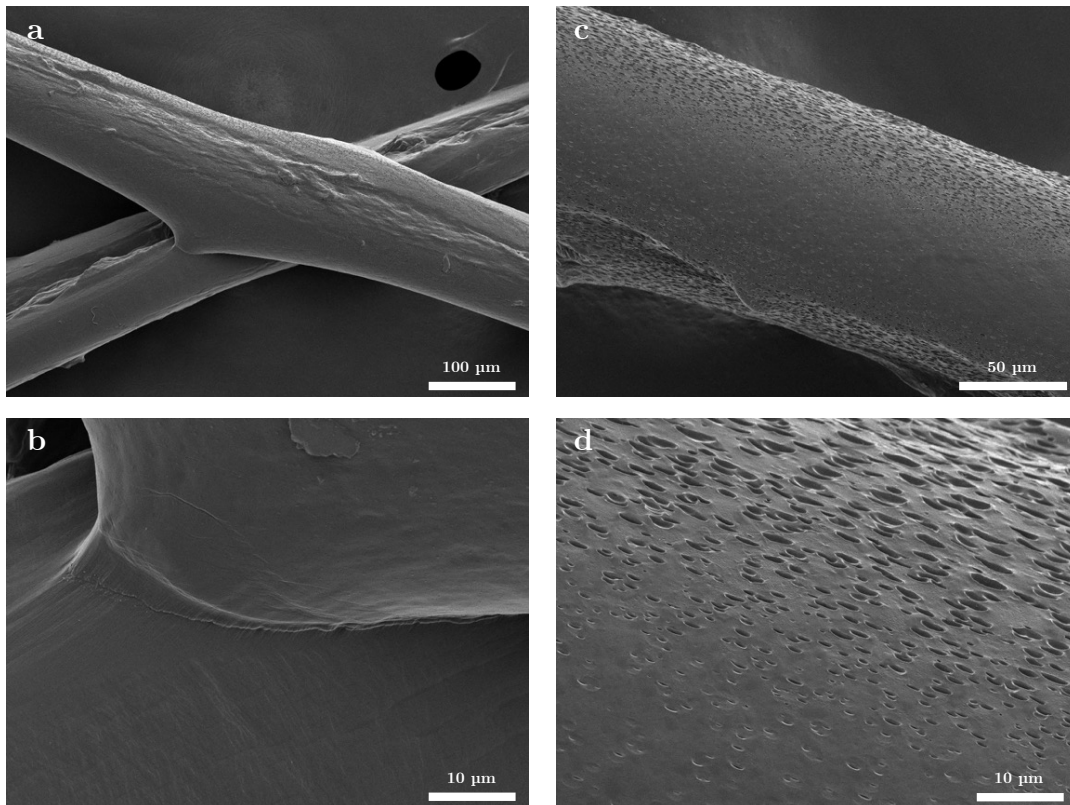


Fig. 3.4 (a) PLLA stent SEM image of the junction between filaments and (b) detail of weld line. (c) Stent SEM images of the micropores distribution and (d) stent cross-section.

Stents crystallinity percentage was evaluated by means of DSC (Figure 3.S3). PLLA pellets were analyzed as received and found to present a crystallinity of $56.0\% \pm 5.2\%$. As expected, a considerable percentage of crystallinity was lost during the conformation process, down to $21.2\% \pm 1.0\%$ for as-printed stents. Subsequent thermal treatment resulted in a slight crystallinity increase, up to $27.3\% \pm 1.6\%$.

Compression tests performed with 3-mm in diameter stents showed a clear difference in mechanical properties among stents (Figure 3.5a). For each stent condition, there was a significant increase in resistance to compression force for thermally-treated stents compared to non-treated ones. Moreover, the force needed to compress stents increased with the mesh density, ranging from 0.02 N/mm for thermally-treated stents with $n_p = 5$ up to 0.16 N/mm for thermally-treated stents with $n_p = 20$. Using initial and final diameter, elastic recovery was computed, and found to be around 90% for untreated stents, and around 95% for treated ones, as shown in Figure 3.5b. No significant trend was found as the mesh density increased. Stents deployment into silicone tubes showed a good attachment to the inner part of the mock vessel. From $n_p = 5$ to $n_p = 20$, upon balloon deflation and removal, deployed stents remained attached inside the tube and showed no sign of collapse. Expansion assays showed that stents were able to sustain up to 16 atm (RBP) without any signs of strut breakage (Figure 3.S4).

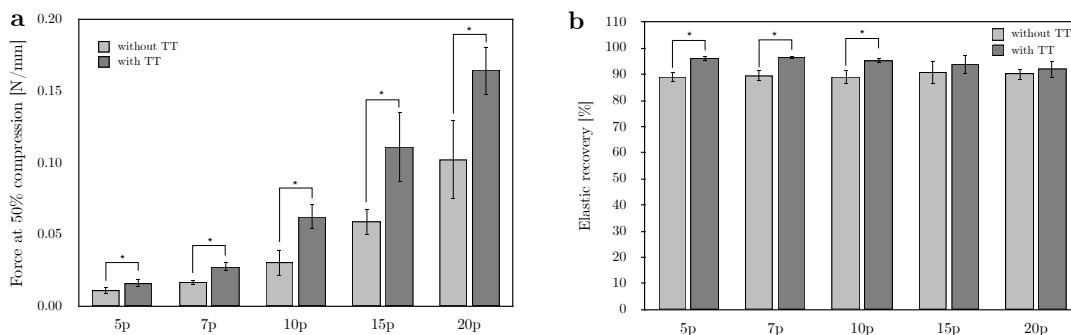


Fig. 3.5 (a) Compression force at 50% deformation for PLLA stents with increasing mesh density, before and after TT. (b) Elastic recovery shown by stents. Statistically significant differences among conditions are shown with an asterisk ($p < 0.05$).

The indirect cytotoxicity test revealed that printed PLLA stents were not cytotoxic for HUVECs. On the one hand, non thermally-treated stents presented a living cell percentage of around 90% for all dilutions, as shown in Figure 3.S5. On the other hand, thermally-treated stents exhibited percentages close to or above 100%, therefore indicating that cell growth was similar using complete medium or with pure extract. Considering that the standard indicates that a sample is considered to be toxic for living cell percentages lower than 70% [45], these results manifest the non-toxicity behaviour of PLLA SC-DW stents.

The thrombogenicity of printed stents was evaluated using an *ex vivo* flow setup. Tested PLLA stents presented a mean strut thickness of $131 \pm 9 \mu\text{m}$, whereas PLLA* showed $83 \pm 12 \mu\text{m}$. In Figure 3.6a, the analysis of LDH/HEM for each donor's blood was done to find the relationship between the total amount of adhered cells and the amount of red blood cells involved in clotting processes. Visual differences were observed between the different stents, observing higher red blood cells attachment for PLLA and the commercial stent compared to PLLA* (Figure 3.6b). The LDH/HEM ratio quantifies the total number of cells (LDH) vs. the total hemoglobin (HEM) which is directly related to the number of red blood cells involved in the coagulation process. A lower value of LDH/HEM indicates that the proportion of red blood cells to the total number of cell is high and thus, a higher thrombogenicity. Stents with thinner struts were less prone to thrombogenicity, whereas thicker strut stents and the commercial stent showed higher thrombogenicity. Differences among conditions were statistically significant. The LDH/HEM ratio showed similar tendencies independently of the tested patient blood.

3.3.3 Radiopaque stents production and characterization

Mixing of PLLA pellets, chloroform and radiopaque agent resulted in homogeneous inks with the proper rheological properties. Iodine-containing inks presented a pink color, which increased in intensity with increasing iodine concentration. On the other hand, TIBA-containing inks were pearl white, whereas BaSO₄-containing inks were

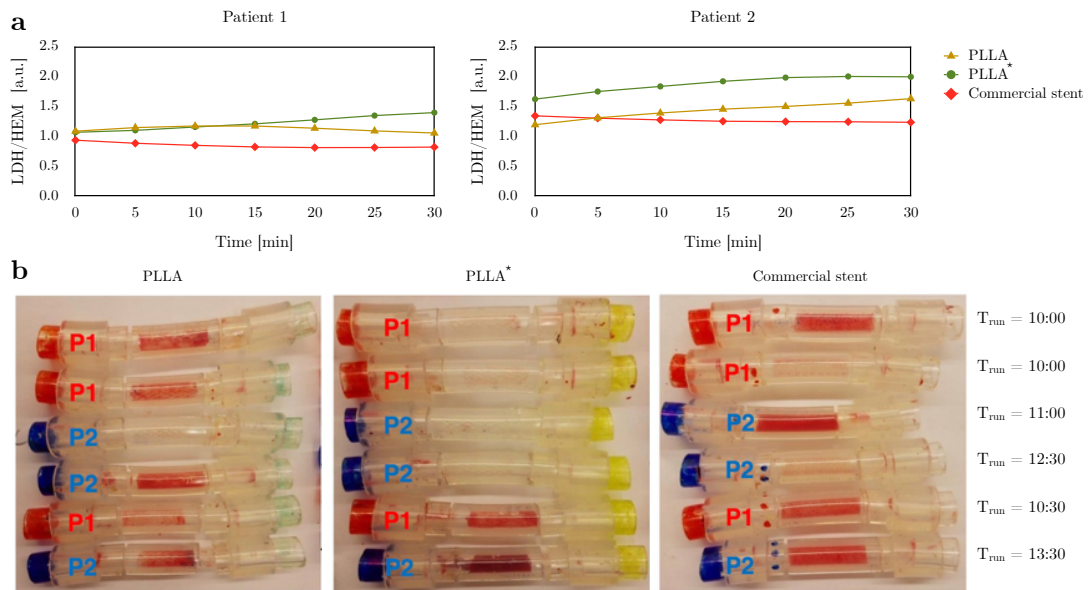


Fig. 3.6 Thrombogenicity results of 3D printed PLLA stents with different strut thickness and a commercial polymeric stent. (a) Average quantification of the total cells/red cells ratio. (b) Images of the clotting process after a certain period of time (min) for both blood donors (P1 and P2).

chalk-white, with no visual agglomerates after sonication. $BaSO_4$ size distribution was found to be from 0.75 to 2 μm , with a mean particle size of 1.5 μm . For PLCL-based inks, a higher polymer to solvent ratio was needed in order to match the viscosity shown by the PLLA ink. Figure 3.2 shows the rheological characterization of PLCL ink. When compared to PLLA ink, a very similar shear-thinning behaviour can be observed, although displaying reduced viscosity.

Radiopaque bioresorbable stents were satisfactorily fabricated through SC-DW. Figure 3.7 shows three pictures of the 3D printing process for (a) a iodine-containing PLLA stent, (b) a $BaSO_4$ -containing PLCL stent and (c) a TIBA-containing PLCL stent.

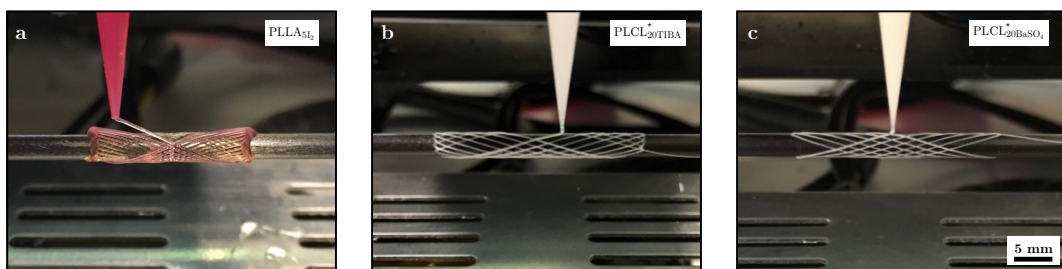


Fig. 3.7 3D printing of a radiopaque stent with (a) iodine, (b) $BaSO_4$ and (c) TIBA. (a) was printed with a 250 μm diameter nozzle, whereas for (b) and (c) a 200 μm diameter nozzle was used.

An overview of all printed conditions can be seen in Figure 3.S6. Iodine-containing stents showed a brownish color as the chloroform evaporated. Subsequent thermal

treatment resulted in a significant color change. Stents with TIBA and BaSO₄ showed no change in color after undergoing TT.

Strut thickness for radiopaque stents resulted in an increase with respect to PLLA stents. The addition of iodine, TIBA or BaSO₄ led to thicker struts, around 200 μm. The effect was especially manifest for the case of PLLA_{10I₂}, with up to 250 μm. The use of a 200 μm diameter nozzle instead of the one with 250 μm allowed for a significant reduction in strut thickness, with 124.6 μm for PLLA_{20I₂}^{*}, 178.1 μm for PLCL_{20BaSO₄}^{*} and 161.3 μm for PLCL_{20TIBA}^{*}, as shown in Table 3.2.

Tab. 3.2 Stents' strut thickness and crystallinity.

Stent	Strut thickness [μm]	Crystallinity [%]
PLLA	132.2 ± 7.1	27.3 ± 1.6
PLLA _{1I₂}	205.3 ± 15.2	24.0 ± 1.4
PLLA _{5I₂}	212.6 ± 10.3	25.2 ± 4.4
PLLA _{10I₂}	245.3 ± 14.1	35.3 ± 4.3
PLLA _{20I₂} [*]	124.6 ± 5.0	45.3 ± 9.4
PLLA _{10BaSO₄}	208.0 ± 4.1	26.7 ± 1.3
PLLA _{10TIBA}	215.2 ± 5.6	31.0 ± 3.3
PLCL	134.0 ± 5.3	21.2 ± 0.8
PLCL _{10BaSO₄}	200.8 ± 20.0	22.1 ± 0.6
PLCL _{20BaSO₄} [*]	178.1 ± 3.1	21.5 ± 0.7
PLCL _{20TIBA} [*]	161.3 ± 6.6	26.7 ± 1.4

Stents were further characterized with SEM. Iodine-containing stents presented a slightly wave-like surface, as one can see in Figure 3.8. Stents with BaSO₄ showed a homogeneous dispersion of microparticles throughout the filaments and TIBA-containing stents displayed formation of TIBA crystals following the printing direction subsequent to chloroform evaporation. Among all printed radiopaque stents, only PLLA_{20I₂}^{*} became brittle and showed numerous fractured struts after undergoing TT.

DSC analysis showed that the highest crystallinity was found for PLLA_{20I₂}^{*} samples, up to 45.3% (Table 3.2 and Figure 3.S3). PLLA_{10BaSO₄} stents presented the same crystallinity as bare PLLA stents, around 27%, whereas PLLA_{10TIBA} showed a higher crystallinity, around 31%. For PLCL-based stents, the addition of 10 wt.% or 20 wt.% BaSO₄ resulted in no change in crystallinity. Finally, as for the PLLA case, PLCL_{20TIBA}^{*} exhibited a remarkable higher crystallinity with respect to BaSO₄ addition.

Mechanical properties of radiopaque stents were evaluated by means of compression and expansion tests. Figure 3.9a presents the force-strain curves for all printed stents. PLLA, PLLA_{1I₂}, PLLA_{5I₂} and PLLA_{10TIBA} showed a resistance to 50% compression in diameter between 1.5 and 2 N; PLLA_{10BaSO₄}, PLCL and PLCL_{10BaSO₄} between 2 and 2.5 N; PLLA_{10I₂} above 3 N and PLLA_{20I₂}^{*}, PLCL_{20BaSO₄}^{*} and PLCL_{20TIBA}^{*}, below 1 N. The latter 3 conditions were printed with a lower diameter nozzle (200 μm instead of 250 μm). Besides, PLLA_{10TIBA} and PLLA_{10BaSO₄} showed a discontinuous profile, and the

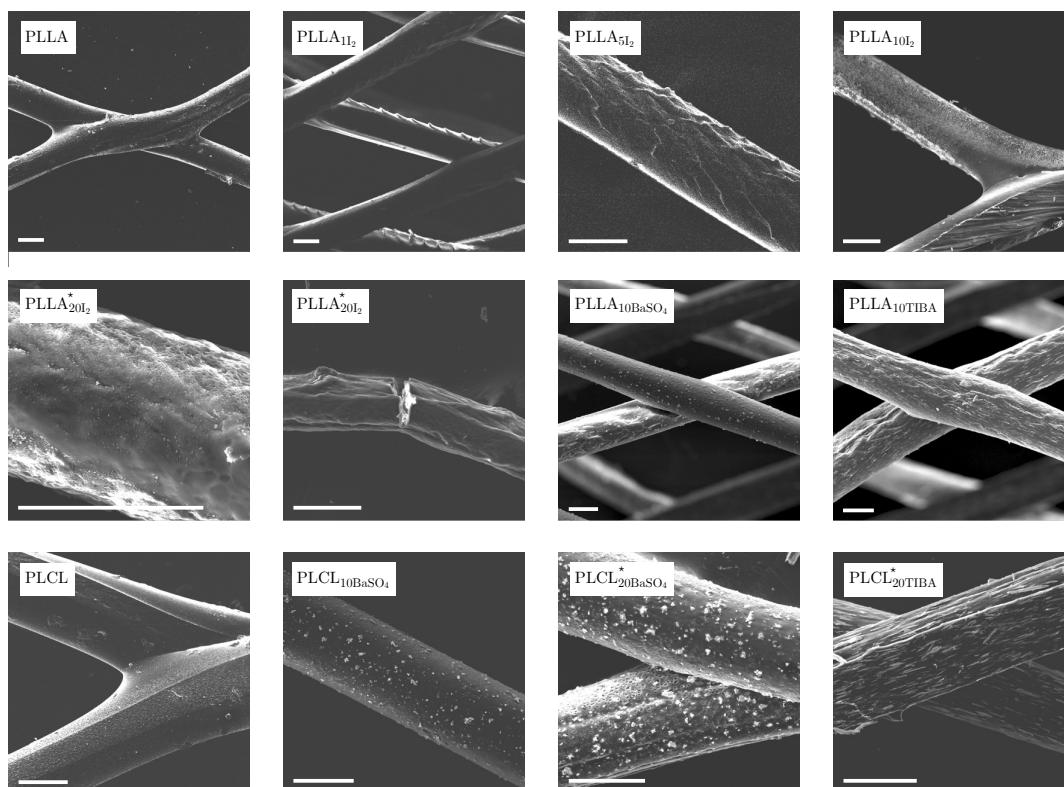


Fig. 3.8 SEM images of printed stents. Iodine-containing stents present wave-like surface, with PLLA^{*}_{20I₂} becoming brittle after thermal treatment. Stents with BaSO₄ show dispersion of microparticles and TIBA-containing stents show TIBA crystals in the printing direction. Scale bar corresponds to 100 μ m.

latter presented the highest resistance to compression at low deformation. Figure 3.9b displays the normalized force at 50% diameter compression (left axis) as well as the computed elastic recovery (right axis). Clearly, stents printed with the smaller diameter nozzle resulted in poorer resistance to compression, whereas it increased with the addition of a radiopaque agent. Elastic recovery was very similar for all cases and found to be around or above 95%. Regarding expansion assays, deployment of radiopaque stents into silicone tubes displayed close attachment to the inner part of the tube. Both PLLA- and PLCL-based radiopaque stents remained attached upon balloon removal, except from PLLA^{*}_{20I₂}, which cracked as pressure increased. Unrestricted expansion assays revealed issues for some conditions. PLLA_{1I₂}, PLLA_{10BaSO₄} and PLLA_{10TIBA} stents displayed strut detachment at certain junctions upon balloon inflation. All other conditions showed that stents were able to sustain at least 16 atm (RBP) without strut breakage (Figure 3.S7).

Stents were micro-CT scanned in order to evaluate their radiopacity. Figure 3.10a presents the resulting reconstruction for all stents. Qualitatively, iodine-containing stents do not seem to appear more highlighted than PLLA or PLCL control stents. On the other hand, there are clear differences among the others, being BaSO₄- and TIBA-

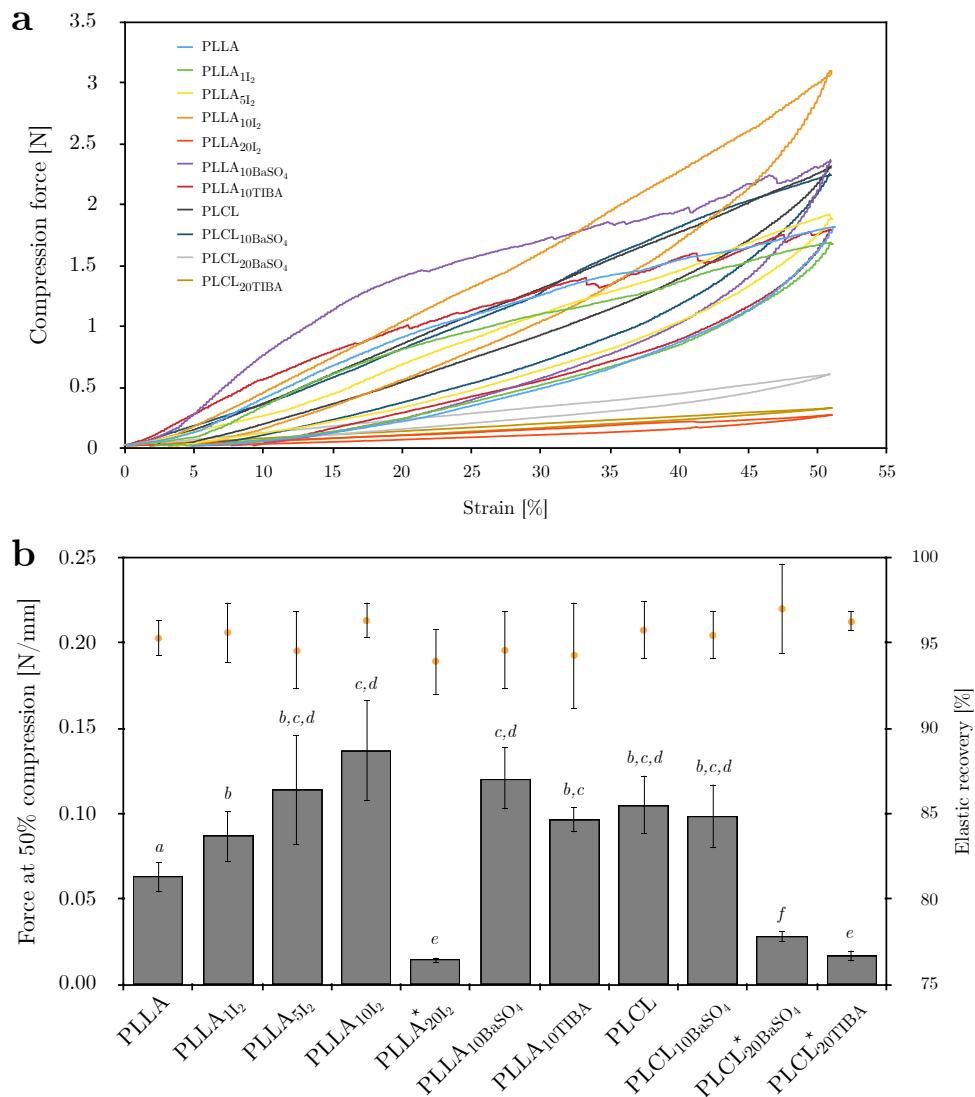


Fig. 3.9 (a) Compression curves for radiopaque stents. Stents were compressed up to 50% reduction in diameter, with crosshead speed set to 1 mm/min, both in loading and unloading. (b) Force at 50% compression (left axis, bars) and elastic recovery (right axis, dots). Conditions *a*, *b*, *c*, *d*, *e* and *f* are statistically different ($p < 0.05$).

containing stents the ones with a better visibility. These differences are quantified in Figure 3.10b, where X-ray attenuation for each stent is shown in HU values. TIBA appears as the most radiopaque agent, with about 2000 HU for PLLA₁₀TIBA and around 3000 HU for PLCL₂₀TIBA when doubling its content. BaSO₄ also renders significant radiopacity, around 1600 HU for PLLA₁₀BaSO₄ and PLCL₁₀BaSO₄, and up to 2500 HU for PLCL₂₀BaSO₄. Finally, iodine-containing stents show no change in X-Ray attenuation with respect to PLLA or PLCL stents, with -250 HU.

Incubated stents in PBS for 3 months at 37 °C were further characterized by means of a compression test and a micro-CT scan. Figure 3.11a shows the normalized force at 50% compression. In general, no change in mechanical properties was found after 3

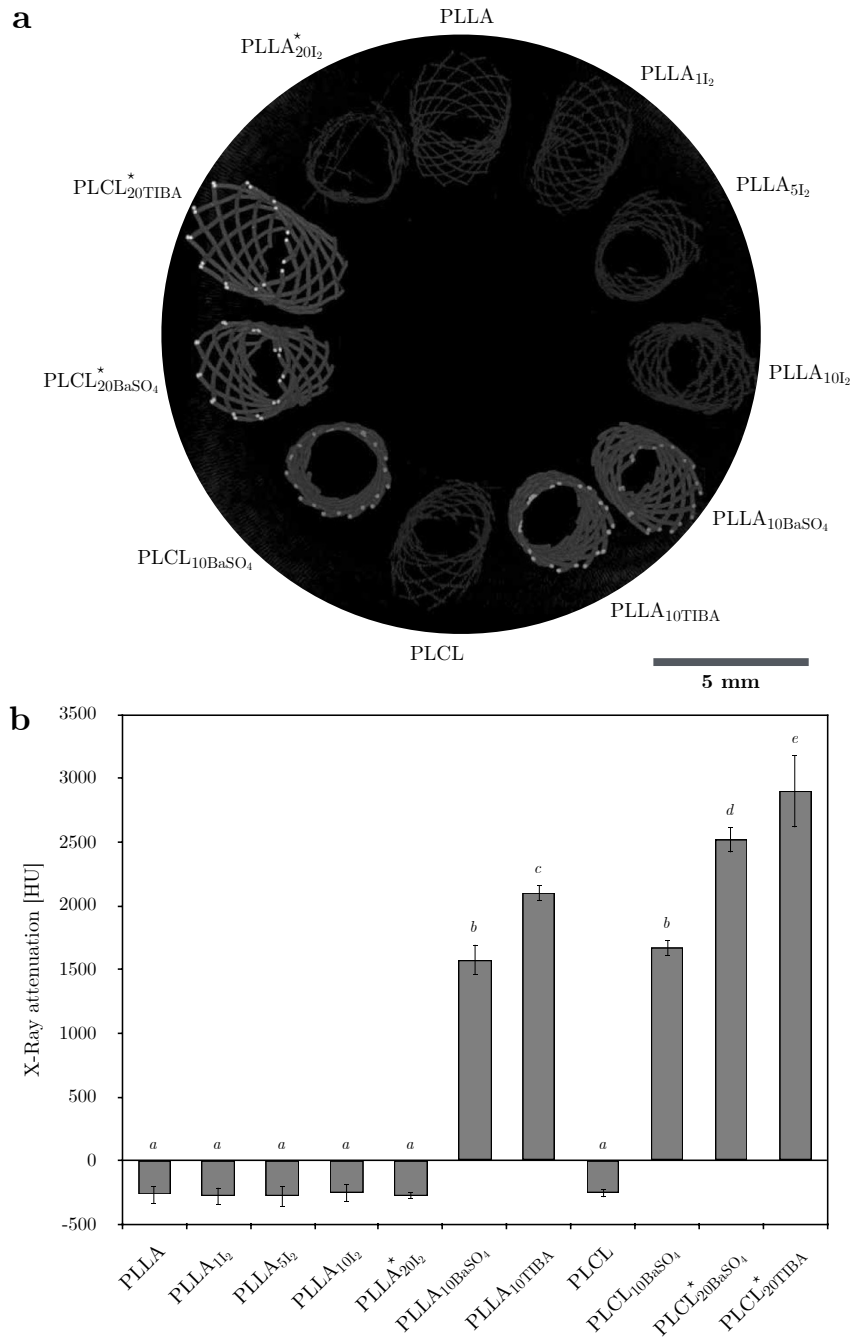


Fig. 3.10 (a) Stents' reconstruction after microCT scan, being white more radiopaque. (b) X-Ray attenuation values for radiopaque stents. Conditions *a*, *b*, *c*, *d* and *e* are statistically different ($p < 0.05$).

months incubation, except for PLLA_{10TIBA}, showing a decrease from 0.096 N/mm to 0.65 N/mm. Regarding elastic recovery, values ranged from 92% for PLLA_{10TIBA} to 96% for PLLA_{5I₂} and PLLA_{10BaSO₄}. No statistically significant differences were found with respect to the elastic recovery shown by non-incubated stents. Analysis of microCT scans demonstrated no significant change in X-ray attenuation compared to non-incubated stents, as shown in Figure 3.11b. Iodine-containing stents kept around -250 HU,

whereas PLLA₁₀BaSO₄ and PLLA₁₀TIBA showed similar X-Ray attenuation values with respect to non-incubated stents.

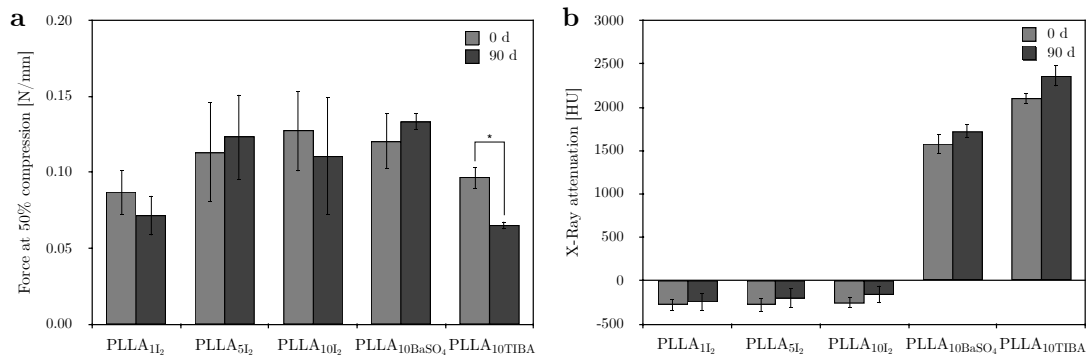


Fig. 3.11 (a) Force at 50% compression of fresh and incubated stents and (b) X-Ray attenuation values of fresh and incubated stents. Statistically significant differences among conditions are shown with an asterisk ($p < 0.05$).

Cytotoxicity of 3D-printed radiopaque stents was evaluated via an indirect cytotoxicity assay (Figure 3.12). On the one hand, cell viability resulted above 70% for iodine-containing stents, as well as for stents printed with BaSO₄, which showed cell viability to be around 80%, for all dilutions. On the other hand, cell viability decreased to around 40% for TIBA-containing stents with pure extract. The effect of the dilutions (1/2 and 1/10) resulted in cell viability close to 100% for PLLA₁₀TIBA and around 70% for PLCL₂₀TIBA.

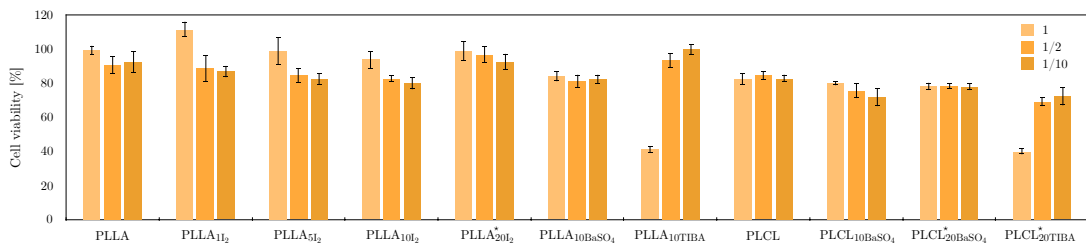


Fig. 3.12 Cell viability test performed on printed stents for pure extract and dilutions 1/2 and 1/10.

3.4 Discussion

The use of biodegradable polymers as a suitable material for cardiovascular stents has been a recurring idea in the treatment of coronary heart disease. Major advances in this technology have been achieved in the last decade, but still more research is needed to overcome some of the limitations shown by BRS. Here we present a versatile approach for BRS fabrication which circumvents the need of high temperatures, associated to FDM processes as previously shown in the literature [32–35]. SC-DW represents a step forward as it allows for a broad versatility with regards to ink composition and patient-specific customization, both in terms of stent design and functionalization.

PLLA dissolution in chloroform resulted in a viscous, printable polymeric solution. At a printing speed of 4 mm/s, the apparent viscosity has been calculated to be 207 Pa·s. In comparison to other printable ink studies, the extrusion applied pressure range is slightly lower, but the overall rheology of our chloroform-based ink is similar to the one reported in [47], which was based on dichloromethane.

Strut coverage area was measured for 3-mm in diameter stents, showing a range from 16% for 5p stents up to 57% for 20p samples. In comparison to commercial stents, the Absorb presents a surface area coverage of 27% at rated burst pressure, which decreases to 22% for the Magnitude stent [48]. Regarding strut thickness, it was measured to be around 130 μm , which is lower than the strut thickness presented by the Absorb, DESolve, Fortitude, Acute, Magmaris, Xinsorb, Art Pure, Ideal or ReZolve stents, all of them equal or greater than 150 μm [49]. The current tendency is to shift towards thinner struts in order to minimize blood turbulence which may lead to thrombotic events. In consequence, more recent designs aim at 125 μm such as the Fantom, or even below 100 μm as the Magnitude or the Falcon [50]. In SC-DW, strut thickness can be further reduced by using thinner micronozzles. The use of a 200 μm diameter nozzle instead of the one with 250 μm allows for a significant reduction in strut thickness for PLLA stents, from 130 μm down to 80 μm . For radiopaque stents, for instance, $\text{PLCL}_{10\text{BaSO}_4}$ presented a strut thickness around 200 μm , whereas when using a 200 μm diameter nozzle instead, strut thickness was reduced to 175 μm for $\text{PLCL}_{20\text{BaSO}_4}^*$.

DSC analysis of as-printed stents showed crystallinity percentage to be around 24%. Posterior thermal treatment above PLLA's glass-transition temperature induced higher crystallinity, close to 30%. Other fabrication techniques such as FDM also render polymeric parts with a low degree of crystallinity, below 5% [51, 52]. Crystallinity constitutes a key factor in semicrystalline materials such as PLLA, as it is closely correlated to its mechanical performance. Therefore, subsequent annealing processes are widely applied in order to increase the fraction of ordered phase, which in turn impacts the mechanical properties and the biodegradation kinetics [52–55].

As for the mechanical properties, compression tests with printed stents showed the importance of performing a thermal treatment after fabrication in order to increase by about 70% the resistance to compression at 50% deformation. As expected, mesh density also influenced resistance to compression, as the increase in n_p correlated with higher resistance, up to 0.16 N/mm for thermally-treated stents with $n_p = 20$. Figure 3.S2b shows the correlation between resistance to compression at 50% deformation with area coverage. Lee *et al.* [33] performed a parallel plate compression test on the Absorb BVS at a velocity of 10 mm/min, obtaining a radial force of 2.14 ± 0.03 N at 50% diameter reduction. In comparison, 10p stents presented a radial force of 1.25 ± 0.16 N, 15p of 2.19 ± 0.41 N and 20p of 3.26 ± 0.36 N. Although the test parameters were not exactly the same, these results show that the mechanical properties of SC-DW

15p and 20p stents are similar or superior to those shown by a commercial polymeric stent such as the Absorb BVS.

Regarding elastic recovery rate, the effect of TT is clearly seen, as it increases from 90% up to 95%. Therefore, thermally-treated stents are able to maintain the greatest part of their initial shape after being compressed up to 50% deformation with respect to their original diameter. These results are in accordance with the analysis carried out by Zhao *et al.* in [56], where poly(p-dioxanone) braided stents were tested. Elastic recovery rate was found to be between 86% and 92%, and increased after performing an annealing treatment. Long-term elastic recovery may be studied under cyclic loading assays [57]. Stent's elasticity is a key factor in stent design, as stents must accompany arteries contraction and expansion in order to keep blood flowing [58]. As for the expansion tests, deployment of stents resulted in a good attachment to the silicone artery and showed no signs of collapse. Regardless of the number of peaks, stents were able to withstand pressures up to 16 atm with no signs of strut breakage or detachment among struts, which corresponded to a stent inner radius of 3.26 mm.

In vitro indirect cytotoxicity test with HUVECs indicated that PLLA printed stents were not cytotoxic. Although traces of chloroform may have an impact for non-treated stents, results showed a percentage of living cells well above 80%. This percentage is even higher for thermally-treated stents and equal to or greater than 100%. These results demonstrate the feasibility of the SC-DW approach, even using organic solvents such as chloroform.

As expected, strut thickness had an influence on the thrombogenicity response of studied stents: the thicker the struts, the more thrombogenicity was detected on PLLA stents. The amount of material in contact with the bloodstream was a crucial parameter to control and thus, thinner struts were better. Kollandaivelu *et al.* showed that 162 μm -strut DES were 1.5-fold more thrombogenic than otherwise identical stents with 81 μm struts [59]. Moreover, in the same study, thick-strut stents implanted in porcine coronary arteries presented more thrombus and fibrin deposition than thin-strut stents at 3 days after implantation, with approximately 60% more thrombus formation [59]. A finite element analysis study of the effect of different stent strut thickness with ISR demonstrated that thinner strut stent resulted in lower stresses in the vessel wall, which is hypothesized to be responsible for the lower restenosis outcome [60]. Finally, the presence of pores distributed on the outer part of the stent did not show to have an impact on stent thrombosis.

The promising results on PLLA stents regarding mechanical and biological properties, together with the versatility of the SC-DW approach, allowed for its modification to render stents radiopaque, with BaSO_4 as a positive control for radiopacity. By mixing

radiopaque agents into the polymeric solution in chloroform, printable inks with very similar rheological properties to the original ink were obtained.

Thermal treatment for iodine-containing stents resulted in a sharp color change, from brownish to pale white. We attribute this variation to the evaporation of iodine molecules, as physical entrapment between PLLA chains may not be enough to avoid their release in gas form due to sublimation. On the other hand, TIBA and BaSO₄-containing stents showed no visual alteration after undergoing TT.

Optical microscopy analysis showed a substantial increase in strut thickness with respect to PLLA or PLCL stents when adding a radiopaque agent and printed with the same nozzle. This increase may be associated to the physical presence of iodine, TIBA or BaSO₄ microparticles, which hamper the optimal folding for polymeric chains. Strut thickness could be reduced by using a thinner extrusion micronozzle of 200 μm, thus achieving thicknesses comparable to those of commercial stents, as previously discussed. PLLA_{20I₂}^{*} stents' brittleness arose most probably from iodine evaporation, as it accounted for 20 wt.%, which left a fragile structure with thin struts. This effect may be the case as well for other iodine-containing stents, although the higher strut thickness and the lower iodine content might have concealed it. Wave-like surface found for iodine-containing stents is most probably due to extrusion instabilities, as the flux was not as constant as for the original PLLA ink. BaSO₄ microparticles rendered a rough surface, whereas TIBA crystals formed along the printing direction.

Regarding DSC curves analysis, the addition of iodine did not result in a change in crystallinity for 1 or 5 wt.% iodine, but higher iodine contents resulted in a crystallinity increase, especially for PLLA_{20I₂}^{*}. Crystallinity was also higher for PLLA_{10TIBA} than for PLLA_{10BaSO₄}, possibly due to the physical constraints shown by BaSO₄ microparticles. PLCL stents crystallinity remained fairly constant for PLCL_{10BaSO₄} and PLCL_{20BaSO₄}^{*}, with the exception of PLCL_{20TIBA}^{*}, which showed a substantial increase. Although crystallinity plays a role in the mechanical properties, crush resistance tests showed that the main contribution to compression force was strut thickness. One can clearly distinguish from the compression curves between stents printed with a 250 μm or a 200 μm micronozzle. Therefore, there is a clear correlation between compression force and strut thickness, which in this case is proportional to surface area coverage, given that the stent design is constant ($n_p = 10$). PLLA_{10I₂} presents the highest normalized force, above 0.13 N/mm, and the highest strut thickness, close to 250 μm.

BaSO₄ addition resulted in a significant reinforcement of PLLA, as previously reported [61, 62], although at the expense of a discontinuous profile during compression testing. Visual inspection of compressed stents evidenced no strut fracture, although some junctions presented detached struts. This behaviour was similar for PLLA_{10TIBA}. In contrast, PLCL-based stents compression curves were smooth and presented no such

behavior. PLCL was chosen as an alternative to PLLA for its well-described additional flexibility given by the caprolactone monomers, while keeping the same overall stiffness. In fact, PLCL stents show a higher force at 50% compression (0.105 ± 0.017 N/mm vs. 0.063 ± 0.008 N/mm for PLLA) with comparable strut thickness.

Expansion assays confirmed that the discontinuous profile found for PLLA_{10BaSO₄} and PLLA_{10TIBA} was due to partial strut detachment rather than fracture. Unrestricted assays showed that junctions at both ends of the stent separated with increasing pressure, but central junctions remained linked. We attribute this spatial pattern to the SC-DW fabrication process. Upon extrusion, filaments are deposited onto the rotating mandrel and start to solidify as chloroform evaporates. If the filament underneath is too dry, welding between filaments is not strong enough. Therefore, chloroform evaporation is a key process parameter in order to render stents with fused unions between struts. This could be achieved by controlling the atmosphere in which stents are manufactured. All other stents showed no strut fracture or detachment up to 16 atm, which corroborated the close relationship between compression and expansion tests in terms of mechanical properties.

As previously discussed, the presence of iodine entrapped in the stents after heat treatment is probably very low due to its evaporation. This claim is supported by X-Ray imaging evidence, as there is no difference in terms of X-Ray attenuation for iodine-containing stents with respect to PLLA and PLCL controls. In contrast, iodine atoms bond in TIBA result in a significant increase in X-Ray attenuation, as well as barium atoms for BaSO₄-containing stents. Degradation of a selected group of radiopaque PLLA-based stents showed no changes in X-Ray attenuation after 3 months incubation, therefore ensuring X-Ray visibility in the mid-term. Finally, compression tests of degraded stents showed no changes in terms of mechanical properties with respect to fresh stents, with the exception of PLLA_{10TIBA}, which showed a significant decrease in compression force. This may be linked to the particular orientation of TIBA crystals along the filament, which may accelerate PLLA degradation following TIBA dissolution.

Concerning cytotoxicity assays, the addition of iodine or BaSO₄ did not result in a cytotoxic effect to cells. Previous studies have investigated iodine's antibacterial effect ([63], [64], [9] and [13]), showing antibacterial properties and biocompatibility both *in vitro* and *in vivo*. Regarding BaSO₄, *in vivo* studies showed good biocompatibility of BaSO₄-containing PLA urethral, pancreatic and biliary stents ([21], [22], and [23]), where BaSO₄ microparticles would be excreted through the gastrointestinal tract. TIBA-containing stents showed a certain degree of cytotoxicity for pure extract, although subsequent dilutions attenuated such effect. This outcome may result as a consequence of the chosen sterilization method, which was UV radiation. It has been reported that TIBA presents photodegradation under exposure to UV radiation [65, 66], which may result in the appearance of toxic species. In order to confirm this, a new cytotoxicity

assay was performed using ethanol soaking as an alternative sterilization method. In this case, cell viability was found to be over 70% for pure extract and subsequent dilutions for the PLCL_{20TIBA}^{*} (87.6 ± 12.5 % for pure extract, 76.6 ± 10.6 % for dilution $1/2$ and 83.8 ± 5.8 % for dilution $1/10$). This result is in accordance with TIBA's reported biocompatibility in literature [19], where exposure of the different extract concentrations of the TIBA-infused sutures had no effect on Hela cells. Therefore, TIBA's cytotoxic effect is attributed to the photodegradation induced by UV radiation, which may be circumvented by using alternative sterilization methods.

3.5 Conclusions

In this work we have developed a novel, versatile SC-DW printing system onto a rotating mandrel to manufacture bioresorbable stents. Chloroform-based PLLA ink presented the required shear-thinning behaviour for extrusion through a micronozzle. A variety of designs with different mesh patterns and densities were successfully fabricated and characterized, with encouraging results regarding mechanical and biological properties. The versatility of the SC-DW approach allowed for ink modification in order to obtain radiopaque polymeric stents. MicroCT analysis evidenced increased X-Ray attenuation for TIBA- and BaSO₄-containing stents with respect to control PLLA or PLCL stents, showing maintained radiopacity after 3 months incubation time.

This preliminary study constitutes a promising starting point in regards of the SC-DW technique's potential for BRS fabrication. The versatility of the approach allows for patient-specific customization in terms of material and printing design in order to achieve sufficient mechanical support with suitable degradation rate. Furthermore, stents with supplementary features may be obtained, such as radiopaque BRS. Future perspectives include the addition of antiproliferative drug into the stents and monitor its release, or surface functionalization with peptides in order to enhance endothelial cell adhesion.

3.6 Supplementary information

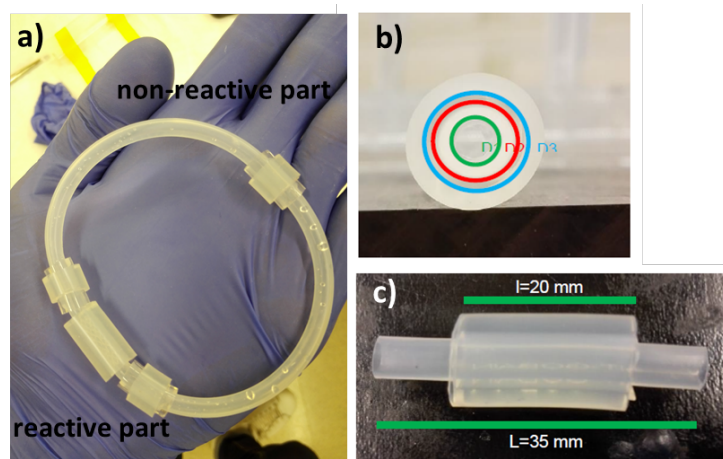


Fig. 3.S1 Silicone loops to test stents thrombogenicity. (a) Complete silicone tubes. (b) Front view of the concentric silicone tubes at the reactive site (c) Top view of the reactive part of the loop.

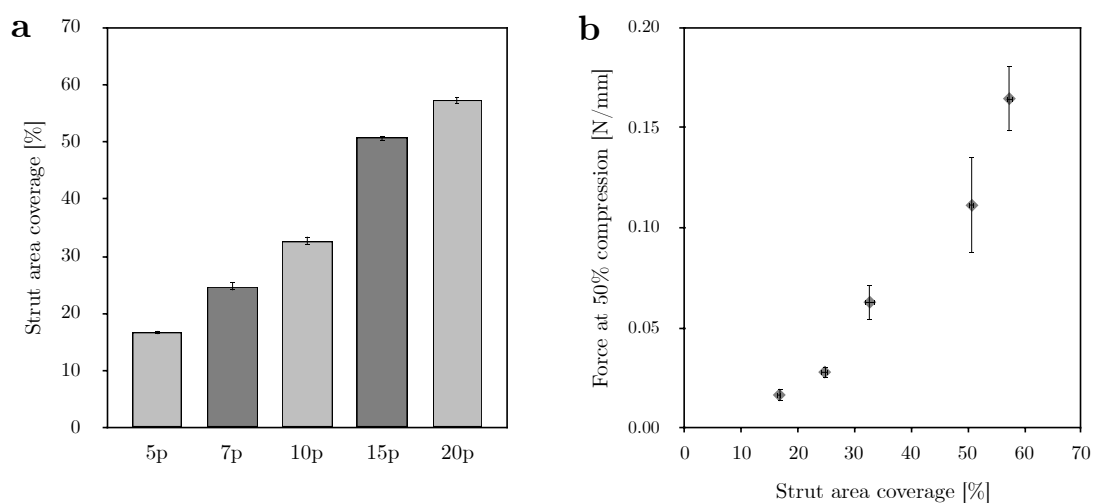


Fig. 3.S2 Stents were axially cut and flattened between two glass plates in order to determine the area percentage covered by stents' struts. Images were post-processed with ImageJ software following ASTM F2081 [67]. (a) Surface area covered by struts as a function of increasing mesh density. (b) Correlation between strut area coverage and compression force at 50% deformation.

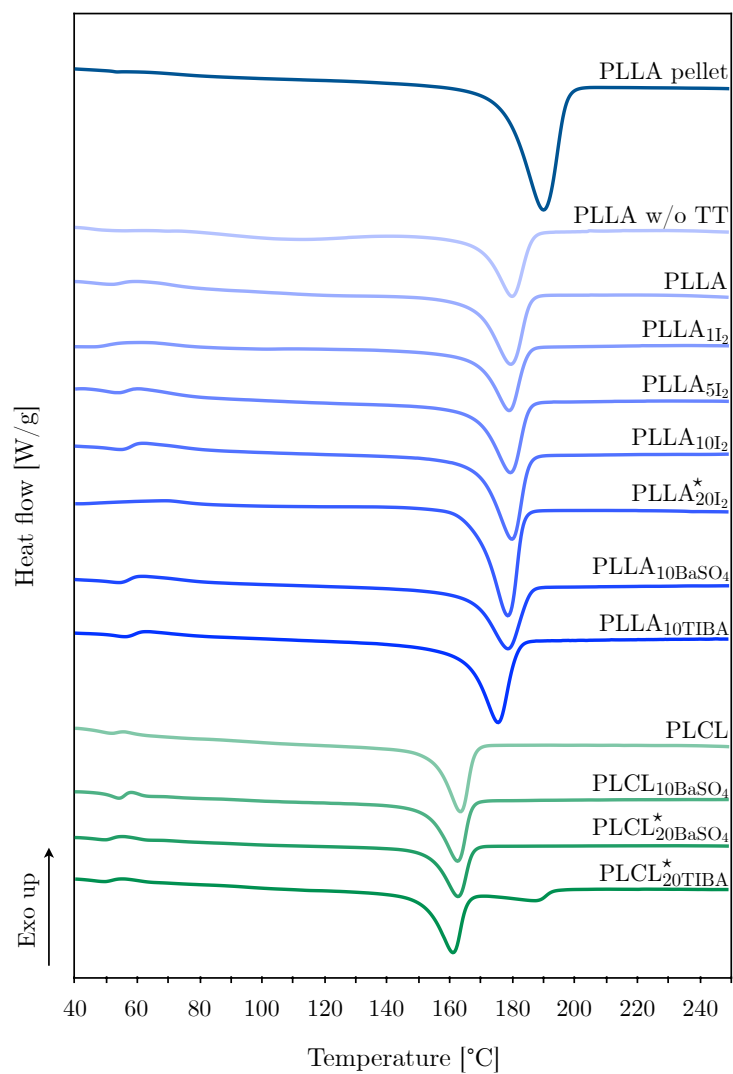


Fig. 3.S3 Heat flow curves for all tested conditions. Samples were heated from room temperature to 250 °C at a rate of 10 °C/min.

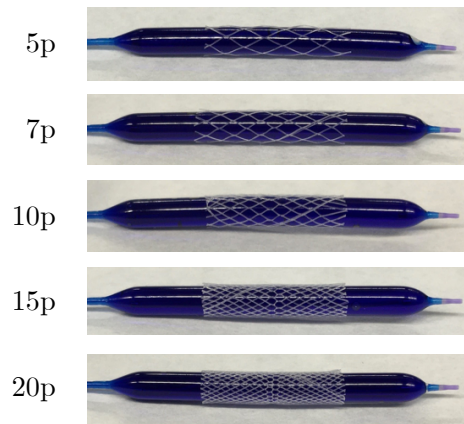


Fig. 3.S4 Expansion test with blue-stained water-filled balloon for PLLA stents with increasing mesh density at 16 atm pressure.

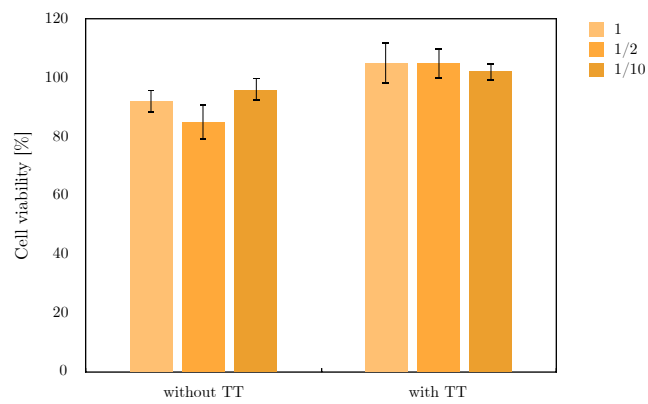


Fig. 3.S5 Cell viability test performed on PLLA stents without and with thermal treatment, for pure extract and dilutions $1/2$ and $1/10$.

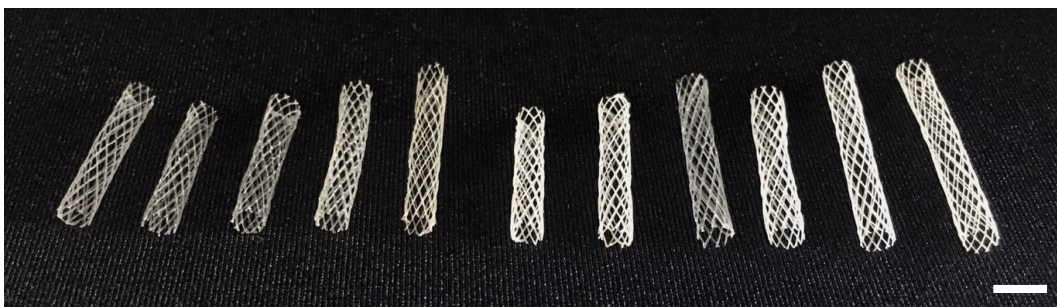


Fig. 3.S6 Overview of printed stents. From left to right: PLLA, PLLA_{1I₂}, PLLA_{5I₂}, PLLA_{10I₂}, PLLA_{20I₂}, PLLA_{10BaSO₄}, PLLA_{10TIBA}, PLCL, PLCL_{10BaSO₄}, PLCL_{20BaSO₄} and PLCL_{20TIBA}. Scale bar corresponds to 5 mm.

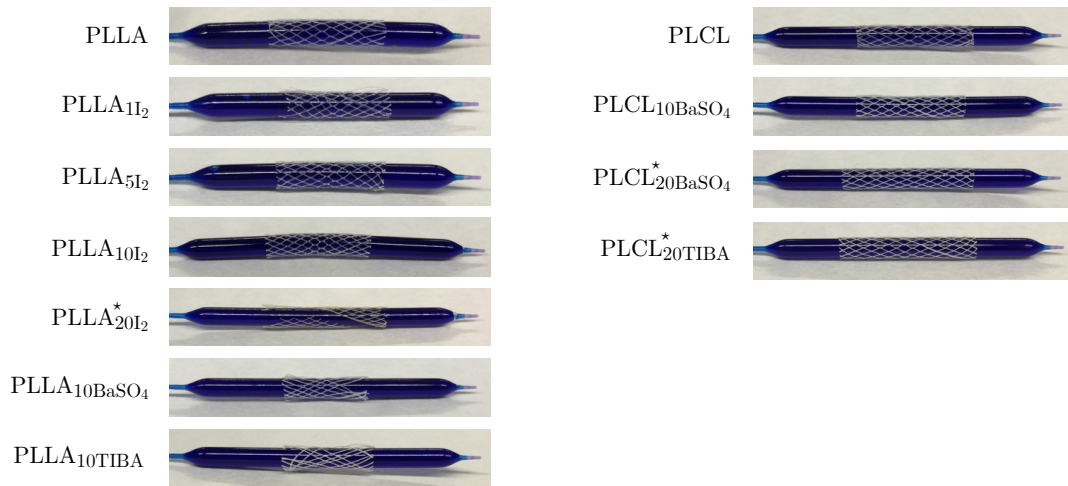


Fig. 3.S7 Expansion test for radiopaque printed stents at 16 atm pressure. (Left) PLLA-based stents and (right) PLCL-based stents.

References

- [1] H. Ang, J. Ng, H. Bulluck, P. Wong, S. Venkatraman, Y. Huang, and N. Foin, “Fundamentals of bioresorbable stents”, in *Functionalised Cardiovascular Stents*, Elsevier, 2018, pp. 75–97.
- [2] G. W. Stone, R. Gao, T. Kimura, D. J. Kereiakes, S. G. Ellis, Y. Onuma, W.-F. Cheong, J. Jones-McMeans, X. Su, Z. Zhang, *et al.*, “1-year outcomes with the Absorb bioresorbable scaffold in patients with coronary artery disease: a patient-level, pooled meta-analysis”, *The Lancet*, vol. 387, no. 10025, pp. 1277–1289, 2016.
- [3] S. Cassese, R. A. Byrne, G. Ndrepepa, S. Kufner, J. Wiebe, J. Repp, H. Schunkert, M. Fusaro, T. Kimura, and A. Kastrati, “Everolimus-eluting bioresorbable vascular scaffolds versus everolimus-eluting metallic stents: a meta-analysis of randomised controlled trials”, *The Lancet*, vol. 387, no. 10018, pp. 537–544, 2016.
- [4] S. G. Ellis, D. J. Kereiakes, G. W. Stone, *et al.*, “Everolimus-eluting bioresorbable vascular scaffolds in patients with coronary artery disease: ABSORB III trial 2-year results”, in *Annual Meeting of the American College of Cardiology*, vol. 18, 2017.
- [5] J. Wiebe, H. M. Nef, and C. W. Hamm, “Current status of bioresorbable scaffolds in the treatment of coronary artery disease”, *Journal of the American College of Cardiology*, vol. 64, no. 23, pp. 2541–2551, 2014.
- [6] S. McMahon, N. Bertollo, E. D. O. Cearbhaill, J. Salber, L. Pierucci, P. Duffy, T. Dürig, V. Bi, and W. Wang, “Bio-resorbable polymer stents: a review of material progress and prospects”, *Progress in Polymer Science*, vol. 83, pp. 79–96, 2018.
- [7] J. Fernandez, A. Etxeberria, and J.-R. Sarasua, “Synthesis, structure and properties of poly (L-lactide-co- ϵ -caprolactone) statistical copolymers”, *Journal of the Mechanical Behavior of biomedical Materials*, vol. 9, pp. 100–112, 2012.
- [8] G. Leibundgut, “A novel, radiopaque, bioresorbable tyrosine-derived polymer for cardiovascular scaffolds”, *Insert to Cardiac Interventions Today Europe*, vol. 2, no. 2, pp. 26–30, 2018.

- [9] K. de Arruda Almeida, A. A. A. de Queiroz, O. Z. Higa, G. A. Abraham, and J. San Román, “Macroporous poly (ϵ -caprolactone) with antimicrobial activity obtained by iodine polymerization”, *Journal of Biomedical Materials Research Part A*, vol. 68, no. 3, pp. 473–478, 2004.
- [10] B. Nottelet, J. Coudane, and M. Vert, “Synthesis of an X-ray opaque biodegradable copolyester by chemical modification of poly (ϵ -caprolactone)”, *Biomaterials*, vol. 27, no. 28, pp. 4948–4954, 2006.
- [11] J.-M. Coutu, A. Fatimi, S. Berrahmoune, G. Soulez, and S. Lerouge, “A new radiopaque embolizing agent for the treatment of endoleaks after endovascular repair: influence of contrast agent on chitosan thermogel properties”, *Journal of Biomedical Materials Research Part B: Applied Biomaterials*, vol. 101, no. 1, pp. 153–161, 2013.
- [12] A. Galperin, D. Margel, J. Baniel, G. Dank, H. Biton, and S. Margel, “Radiopaque iodinated polymeric nanoparticles for X-ray imaging applications”, *Biomaterials*, vol. 28, no. 30, pp. 4461–4468, 2007.
- [13] S. I. Goreninskii, K. S. Stankevich, A. L. Nemoykina, E. N. Bolbasov, S. I. Tverdokhlebov, and V. D. Filimonov, “A first method for preparation of biodegradable fibrous scaffolds containing iodine on the fibre surfaces”, *Bulletin of Materials Science*, vol. 41, no. 4, p. 100, 2018.
- [14] K. Lei, W. Shen, L. Cao, L. Yu, and J. Ding, “An injectable thermogel with high radiopacity”, *Chemical communications*, vol. 51, no. 28, pp. 6080–6083, 2015.
- [15] K. Lei, Y. Chen, J. Wang, X. Peng, L. Yu, and J. Ding, “Non-invasive monitoring of in vivo degradation of a radiopaque thermoreversible hydrogel and its efficacy in preventing post-operative adhesions”, *Acta biomaterialia*, vol. 55, pp. 396–409, 2017.
- [16] X. Li, N. Anton, G. Zuber, M. Zhao, N. Messaddeq, F. Hallouard, H. Fessi, and T. F. Vandamme, “Iodinated α -tocopherol nano-emulsions as non-toxic contrast agents for preclinical X-ray imaging”, *Biomaterials*, vol. 34, no. 2, pp. 481–491, 2013.
- [17] D. Mawad, L. A. Poole-Warren, P. Martens, L. H. Koole, T. L. Slots, and C. S. v. Hooy-Corstjens, “Synthesis and characterization of radiopaque iodine-containing degradable PVA hydrogels”, *Biomacromolecules*, vol. 9, no. 1, pp. 263–268, 2007.
- [18] R. Samuel, E. Girard, G. Chagnon, S. Dejean, D. Favier, J. Coudane, and B. Nottelet, “Radiopaque poly (ϵ -caprolactone) as additive for X-ray imaging of temporary implantable medical devices”, *Rsc Advances*, vol. 5, no. 102, pp. 84 125–84 133, 2015.
- [19] B. Singhana, A. Chen, P. Slattery, I. K. Yazdi, Y. Qiao, E. Tasciotti, M. Wallace, S. Huang, M. Eggers, and M. P. Melancon, “Infusion of iodine-based contrast agents into poly(p-dioxanone) as a radiopaque resorbable IVC filter”, *Journal of Materials Science: Materials in Medicine*, vol. 26, no. 3, p. 124, 2015.
- [20] F. Zhao, H. Xu, W. Xue, Y. Li, J. Sun, F. Wang, G. Jiang, L. Li, and L. Wang, “Iodinated poly(p-dioxanone) as a facile platform for X-ray imaging of resorbable implantable medical devices”, *Journal of biomaterials applications*, vol. 35, no. 1, pp. 39–48, 2020.
- [21] T. Isotalo, E. Alarakkola, M. Talja, T. Tammela, T. Välimaa, and P. Törmälä, “Biocompatibility testing of a new bioabsorbable X-ray positive SR-PLA 96/4 urethral stent”, *The Journal of urology*, vol. 162, no. 5, pp. 1764–1767, 1999.

- [22] T. Lämsä, H. Jin, J. Mikkonen, J. Laukkarinen, J. Sand, and I. Nordback, “Biocompatibility of a new bioabsorbable radiopaque stent material (BaSO₄ containing Poly-L,D-Lactide) in the rat pancreas”, *Pancreatology*, vol. 6, no. 4, pp. 301–305, 2006.
- [23] J. Laukkarinen, I. Nordback, J. Mikkonen, P. Kärkkäinen, and J. Sand, “A novel biodegradable biliary stent in the endoscopic treatment of cystic-duct leakage after cholecystectomy”, *Gastrointestinal endoscopy*, vol. 65, no. 7, pp. 1063–1068, 2007.
- [24] A. Scafa Udriste, A.-G. Niculescu, A. M. Grumezescu, and E. Bădilă, “Cardiovascular stents: a review of past, current, and emerging devices”, *Materials*, vol. 14, no. 10, p. 2498, 2021.
- [25] C. Pan, Y. Han, and J. Lu, “Structural design of vascular stents: a review”, *Micromachines*, vol. 12, no. 7, p. 770, 2021.
- [26] R. A. Buiten, E. H. Ploumen, P. Zocca, C. J. Doggen, L. C. Van Der Heijden, M. M. Kok, P. W. Danse, C. E. Schotborgh, M. Scholte, F. H. De Man, *et al.*, “Outcomes in patients treated with thin-strut, very thin-strut, or ultrathin-strut drug-eluting stents in small coronary vessels: a prespecified analysis of the randomized bio-resort trial”, *JAMA cardiology*, vol. 4, no. 7, pp. 659–669, 2019.
- [27] P. Guedeney, B. E. Claessen, R. Mehran, D. E. Kandzari, M. Aquino, S. Davis, L. Tamis, J. C. Wang, I. Othman, O. S. Gigliotti, *et al.*, “Small-vessel PCI outcomes in men, women, and minorities following platinum chromium everolimus-eluting stents: insights from the pooled PLATINUM diversity and PROMUS Element Plus Post-Approval studies”, *Catheterization and Cardiovascular Interventions*, vol. 94, no. 1, pp. 82–90, 2019.
- [28] N. Bink, V. B. Mohan, and S. Fakirov, “Recent advances in plastic stents: a comprehensive review”, *International Journal of Polymeric Materials and Polymeric Biomaterials*, vol. 70, no. 1, pp. 54–74, 2021.
- [29] A. B. ALAli, M. F. Griffin, and P. E. Butler, “Three-dimensional printing surgical applications”, *Eplasty*, vol. 15, 2015.
- [30] J. Goole and K. Amighi, “3D printing in pharmaceuticals: a new tool for designing customized drug delivery systems”, *International journal of pharmaceuticals*, vol. 499, no. 1-2, pp. 376–394, 2016.
- [31] R. Van Lith, E. Baker, H. Ware, J. Yang, A. C. Farsheed, C. Sun, and G. Ameer, “3D-printing strong high-resolution antioxidant bioresorbable vascular stents”, *Advanced Materials Technologies*, vol. 1, no. 9, p. 1600138, 2016.
- [32] S. A. Park, S. J. Lee, K. S. Lim, I. H. Bae, J. H. Lee, W. D. Kim, M. H. Jeong, and J.-K. Park, “In vivo evaluation and characterization of a bio-absorbable drug-coated stent fabricated using a 3D-printing system”, *Materials Letters*, vol. 141, pp. 355–358, 2015.
- [33] S. J. Lee, H. H. Jo, K. S. Lim, D. Lim, S. Lee, J. H. Lee, W. D. Kim, M. H. Jeong, J. Y. Lim, I. K. Kwon, *et al.*, “Heparin coating on 3D printed poly (l-lactic acid) biodegradable cardiovascular stent via mild surface modification approach for coronary artery implantation”, *Chemical Engineering Journal*, vol. 378, p. 122116, 2019.
- [34] A. J. Guerra and J. Ciurana, “3D-printed bioabsorbable polycaprolactone stent: the effect of process parameters on its physical features”, *Materials & Design*, vol. 137, pp. 430–437, 2019.
- [35] A. J. Guerra, P. Cano, M. Rabionet, T. Puig, and J. Ciurana, “3D-printed PCL/PLA composite stents: Towards a new solution to cardiovascular problems”, *Materials*, vol. 11, no. 9, p. 1679, 2018.

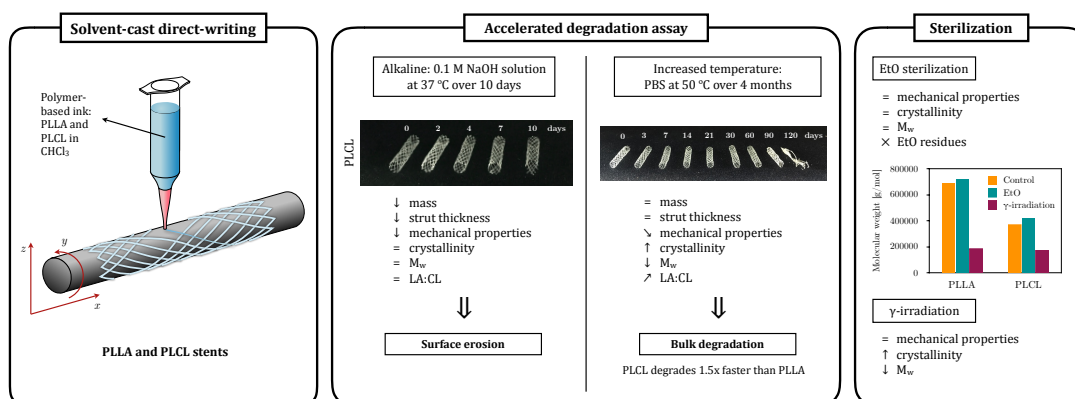
- [36] C. J. Boyer, M. Boktor, H. Samant, L. A. White, Y. Wang, D. H. Ballard, R. C. Huebert, J. E. Woerner, G. E. Ghali, and J. S. Alexander, “3D printing for bio-synthetic biliary stents”, *Bioengineering*, vol. 6, no. 1, p. 16, 2019.
- [37] R. Schieber, Y. Raymond, C. Caparrós, J. Bou, E. Herrero Acero, G. M. Guebitz, C. Canal, and M. Pegueroles, “Functionalization strategies and fabrication of solvent-cast PLLA for bioresorbable stents”, *Applied Sciences*, vol. 11, no. 4, p. 1478, 2021.
- [38] J. Bruneaux, D. Therriault, and M.-C. Heuzey, “Micro-extrusion of organic inks for direct-write assembly”, *Journal of Micromechanics and Microengineering*, vol. 18, no. 11, p. 115 020, 2008.
- [39] S.-Z. Guo, M.-C. Heuzey, and D. Therriault, “Properties of polylactide inks for solvent-cast printing of three-dimensional freeform microstructures”, *Langmuir*, vol. 30, no. 4, pp. 1142–1150, 2014.
- [40] E. Fischer, H. J. Sterzel, and G. Wegner, “Investigation of the structure of solution grown crystals of lactide copolymers by means of chemical reactions”, *Kolloid-Zeitschrift und Zeitschrift für Polymere*, vol. 251, no. 11, pp. 980–990, 1973.
- [41] ISO 25539-2, *Cardiovascular implants. endovascular devices. part 1: vascular stents*. International Organization for Standardization, 2012.
- [42] H. Kahraman, M. Ozaydin, E. Varol, S. M. Aslan, A. Dogan, A. Altinbas, M. Demir, O. Gedikli, G. Acar, and O. Ergene, “The diameters of the aorta and its major branches in patients with isolated coronary artery ectasia”, *Texas Heart Institute Journal*, vol. 33, no. 4, p. 463, 2006.
- [43] K. Kolandaivelu and E. R. Edelman, “Low background, pulsatile, in vitro flow circuit for modeling coronary implant thrombosis”, *J. Biomech. Eng.*, vol. 124, no. 6, pp. 662–668, 2002.
- [44] —, “Environmental influences on endovascular stent platelet reactivity: an in vitro comparison of stainless steel and gold surfaces”, *Journal of Biomedical Materials Research Part A*, vol. 70, no. 2, pp. 186–193, 2004.
- [45] ISO 10993-5, *Biological evaluation of medical devices — part 5: tests for in vitro cytotoxicity*, International Organization for Standardization, 2009.
- [46] ISO 10993-12, *Biological evaluation of medical devices — part 12: sample preparation and reference materials*. International Organization for Standardization, 2007.
- [47] S.-Z. Guo, F. Gosselin, N. Guerin, A.-M. Lanouette, M.-C. Heuzey, and D. Therriault, “Solvent-cast three-dimensional printing of multifunctional microsystems”, *Small*, vol. 9, no. 24, pp. 4118–4122, 2013.
- [48] Y. Cheng, P. Gasior, K. Ramzipoor, C. Lee, J. C. McGregor, G. B. Conditt, T. McAndrew, G. L. Kaluza, and J. F. Granada, “In vitro mechanical behavior and in vivo healing response of a novel thin-strut ultrahigh molecular weight poly-l-lactic acid sirolimus-eluting bioresorbable coronary scaffold in normal swine”, *International journal of cardiology*, vol. 286, pp. 21–28, 2019.
- [49] H. Y. Ang, H. Bulluck, P. Wong, S. S. Venkatraman, Y. Huang, and N. Foin, “Bioresorbable stents: current and upcoming bioresorbable technologies”, *International journal of cardiology*, vol. 228, pp. 931–939, 2017.

- [50] D. Capodanno, “Bioresorbable scaffolds in coronary intervention: unmet needs and evolution”, *Korean circulation journal*, vol. 48, no. 1, pp. 24–35, 2018.
- [51] M. A. Cuiffo, J. Snyder, A. M. Elliott, N. Romero, S. Kannan, and G. P. Halada, “Impact of the fused deposition (FDM) printing process on polylactic acid (PLA) chemistry and structure”, *Applied Sciences*, vol. 7, no. 6, p. 579, 2017.
- [52] R. A. Wach, P. Wolszczak, and A. Adamus-Wlodarczyk, “Enhancement of mechanical properties of FDM-PLA parts via thermal annealing”, *Macromolecular Materials and Engineering*, vol. 303, no. 9, p. 1 800 169, 2018.
- [53] T. R. Welch, R. C. Eberhart, J. Reisch, and C.-J. Chuong, “Influence of thermal annealing on the mechanical properties of PLLA coiled stents”, *Cardiovascular Engineering and Technology*, vol. 5, no. 3, pp. 270–280, 2014.
- [54] J. Sarasua, N. López-Rodríguez, E. Zuza, S. Petisco, B. Castro, M. Del Olmo, T. Palomares, and A. Alonso-Varona, “Crystallinity assessment and in vitro cytotoxicity of polylactide scaffolds for biomedical applications”, *Journal of Materials Science: Materials in Medicine*, vol. 22, no. 11, pp. 2513–2523, 2011.
- [55] N. Vasanthan and O. Ly, “Effect of microstructure on hydrolytic degradation studies of poly (l-lactic acid) by FTIR spectroscopy and differential scanning calorimetry”, *Polymer Degradation and Stability*, vol. 94, no. 9, pp. 1364–1372, 2009.
- [56] F. Zhao, W. Xue, F. Wang, C. Yu, H. Xu, Y. Hao, and L. Wang, “A new approach to improve the local compressive properties of PPDO self-expandable stent”, *Journal of the mechanical behavior of biomedical materials*, vol. 68, pp. 318–326, 2017.
- [57] H. Jaziri, S. Mokhtar, N. Chakfe, F. Heim, and S. B. Abdessalem, “Elastic recovery of polymeric braided stents under cyclic loading: preliminary assessment”, *Journal of the mechanical behavior of biomedical materials*, vol. 98, pp. 131–136, 2019.
- [58] A. Freitas, M. de Araujo, W. Zu, and R. Fangueiro, “Development of weft-knitted and braided polypropylene stents for arterial implant”, *The Journal of the Textile Institute*, vol. 101, no. 12, pp. 1027–1034, 2010.
- [59] K. Kolandaivelu, R. Swaminathan, W. J. Gibson, V. B. Kolachalama, K.-L. Nguyen-Ehrenreich, V. L. Giddings, L. Coleman, G. K. Wong, and E. R. Edelman, “Stent thrombogenicity early in high-risk interventional settings is driven by stent design and deployment and protected by polymer-drug coatings”, *Circulation*, vol. 123, no. 13, pp. 1400–1409, 2011.
- [60] H. Zahedmanesh and C. Lally, “Determination of the influence of stent strut thickness using the finite element method: implications for vascular injury and in-stent restenosis”, *Medical & biological engineering & computing*, vol. 47, no. 4, p. 385, 2009.
- [61] I. M. de Arenaza, N. Sadaba, A. Larrañaga, E. Zuza, and J. Sarasua, “High toughness biodegradable radiopaque composites based on polylactide and barium sulphate”, *European Polymer Journal*, vol. 73, pp. 88–93, 2015.
- [62] J.-P. Nuutinen, C. Clerc, and P. Törmälä, “Mechanical properties and in vitro degradation of self-reinforced radiopaque bioresorbable polylactide fibres”, *Journal of Biomaterials Science, Polymer Edition*, vol. 14, no. 7, pp. 665–676, 2003.
- [63] T. Shirai, T. Shimizu, K. Ohtani, Y. Zen, M. Takaya, and H. Tsuchiya, “Antibacterial iodine-supported titanium implants”, *Acta Biomaterialia*, vol. 7, no. 4, pp. 1928–1933, 2011.

- [64] H. Tsuchiya, T. Shirai, H. Nishida, H. Murakami, T. Kabata, N. Yamamoto, K. Watanabe, and J. Nakase, “Innovative antimicrobial coating of titanium implants with iodine”, *Journal of Orthopaedic Science*, vol. 17, no. 5, pp. 595–604, 2012.
- [65] R. Jarboe Jr, J. Data, and J. Christian, “Photodisintegration studies of ^{14}C -carboxyl 2,3,5-triiodobenzoic acid”, *Journal of pharmaceutical sciences*, vol. 57, no. 2, pp. 323–325, 1968.
- [66] S. Allard, J. Criquet, A. Prunier, C. Falantin, A. Le Person, J. Y.-M. Tang, and J.-P. Croué, “Photodecomposition of iodinated contrast media and subsequent formation of toxic iodinated moieties during final disinfection with chlorinated oxidants”, *Water research*, vol. 103, pp. 453–461, 2016.
- [67] ASTM Standard F2081-06(13), *Characterization and presentation of the dimensional attributes of vascular stents*, ASTM International, 2013.

Chemical vs thermal accelerated hydrolytic degradation of 3D-printed PLLA/PLCL bioresorbable stents: characterization and influence of sterilization

Bioresorbable stents (BRS) are designed to provide initial sufficient mechanical support to prevent vessel recoil while being degraded until their complete resorption. Therefore, degradation rate of BRS plays a crucial role in successful stent performance. This work presents a complete study on the degradation of poly-L-lactic acid (PLLA) and poly(L-lactic-co- ϵ -caprolactone) (PLCL) stents fabricated by solvent-cast direct-writing (SC-DW) through two different accelerated assays: alkaline medium at 37 °C for 10 days and PBS at 50 °C for 4 months. On retrieval, degraded stents were characterized in terms of mass loss, molecular weight (M_w), thermal and mechanical properties. The results showed that under alkaline conditions, stents underwent surface erosion, whereas stents immersed in PBS at 50 °C experienced bulk degradation. M_n decrease was accurately described by the autocatalyzed kinetic model, with PLCL showing a degradation rate 1.5 times higher than PLLA. Additionally, stents were subjected to γ -irradiation and ethylene oxide (EtO) sterilization. Whereas EtO-sterilized stents remained structurally unaltered, γ -irradiated stents presented severe deterioration as a result of extensive chain scission.



V. Chausse, C. Iglesias, E. Bou-Petit, M.-P. Ginebra, M. Pegueroles, *Chemical vs thermal accelerated hydrolytic degradation of 3D-printed PLLA/PLCL bioresorbable stents: Characterization and influence of sterilization*, Polymer Testing 117 (2023) 107817.

4.1 Introduction

Bioresorbable stents (BRS) are envisaged to revolutionize restenosis treatment by providing a temporary support to the vessel in contrast to permanent stents [1]. In the first months after implantation, BRS should present sufficient mechanical strength to prevent vessel recoil, while minimizing the resorption time in order to reduce late undesirable events [2]. The idea of dissolvable scaffolds is not novel, as it dates to the description of Tamai *et al.* [3] of the first successful use of a fully degradable poly-L-lactic acid (PLLA) stent in the early 1990s. Although initially set aside due to the early success of permanent stents, the revelation of associated risks in the long-term such as late stent thrombosis resulted in BRS redevelopment with a variety of devices [4].

Currently, the majority of BRS are manufactured with polymers, being PLLA the most used in the field, in the Absorb BVS, DESolve or Fortitude stents, among others [2]. Semi-crystalline PLLA is composed of crystalline lamellae linked with amorphous tie chains. With increasing molecular weight (M_w), lamellae are more close-packed, leading to increased crystallinity and improved mechanical properties [5, 6]. Alternatively, PLLA may be combined with other aliphatic polyesters in order to render polymers with tailored mechanical properties. For instance, with the aim to increase PLLA's elasticity, poly(ϵ -caprolactone) (PCL) has been used to manufacture poly(L-lactic-co- ϵ -caprolactone) copolymers (PLCL) with varying lactide-to-caprolactone ratios [7].

Degradation of BRS plays a crucial role in the performance of stents while implanted, as aliphatic polyesters degrade *in vivo* through random bulk hydrolysis [8]. In the first stage, hydrolysis of amorphous regions via ester bond scission occurs, leading to a decrease in M_w with little effect on the mechanical properties [9]. In a second stage, hydrolysis is shifted to crystalline regions, resulting in a decrease in radial strength and eventually, mass loss, until complete resorption of the polymer. The degradation rate of PLLA strongly depends on its M_w and crystallinity, and it may take between two to three years [10]. Besides, copolymers such as PLCL also present particular degradation rates, different from their homopolymers, depending on their specific composition.

In order to simulate *in vivo* degradation of polyesters *in vitro*, immersion in phosphate buffered saline (PBS) at 37 °C is widely used [8, 11–13]. However, in view of the lengthiness of the process, hydrolysis may be accelerated by using acidic or basic media, enzymes or increased temperatures [14]. Accelerated degradation in alkaline conditions has been reported for PLLA films and fibers in 0.01 M NaOH at 37 °C [15], PLLA films in 0.1 M NaOH at room temperature [16], PCL scaffolds in 5 M NaOH at 37 °C [12] and PCL-PLLA semi-interpenetrating networks in 1 M NaOH at 37 °C [13]. The use of increased temperatures has been applied for PLLA samples in PBS at 50 °C and 70 °C [17], PLLA and PLCL 95/5 filaments in PBS at 60 °C [18], PLLA tubes in PBS at 50 °C

[19] and PLLA fibers at 80 °C both in PBS and in 0.01 M NaOH [20]. Nevertheless, the validity of accelerated testing above T_g to predict degradation below T_g is a matter of discussion. Although Weir *et al.* [17] speculated that for semicrystalline polymers this assumption may be valid due to their greater volume in less-accessible crystalline domains, other authors showed that at temperatures lower than T_g a change of slope in the kinetics was detected with respect to data obtained over T_g [21]. Similarly, Agrawal *et al.* evaluated the degradation of poly(lactic-co-glycolic) acid (PLGA) copolymers and concluded that elevated temperature studies should be performed only at temperatures below T_g to assess the performance of materials with operating temperatures below T_g [22]. Thus, the experimental accelerated degradation assay that mimics *in vivo* conditions is not yet clarified.

Regarding the different sterilization techniques for medical devices, ethylene oxide (EtO) and gamma irradiation are the most extensively used [23–25]. However, the sterilization procedure may affect the degradation rate of aliphatic polyesters. Several studies have investigated the effects of γ -irradiation and EtO on M_w , crystallinity and mechanical properties for PLLA samples [26], knitted PLLA stents [27], PLCL 70/30 balloon implants [28] and 3D printed PLA samples [29], together with the use of hydrogen peroxide (H_2O_2) plasma for laser-machined PLLA stents and PLA nanofiber scaffolds [30, 31]. Still, thorough studies on PLCL with specific lactide-to-caprolactone ratios are yet to be performed.

Recent advances in additive manufacturing (AM) approaches have resulted in the fabrication of different BRS. Van Lith *et al.* [32] developed a polydiolcitrate-based vascular stent via stereolithography and photopolymerization by exposure to UV light. Park *et al.* designed a 3D printing system to deposit molten PCL or PLLA onto a rotating cylinder to obtain polymeric stents [33, 34]. Similarly, Guerra *et al.* [35] developed a system based on Fused Filament Fabrication (FFF) to print PCL onto a rotating mandrel, and applied this approach to manufacture PCL/PLA composite stents [36]. Finally, Chausse *et al.* presented a novel solvent-cast direct-write (SC-DW) printing system using PLLA and PLCL inks to manufacture BRS onto a rotating cylinder [37]. Although printed stents were characterized in terms of mechanical, thermal and biological properties, further investigations regarding degradation and effects of sterilization were needed.

This work presents a complete study on the degradation of SC-DW PLLA and PLCL stents comparing chemical vs. thermal accelerated degradation assays. The aim is to determine the structural degradation mechanism that stents undergo in different conditions: alkaline medium at 37 °C for 10 days and PBS at 50 °C for 4 months. Stents were characterized by means of mass change, scanning electron microscopy (SEM), compression tests, differential scanning calorimetry (DSC) and gel permeation chromatography (GPC). Additionally, nuclear magnetic resonance (1H -NMR) was used to determine the chemical composition of PLCL stents. Finally, stents were subjected

to gamma irradiation and EtO sterilization in order to evaluate changes in molecular weight, mechanical properties and crystallinity, as well as EtO residuals by fourier transform infrared spectroscopy (FTIR).

4.2 Materials and methods

4.2.1 Chemicals and materials

Medical grade PLLA (Purasorb[®] PL 65; inherent viscosity 6.5 dl/g, $M_w=1675000$ g/mol) and PLCL (Purasorb[®] PLC 9538, 95:5 lactic-to-caprolactone molar ratio, 3.8 dl/g, $M_w=700000$ g/mol) were purchased from Corbion (Netherlands). Sodium hydroxide pellets (PanReac AppliChem ITW Reagents, Germany), phosphate buffered saline (PBS tablets, Gibco, ThermoFisher Scientific, USA) and chloroform ($\geq 99.5\%$, Sigma-Aldrich, USA) were used as received.

4.2.2 3D Printing of stents

PLLA and PLCL stents were fabricated by means of SC-DW technique, as described elsewhere [37]. In short, printable inks were prepared by dissolution of PLLA or PLCL pellets in chloroform at a 10% or 12.5% ratio (w/v), respectively. The 3D printer (BCN 3D+, BCN 3D technologies, Spain) was modified by substituting its y axis for a 3-mm in diameter rotating mandrel to allow for cylindrical printing using a 250 μm nozzle (Optimum[®] SmoothFlow[™], Nordson, USA). Stents were designed with rhombic cell structure, 30 mm in length, 3 mm in diameter and number of peaks equal to 10. After fabrication, stents underwent a thermal treatment at 80 °C for 12 hours.

4.2.3 Accelerated *in vitro* degradation

Chemical vs thermal accelerated degradation of printed stents was assessed by two assays with different media and temperatures: (i) alkaline medium at 37 °C and (ii) PBS at 50 °C. For the former, each stent was immersed in 10 mL of 0.1 M NaOH aqueous solution in sealed glass vials and maintained at 37 °C. Samples were retrieved at time points corresponding to 2, 4, 7 and 10 days. For the latter, each stent was immersed in 10 mL of PBS and maintained at 50 °C, being retrieved at 3, 7, 14, 21, 30, 60, 90 and 120 days. The pH of the solution was monitored throughout the duration of each of the assays. After removal, stents were thoroughly rinsed with deionized water, dried in an oven at 37 °C for 24 hours and stored in a desiccator until further analysis.

4.2.4 Stents characterization

Mass change

Prior to the degradation assay, stents were weighed and their initial mass recorded ($n = 11$ for alkaline degradation, $n = 8$ for temperature degradation). Stents were reweighed after retrieval and drying to obtain the mass at time t . The mass change in percentage was calculated with respect to the initial mass.

Microscopy

Visual examination of degraded stents was performed under microscope Olympus BX51 (Olympus, Japan) to measure strut thickness (AnalySIS Docu, Olympus, Japan). Stents were further examined under SEM (JEOL JSM-7001F, Jeol, Japan) at 2 kV acceleration voltage after being coated with platinum-palladium (80:20).

Mechanical properties

A compression resistance parallel plate test was performed in order to measure stents' radial strength throughout the degradation assay. Stents ($n = 5$) were compressed using a rheometer equipped with a load cell of 50 N (Discovery HR-2, TA instruments, USA) with the upper plate advancing towards the lower plate at 1 mm/min following ISO 25539-2 [38]. At 50% reduction in diameter, radial force was noted and normalized by stent length (N/mm).

Thermal properties

Thermal properties of stents ($n = 3$) were analyzed by means of a DSC assay (DSC2920, TA instruments, USA). The samples were scanned at a heating rate of 10 °C/min from room temperature to 250 °C using nitrogen as purge gas to determine their glass transition temperature (T_g) and melting temperature (T_m). The crystallinity percentage was computed from the heat flow curves as

$$\chi_c(\%) = \frac{\Delta H_m}{\Delta H_m^0 \times X_{\text{PLLA}}} \times 100 \quad (4.1)$$

where ΔH_m is the fusion enthalpy of the polymer, X_{PLLA} is the mass fraction of PLLA in the sample and ΔH_m^0 is the theoretical fusion enthalpy of a 100% crystalline PLLA sample (93 J/g [39]). In the case of PLCL stents, only lactide units were assumed to be able to crystallize [7].

Molecular weight

The molecular weight of degraded stents ($n = 1$) was determined by GPC in an Agilent chromatograph (HPLC 1260 Infinity series, Agilent Technologies, USA). The separation

was carried in an Agilent PL HFIP gel column (USA) using hexafluoro-2-propanol (HFIP, Apollo Scientific, UK) containing 0.05 mol/L of sodium trifluoroacetate (Sigma Aldrich, USA) as eluent. Sample concentration used for analysis was 2 mg/mL. The used flow was 0.3 mL/min and the injection volume was 10 μ L. Molecular weights were calculated after calibration with PMMA standards from Sigma-Aldrich (USA), the molecular weight calibration range being from 2.7 million to 2000 Dalton. Calculations were performed with Chemstation Software (Agilent Technologies) to obtain weight average molecular weight (M_w), number average molecular weight (M_n) and polydispersity index (PDI) as its ratio (M_w/M_n).

Nuclear magnetic resonance (NMR)

In order to determine the chemical composition of PLCL stents ($n = 3$) throughout the degradation assay $^1\text{H-NMR}$ was performed in a Bruker NMR Ascend 400 of 400 MHz (Bruker, USA). Stents were dissolved in deuterated chloroform (CDCl_3 , 99.80%, Euriso-top, France) using tetramethylsilane (TMS, 0.03%) as internal standard for calibration. Obtained spectra were analyzed with Topspin software (Bruker, USA). The lactide-to-caprolactone (LA/CL) molar ratio was determined as the integration ratio of peaks characteristic to each unit, being $\delta 5.1$ ppm for LA and $\delta 4.1$ ppm for CL.

4.2.5 Sterilization methods

Degradation of PLLA and PLCL stents was characterized after two different sterilization methods: (i) gamma irradiation and (ii) ethylene oxide gas. The former was performed at Aragogamma (Barcelona, Spain) using a source of ^{60}Co at a dose of 8 kGy following ISO 13485 and 11137 standards [40, 41]. The latter was performed at Soadco (Escaldes-Engordany, Andorra) according to ISO 11135 standards [42]. Briefly, EtO concentration of 750 g/cm³ was used during 120 minutes treatment time at 50 °C, followed by 18 h degassing time. Sterilized stents were characterized with GPC, DSC and compression tests and compared to control PLLA and PLCL stents. After EtO sterilization, stents were further analyzed by FTIR (Nicolet 6700 FTIR spectrometer, Thermo Scientific, USA), used in attenuated total reflection (ATR) mode and equipped with a Ge crystal. A spectral range between 4000 and 675 cm^{-1} was obtained, with a resolution of 2 cm^{-1} and 64 scans.

4.2.6 Statistical analysis

Statistical analysis was performed using Minitab software (Minitab Inc., USA). An equality of variances test (ANOVA) was used to determine statistically significant differences (p-value < 0.05 between the different groups and 95% confidence interval) for normally-distributed data. All data are represented as mean values \pm standard deviation (SD).

4.3 Results

4.3.1 Accelerated alkaline degradation

Figure 4.1 shows the parameters evaluated after chemical degradation. PLLA and PLCL stents immersed in NaOH 0.1 M solution over 10 days experienced a noticeable degradation. The monitoring of pH evidenced a constant pH around 12.75 until day 10, when a slight pH decrease was detected, as shown in Figure 4.1a. After drying, stents were weighed and their mass compared to the one before the degradation assay. Figure 4.1b displays the mass change in percentage shown by PLLA and PLCL stents over 10 days of incubation. Starting from day 2, both PLLA and PLCL stents experienced significant mass loss, between 20 and 30%, up until day 10, where PLLA stents mass loss was over 90%. As the degradation proceeded, strut thickness gradually decreased. This was confirmed upon inspection with an optical microscope. A reduction of strut thickness from day 0 to day 10 was found, from 120.9 μm down to 43.9 μm for PLLA and from 151.6 μm to 53.3 μm for PLCL, as shown in Figure 4.1c.

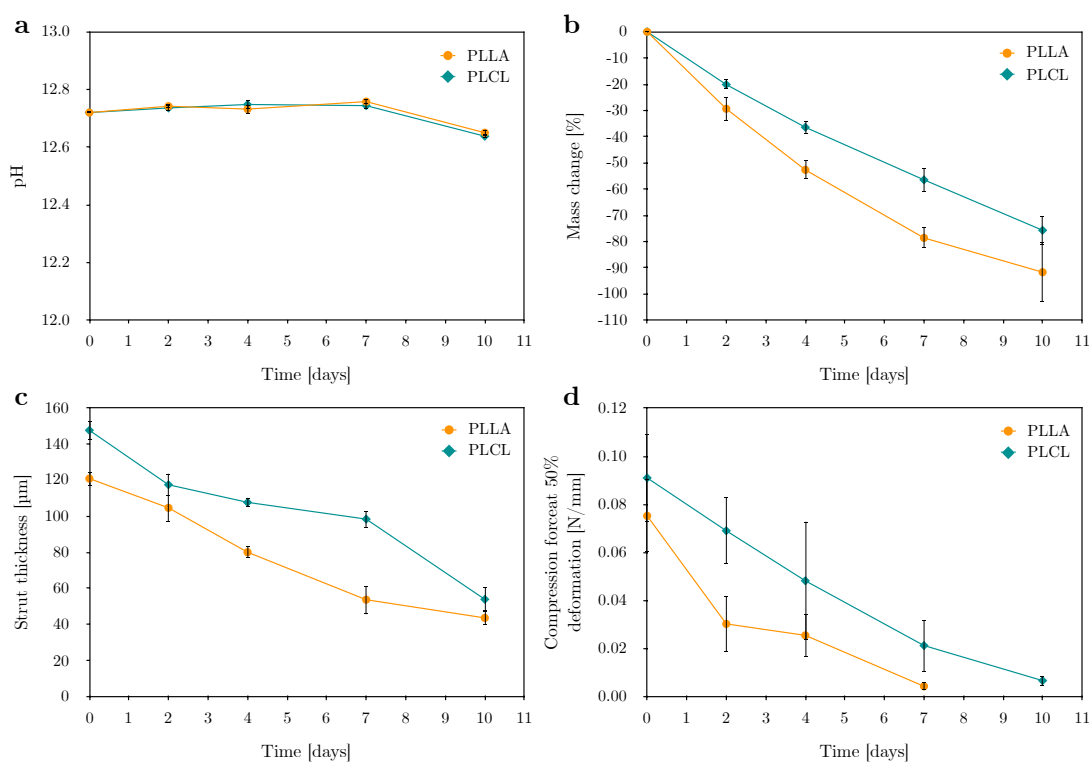


Fig. 4.1 *in vitro* accelerated degradation of PLLA and PLCL stents in 0.1 M NaOH solution at 37 °C over 10 days. (a) Medium pH, (b) stents mass change, (c) strut thickness and (d) compression force at 50% deformation as a function of degradation time.

Stents morphology changed throughout the experiment, as one can observe in Figure 4.2a. Both PLLA and PLCL stents fragilized over time. Nevertheless, while PLLA presented a more accelerated degradation, specially at day 10, PLCL kept its structure although some parts of the stents were disintegrated.

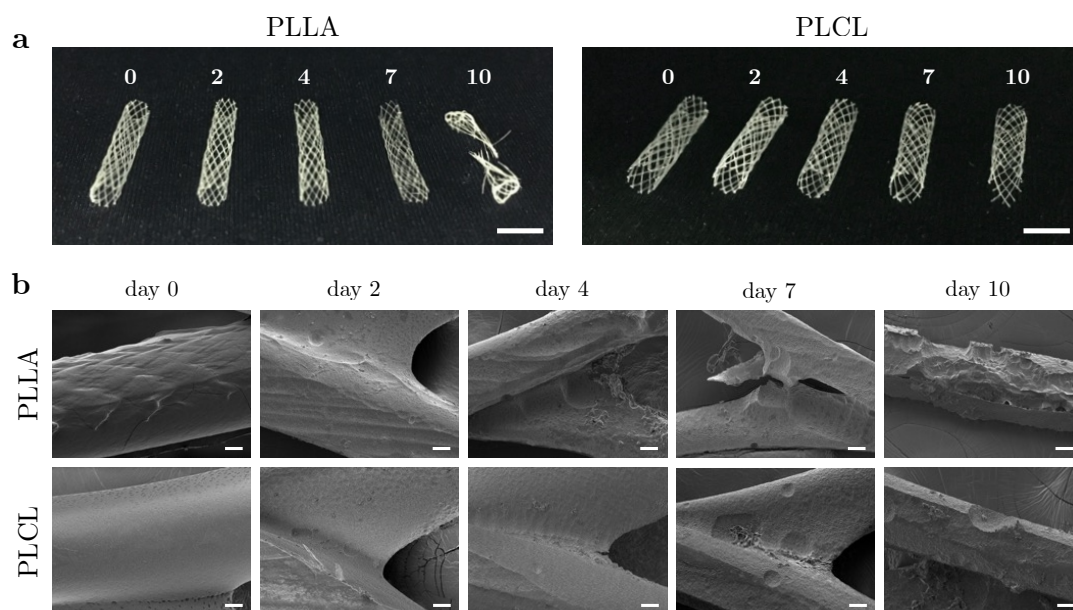


Fig. 4.2 (a) Stents appearance as a function of degradation time in alkaline solution. Scale bar corresponds to 5 mm. (b) SEM images of degraded stents' surface. Scale bar corresponds to 20 μm .

PLLA and PLCL stents were further examined under SEM (Figure 4.2b), which revealed the thinning of the stent struts, where the material appeared to be shaved off from the bulk. Although strut thickness decreased with degradation, unions between struts maintained welded, except for PLLA at day 10, where strut unions presented extensive detachment. PLLA stents presented more quantity of eroded cavities in comparison to PLCL stents as the degradation time increased. As expected, the decrease in strut thickness caused a considerable decrease in mechanical properties, which was found to be more pronounced for PLLA than for PLCL, with a more gradual decrease, as shown in Figure 4.1d. Starting from 0.09 N/mm before degradation, PLCL stents compression force at 50% deformation decreased gradually, reaching 0.01 N/mm at day 10. In the case of PLLA, compression force experienced a very pronounced decline after two days, which moderated in the following time-points.

Regarding DSC analysis, PLLA stents showed a glass transition temperature close to 70 °C and a melting temperature around 178 °C, constant for the entire assay (Table 4.1 and Figure 4.S1). Similarly, PLCL stents presented lower values, being 60 °C and 162 °C, respectively. Regarding crystallinity percentage, PLLA presented a higher value than PLCL (25% vs 21%), although these values remained unaltered over degradation time.

Tab. 4.1 Glass transition temperature (T_g), melting temperature (T_m) and crystallinity percentage (χ_c) for PLLA and PLCL stents as a function of degradation time in alkaline solution.

Degradation time [days]	PLLA			PLCL		
	T_g [°C]	T_m [°C]	χ_c [%]	T_g [°C]	T_m [°C]	χ_c [%]
0	69.9 ± 2.0	178.8 ± 0.5	25.8 ± 0.9	59.4 ± 0.2	162.5 ± 0.3	20.8 ± 0.4
2	69.3 ± 0.9	178.0 ± 0.6	24.1 ± 0.5	60.2 ± 0.8	162.2 ± 0.1	20.5 ± 0.2
4	68.9 ± 0.7	178.3 ± 0.1	24.1 ± 0.7	59.8 ± 2.8	162.1 ± 0.1	20.4 ± 0.5
7	69.2 ± 1.3	179.1 ± 0.1	25.5 ± 1.0	59.3 ± 0.6	162.1 ± 0.2	21.1 ± 1.2
10	68.6 ± ./.	180.5 ± ./.	21.8 ± ./.	59.8 ± 0.5	162.7 ± 0.6	20.0 ± 0.6

Analogously, gel permeation chromatography revealed that M_w and M_n remained fairly constant throughout the degradation assay for both types of stents, as one can see in Table 4.2, with minimal batch-related variations. PLLA presented higher molecular weight, around 700,000 g/mol, whereas PLCL's values were around 380,000 g/mol. Polydispersity was found to be around 2.5 for PLLA and 2.0 for PLCL stents. The weight distribution curves remained monomodal throughout degradation (Figure 4.S2).

Tab. 4.2 Weight average molecular weight (M_w), number average molecular weight (M_n) and polydispersity (PDI) for PLLA and PLCL stents as a function of degradation time in alkaline solution.

Degradation time [days]	PLLA			PLCL		
	M_w	M_n	PDI	M_w	M_n	PDI
0	688,050	258,210	2.66	367,840	185,690	1.98
2	673,510	268,300	2.51	363,680	184,680	1.97
4	690,070	271,880	2.54	359,870	179,710	2.00
7	676,830	267,140	2.53	395,510	191,670	2.06
10	747,590	302,530	2.47	406,750	194,830	2.09

The $^1\text{H-NMR}$ spectrum of PLCL presented characteristic PLLA signals at δ 1.6 (CH_3) and δ 5.1 (CH), and PCL signals at δ 1.35-1.67 ($\text{CH}_2\text{CH}_2\text{CH}_2$), δ 2.3 (CH_2CO) and δ 4.1 (CH_2O) (Figure 4.3). Additional signals corresponding to lactide-caprolactone (LA-CL) junctions were found at 2.4, 4.1 and 5.0 ppm. Integration of peaks of samples at days 0, 2, 4, 7 and 10 evidenced no preferential degradation, as initial values around 97% for LA and 3% for CL remained constant throughout the degradation assay.

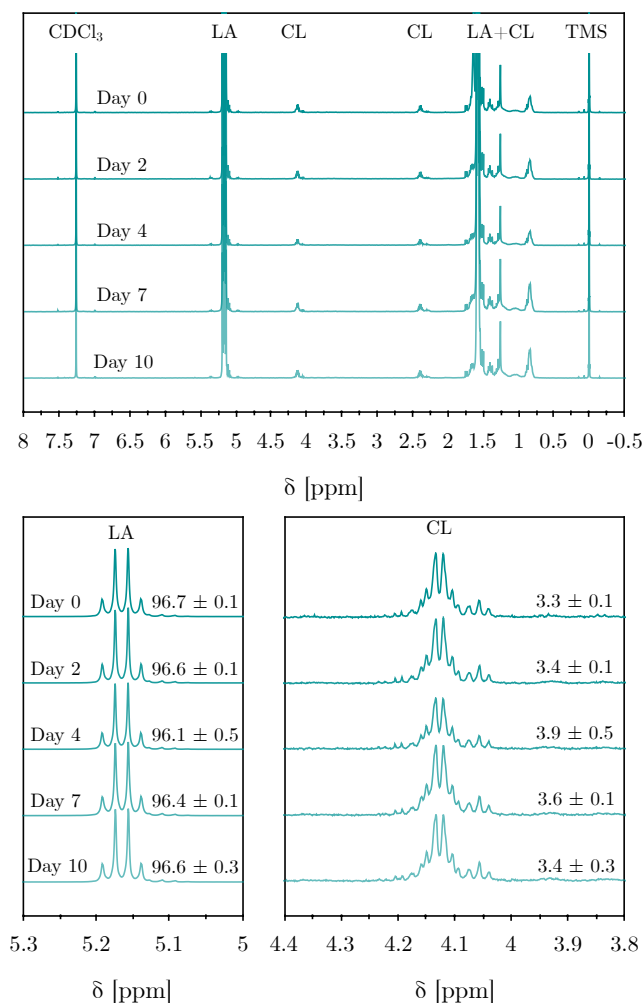


Fig. 4.3 $^1\text{H-NMR}$ spectra of PLCL stents degraded in alkaline medium, with details at 5.1 ppm corresponding to LA units (left) and at 4.1 ppm corresponding to CL units (right). PLCL composition regarding LA and CL units is given in percentage.

4.3.2 Accelerated temperature degradation

To evaluate thermal degradation, PLLA and PLCL stents were immersed in PBS and kept at 50 °C for 4 months. The measured parameters and the morphology images are shown in Figure 4.4 and Figure 4.5, respectively. The pH of the solution was monitored throughout the assay, showing constant pH values for PLLA samples, around 7.4 (Figure 4.4a). In contrast, PBS in contact with PLCL stents presented acidification in the later stage, with pH values reaching 7.1 after 120 days.

Stents appearance changed over time, from being transparent at the beginning of the assay to progressively turning whitish as the degradation proceeded, as one can see in Figure 4.5a. Concurrently, stents became increasingly brittle, specially at day 120 for PLLA and at days 90 and 120 for PLCL

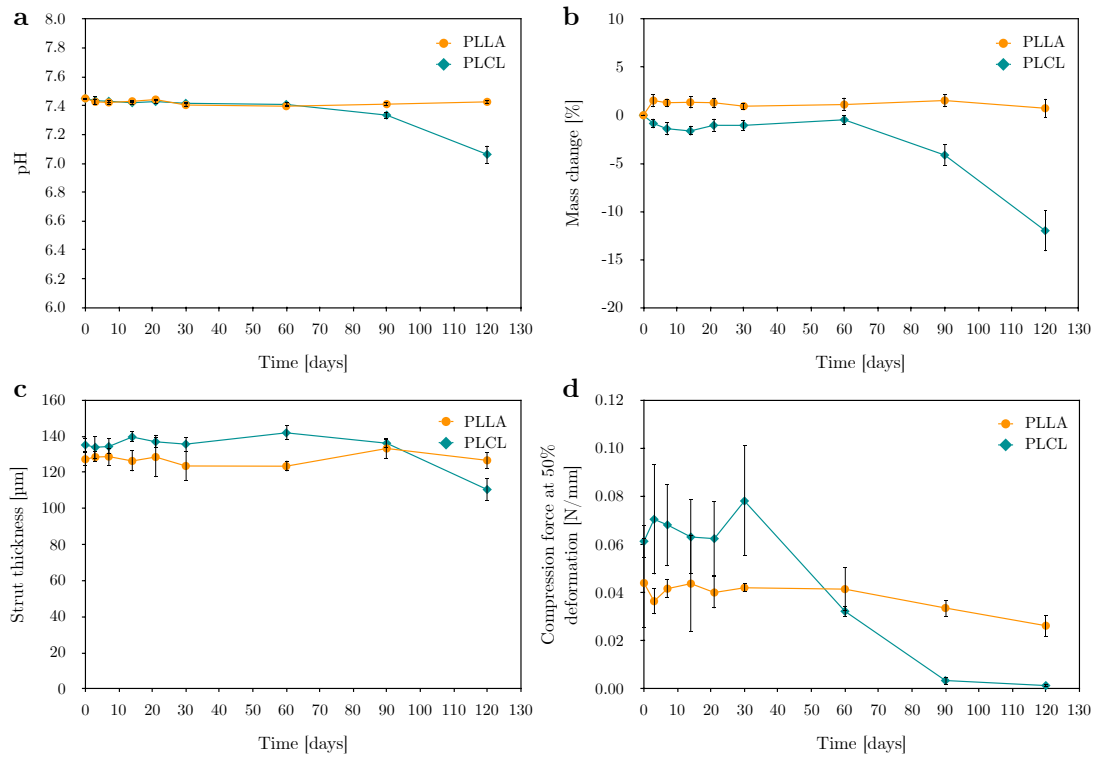


Fig. 4.4 *in vitro* accelerated degradation of PLLA and PLCL stents in PBS at 50 °C over 4 months. (a) Medium pH, (b) stents mass change, (c) strut thickness and (d) compression force at 50% deformation as a function of degradation time.

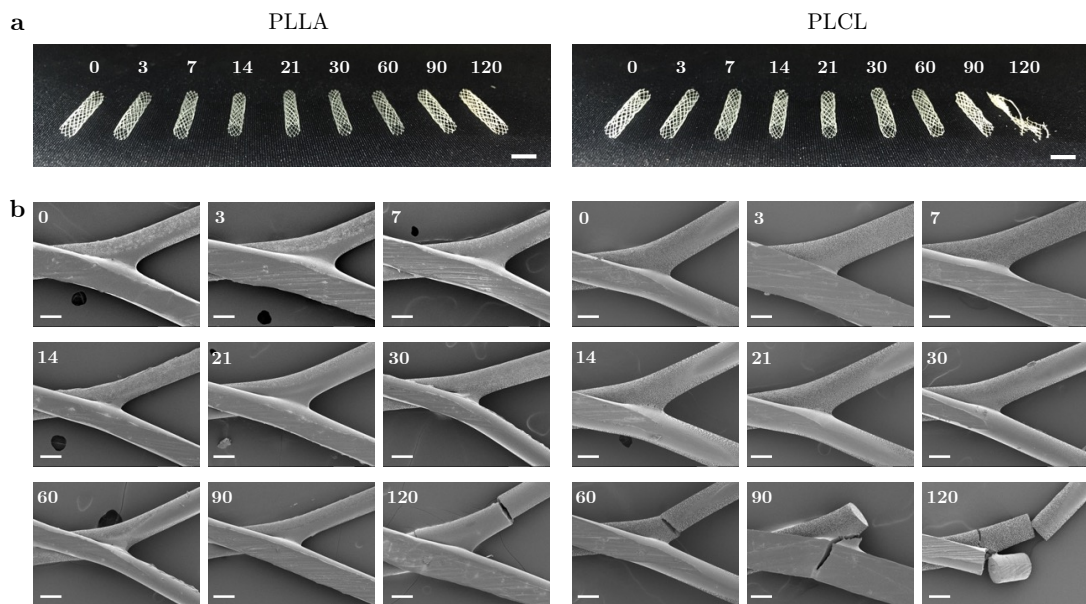


Fig. 4.5 (a) Stents appearance over degradation time in PBS solution. Scale bar corresponds to 5 mm. (b) SEM images of degraded stents' surface. Scale bar corresponds to 100 μm .

Mass change followed a similar trend to that observed for pH. Whereas PLLA stents suffered no change in mass for the whole of the degradation assay, PLCL stents showed 5% mass loss at day 90, which increased up to 12% after 120 days (Figure 4.4b). Regarding strut thickness, PLLA stents presented constant values, around 130 μm , until the end of the assay (Figure 4.4c). Conversely, strut thickness of PLCL stents remained constant around 140 μm except for the last time point, when it decreased significantly to 110 μm . SEM examination of degraded stents displayed no striking differences in terms of superficial appearance. Degraded PLLA and PLCL stents looked topographically indistinguishable with respect to control stents prior to degradation (Figure 4.5b). Nonetheless, hydrolysis resulted in internal changes leading to a brittle behavior, visible for PLLA at day 120 and for PLCL starting at day 60.

Mechanical properties of degraded stents remained constant for the first weeks, but eventually effects of degradation became noticeable (Figure 4.4d). For PLLA, compression force at 50% deformation was found to be around 0.04 N/mm until days 90 and 120, showing a slight decreasing trend. In contrast, PLCL stents initially presented higher resistance to compression, around 0.07 N/mm, followed by a steep decrease after day 30 and complete collapse at days 90 and 120.

Thermal analysis evidenced extensive internal changes throughout the degradation assay. Both PLLA and PLCL stents experienced a sustained increment in crystallinity percentage, from 27.2% to 51.5% for PLLA, and from 21.6% to 55.3% for PLCL (Table 4.3 and Figure 4.S3). Additionally, PLCL showed an initial melting temperature of 162.5 $^{\circ}\text{C}$, which rose to 167.3 $^{\circ}\text{C}$ at day 60, only to reduce to 154.1 $^{\circ}\text{C}$ at the end of the assay. Glass transition temperatures were also found to increase prior to decreasing and to ultimately becoming undetectable. Similar trends were found for PLLA, although less marked.

Tab. 4.3 Glass transition temperature (T_g), melting temperature (T_m) and crystallinity percentage (χ_c) for PLLA and PLCL stents as a function of degradation time in PBS at 50 $^{\circ}\text{C}$.

Degradation time [days]	PLLA			PLCL		
	T_g [$^{\circ}\text{C}$]	T_m [$^{\circ}\text{C}$]	χ_c [%]	T_g [$^{\circ}\text{C}$]	T_m [$^{\circ}\text{C}$]	χ_c [%]
0	72.1 \pm 1.1	178.1 \pm 0.2	27.2 \pm 0.2	59.4 \pm 0.2	162.5 \pm 0.2	21.6 \pm 1.1
3	71.8 \pm 0.2	178.1 \pm 0.3	27.7 \pm 0.6	59.9 \pm 0.7	162.6 \pm 0.2	21.9 \pm 0.8
7	72.9 \pm 0.9	178.4 \pm 0.3	28.0 \pm 0.2	66.4 \pm 0.3	163.1 \pm 0.1	22.1 \pm 0.1
14	71.5 \pm 0.7	178.6 \pm 0.1	29.5 \pm 0.4	64.7 \pm 1.2	163.6 \pm 0.3	24.6 \pm 0.6
21	73.5 \pm 0.8	179.2 \pm 0.2	30.8 \pm 0.8	62.0 \pm 3.2	164.6 \pm 0.2	26.9 \pm 0.4
30	74.5 \pm 1.4	179.2 \pm 0.2	34.2 \pm 2.7	58.1 \pm 1.0	166.4 \pm 0.6	29.6 \pm 1.1
60	72.0 \pm 0.5	179.1 \pm 0.2	41.9 \pm 2.1	./.	167.3 \pm 0.2	38.7 \pm 0.2
90	./.	177.8 \pm 0.6	49.7 \pm 2.6	./.	156.4 \pm 0.4	49.1 \pm 2.0
120	./.	177.2 \pm 0.5	51.5 \pm 1.8	./.	154.1 \pm 0.6	55.3 \pm 3.5

Table 4.4 displays the data gathered from GPC. PLLA stents initially presented M_w around 850,000 g/mol, whereas this value was about half for PLCL stents, around 450,000. Hydrolytic degradation in PBS resulted in a steady decrease over time in M_w and M_n for both materials, until reaching values around 130,000 for PLLA and 20,000 for PLCL. Regarding PLLA's polydispersity index, it was found to be between 3.5 and 4 for the first two months, after which it increased around 5, whereas PLCL showed invariable PDI around 3. The GPC chromatograms remained monomodal throughout the assay and presented a shift towards lower molecular weights as degradation proceeded (Figure 4.S4).

Tab. 4.4 Weight average molecular weight (M_w), number average molecular weight (M_n) and polydispersity (PDI) for PLLA and PLCL stents as a function of degradation time in PBS at 50 °C.

Degradation time [days]	PLLA			PLCL		
	M_w	M_n	PDI	M_w	M_n	PDI
0	863,780	232,580	3.71	452,250	148,210	3.05
3	796,960	231,290	3.45	454,460	147,890	3.07
7	974,900	250,570	3.89	420,520	136,520	3.08
14	725,660	211,460	3.43	372,110	130,530	2.85
21	604,790	173,710	3.48	261,160	103,620	2.52
30	528,010	153,340	3.44	243,290	96,496	2.52
60	384,060	97,152	3.95	115,980	38,419	3.02
90	233,930	49,298	4.75	34,365	10,118	3.40
120	131,700	25,024	5.26	18,049	6,797	2.66

Analysis of $^1\text{H-NMR}$ spectra of PLCL stents (Figure 4.6) showed no changes in composition until day 60 of degradation, as LA units accounted for 97.1% of total units and CL units, for 2.9%. At day 90, CL percentage decreased slightly to 2.7%, which was further reduced to 2.0% at the last time point. Besides, two additional peaks appeared as the degradation proceeded: a peak corresponding to terminal LA units at $\delta 4.36$ and its counterpart for CL units, at $\delta 3.65$, detectable from day 60 onwards.

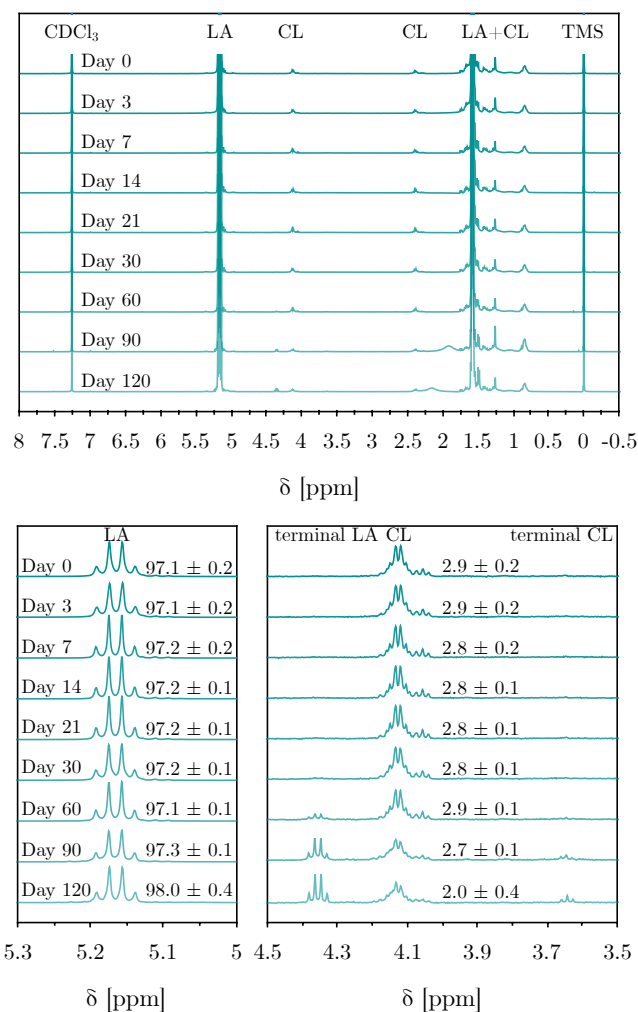


Fig. 4.6 $^1\text{H-NMR}$ spectra of PLCL stents degraded in PBS at 50 °C, with detailed regions at $\delta 5.1$ ppm corresponding to LA units (left) and between $\delta 4.5$ and $\delta 3.5$ ppm showing terminal LA peak at $\delta 4.36$, CL units at $\delta 4.1$ and terminal CL peak at $\delta 3.65$ (right). PLCL composition regarding LA and CL units is given in percentage.

4.3.3 Effects of γ -irradiation and EtO sterilization

The effects of sterilization on PLLA and PLCL stents were examined with GPC, DSC and compression tests to evaluate sterilization effects on stent's crystallinity, molecular weight and mechanical properties. GPC showed how EtO sterilization did not have an effect on PLLA and PLCL molecular weight, as shown in Table 4.5 and Figure 4.S5. However, γ -irradiation resulted in a M_w sharp decrease, from 688,000 g/mol down to 187,000 g/mol for PLLA and from 368,000 g/mol to 171,000 g/mol for PLCL. Regarding crystallinity, γ -irradiation effects on the polymer were significant, with crystallinity increasing from 26% up to 40% for PLLA and from 21% to 29% for PLCL. On the contrary, EtO-sterilized stents presented the same crystallinity as control PLLA or PLCL stents. Figure 4.7a shows that both sterilization methods did not result in a decrease in mechanical properties for PLLA stents. In the case of PLCL stents, compression

force appeared to increase after EtO and γ -irradiation although differences were not statistically significant. Additionally, stents exposed to EtO were further characterized with FTIR. Figure 4.7b shows the obtained spectra for EtO-sterilized PLLA and PLCL stents, as well as for control stents. No differences were found in terms of bands or band shifting when comparing control to sterilized stents.

Tab. 4.5 Weight average molecular weight (M_w), number average molecular weight (M_n), polydispersity (PDI), glass transition temperature (T_g), melting temperature (T_m) and crystallinity percentage (χ_c) for PLLA and PLCL stents as a function of sterilization method.

	Material	M_w	M_n	PDI	T_g	T_m	χ_c
PLLA	Control	688,050	258,210	2.66	69.9 ± 2.0	178.8 ± 0.4	25.8 ± 0.9
	EtO	720,460	309,790	2.33	69.2 ± 1.1	179.3 ± 0.5	26.5 ± 0.6
	γ -irradiation	186,900	119,220	1.57	./.	179.0 ± 0.6	39.6 ± 0.9
PLCL	Control	367,840	185,690	1.98	59.4 ± 0.1	162.5 ± 0.3	20.8 ± 0.4
	EtO	417,630	198,430	2.10	60.5 ± 0.6	163.5 ± 0.2	21.8 ± 0.5
	γ -irradiation	171,300	102,690	1.67	58.4 ± 1.0	167.0 ± 0.1	29.0 ± 0.1

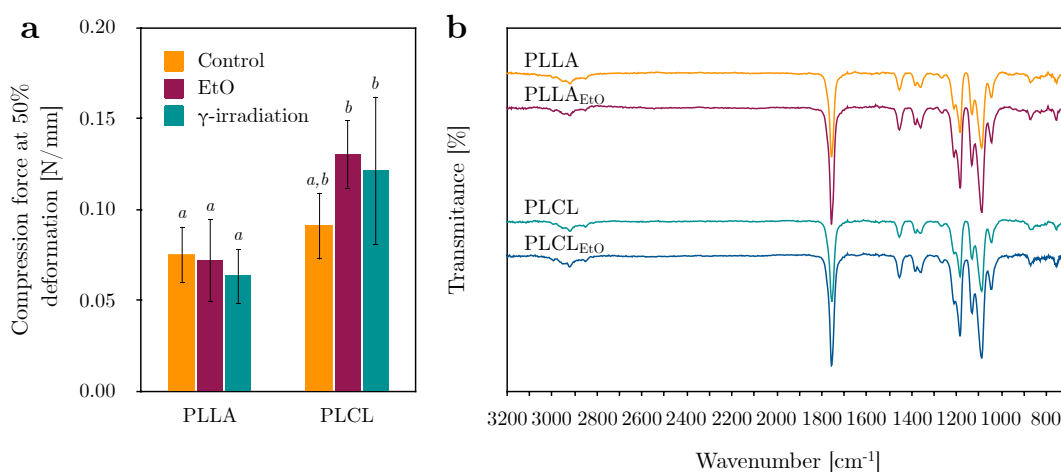


Fig. 4.7 Stents characterization after sterilization with γ -irradiation or EtO. (a) Stents force at 50% deformation under compression assay and (b) FTIR spectra of PLLA and PLCL stents before and after EtO sterilization. Conditions *a* and *b* are statistically different ($p < 0.05$).

4.4 Discussion

BRS are temporary implants with dynamic properties since they should present sufficient mechanical properties throughout the degradation timeframe and biocompatibility, related to degradation products. Thus, an adequate degradation evaluation should always be performed. In that sense, accelerated degradation studies are of interest to shorten the assay time. However, such assays should reproduce the degradation behavior *in vivo*. The present work evaluates chemical vs thermal accelerated degradation in order to determine the appropriate conditions to mimic *in vivo* degradation.

Degradation of aliphatic polyesters is driven by a competition between two effects, namely water diffusion into the polymer and hydrolytic chain scission. The former is highly dependent on the polymer's chemical composition, hydrophobicity, size and design, all of which determine the accessibility of water molecules within the polymer [12]. The latter consists in the reaction of water molecules with the ester bonds that constitute the backbone of the polymeric chains, which are fragmented into carboxylic acid and alcohol groups [43].

When the hydrolysis rate is faster than the diffusion of water molecules inside the polymer's bulk, surface erosion occurs. In this case, only surface chains are hydrolyzed whereas the bulk of the polymer remains intact. As a result, the polymer undergoes a thinning effect as degradation by-products are shaved off from the surface and diffuse into the media [44]. This effect leaves an unchanged polymer core in terms of molecular weight, crystallinity percentage or mechanical properties.

Stents subjected to chemical degradation and thus immersed in 0.1 M NaOH solution at 37 °C showed this kind of degradation behavior. The pH of the supernatant remained constant until day 10, when the solution turned slightly more acidic. Upon increasing times of immersion, stents appeared to become fragile as their strut thickness decreased, from 120.9 μm down to 43.9 μm for PLLA and from 151.6 μm to 53.3 μm for PLCL. Moreover, after 2 days stents presented significant mass loss as the material was removed from the surface, until reaching 90% mass loss for PLLA and 75% for PLCL. SEM examination evidenced extensive surface degradation, showing a marked thinning effect and eroded cavities for increased degradation time. In close agreement to strut thickness reduction, stents' resistance to compression progressively decreased. Regarding DSC analysis, T_g , T_m and χ_c remained constant for the totality of the assay, as expected from samples undergoing surface erosion. This was also the case for GPC results, which showed no changes in molecular weight with respect to undegraded stents. Finally, the analysis of $^1\text{H-NMR}$ spectra for PLCL degraded stents displayed no preferential degradation for lactide or caprolactone units as the lactide-to-caprolactone ratio kept invariable throughout the assay.

These results are in concordance with those previously reported in literature, where alkaline degradation in NaOH solution at different concentrations (between 5 M and 0.01 M) was used for aliphatic polyesters [12, 13, 15, 16]. In general, degraded samples presented extensive mass loss from the beginning of the assay and steady molecular weight, with the exception of the study by Yuan *et al.* [20]. In this case, although immersion of PLLA fibers in 0.01 M NaOH at 80 °C led to mass loss together with a decrease in molecular weight, the authors attributed the latter to the elevated temperature of the assay, which induced a combination of surface erosion and bulk degradation.

Essentially, bulk degradation takes place when the diffusion of water molecules into the polymer is faster than the rate of chain scission. In this case, the polymer is fully hydrated and the hydrolysis reaction occurs uniformly throughout the polymer. The cleavage of ester bonds results in the formation of new terminal carboxyl groups, leading to pH reduction and increased hydrolysis rate in an autocatalytic process. Therefore, the polymer experiences a decrease in molecular weight and eventually mass loss once the degradation by-products, namely oligomers and monomers, are able to diffuse out of the polymer matrix [44]. However, when oligomers accumulate in the core of the polymer, pH locally decreases due to carboxylic acid catalysis and the degradation rate is accelerated in the core with respect to the surface. In consequence, dissimilar degradation rate may lead to bimodal molecular weight distribution, with high M_w surface and low M_w core [12].

In contrast to the surface erosion mechanism showed by the degradation of PLLA and PLCL stents in alkaline medium, stents subjected to thermal degradation, i.e., immersed in PBS at 50 °C underwent bulk degradation. As stents were retrieved from the degradation media, PLCL stents were found to become fragile as degradation time increased, in accordance with mass loss onset observed at day 90. Consequently, the pH of the solution also decreased as a result of acidic degradation by-products release in the surrounding media [22]. On the contrary, PLLA stents presented no mass loss during the assay timeframe and thus the pH of the solution remained constant. Regarding strut thickness, significant reduction was found for PLCL stents at day 120, from about 140 μm to 110 μm , while remaining invariable for PLLA stents. Initial stages of strut breakage due to fragility were observed under SEM examination, with PLLA showing no such signs until day 120, whereas at day 60 PLCL stents already presented preliminary cracks, which generalized for days 90 and 120. Subsequent compression test results were in agreement with these findings, as PLLA stents displayed very similar resistance to compression with a slight decreasing trend. Conversely, although PLCL stents performance was initially higher, effects of brittleness appeared at day 60 as the resistance to compression plummeted for the final time points. DSC curves analysis indicated initial degradation of amorphous parts of the polymer in view of the sustained increment in crystallinity, until reaching percentages over 50% for both PLLA and PLCL. Therefore, as amorphous regions were hydrolyzed, the polymers became less elastic and brittleness arose, as shown previously by SEM and compression tests. Although GPC confirmed considerable molecular weight decrease throughout the assay, PLLA stents retained their mechanical properties longer than PLCL stents. This may be partly attributed to initial higher M_w (863,780 vs 452,250 g/mol), even if PLLA's degradation rate appears to be lower than that of PLCL. According to the essentially monomodal nature of the weight distribution curves, the degradation rate of the surface and the core appeared to be homogeneous. Finally, $^1\text{H-NMR}$ of PLCL stents indicated no clear preferential degradation in the early stages, but towards the end of the assay CL percentage was reduced. Moreover, the manifestation of terminal LA and CL peaks is in

agreement with the decrease in M_w , as the relative concentration of terminal groups must increase over time as a result of chain scission.

Accelerated degradation of polyesters through increased temperature has been reported to occur via bulk degradation. Naseem *et al.* investigated the degradation behavior of high M_w PLLA in PBS at 50 °C, with minimal mass loss over 120 days of incubation and a great decline in M_w (from 338,000 to 8,000 g/mol) [19]. Similar findings on mass loss and M_w were published by Shi *et al.* on the degradation of PLLA and PLCL 95/5 filaments in PBS at 60 °C over 21 days [18]. However, no increase in crystallinity was found as initial crystallinity was already very high, over 60% for PLLA and around 50% for PLCL. In contrast, as-printed SC-DW stents presented lower crystallinity percentage, around 26% for PLLA and 20% for PLCL, thus allowing for an increase in crystallinity as the degradation proceeded. Additionally, Shi *et al.* reported that the melting temperature for PLCL increased from 162.6 °C to 166.3 °C to eventually decrease to 152.6 °C, a fact attributed to initial regularization of the molecular chains followed by further degradation. The same behavior was found for SC-DW PLCL stents, as T_m increased from 162.5 °C to 167.3 °C and then decreased to 154.1 °C.

Furthermore, Weir *et al.* studied the degradation of PLLA samples in PBS at 50 °C over 115 days and at 70 °C over 23 days and compared the degradation mechanisms at elevated temperature with respect to those obtained over 44 weeks *in vitro* at 37 °C and *in vivo* [8, 17]. The authors concluded that PLLA degraded at the same rate *in vitro* at 37 °C and *in vivo* following bulk degradation. Moreover, the degradation mechanism at 50 °C and 70 °C (below and above PLLA's T_g) proved to be very similar to the one obtained at 37 °C, in terms of mass loss, crystallinity, molecular weight and mechanical properties, although in an accelerated manner.

Regarding sterilization, effects on crystallinity, M_w and mechanical properties were dissimilar depending on the sterilization procedure. EtO-sterilized stents presented no EtO residues following FTIR analysis, and presented equivalent M_w , crystallinity percentage and resistance to compression with respect to control PLLA or PLCL stents. In contrast, effects of γ -irradiation included a 73% decrease in M_w for PLLA and of 54% for PLCL, in conjunction with a significant increase in crystallinity, whereas resistance to compression was maintained. These results are consistent with the findings reported by several authors on PLLA, showing increased crystallinity and a decrease in M_w as a result of chain scission upon γ -irradiation [24, 27, 30], and unchanged M_w upon EtO sterilization [26]. Regarding PLCL, Haim *et al.* concluded that no chemical changes were caused by EtO on PLCL 70/30 balloons while γ -irradiation induced extensive chain scission [28]. Therefore, γ -irradiated stents present a substantial risk of early degradation as M_w is severely deteriorated, whereas EtO-sterilized PLLA and PLCL stents showed no significant alterations in their polymer structure. For this reason, EtO-

sterilized stents are expected to reproduce the degradation displayed by unsterilized stents in terms of degradation mechanism and timeframe.

Finally, one may model stent degradation kinetics from the experimental data obtained under thermal degradation at 50 °C. To that end, Anderson [45] reported a statistical model for the temporal evolution of M_n under hydrolysis until the point of mass loss as

$$\frac{1}{M_{n_t}} = \frac{1}{M_{n_0}} + k_1 t \quad (4.2)$$

where M_{n_t} is M_n at time t and M_{n_0} , at time 0, k_1 is the rate constant and t is time [46]. However, this model does not account for the increasing concentration of carboxylic acid end groups that trigger autocatalysis. Therefore, an alternative relationship was derived by Pitt and Gu [47] as

$$M_{n_t} = M_{n_0} \cdot e^{-k_2 t} \quad (4.3)$$

where k_2 is the rate constant for the autocatalyzed model. Figures 4.8a and 4.8b show the plot of $1/M_{n_t} - 1/M_{n_0}$ as a function of time for the uncatalyzed model and $\ln(M_{n_t}/M_{n_0})$ for the autocatalyzed one. The rate constants k_1 and k_2 , corresponding to the uncatalyzed and autocatalyzed models, respectively, were determined from the linear regression and are summarized in Table 4.6. Considering the correlation coefficients (R^2), the autocatalyzed model appears to model the degradation of both PLLA and PLCL better than the uncatalyzed model, with PLCL showing increased degradation rate. Figure 4.8c presents the close agreement between M_n degradation data and the predicted behavior by the autocatalyzed model at 50 °C. Besides, this work presents very similar values for the rate constants regarding PLLA degradation at 50 °C in comparison to previously reported values by Weir *et al.* (2.64×10^{-7} vs 3×10^{-7} for k_1 and 0.0188 vs 0.0196 for k_2) [8, 17]. Furthermore, by applying the Arrhenius equation,

$$k = A e^{-E_a/RT} \quad (4.4)$$

where A is a constant, E_a is the activation energy, R is the universal gas constant and T is the temperature, Weir *et al.* calculated the activation energy for PLLA in the temperature range between 37 °C and 70 °C, and found it to be 100.5 kJ/mol [17]. Therefore, with E_a known, it is possible to extrapolate PLLA stents degradation behavior from 50 °C to 37 °C, as shown in Figure 4.8d, with the degradation constant

calculated to be $k_{37^\circ\text{C}, \text{PLLA}} = 0.0039$. Regarding PLCL, as no value for E_a is available in the literature, 100.5 kJ/mol has been taken as a reference, giving $k_{37^\circ\text{C}, \text{PLCL}} = 0.0058$. The extrapolation indicates that complete degradation of PLCL would take around 2 years at 37 °C, whereas longer degradation time would be expected for PLLA.

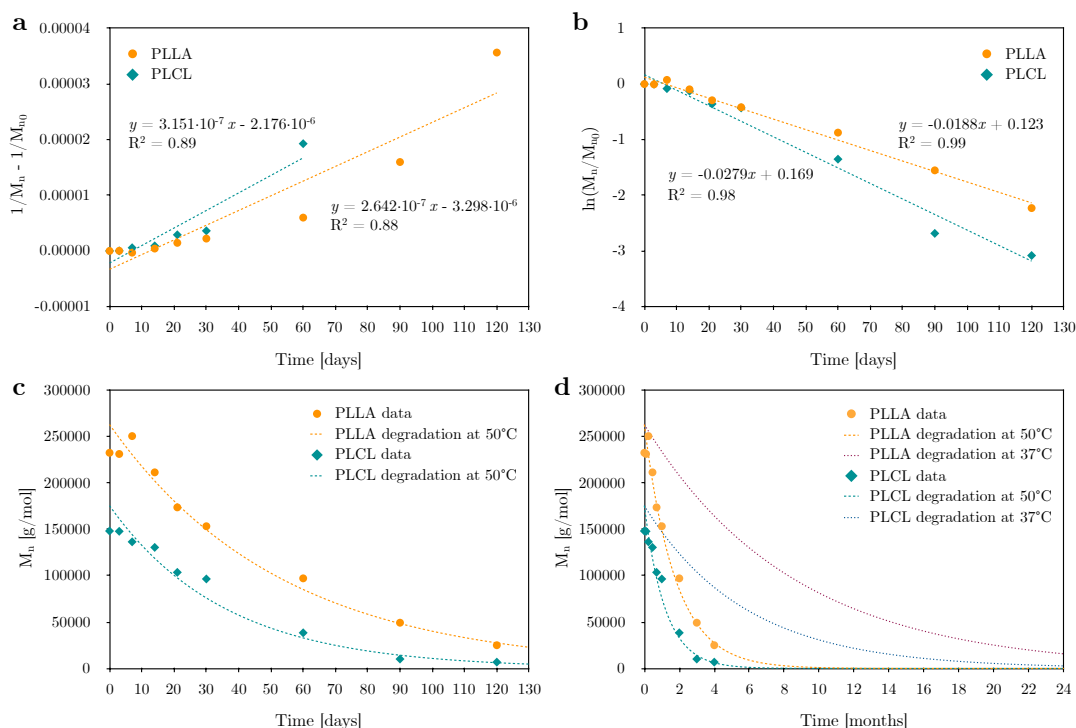


Fig. 4.8 Degradation models: (a) plot of $1/M_{n_t} - 1/M_{n_0}$ as a function of time for the uncatalyzed model and (b) $\ln(M_{n_t}/M_{n_0})$ for the autocatalyzed, (c) M_n as a function of time with measured time points and as predicted by the autocatalyzed model and (d) extrapolation of M_n degradation curves from 50 °C to 37 °C over 24 months using Arrhenius equation.

Tab. 4.6 Rate constants k_1 and k_2 and correlation coefficients as determined from linear regression for uncatalyzed and autocatalyzed degradation models.

Material	Temperature	Uncatalyzed		Autocatalyzed		Source
		k_1 (days ⁻¹)	R^2	k_2 (days ⁻¹)	R^2	
PLLA	50 °C	2.64×10^{-7}	0.88	0.0188	0.99	-
PLCL		3.15×10^{-7}	0.89	0.0279	0.98	
PLLA	37 °C	9×10^{-8}	0.63	0.0052	0.85	[17]
	50 °C	3×10^{-7}	0.90	0.0196	0.96	
	70 °C	4×10^{-6}	0.99	0.2155	0.95	
PLLA	60 °C	./.	./.	0.06	./.	[18]
PLCL 95/5		./.	./.	0.15	./.	

These results suggest the feasibility of performing accelerated degradation assays in order to extrapolate aliphatic polyester degradation at operating conditions. Nevertheless, estimations may be compromised when the samples undergo a different degradation mechanism. Although degradation of PLLA and PLCL stents in PBS at 50 °C led to bulk degradation, the use of alkaline medium (0.1 M NaOH solution) induced surface erosion

instead. In fact, in alkaline medium, due to surface erosion, the most determining parameter on degradation was strut thickness, and consequently PLLA stents degraded faster, as they initially presented filaments around 120 μm versus 150 μm for PLCL stents. Conversely, PLCL degraded 1.5 times faster than PLLA at 50 °C. On the one hand, it is well accepted that PCL degrades slower than PLA due to its higher hydrophobicity. On the other hand, hydrolysis initially occurs in amorphous regions as water diffusion is hindered in crystalline domains. Altogether, the reduced crystallinity and increase in water penetration leads to more rapid degradation for copolymers than for homopolymers [48]. In fact, the reduction of CL units percentage as shown by $^1\text{H-NMR}$ towards the end of the assay is consistent with CL units in amorphous regions degrading earlier than LA units located in crystalline domains. Hence the importance of achieving the desired degradation mechanism when conducting accelerated degradation assays in order to accurately mimic *in vivo* degradation.

4.5 Conclusions

In this work we have presented the results for two accelerated degradation assays on PLLA and PLCL 3D-printed stents. Under alkaline conditions, stents degraded via surface erosion given the sustained mass loss, reduced strut thickness, invariable crystallinity percentage and constant M_w . On the contrary, when immersed in PBS at 50°C, stents underwent bulk degradation, due to considerable decrease in M_w and an increase in crystallinity, with PLLA stents showing neither mass loss nor decreased strut thickness throughout the assay. The autocatalyzed kinetic model described the experimental data decrease for M_n better than the uncatalyzed model. The degradation rate of PLCL was found to be 1.5 times faster than that of PLLA due to the higher availability of amorphous regions, which are hydrolyzed prior to more impervious crystalline domains. Finally, γ -irradiation triggered extensive chain scission and severe polymer deterioration, whereas no significant structural alterations were found on EtO-sterilized stents.

Considering that aliphatic polyesters degrade *in vivo* through random bulk hydrolysis, chemical degradation of stents in alkaline media has been found unsuitable to accurately mimic *in vivo* conditions. Conversely, results obtained at elevated temperature suggest the feasibility of extrapolating the degradation rate of PLLA and PLCL stents to estimate *in vivo* degradation until complete resorption. Furthermore, the versatility of the SC-DW approach allows for the fabrication of stents with supplementary features, such as drug-eluting BRS, for which polymer degradation behavior constitutes a critical parameter in terms of drug release timeframe.

4.6 Supplementary information

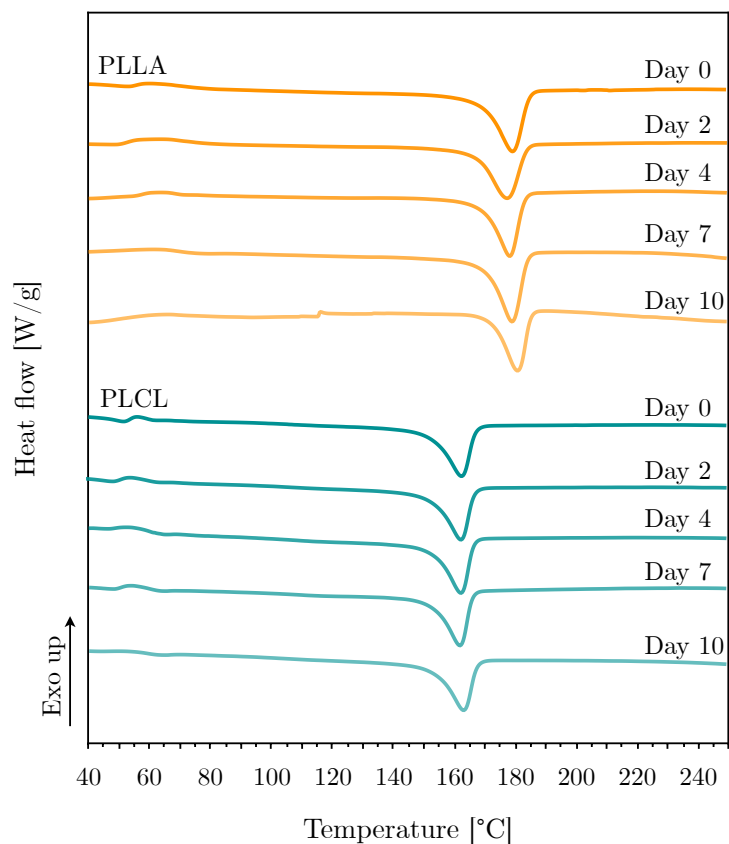


Fig. 4.S1 Heat flow curves for PLLA and PLCL stents under alkaline degradation. Samples were heated from room temperature to 250 °C at a rate of 10 °C/min.

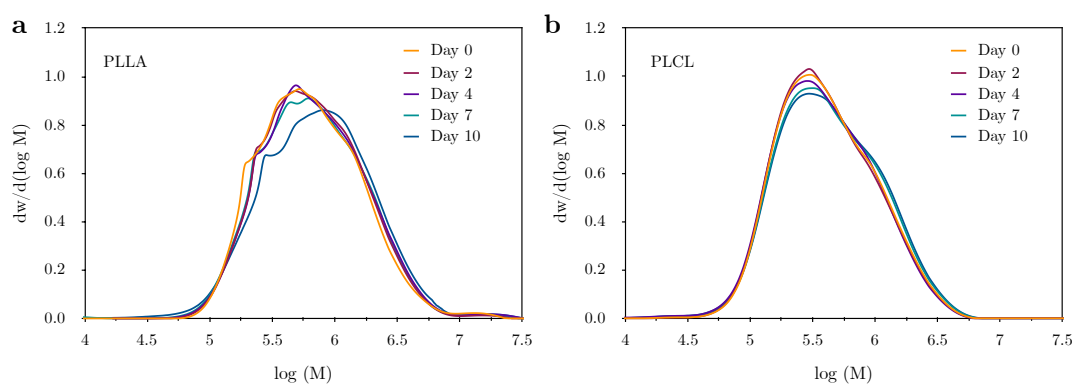


Fig. 4.S2 Molecular weight distribution as a function of the logarithm of molar mass (M) for (a) PLLA and (b) PLCL stents degraded in 0.1 M NaOH solution at 37 °C.

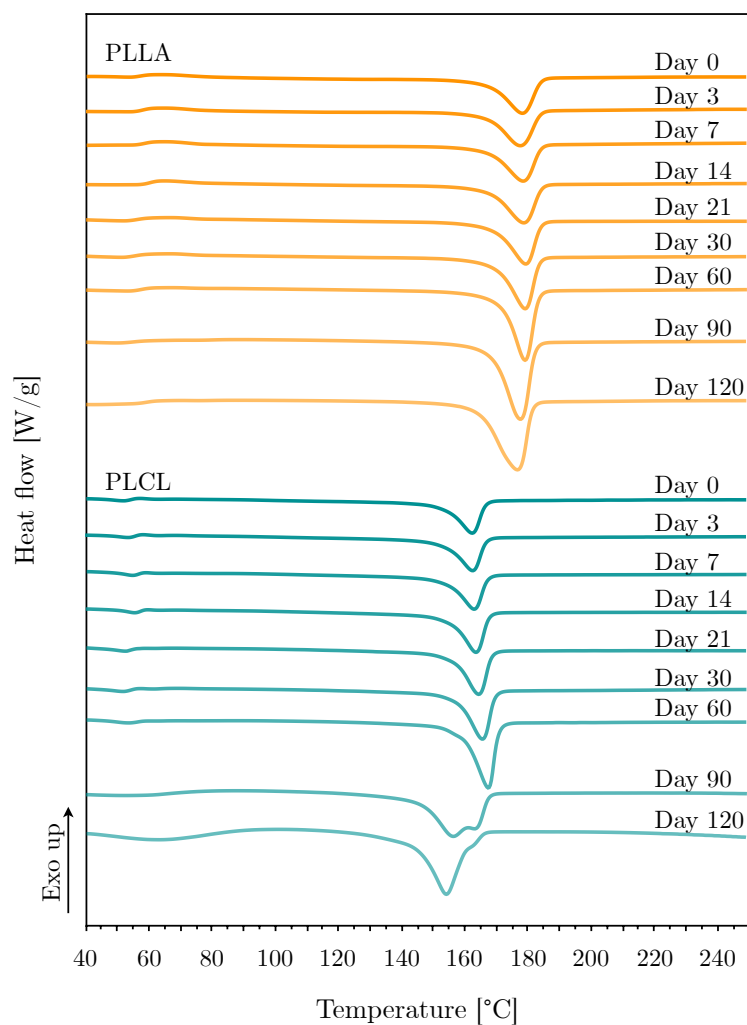


Fig. 4.S3 Heat flow curves for PLLA and PLCL stents degraded in PBS at 50 °C. Samples were heated from room temperature to 250 °C at a rate of 10 °C/min.

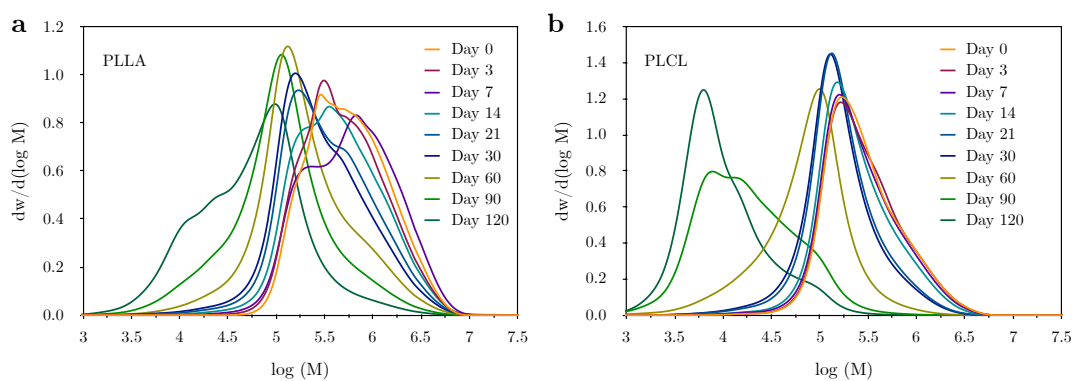


Fig. 4.S4 Molecular weight distribution as a function of the logarithm of molar mass (M) for (a) PLLA and (b) PLCL stents degraded in PBS at 50 °C.

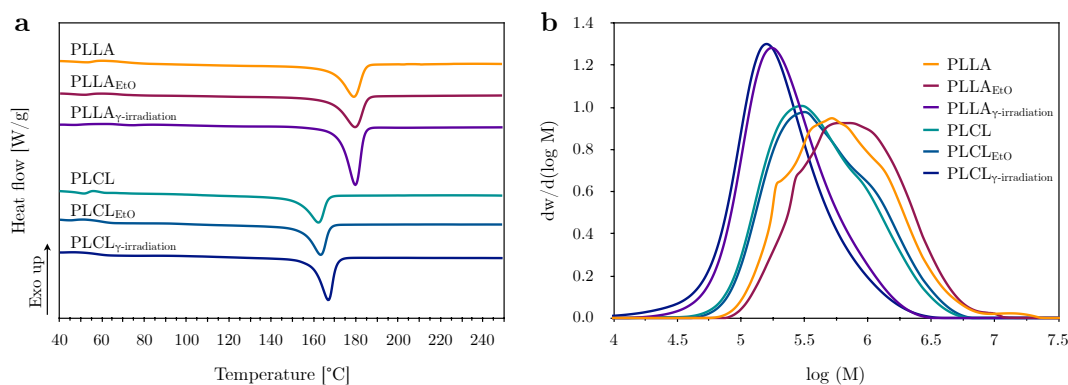


Fig. 4.S5 Effects of EtO or γ -irradiation sterilization on PLLA and PLCL stents regarding (a) heat flow curves and (b) molecular weight distribution.

References

- [1] C. Indolfi, S. De Rosa, and A. Colombo, “Bioresorbable vascular scaffolds—basic concepts and clinical outcome”, *Nature Reviews Cardiology*, vol. 13, no. 12, p. 719, 2016.
- [2] H. Ang, J. Ng, H. Bulluck, P. Wong, S. Venkatraman, Y. Huang, and N. Foin, “Fundamentals of bioresorbable stents”, in *Functionalised Cardiovascular Stents*, Elsevier, 2018, pp. 75–97.
- [3] H. Tamai, K. Igaki, E. Kyo, K. Kosuga, A. Kawashima, S. Matsui, H. Komori, T. Tsuji, S. Motohara, and H. Uehata, “Initial and 6-month results of biodegradable poly-L-lactic acid coronary stents in humans”, *Circulation*, vol. 102, no. 4, pp. 399–404, 2000.
- [4] J. Wiebe, H. M. Nef, and C. W. Hamm, “Current status of bioresorbable scaffolds in the treatment of coronary artery disease”, *Journal of the American College of Cardiology*, vol. 64, no. 23, pp. 2541–2551, 2014.
- [5] G. Perego, G. D. Cella, and C. Bastioli, “Effect of molecular weight and crystallinity on poly (lactic acid) mechanical properties”, *Journal of Applied Polymer Science*, vol. 59, no. 1, pp. 37–43, 1996.
- [6] T. R. Welch, R. C. Eberhart, J. Reisch, and C.-J. Chuong, “Influence of thermal annealing on the mechanical properties of PLLA coiled stents”, *Cardiovascular Engineering and Technology*, vol. 5, no. 3, pp. 270–280, 2014.
- [7] J. Fernandez, A. Etxeberria, and J.-R. Sarasua, “Synthesis, structure and properties of poly (L-lactide-co- ϵ -caprolactone) statistical copolymers”, *Journal of the Mechanical Behavior of biomedical Materials*, vol. 9, pp. 100–112, 2012.
- [8] N. Weir, F. Buchanan, J. Orr, and G. Dickson, “Degradation of poly-L-lactide. part 1: in vitro and in vivo physiological temperature degradation”, *Proceedings of the Institution of Mechanical Engineers, Part H: Journal of Engineering in Medicine*, vol. 218, no. 5, pp. 307–319, 2004.
- [9] S. McMahon, N. Bertollo, E. D. O. Cearbhaill, J. Salber, L. Pierucci, P. Duffy, T. Dürig, V. Bi, and W. Wang, “Bio-resorbable polymer stents: a review of material progress and prospects”, *Progress in Polymer Science*, vol. 83, pp. 79–96, 2018.

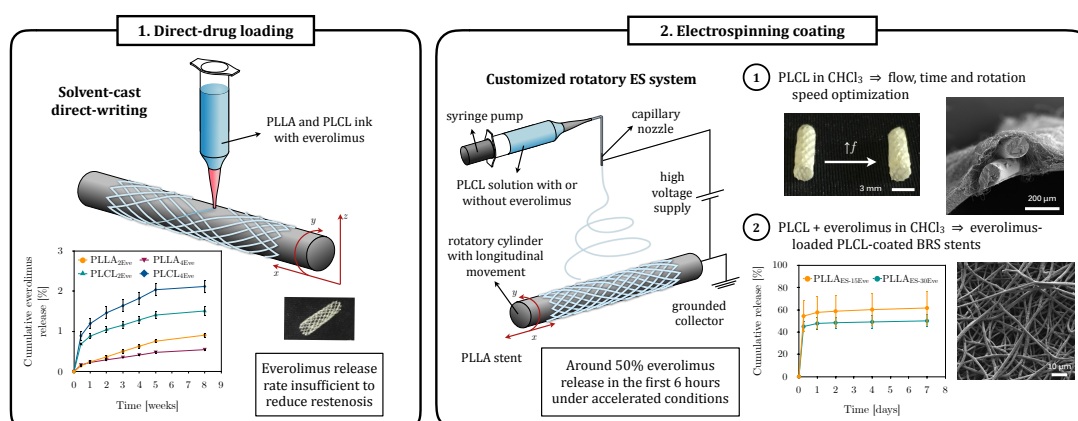
- [10] T. Hu, C. Yang, S. Lin, Q. Yu, and G. Wang, “Biodegradable stents for coronary artery disease treatment: recent advances and future perspectives”, *Materials Science and Engineering: C*, vol. 91, pp. 163–178, 2018.
- [11] K. Garkhal, S. Verma, S. Jonnalagadda, and N. Kumar, “Fast degradable poly(L-lactide-co- ϵ -caprolactone) microspheres for tissue engineering: synthesis, characterization, and degradation behavior”, *Journal of polymer science part A: Polymer chemistry*, vol. 45, no. 13, pp. 2755–2764, 2007.
- [12] C. X. Lam, M. M. Savalani, S.-H. Teoh, and D. W. Huttmacher, “Dynamics of in vitro polymer degradation of polycaprolactone-based scaffolds: accelerated versus simulated physiological conditions”, *Biomedical materials*, vol. 3, no. 3, p. 034 108, 2008.
- [13] L. N. Woodard and M. A. Grunlan, “Hydrolytic degradation of PCL–PLLA semi-IPNs exhibiting rapid, tunable degradation”, *ACS biomaterials science & engineering*, vol. 5, no. 2, pp. 498–508, 2018.
- [14] N. F. Zaaba and M. Jaafar, “A review on degradation mechanisms of polylactic acid: hydrolytic, photodegradative, microbial, and enzymatic degradation”, *Polymer Engineering & Science*, vol. 60, no. 9, pp. 2061–2075, 2020.
- [15] D. Cam, S.-h. Hyon, and Y. Ikada, “Degradation of high molecular weight poly (L-lactide) in alkaline medium”, *Biomaterials*, vol. 16, no. 11, pp. 833–843, 1995.
- [16] N. Vasanthan and O. Ly, “Effect of microstructure on hydrolytic degradation studies of poly (L-lactic acid) by FTIR spectroscopy and differential scanning calorimetry”, *Polymer Degradation and Stability*, vol. 94, no. 9, pp. 1364–1372, 2009.
- [17] N. Weir, F. Buchanan, J. Orr, D. Farrar, and G. Dickson, “Degradation of poly-L-lactide. part 2: increased temperature accelerated degradation”, *Proceedings of the Institution of Mechanical Engineers, Part H: Journal of Engineering in Medicine*, vol. 218, no. 5, pp. 321–330, 2004.
- [18] D. Shi, Y. Kang, G. Zhang, C. Gao, W. Lu, C. Yang, H. Zou, and H. Jiang, “A comparative study on in vitro degradation behavior of PLLA-based copolymer monofilaments”, *Polymer Degradation and Stability*, vol. 158, pp. 148–156, 2018.
- [19] R. Naseem, L. Zhao, S. K. Eswaran, and H. Willcock, “Characterization of biodegradable poly (L-lactide) tube over accelerated degradation”, *Polymer Engineering & Science*, vol. 60, no. 7, pp. 1430–1436, 2020.
- [20] X. Yuan, A. F. Mak, and K. Yao, “Comparative observation of accelerated degradation of poly (L-lactic acid) fibres in phosphate buffered saline and a dilute alkaline solution”, *Polymer degradation and stability*, vol. 75, no. 1, pp. 45–53, 2002.
- [21] G. Gorrasi and R. Pantani, “Hydrolysis and biodegradation of poly(lactic acid)”, in *Synthesis, Structure and Properties of Poly(lactic acid)*. Cham: Springer International Publishing, 2018, ch. 4, pp. 119–151.
- [22] C. M. Agrawal, D. Huang, J. Schmitz, and K. Athanasiou, “Elevated temperature degradation of a 50:50 copolymer of PLA-PGA”, *Tissue engineering*, vol. 3, no. 4, pp. 345–352, 1997.
- [23] B. J. Lambert, T. A. Mendelson, and M. D. Craven, “Radiation and ethylene oxide terminal sterilization experiences with drug eluting stent products”, *Aaps Pharmscitech*, vol. 12, no. 4, pp. 1116–1126, 2011.

- [24] Z. Dai, J. Ronholm, Y. Tian, B. Sethi, and X. Cao, “Sterilization techniques for biodegradable scaffolds in tissue engineering applications”, *Journal of tissue engineering*, vol. 7, p. 2 041 731 416 648 810, 2016.
- [25] N. P. Tipnis and D. J. Burgess, “Sterilization of implantable polymer-based medical devices: a review”, *International journal of pharmaceuticals*, vol. 544, no. 2, pp. 455–460, 2018.
- [26] N. Weir, F. Buchanan, J. Orr, D. Farrar, and A. Boyd, “Processing, annealing and sterilisation of poly-L-lactide”, *Biomaterials*, vol. 25, no. 18, pp. 3939–3949, 2004.
- [27] J.-P. Nuutinen, T. Välimaa, C. Clerc, and P. Törmälä, “Mechanical properties and in vitro degradation of bioresorbable knitted stents”, *Journal of Biomaterials Science, Polymer Edition*, vol. 13, no. 12, pp. 1313–1323, 2002.
- [28] M. Haim Zada, A. Kumar, O. Elmalak, G. Mechrez, and A. J. Domb, “Effect of ethylene oxide and gamma (γ -) sterilization on the properties of a PLCL polymer material in balloon implants”, *ACS omega*, vol. 4, no. 25, pp. 21 319–21 326, 2019.
- [29] C. West, R. McTaggart, T. Letcher, D. Raynie, and R. Roy, “Effects of gamma irradiation upon the mechanical and chemical properties of 3D-printed samples of polylactic acid”, *Journal of Manufacturing Science and Engineering*, vol. 141, no. 4, 2019.
- [30] N. Grabow, M. Schlun, K. Sternberg, N. Hakansson, S. Kramer, and K.-P. Schmitz, “Mechanical properties of laser cut poly (L-lactide) micro-specimens: implications for stent design, manufacture, and sterilization”, *Journal of biomechanical engineering*, vol. 127, no. 1, pp. 25–31, 2005.
- [31] I. Mendieta-Barrañon, O. A. Chanes-Cuevas, M. A. Álvarez-Pérez, P. González-Alva, L. A. Medina, M. Aguilar-Franco, and J. Serrano-Bello, “Physicochemical and tissue response of PLA nanofiber scaffolds sterilized by different techniques”, *Odovtos-International Journal of Dental Sciences*, vol. 21, no. 3, pp. 77–88, 2019.
- [32] R. Van Lith, E. Baker, H. Ware, J. Yang, A. C. Farsheed, C. Sun, and G. Ameer, “3D-printing strong high-resolution antioxidant bioresorbable vascular stents”, *Advanced Materials Technologies*, vol. 1, no. 9, p. 1 600 138, 2016.
- [33] S. A. Park, S. J. Lee, K. S. Lim, I. H. Bae, J. H. Lee, W. D. Kim, M. H. Jeong, and J.-K. Park, “In vivo evaluation and characterization of a bio-absorbable drug-coated stent fabricated using a 3D-printing system”, *Materials Letters*, vol. 141, pp. 355–358, 2015.
- [34] S. J. Lee, H. H. Jo, K. S. Lim, D. Lim, S. Lee, J. H. Lee, W. D. Kim, M. H. Jeong, J. Y. Lim, I. K. Kwon, *et al.*, “Heparin coating on 3D printed poly (l-lactic acid) biodegradable cardiovascular stent via mild surface modification approach for coronary artery implantation”, *Chemical Engineering Journal*, vol. 378, p. 122 116, 2019.
- [35] A. J. Guerra and J. Ciurana, “3D-printed bioabsorbable polycaprolactone stent: the effect of process parameters on its physical features”, *Materials & Design*, vol. 137, pp. 430–437, 2019.
- [36] A. J. Guerra, P. Cano, M. Rabionet, T. Puig, and J. Ciurana, “3D-printed PCL/PLA composite stents: Towards a new solution to cardiovascular problems”, *Materials*, vol. 11, no. 9, p. 1679, 2018.
- [37] V. Chausse, R. Schieber, Y. Raymond, B. Ségry, R. Sabaté, K. Kolandaivelu, M.-P. Ginebra, and M. Pegueroles, “Solvent-cast direct-writing as a fabrication strategy for radiopaque stents”, *Additive Manufacturing*, p. 102 392, 2021.

- [38] ISO 25539-2, *Cardiovascular implants. endovascular devices. part 1: vascular stents*. International Organization for Standardization, 2012.
- [39] E. Fischer, H. J. Sterzel, and G. Wegner, “Investigation of the structure of solution grown crystals of lactide copolymers by means of chemical reactions”, *Kolloid-Zeitschrift und Zeitschrift für Polymere*, vol. 251, no. 11, pp. 980–990, 1973.
- [40] ISO 13485, *Medical devices — quality management systems — requirements for regulatory purposes*, International Organization for Standardization, 2016.
- [41] ISO 11137, *Sterilization of health care products — radiation — requirements for development, validation and routine control of a sterilization process for medical devices — establishing the sterilization dose — guidance on dosimetric aspects of development, validation and routine control*, International Organization for Standardization, 2018.
- [42] ISO 11135, *Sterilization of health-care products — ethylene oxide — requirements for the development, validation and routine control of a sterilization process for medical devices*, International Organization for Standardization, 2014.
- [43] S. Teixeira, K. M. Eblagon, F. Miranda, M. F. R. Pereira, and J. L. Figueiredo, “Towards controlled degradation of poly (lactic) acid in technical applications”, *C*, vol. 7, no. 2, p. 42, 2021.
- [44] T. Casalini, F. Rossi, A. Castrovinci, and G. Perale, “A perspective on polylactic acid-based polymers use for nanoparticles synthesis and applications”, *Frontiers in bioengineering and biotechnology*, vol. 7, p. 259, 2019.
- [45] J. Anderson, “Perspectives on the in vivo responses of biodegradable polymers”, *Biomedical applications of synthetic biodegradable polymers*, pp. 223–233, 1995.
- [46] D. Farrar, “Modelling of the degradation process for bioresorbable polymers”, in *Degradation rate of bioresorbable materials*, Elsevier, 2008, pp. 183–206.
- [47] C. G. Pitt and G. Zhong-wei, “Modification of the rates of chain cleavage of poly (ϵ -caprolactone) and related polyesters in the solid state”, *Journal of Controlled Release*, vol. 4, no. 4, pp. 283–292, 1987.
- [48] S. I. Jeong, B.-S. Kim, S. W. Kang, J. H. Kwon, Y. M. Lee, S. H. Kim, and Y. H. Kim, “In vivo biocompatibility and degradation behavior of elastic poly (l-lactide-co- ϵ -caprolactone) scaffolds”, *Biomaterials*, vol. 25, no. 28, pp. 5939–5946, 2004.

Solvent-cast direct-writing and electrospinning as a dual fabrication strategy for drug-eluting polymeric bioresorbable stents

Bioresorbable stents (BRS) are conceived to retain sufficient radial strength after implantation while releasing an antiproliferative drug in order to prevent vessel restenosis until complete resorption. Ongoing research trends involve the use of innovative manufacturing techniques to achieve thinner struts combined with optimized local drug delivery. This work presents a combination of solvent-cast direct-writing (SC-DW) and electrospinning (ES) using poly-L-lactic acid (PLLA) and poly(L-lactic-co- ϵ -caprolactone) (PLCL) as a new approach to generate everolimus-eluting BRS for cardiovascular applications. A Design of Experiment (DoE) was conducted to determine the optimal parameters to obtain a homogeneous coating with high specific surface. Manufactured stents were characterized by means of mechanical tests and scanning electron microscopy (SEM), with everolimus release in accelerated conditions quantified through High Performance Liquid Chromatography (HPLC). Drug loading was achieved either encapsulated in the struts of the stent or in an electrospun PLCL membrane covering the stent. In the former case, everolimus release was found to be insufficient, less than 3% of total drug loading after 8 weeks. In the latter, everolimus release considerably increased with respect to drug-loaded 3D-printed stents, with over 50% release in the first 6 hours of the test. In conclusion, everolimus release from PLCL-coated 3D-printed stents would match the dose and timeframe required for *in vivo* applications, while providing thinner struts than SC-DW drug-loaded stents.



V. Chausse, E. Casanova-Batlle, C. Canal, M.-P. Ginebra, J. Ciurana, M. Pegueroles, *Solvent-cast direct-writing and electrospinning as a dual fabrication strategy for drug-eluting polymeric bioresorbable stents* (under revision in Additive Manufacturing).

5.1 Introduction

The development of drug-eluting stents (DES) constituted a revolution in stent conceptualization. DES loaded with antirestenotic drugs to avoid the overproliferation of smooth muscle cells (SMCs) provided localised drug delivery directly to the affected lesion in high concentrations [1, 2]. When compared to bare metal stents, restenosis rate decreased from 36.3% down to 8.9% ($p < 0.001$) at 9 month follow-up [3]. Initially, two antiproliferative drugs showed significant efficacy in clinical trials: sirolimus and paclitaxel [4, 5]. Sirolimus is an antibiotic which causes an inhibition of the immune response through inhibition of T-lymphocyte activation, and also has an antiproliferative effect on SMCs [6]. Paclitaxel is an antineoplastic drug with an effect on stabilising the microtubules during mitosis, therefore inhibiting cell cycle and the proliferation of SMCs [7]. Nevertheless, although DES significantly reduced in-stent restenosis, delayed arterial healing accompanied by denuded exposure of the biomaterial to the bloodstream led to increased risk of late stent thrombosis with a rate as high as 9.4% at 5 years [8]. This was related to the fact that antiproliferative drugs inhibited endothelial cells (ECs) proliferation at the same concentration required to inhibit SMCs proliferation [9, 10], thus hindering endothelium recovery.

In order to overcome the limitations of DES, bioresorbable stents (BRS) were developed with the aim to provide a transient support for the endothelium to heal. Ideally, stents would retain sufficient radial strength after implantation to prevent acute vessel recoil while releasing the antiproliferative drug [11]. After the healing period, they would degrade and be resorbed completely, leaving an open vessel with a healthy endothelium [12]. Nonetheless, BRS without drugs were associated with neointimal hyperplasia, therefore suggesting the indispensability of drug loading to enable clinical application [13]. Although the majority of BRS in development use sirolimus as antiproliferative drug, other stents have been loaded with alternative drugs from the same family such as myolimus and everolimus [14, 15]. Everolimus is more lipophilic than sirolimus due to its chemical structure and therefore it is more swiftly absorbed in the arterial wall [16].

Regarding drug loading strategies, drugs may be physically entrapped during the material synthesis process or deposited on the surface, either unspecifically adsorbed, covalently linked or attached by physical interactions [17]. Release kinetics has a significant role in the revascularization of the artery wall, and rapid vs slow drug release offers advantages and drawbacks. In some cases, the restenotic process is still active several months after implantation and only stents with long drug release could prevent this phenomenon. However, a slower release profile would in turn delay endothelialization for longer time and late stent thrombosis may occur [18]. Overall, a drug release time of about 3 months with the appropriate dose constitutes a good

compromise between short- and long-term kinetics [15]. Therefore, the release profile must be stable in time, and that is why physical entrapment is the preferred drug loading technique, as the drug diffuses following matrix erosion [17].

Nevertheless, drug-loaded BRS may present altered mechanical properties with respect to the polymeric material alone, and also different degradation mechanisms. This is the reason why drugs are sometimes loaded in a polymeric coating, different from the core of the stent [19]. For instance, the Absorb stent (BVS, Abbott Vascular, USA) consisted of a platform made of semi-crystalline poly-L-lactic acid (PLLA) with a 2-4 μm coating of poly-D,L-lactic acid containing everolimus [15]. On the other hand, this coating may also affect the degradation timeframe of the stent [13].

Concerning BRS manufacturing, recent advances in additive manufacturing (AM) may facilitate drug loading approaches [14]. On the one hand, fused deposition modelling (FDM) requires a thermoplastic material but high temperature conditions hamper the addition of drugs to the polymer as they may degrade. On the other hand, solvent-cast direct-writing (SC-DW), where a polymer is dissolved in a solvent and extruded through pressure-assisted microsyringes, allows for the loading of drugs to the polymeric ink without the limitations of FDM, as the procedure can be performed at room temperature.

Drug-eluting stents are generally obtained by coating bare metal stents (BMS) with drug-loaded polymers through dip coating or spray coating [20]. These approaches have been used for a combined paclitaxel and sirolimus release from a biodegradable bilayer coating for endovascular stents [21], everolimus-eluting self-assembled monolayers for DES [22], BMS coated by means of an ultrasonic spray with sirolimus-loaded poly(D,L)-lactide-co-glycolide (PLGA) grafted with poly ethylene glycol [23], or stainless steel 316L BMS coated with a sirolimus-containing polymer using electrospray [24]. Finally, Liu *et al.* spray coated a poly(ϵ -caprolactone) (PCL) stent with paclitaxel to obtain a drug-eluting BRS [25].

Besides, electrospinning (ES) appears as a versatile technique in terms of polymer and drug choice to obtain nanofibers (NFs) with high specific area for biomedical applications. Recent advances in the use of ES in stent manufacturing include polyurethane electrospun NFs on BMS for treating cerebral aneurysms [26], paclitaxel-loaded PCL electrospun covered stents for benign cardiac stricture [27], rosuvastatin-loaded PLGA electrospun fibers on a BMS to accelerate re-endothelialization and inhibit neointimal hyperplasia [28], paclitaxel-loaded silica nanoparticles within electrospun PLA fibers on a BMS [29], chitosan-based NFs loaded with simvastatin on Nitinol stents for restenosis prevention [30], and sirolimus-loaded methylacrylated gelatin-polyethylene glycol diacrylate with polycaprolactone composite NFs on 316L stainless steel stents to prevent in-stent restenosis [31]. Finally, a different approach was performed by Guerra *et al.*

by engineering electrospun tubular PCL scaffolds for stenting applications, without the use of BMS as a support [32]. Nevertheless, to the best of our knowledge, the manufacturing of drug-eluting electrospun-covered 3D-printed bioresorbable stents has never been reported.

To overcome the different limitations discussed, this work presents a combination of SC-DW and ES to generate new drug-eluting PLLA and poly(L-lactic-co- ϵ -caprolactone) (PLCL) BRS for cardiovascular applications. 3D-printed stents by SC-DW technique loaded with everolimus were manufactured and characterized by means of scanning electron microscopy (SEM) and mechanical tests. Alternatively, a customized rotatory ES system was used in order to coat PLLA 3D-printed stents with a thin polymeric membrane of PLCL electrospun fibers. A Design of Experiment (DoE) was conducted to determine the parameters necessary for optimal homogeneous coating. Finally, everolimus/PLCL-coated 3D-printed stents were obtained, and the release of everolimus was quantified with High Performance Liquid Chromatography (HPLC).

5.2 Materials and methods

5.2.1 Chemicals and materials

Medical grade PLLA (Purasorb[®] PL 65; inherent viscosity 6.5 dL/g, $M_w = 1,675,000$ g/mol) and PLCL (Purasorb[®] PLC 9538, 95:5 lactic-to-caprolactone molar ratio, 3.8 dL/g, $M_w = 700,000$ g/mol) were purchased from Corbion (Netherlands). Triton X-405 (Acros Organics, Belgium), potassium dihydrogen phosphate (PanReac AppliChem ITW Reagents, Germany), potassium hydrogen phosphate trihydrate (Sigma-Aldrich, USA), ammonium acetate (Sigma-Aldrich, USA), acetonitrile (ACN, PanReac AppliChem ITW Reagents, Germany) and chloroform ($\geq 99.5\%$, Sigma-Aldrich, USA) were used as received.

5.2.2 3D Printing of stents

SC-DW was used to manufacture PLLA and PLCL stents as described in Chausse *et al.* [33] (Figure 5.1). Briefly, PLLA or PLCL pellets were dissolved in chloroform at a 10% or 12.5% ratio (w/v), respectively, in order to obtain printable inks. The 3D printer (BCN 3D+, BCN 3D technologies, Spain) was modified by substituting its y axis for a 3-mm in diameter rotating mandrel to allow for tubular printing using a 250 μm nozzle (Optimum[®] SmoothFlow[™], Nordson, USA). Stents design followed rhombic cell structure, with 30 mm in length, 3 mm in diameter and 10 peaks. After printing, stents underwent a thermal treatment at 80 °C for 12 hours. Inks were further modified with the addition of the antiproliferative drug everolimus at 2 wt.% and 4 wt.% with respect

to polymer content to obtain everolimus-loaded stents, labeled as PLLA_{2Eve}, PLLA_{4Eve}, PLCL_{2Eve} and PLCL_{4Eve}. The quantity of everolimus was chosen to be in agreement with the amount of everolimus present in commercially available everolimus-eluting stents [15].

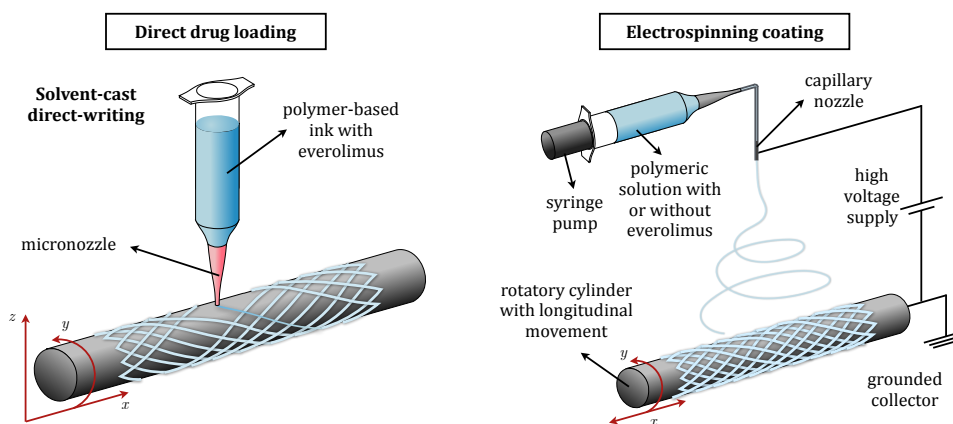


Fig. 5.1 Scheme of the two drug-loading techniques applied in this project. Printing setup for everolimus-loaded stents, where the drug is dissolved in the polymeric ink (left) and combination of SC-DW and ES to obtain everolimus/PLCL-coated PLLA stents (right).

5.2.3 ES coating of stents

An alternative drug-loading method was developed by means of ES by dissolution of PLCL pellets in chloroform and ethanol (7:3 ratio) at 6.25% (w/v). 3D-printed PLLA stents were mounted onto a grounded collector mandrel showing both rotation and longitudinal movement (Figure 5.1). A DoE employing the central composite design (6 centre points*, alpha 1.682 and 3 replicas) was conducted to evaluate effects of flow (f : 0.35 – 1 mL/h), time (t : 90 – 180 s) and rotation speed (s : 5.33 – 10.67 rpm) on material deposition, membrane thickness, fiber diameter and fiber orientation. Thus, 66 stents were coated (Table 5.1) with a G20 needle. The rest of the ES parameters were fixed throughout the experiment as follows: longitudinal speed was set to 2.5 mm/s, distance from nozzle to collector at 90 mm and operating voltage at 9 kV. Stents were weighed before and after ES coating and examined under SEM to measure membrane thickness, fiber diameter and fiber orientation. Each condition was tested in triplicate. The optimal parameters required for optimal homogeneous coating were derived with the aim to obtain fibers with the highest possible surface area for drug release purposes.

Once the optimal parameters were determined, ES solution was modified by the addition of everolimus at a ratio of 15 wt.% and 30 wt.% with respect to PLCL content in order to match the quantity of everolimus present in everolimus-loaded 3D-printed stents. Stents were coated at a flow of 0.8 mL/h for 125 s time and rotation speed of 8 rpm.

Tab. 5.1 Design of Experiment. ES-coated samples as a function of flow (f), time (t) and rotation speed (s) ($n = 3$).

Sample	Flow [mL/h]	Time [s]	Rotation speed [rpm]
1	0.35	90	5.33
2	2	90	5.33
3	0.35	90	10.67
4	1	90	10.67
5	0.35	180	5.33
6	1	180	5.33
7	0.35	180	10.67
8	1	180	10.67
9	0.675	59.32	8
10	0.675	210.68	8
11	0.675	135	3.51
12	0.675	135	12.49
13	0.128	135	8
14	1.222	135	8
15	0.675	135	8
16	0.675	135	8
17	0.675	135	8
18	0.675	135	8
19	0.675	135	8
20	0.675	135	8
21	0.675	135	8
22	0.675	135	8

The obtained everolimus-loaded PLCL-coated PLLA stents were characterized with SEM and labeled as PLLA_{ES-15Eve} and PLLA_{ES-30Eve}.

5.2.4 Stents characterization

Microscopy

Microscope Olympus BX51 (Olympus, Japan) was used to visually inspect printed stents and to measure their strut thickness (AnalySIS Docu, Olympus, Japan). For SEM visualization, stents were either sputtered with carbon and examined using Phenom XL (PhenomWorld, USA) at an operating voltage of 5 kV or with platinum–palladium (80:20) and examined using JEOL JSM-7001F (Jeol, Japan) at 2 kV acceleration voltage. Subsequent analysis of fiber distribution was performed with ImageJ Directionality plugin. As a result, a histogram of orientations was obtained, with the highest peak, if present, fitted by a Gaussian function and given as mean \pm standard deviation.

Mechanical properties

Stents' radial strength after everolimus-loading was analyzed with a compression resistance parallel plate test. Stents ($n = 5$) were compressed using a rheometer (Discovery HR-2, TA instruments, USA) equipped with a load cell of 50 N, having the upper plate advance towards the lower plate at a rate of 1 mm/min following ISO 25539-2 [34]. Radial force was noted at 50% reduction in diameter and normalized

by stent length (N/mm). Using final and initial diameter, stent elastic recovery was calculated as its ratio, in percentage.

5.2.5 In vitro accelerated everolimus release study

Everolimus release was evaluated by incubation of everolimus-loaded stents in 5 mL of release medium (0.7% Triton X-405 in 0.01 M potassium phosphate buffer pH 6 at 37 °C in 7% ACN), which was replaced by fresh medium at selected time points [35, 36]. For SC-DW drug-loaded PLLA_{2Eve}, PLLA_{4Eve}, PLCL_{2Eve} and PLCL_{4Eve}, everolimus release was monitored for 8 weeks. Retrieved stents were characterized by SEM and mechanical compression tests to study changes in surface appearance or mechanical properties, respectively. In the case of ES-coated PLLA_{ES-15Eve} and PLLA_{ES-30Eve}, the assay spanned 7 days, and SEM was used to monitor surface appearance.

The release of everolimus in medium was quantified using reversed-phase HPLC (Prominence XR, Shimadzu, Japan) equipped with a LC-20AD pump, a SIL-20AC cooling autosampler, a CTO-10AS column oven and a SPD-M20A photodiode array detector. A reversed-phase XBridge (Waters) C18 (4.6 × 100 mm, 3.5 μm) column was used. Analyte separation was achieved under isocratic conditions using a mobile phase of acetonitrile:ammonium acetate (pH 6.8; 0.02 M) (70:30) at a flow rate of 0.6 mL/min and maintained 50 °C. Injection volume was 50 μL and optimal wavelength for everolimus determination was 278 nm. In parallel, a calibration curve of well-known everolimus concentrations, from 0.05 μg/mL up to 50 μg/mL, was performed for each analytical run and used to calculate the concentrations of everolimus in the unknown samples.

5.2.6 Statistical analysis

Statistical analysis was performed using Minitab software (Minitab Inc., USA). An equality of variances test (ANOVA) with Tukey post-hoc test was used to determine statistically significant differences ($p < 0.05$ between the different groups and 95% confidence interval) for normally-distributed data. All data are represented as mean values ± standard deviation (SD).

5.3 Results

5.3.1 Everolimus-loaded PLLA and PLCL stents

Control PLLA and PLCL stents were successfully obtained by SC-DW. Dissolution of everolimus (2 and 4 wt.%) in the chloroform-based polymeric solutions rendered inks with printability equivalent to the original inks. Everolimus-loaded stents were obtained

without further 3D-printing parameter optimization. Figure 5.2a shows an image of the obtained stents, with everolimus-loaded stents looking visually indistinguishable from control stents. However, analysis under the microscope revealed a significant increase in strut thickness, from $132.2 \pm 7.1 \mu\text{m}$ up to over $180 \mu\text{m}$ for PLLA, and from $134.0 \pm 5.3 \mu\text{m}$ to over $210 \mu\text{m}$ for PLCL (Figure 5.2b).

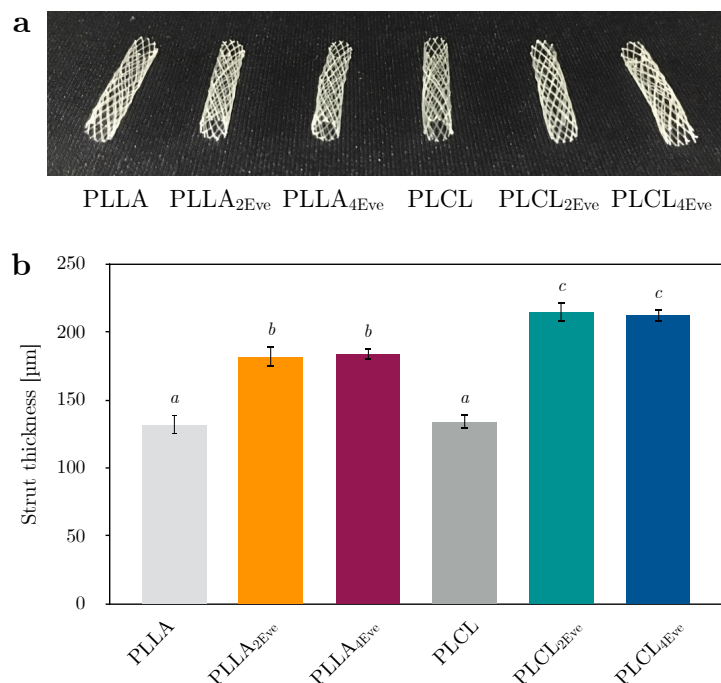


Fig. 5.2 3D-printed everolimus-loaded PLLA and PLCL stents. (a) Stents external appearance. (b) Stents strut thickness. Conditions *a*, *b* and *c* are statistically different ($p < 0.05$).

Further examination under SEM showed no signs of everolimus crystals on the surface of the stents, with all of them presenting a very similar surface morphology characterized by the presence of shallow micropores (Figure 5.3a). Mechanical characterization of printed stents showed no significant changes in terms of compression force at 50% deformation for everolimus-loaded stents with respect to control PLLA or PLCL stents (Figure 5.3b), with values ranging from 0.08 N/mm to 0.11 N/mm. Similarly, the addition of everolimus did not result in detrimental elastic properties, as elastic recovery was found to be above 95% for all tested conditions.

Regarding everolimus release quantification with HPLC, Figure 5.S1a presents representative chromatograms of everolimus in release medium (0.7% Triton X-405 in 0.01 M potassium phosphate buffer pH 6 in 7% ACN) at different concentrations to perform the calibration curve. The initial broad peak was attributed to Triton X-405 [36, 37], with everolimus eluting at a retention time of 6.51 minutes and its isomer at 7.29 minutes. The calibration curves with concentration versus peak area were plotted. Upon linear regression analysis, the regression line fitted with $R^2 > 0.99$ (Figure 5.S1b). The concentrations of everolimus in the release medium were calculated from the calibration

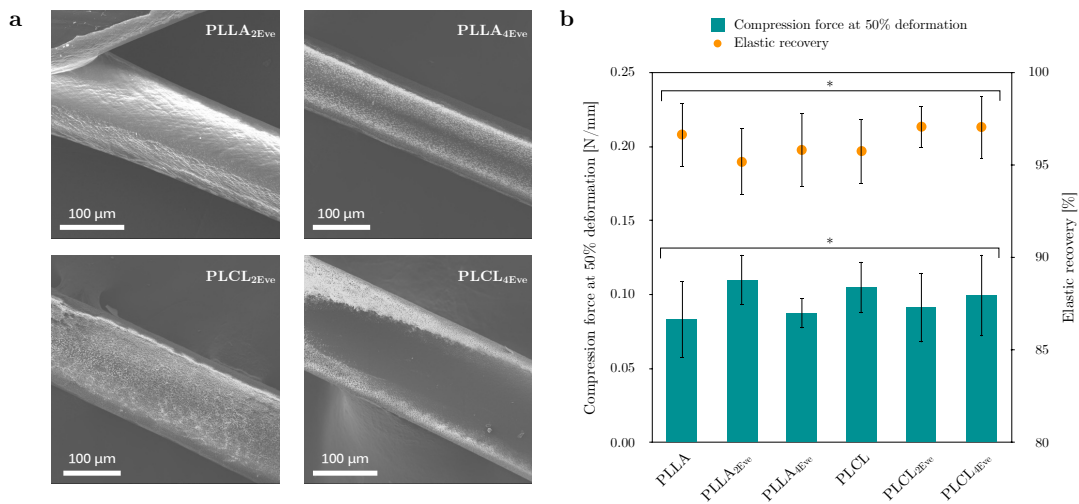


Fig. 5.3 3D-printed everolimus-loaded PLLA and PLCL stents. (a) Surface morphology under SEM. (b) Compression force at 50% deformation (left axis, bars) and elastic recovery (right axis, dots) for everolimus-loaded stents. Conditions with an asterisk are statistically equivalent ($p > 0.05$).

curves for each time point. Figure 5.4a presents total cumulated release, with PLCL_{4Eve} showing the highest release, over 7 μg after 8 weeks time (corresponding to 2% release). Everolimus release into the receptor media was found to be greater for PLCL stents than for PLLA stents. For those loaded with higher amounts of drug (4 wt.%), everolimus release was found to be increased. The release profile was characterized by an initial burst release followed by a linear stabilization starting from week 2 until reaching a plateau after week 5. Nevertheless, when normalizing drug release with respect to the actual drug loading, it can be seen that total release over 2 months accounts only for just 2% of the initial drug loaded in the case of PLCL_{4Eve} (Figure 5.4b).

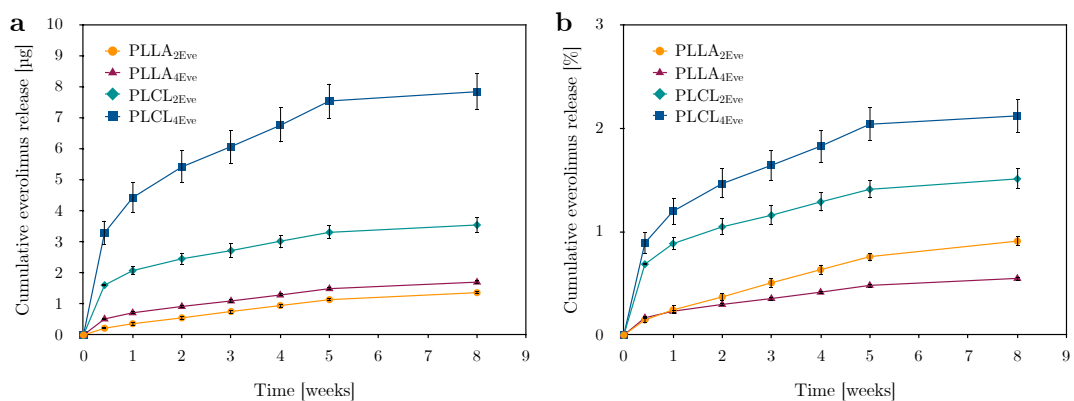


Fig. 5.4 Everolimus release from PLLA and PLCL stents immersed in release media for 8 weeks time, (a) in absolute numbers and (b) normalized to the drug loading of each stent, in percentage.

Stents immersed in release medium over 4 or 8 weeks presented no apparent surface alterations, as shown in Figure 5.5a. Both PLLA and PLCL stents with 2 or 4 wt.% everolimus content displayed a heterogeneous distribution of micropores as found

for as-printed stents. No traces of everolimus residuals were visible on the stents' surface. Regarding mechanical properties, compression assays of stents before and after immersion revealed that stents retained their compression strength even after 8 weeks immersion time (Figure 5.5b), with no differences among conditions. Likewise, elastic recovery was maintained throughout the immersion period, as shown in Figure 5.5c.

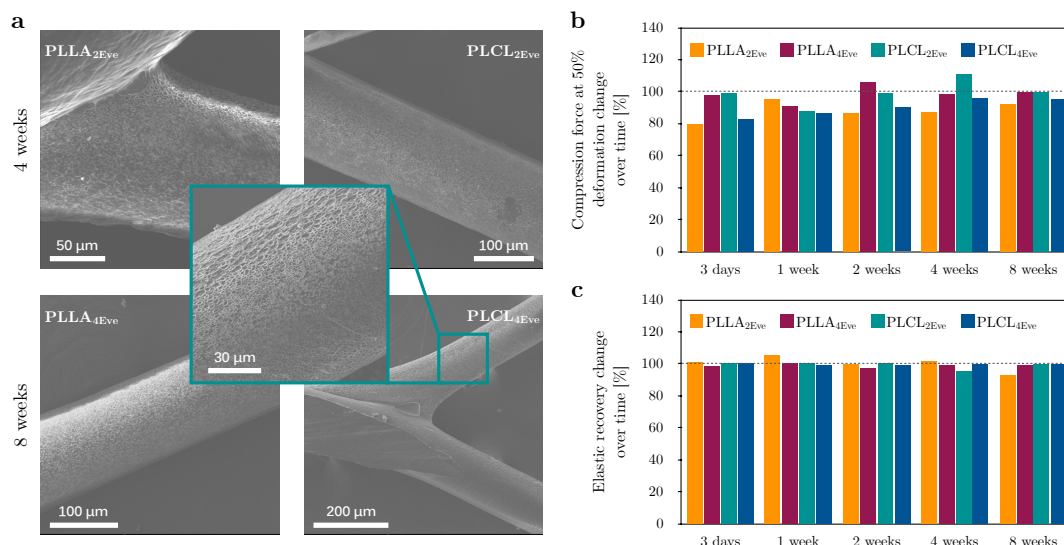


Fig. 5.5 Everolimus-loaded PLLA and PLCL stents immersed for up to 8 weeks in drug release media. (a) SEM pictures of samples after 4 and 8 weeks immersion time. (b) Compression force at 50% deformation and (c) elastic recovery of stents after different times of immersion, normalized to initial values before immersion and given in %.

5.3.2 ES coating of stents

3D-printed stents were successfully coated with a membrane of electrospun PLCL fibers. The coating process commences at the voids left in between stent struts, as they are insulating and the fibers preferentially deposit onto the conductive rotating mandrel, as shown in Figure 5.6a. Only after the voids were filled, a homogenous and continuous membrane coating was formed throughout the abluminal surface of the stent (Figure 5.6b), with PLCL fibers of diameter in the range of the micrometers (Figure 5.6c).

Three design parameters were identified to conduct a DoE: flow, time and rotation speed. Figure 5.6d shows the coated samples as a function of the design parameters. By visual inspection, no apparent differences were found in terms of coating homogeneity regarding flow and rotation speed extreme values, whereas stents coated for a low period of time presented only partial coverage. Upon SEM examination, the cross-section of the stents revealed that denser meshes were obtained for increasing rotation speeds. Regarding flow, no clear correlation was found in terms of membrane coverage for increasing flow rate.

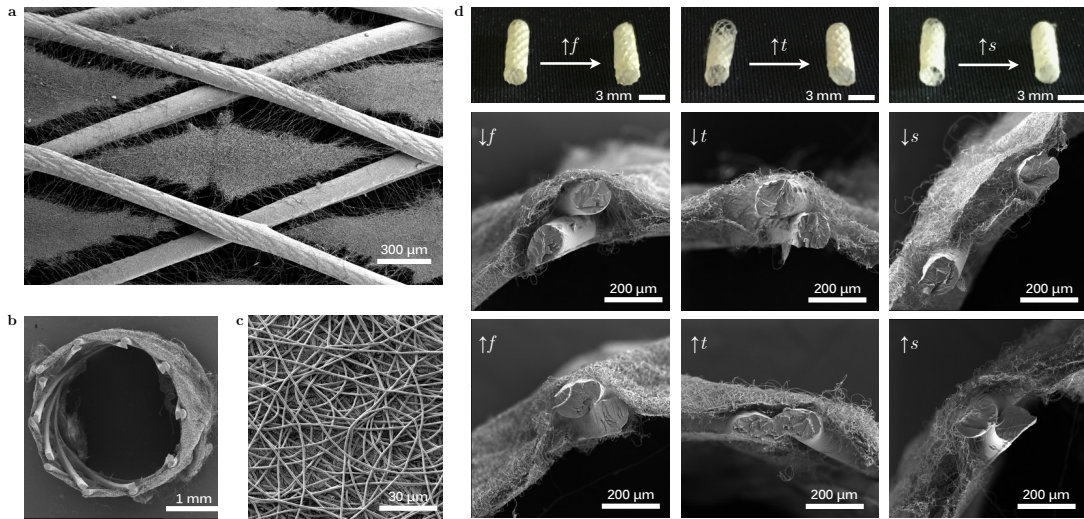


Fig. 5.6 PLLA stents with ES coating. (a) ES process with incomplete coating, showing PLCL fibers initial deposition onto the metallic collector in between stent struts. (b) Stent cross-section showing homogeneous electrospun membrane coating covering the abluminal surface of the stent. (c) PLCL fibers detail, with diameter in the range of the micrometers. (d) Coated stents at different tested parameters, from left to right, at increasing flow (f), time (t) and rotation speed (s). Below, stent cross sections corresponding to parameters with low (top) and high (bottom) parameter values.

The effects of processing parameters on material deposition, membrane thickness, fiber diameter and orientation for PLCL-coated PLLA stents without everolimus are presented in Table 5.2. Material deposition ranged from a minimum of 0.30 mg up to 1.23 mg and membrane thickness from 19.81 μm to 70.70 μm . Fiber diameter was found to be around 1 μm for all conditions, ranging from 0.84 μm to 1.16 μm . Regarding fiber orientation, Figure 5.S2 presents the polar histograms obtained by analyzing the directions in which fibers were aligned. In general, one can perceive a preferential alignment in the 0° – 180° axis, that is, along the longitudinal direction of the stents.

Material deposition was strongly influenced by time, obtaining more electrospun PLCL fibers onto 3D-printed stents with increasing time and flow, as shown in Figure 5.7a, up to 1 mg. Equation 5.1 describes material deposition in mass as a function of flow (f), time (t) and rotation speed (s).

$$\begin{aligned}
 \text{Material deposition } (f, t, s) = & -0.000325 + 0.000108s + 0.0007227f \\
 & + 2.8812 \cdot 10^{-6}t - 1.1947 \cdot 10^{-5}s^2 \\
 & - 0.0011968f^2 + 7.629 \cdot 10^{-7}st \\
 & + 6.8376 \cdot 10^{-6}ft - 3.0419 \cdot 10^{-8}t^2
 \end{aligned} \tag{5.1}$$

Tab. 5.2 Material deposition, membrane thickness, fiber diameter and preferential fiber orientation, with 0° indicating the longitudinal direction of the stent, as a function of design parameters ($n = 3$), for PLCL-coated PLLA stents without everolimus.

Sample	Material deposition [mg]	Membrane thickness [μm]	Fiber diameter [μm]	Fiber orientation [°]
1	0.57 ± 0.21	20.91 ± 2.63	0.98 ± 0.05	-10.0 ± 23.5
2	0.37 ± 0.12	18.91 ± 5.58	0.96 ± 0.06	./.
3	0.43 ± 0.12	25.05 ± 5.20	0.96 ± 0.04	-13.5 ± 60.0
4	0.30 ± 0.10	13.32 ± 11.54	0.84 ± 0.14	-8.0 ± 19.7
5	0.70 ± 0.30	37.98 ± 11.95	0.90 ± 0.11	-9.3 ± 30.6
6	0.93 ± 0.21	49.99 ± 2.18	1.09 ± 0.07	-9.0 ± 22.2
7	0.97 ± 0.15	48.25 ± 4.48	0.90 ± 0.13	./.
8	1.20 ± 0.26	70.70 ± 2.42	1.16 ± 0.10	-15.3 ± 25.2
9	0.53 ± 0.15	19.81 ± 4.77	0.99 ± 0.06	-16.8 ± 55.3
10	1.23 ± 0.06	41.24 ± 3.17	1.10 ± 0.10	./.
11	0.70 ± 0.17	43.64 ± 13.80	0.97 ± 0.10	-11.2 ± 56.9
12	0.93 ± 0.25	34.57 ± 4.57	0.97 ± 0.07	3.0 ± 33.2
13	0.70 ± 0.17	28.54 ± 8.43	1.00 ± 0.10	-2.5 ± 27.8
14	0.70 ± 0.00	30.72 ± 11.45	1.01 ± 0.06	-3.4 ± 17.7
15	1.10 ± 0.20	28.11 ± 4.71	1.08 ± 0.04	-26.0 ± 36.7
16	0.93 ± 0.23	36.79 ± 10.78	0.99 ± 0.18	-8.5 ± 24.9
17	0.97 ± 0.15	49.61 ± 7.06	1.11 ± 0.18	-15.5 ± 40.0
18	1.03 ± 0.15	41.32 ± 16.15	0.93 ± 0.10	./.
19	1.03 ± 0.21	34.33 ± 1.64	0.93 ± 0.05	-12.7 ± 24.6
20	0.97 ± 0.21	33.41 ± 3.90	0.93 ± 0.01	./.
21	0.93 ± 0.29	27.29 ± 3.95	0.88 ± 0.11	-7.7 ± 23.3
22	1.00 ± 0.20	28.87 ± 8.41	0.92 ± 0.11	1.6 ± 25.1
Mean	0.83 ± 0.30	34.70 ± 16.09	0.98 ± 0.16	-6.8 ± 21.3

A similar effect was found for membrane thickness (Figure 5.7b), with a maximum for increasing time and flow of around 60 μm . Equation 5.2 parametrizes membrane thickness as a function of flow, time and rotation speed.

$$\begin{aligned} \text{Membrane thickness } (f, t, s) = & 55.373 - 3.306s - 43.064f \\ & - 0.216t + 0.0284st + 0.3682ft \end{aligned} \quad (5.2)$$

Regarding fiber diameter, a range between 800 nm and 1.2 μm was obtained as a function of flow and time, with rotation speed showing no influence on fiber diameter (Figure 5.7c). Equation 5.3 shows fiber diameter as a function of flow and time.

$$\begin{aligned} \text{Fiber diameter } (f, t) = & 1.2825 - 0.6033f \\ & - 0.0026t + 0.0050ft \end{aligned} \quad (5.3)$$

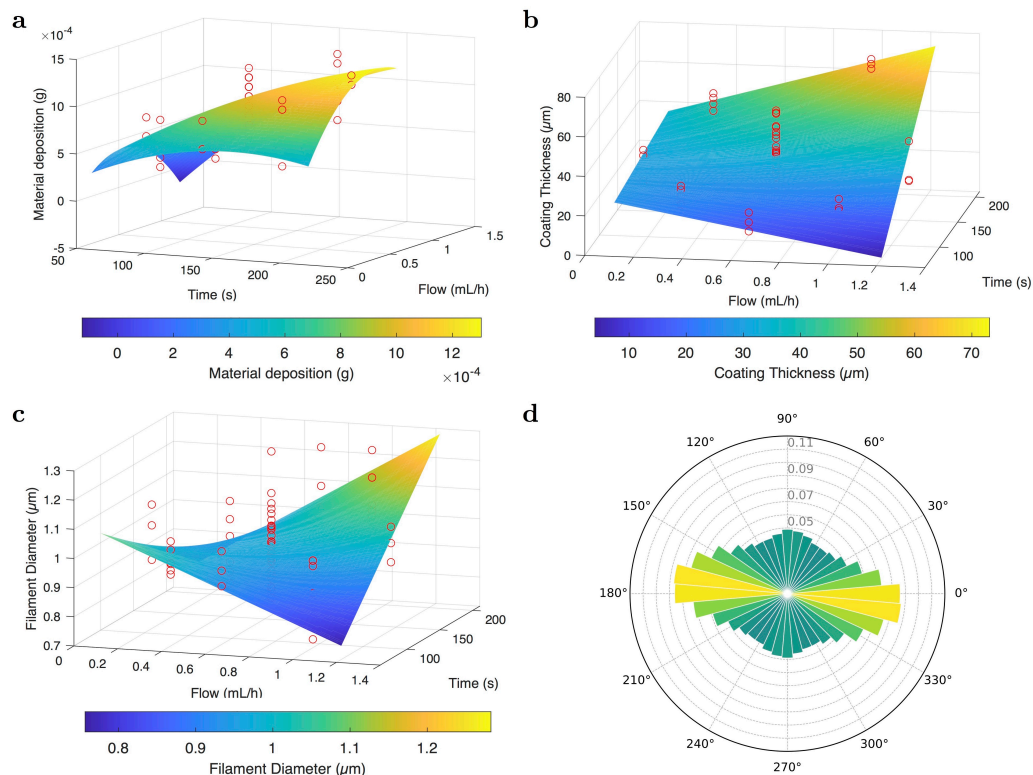


Fig. 5.7 ES coating optimization through Design of Experiment. (a) PLCL fiber deposition onto 3D-printed stents, (b) membrane thickness and (c) fiber diameter as a function of flow (f) and time (t), with fixed rotation speed (s) at 8 rpm. (d) Polar histogram showing the mean frequency distribution of fiber orientations, with the axis 0° – 180° indicating the longitudinal direction of the stent.

Taking into account all these results, an optimal combination of parameters was chosen in order to obtain a continuous coating with thin electrospun fibers. With the aim to attain the smallest possible fiber diameter, the optimal flow and time were derived from the saddle point in Equation 5.3, giving a flow of 0.55 mL/min and 125 s of time. As for the rotation speed, a value of 8 rpm was chosen as intermediate between the upper and lower tested limits.

5.3.3 Everolimus/PLCL-coated 3D-printed stents

The ES solution was further modified with the addition of everolimus at a ratio of 15 wt.% and 30 wt.% with respect to PLCL content. Regarding the ES parameters, the optimal values obtained from the DoE were used with the exception of the flow, which had to be increased to 0.8 mL/min in order to render continuous fibers. Obtained everolimus-loaded PLCL-coated PLLA stents are shown in Figure 5.8a. Both $\text{PLLA}_{\text{ES-15Eve}}$ and $\text{PLLA}_{\text{ES-30Eve}}$ presented a coating mass of 0.85 ± 0.19 mg (Table 5.3). In terms of everolimus loading, the former presented 139 ± 31 μg , and the latter, 250 ± 54 μg . Subsequent SEM analysis showed a similar fiber morphology compared to samples without drug, with a homogeneous and dispersed distribution of everolimus

throughout the fibers (Figure 5.8b). Nevertheless, the mean diameter was found to be increased, around $1.5 \mu\text{m}$ for $\text{PLLA}_{\text{ES-15Eve}}$ and over $1.2 \mu\text{m}$ for $\text{PLLA}_{\text{ES-30Eve}}$. Membrane thickness was found to be around $30 \mu\text{m}$ for both conditions. Figure 5.8d presents the fiber orientation of the specimens, showing preferential alignment in the longitudinal direction.

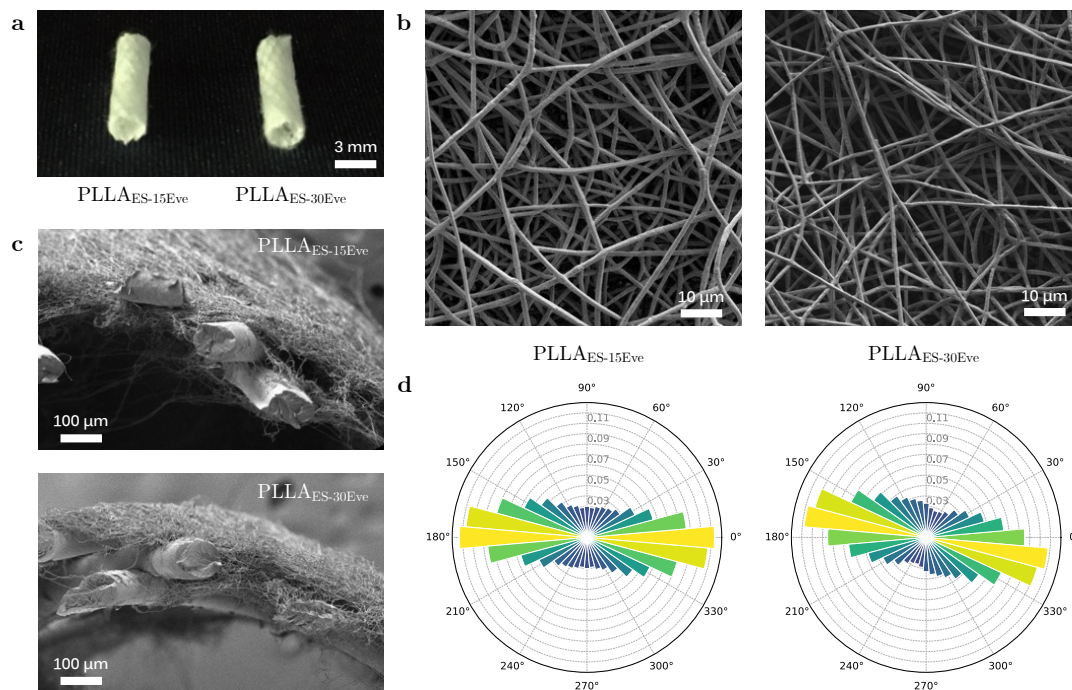


Fig. 5.8 Everolimus-loaded PLCL-coated PLLA stents. (a) Stents external appearance, (b) surface fiber morphology under SEM, (c) stent cross sections and (d) preferred fiber orientation, with 0° indicating the longitudinal direction of the stent.

Tab. 5.3 Everolimus-loaded PLCL-coated PLLA stents. Material deposition, membrane thickness, fiber diameter and preferred fiber orientation, with 0° indicating the longitudinal direction of the stent ($n = 3$).

Sample	Material deposition [mg]	Everolimus loading [μg]	Membrane thickness [μm]	Fiber diameter [μm]	Fiber orientation [$^\circ$]
$\text{PLLA}_{\text{ES-15Eve}}$	0.85 ± 0.19	139 ± 31	31.39 ± 5.55	1.49 ± 0.24	-4.6 ± 20.6
$\text{PLLA}_{\text{ES-30Eve}}$	0.85 ± 0.19	250 ± 54	31.05 ± 7.52	1.22 ± 0.18	-12.1 ± 22.9

Regarding everolimus release from coated stents, Figure 5.9a presents accumulated release, with $\text{PLLA}_{\text{ES-15Eve}}$ having released over $60 \mu\text{g}$ of everolimus in the first 6 hours, and $\text{PLLA}_{\text{ES-30Eve}}$ close to $140 \mu\text{g}$. In terms of percentage, both conditions presented around 50% release in the first 6 hours with surface-available drug. In the following days, the initial burst release slowed down and presented linear release from day 2 to day 7. SEM images of the fibers are shown in Figure 5.9b as a function of immersion time in release medium. PLCL fibers displayed no noticeable differences in terms of surface appearance and looked indistinguishable with respect to coated stents prior to immersion.

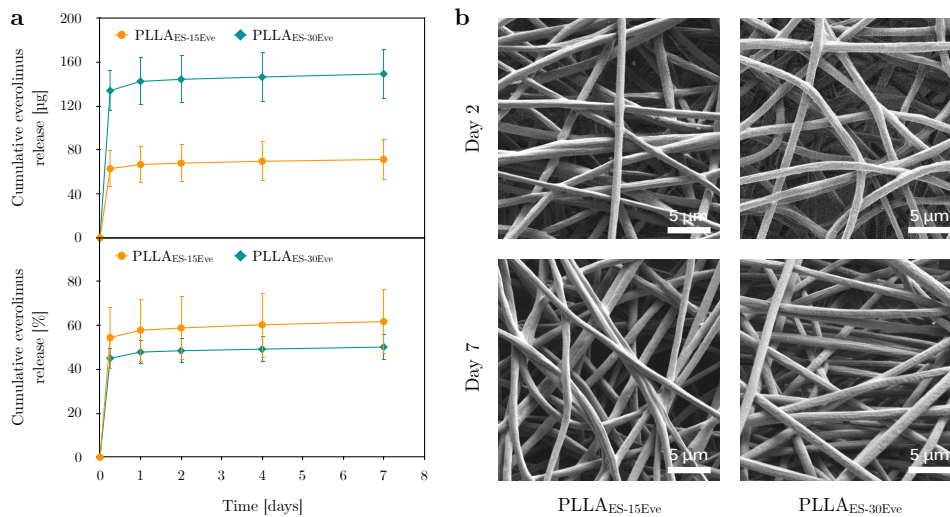


Fig. 5.9 (a) Everolimus release from everolimus-loaded PLCL-coated PLLA stents immersed in release media for 1 week, in absolute numbers and normalized to the drug loading of each stent, in percentage. (b) Surface fiber morphology as a function of immersion time in release medium.

5.4 Discussion

Even though major advances in DES development have been achieved in the last few decades, incomplete arterial healing due to the permanent presence of the medical implant still remains a concern. As a result, the use of biodegradable polymers has been a recurrent idea as a preferable material for cardiovascular stents. Additionally, BRS should maintain the drug-eluting capabilities of DES, showing the desired release kinetics to match SMCs inhibition and endothelialization. The present work investigates two different loading strategies for everolimus loading in BRS, either encapsulated in the struts of the stent or in an electrospun membrane covering the stent.

In the first case, addition of everolimus in the PLLA and PLCL inks permitted to directly print drug-loaded BRS. As the whole procedure was performed at room temperature, potential drug thermal degradation associated to FDM processes was circumvented. However, when compared to control PLLA or PLCL stents, everolimus-loaded stents presented significantly greater strut thickness, around 184 µm for PLLA and around 215 µm for PLCL. Although most BRS under development present strut thickness in the range of 100 to 200 µm, thicker struts are associated with impaired vascular healing [38]. Strut protrusion inside the vessel lumen is directly proportional to greater flow disruption and blood flow turbulence, which in turn enhances platelet deposition, greater acute thrombogenicity, delayed re-endothelialization and ultimately a higher risk of device-associated thrombosis [39–42]. Consequently, current trends in BRS design aim for miniaturizing strut thickness [15].

Here, the increase in strut thickness did not result in improved mechanical properties, as there were no significant changes in terms of compression force at 50% deformation or elastic recovery for everolimus-loaded stents with respect to control stents. Still, stents immersed in release medium retained their compression strength and elastic recovery throughout the immersion period of 8 weeks time. Analysis of the release medium by means of HPLC evidenced everolimus release, although at a very slow rate. In the first 3 days, release was below 1 μg for PLLA stents, and only over 3 μg for PLCL_{4Eve}, which was the condition showing the highest release. In the following time points, the release rate presented linear stabilization, only to reach a plateau after week 5. In terms of release with respect to actual drug loading, one can see that only between 1% and 2% of everolimus was released in 2 months time for PLCL stents. In the case of PLLA, less than 1% of the drug was released into the receptor medium.

The fact that PLCL stents showed increased release with respect to PLLA may be attributed to its constitutional structure. As shown in previous studies [43], PLCL presents lower crystallinity as a result of a higher availability of amorphous regions, which are hydrated prior to more crystalline domains. Thus, the degradation rate of PLCL was found to be 1.5 times faster than that of PLLA. Even so, complete degradation of PLCL would take around 2 years at 37 °C in physiological conditions. Therefore, only surface available drug is released in the initial stages of immersion, with subsequent diffusion from the interior hampered by the physical entrapment of the drug within the polymeric matrix. As a consequence, everolimus release would be subjected to the lengthy degradation timeframe of PLLA and PLCL.

The aforementioned release values are too low in terms of dose and percentage for an appropriate release kinetics to inhibit SMCs overproliferation after stent implantation. Therefore, an alternative method in terms of drug loading was sought in order to obtain the desired release kinetics. In that sense, electrospun fibers present very high specific surface area, in such a way that surface-available drug would be dramatically increased when compared to as-printed stent struts. On that account, a customized rotatory ES system was manufactured to coat PLLA 3D-printed stents with a membrane of PLCL fibers.

Initially, a DoE was conducted to determine the parameters necessary for optimal homogeneous coating regarding flow, time and rotation speed. The totality of the samples were successfully coated with a membrane of electrospun PLCL fibers with different processing parameters. Material deposition was strongly influenced by time, obtaining more electrospun PLCL fibers onto 3D-printed stents with increasing time, up to 1 mg. A similar effect was found for membrane thickness, with a maximum for increasing time and flow of around 60 μm . Regarding fiber diameter, a range between 800 nm and 1.2 μm was obtained as a function of flow and time, with rotation speed showing no influence on fiber diameter. Finally, analysis of the orientation of fibers

evidenced that, globally, there was preferential alignment in the longitudinal direction of the stents, as shown in Figure 5.S2.

In general, due to the bending instability associated with the ES process, electrospun fibers are mostly deposited in a randomly oriented distribution [44]. Nevertheless, in certain fields, such as in tissue engineering, fiber alignment may modulate cell behavior such as cell shape, migration or differentiation [45]. In this regard, several strategies have been implemented in order to obtain oriented nanofibers. Among them, using a rotating collector appears as the simplest way to fabricate aligned fibers in the circumferential direction, by matching the evaporating jet deposition to the velocity of the rotating cylinder, usually well above 1000 rpm [46]. Conversely, in this work the velocity was much lower, between 5.33 and 10.67 rpm, and the fibers were not oriented circumferentially but rather axially, following the longitudinal direction of the stents. We attribute this behavior to the fact that the deposition occurs on a grounded metal cylinder with a polymeric insulator on its surface. This phenomenon has been conceptually described as gap electrospinning, that is, two grounded electrodes separated by an empty space or a substrate that acts as an insulator [47]. In this configuration, random filaments are formed within the electrodes or stent cells, as well as oriented fibers between the stent cells (Figure 5.6a). Additionally, the customized rotatory ES system reported in this study presents a longitudinally moving collector. Fiber orientation as a consequence of collectors in motion, from 0 to 3 m/s, has been previously reported [48]. Therefore, the fiber distribution described by the polar histograms in Figure 5.S2 may be attributed to a combination of gap electrospinning and longitudinal collector movement.

Several studies have reported that scaffolds with aligned topographies may be useful in forming a confluent endothelium with enhanced ECs adhesion [49–51]. Heath *et al.* showed that scaffold fiber alignment would result in a preferentially elongated cell morphology paralleling the direction of the fibers, and Gaharwar *et al.* indicated that ECs on the aligned scaffolds exhibited higher proliferation compared to those cultures on randomly oriented fibrous scaffolds [52, 53]. Therefore, the orientation found in ES-covered stents would constitute a favourable environment for enhanced migration of endothelial cells towards complete colonization of the scaffold.

The rationale for determining the optimal coating parameters was related to the ultimate goal of this work, that is, to successfully release everolimus from additive manufactured BRS. Everolimus encapsulated in the polymeric structure, physically confined within stent struts, was not able to readily diffuse out, hence the proportion of surface-available everolimus needed to be increased. As specific surface increases with decreasing fiber diameter, the optimal combination of parameters was derived from Equations 5.1 to 5.3 with the aim to attain the lowest possible fiber diameter. This way, flow was set to 0.55 mL/min, time to 125 s and rotation speed to 8 rpm. With these parameters, by applying

Equations 5.1, 5.2 and 5.3, a PLCL coating of 927 μg , 32 μm in thickness and fibers of 0.97 μm in diameter would be obtained. Nevertheless, when adding everolimus to the polymeric ES solution, the flow had to be increased to 0.8 mL/min to obtain continuous fibers. As a result, coated stents presented higher mean fiber diameter, in the range between 1.2 and 1.5 μm .

Regarding everolimus release, in the first 6 hours there was over 60 μg of everolimus released into the receptor media from PLLA_{ES-15Eve} stents, and close to 140 μg from PLLA_{ES-30Eve} stents. These results constitute a 50 times increase with respect to everolimus-loaded 3D-printed stents, where in the first 3 days, only 3 μg of everolimus were released from PLCL_{4Eve}, that is, the condition showing the highest release. As both loading strategies presented equivalent everolimus amount, it is clear that the electrospun membrane offers a more suitable platform in terms of everolimus release rate than encapsulation in the stent struts.

To investigate drug release *in vitro*, immersion of drug-loaded stents in phosphate buffered saline (PBS) at 37 °C is widely used [54, 55]. Nevertheless, as some drugs such as sirolimus may degrade in PBS, and in view of the considerable time span, accelerated release studies are of interest to shorten the assay time. In that sense, several studies have described the use of surfactants such as Tween or Triton, or addition of organic solvents such as ACN or isopropanol [56, 57]. Kamberi *et al.* reported the use of a release medium containing 0.7% Triton X-405 in 0.01 M potassium phosphate buffer at pH 6 for everolimus release quantification [36, 37]. Similarly, 0.4% Tween20 and 10 mM sodium acetate (pH 5.0) with ACN at 7% (v/v) was used and compared to long-term *in vitro* release medium, porcine serum with 0.1% sodium azide [35]. A correlation between simulated physiological conditions and accelerated conditions was established, with equivalent release of everolimus in 24 hours and in 30 days, respectively. The Synergy stent (Boston Scientific, USA), a platinum chromium everolimus-eluting stent with a 4 μm PLGA coating on the abluminal surface, has been shown to release 100% of the drug in 90 days in a porcine model [2, 16]. Similarly, the Absorb stent, a BRS made of semi-crystalline PLLA with a 2–4 μm everolimus/PDLLA coating, releases 75% of loaded everolimus within 30 days [40]. Therefore, release from everolimus-loaded PLCL-coated PLLA 3D-printed stents (Figure 5.9), about 50% in 1 day under accelerated conditions, would match the appropriate dose in the required timeframe for *in vivo* application.

5.5 Conclusions

In this work we have presented a combination of SC-DW and ES to fabricate drug-eluting PLLA and PLCL BRS for cardiovascular applications. Firstly, 3D-printed stents by SC-DW technique loaded with everolimus were successfully manufactured and characterized,

although their drug release rate was found to be too modest, less than 3% of the total loaded drug. Secondly, a customized rotatory ES system was designed and built to effectively coat 3D-printed stents with a membrane of PLCL electrospun fibers, between 800 nm and 1.2 μm in diameter. Results from the DoE permitted to select the optimal parameters in terms of flow, time and rotation speed. Finally, everolimus-loaded PLCL-coated stents were fabricated, with everolimus release dramatically increased with respect to everolimus-loaded 3D-printed stents, around 50% in the first 6 hours. These values, obtained under an accelerated release assay, would be in agreement with the required timeframe for *in vivo* release shown by commercial stents.

The versatility of the AM approach used in this study constitutes an encouraging starting point for supplementary features. For instance, the antiproliferative drug release from the electrospun coating, mostly needed in the first weeks after implantation, could be combined with an anti-thrombogenic drug loaded in the stent struts, which would be released in accordance with polymer degradation. Moreover, together with the preferential alignment of fibers in the longitudinal direction, the electrospun membrane may be functionalized in order to guide endothelial cell proliferation until complete re-endothelialization of the scaffold.

5.6 Supplementary information

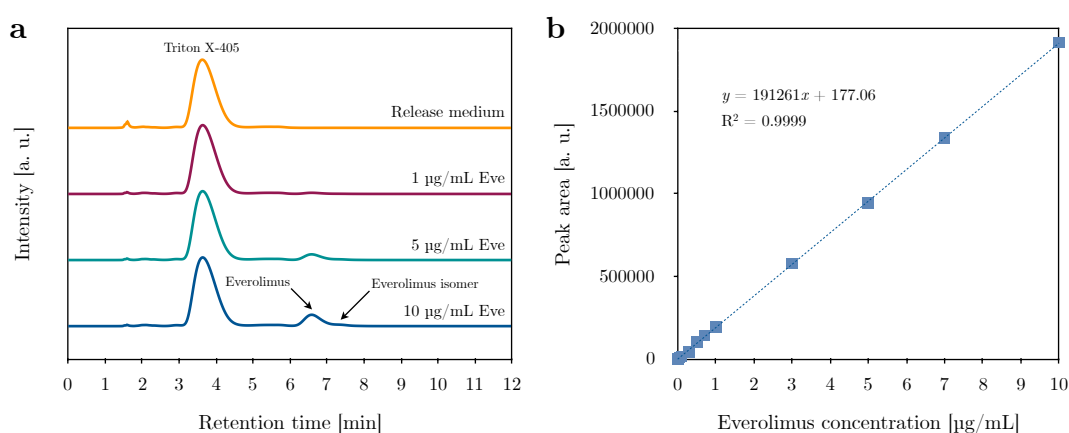


Fig. 5.S1 (a) Representative chromatograms for increasing concentration of everolimus in release medium (0.7% Triton X-405 in 0.01 M potassium phosphate buffer pH 6 in 7% ACN), from 1 $\mu\text{g/mL}$ up to 50 $\mu\text{g/mL}$. Peaks: 1, release medium (Triton X-405); 2, everolimus; 3, everolimus isomer. (b) Calibration curve with everolimus concentration versus peak area.

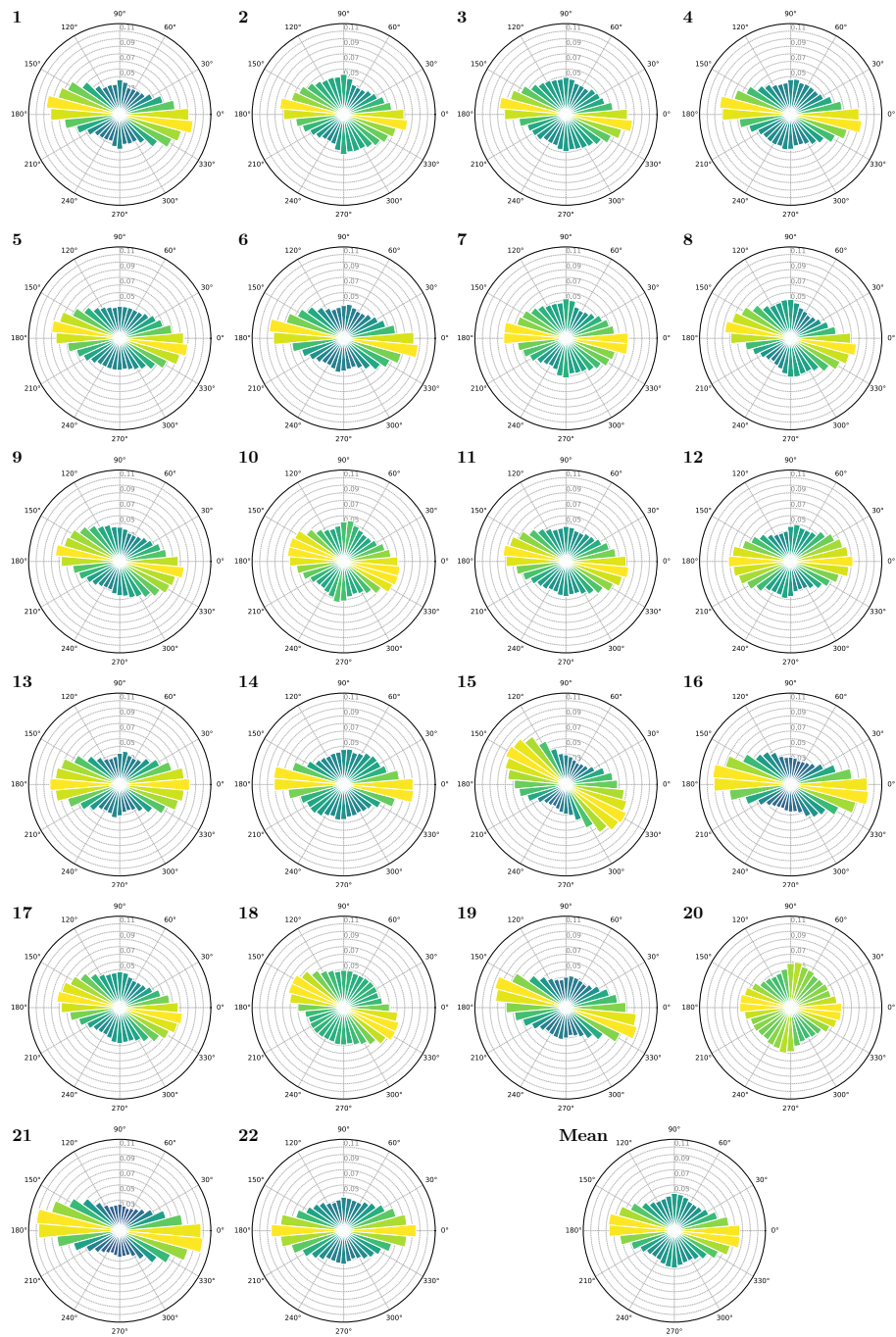


Fig. 5.S2 Polar histograms showing fiber orientation as a function of design parameters. The axis 0°–180° indicates the longitudinal direction of the stent.

References

- [1] N. Foin, R. D. Lee, R. Torii, J. L. Guitierrez-Chico, A. Mattesini, S. Nijjer, S. Sen, R. Petraco, J. E. Davies, C. Di Mario, *et al.*, “Impact of stent strut design in metallic stents and biodegradable scaffolds”, *International journal of cardiology*, vol. 177, no. 3, pp. 800–808, 2014.
- [2] A. Akinapelli, J. P. Chen, K. Roy, J. Donnelly, K. Dawkins, B. Huibregtse, and D. Hou, “Current state of bioabsorbable polymer-coated drug-eluting stents”, *Current cardiology reviews*, vol. 13, no. 2, pp. 139–154, 2017.
- [3] J. W. Moses, M. B. Leon, J. J. Popma, P. J. Fitzgerald, D. R. Holmes, C. O’Shaughnessy, R. P. Caputo, D. J. Kereiakes, D. O. Williams, P. S. Teirstein, *et al.*, “Sirolimus-eluting stents versus standard stents in patients with stenosis in a native coronary artery”, *New England Journal of Medicine*, vol. 349, no. 14, pp. 1315–1323, 2003.
- [4] S. Garg, C. Bourantas, and P. W. Serruys, “New concepts in the design of drug-eluting coronary stents”, *Nature Reviews Cardiology*, vol. 10, no. 5, p. 248, 2013.
- [5] D. Y. Kwon, J. I. Kim, H. J. Kang, B. Lee, K. W. Lee, M. S. Kim, *et al.*, “Biodegradable stent”, *Journal of Biomedical Science and Engineering*, vol. 5, no. 04, p. 208, 2012.
- [6] S. O. Marx and A. R. Marks, *Bench to bedside: the development of rapamycin and its application to stent restenosis*, 2001.
- [7] S. J. Sollott, L. Cheng, R. R. Pauly, G. M. Jenkins, R. E. Monticone, M. Kuzuya, J. P. Froehlich, M. T. Crow, E. G. Lakatta, and E. K. Rowinsky, “Taxol inhibits neointimal smooth muscle cell accumulation after angioplasty in the rat”, *The Journal of clinical investigation*, vol. 95, no. 4, pp. 1869–1876, 1995.
- [8] P. W. Serruys, Y. Onuma, S. Garg, P. Vranckx, B. De Bruyne, M.-C. Morice, A. Colombo, C. Macaya, G. Richardt, J. Fajadet, *et al.*, “5-year clinical outcomes of the ARTS II (arterial revascularization therapies study II) of the sirolimus-eluting stent in the treatment of patients with multivessel de novo coronary artery lesions”, *Journal of the American College of Cardiology*, vol. 55, no. 11, pp. 1093–1101, 2010.
- [9] T. J. Parry, R. Brosius, R. Thyagarajan, D. Carter, D. Argentieri, R. Falotico, and J. Siekierka, “Drug-eluting stents: sirolimus and paclitaxel differentially affect cultured cells and injured arteries”, *European journal of pharmacology*, vol. 524, no. 1-3, pp. 19–29, 2005.
- [10] P. Qi, S. Chen, T. Liu, J. Chen, Z. Yang, Y. Weng, J. Chen, J. Wang, M. F. Maitz, and N. Huang, “New strategies for developing cardiovascular stent surfaces with novel functions”, *Biointerphases*, vol. 9, no. 2, p. 029 017, 2014.
- [11] A. Scafa Udriste, A.-G. Niculescu, A. M. Grumezescu, and E. Bădilă, “Cardiovascular stents: a review of past, current, and emerging devices”, *Materials*, vol. 14, no. 10, p. 2498, 2021.
- [12] H. Ang, J. Ng, H. Bulluck, P. Wong, S. Venkatraman, Y. Huang, and N. Foin, “Fundamentals of bioresorbable stents”, in *Functionalised Cardiovascular Stents*, Elsevier, 2018, pp. 75–97.
- [13] T. Hu, C. Yang, S. Lin, Q. Yu, and G. Wang, “Biodegradable stents for coronary artery disease treatment: recent advances and future perspectives”, *Materials Science and Engineering: C*, vol. 91, pp. 163–178, 2018.

- [14] N. Beshchasna, M. Saqib, H. Kraskiewicz, Ł. Wasyluk, O. Kuzmin, O. C. Duta, D. Ficai, Z. Ghizdavet, A. Marin, A. Ficai, *et al.*, “Recent advances in manufacturing innovative stents”, *Pharmaceutics*, vol. 12, no. 4, p. 349, 2020.
- [15] S. McMahon, N. Bertollo, E. D. O. Cearbhaill, J. Salber, L. Pierucci, P. Duffy, T. Dürig, V. Bi, and W. Wang, “Bio-resorbable polymer stents: a review of material progress and prospects”, *Progress in Polymer Science*, vol. 83, pp. 79–96, 2018.
- [16] J. Bennett and C. Dubois, “A novel platinum chromium everolimus-eluting stent for the treatment of coronary artery disease”, *Biologics: targets & therapy*, vol. 7, p. 149, 2013.
- [17] P. Díaz-Rodríguez and M. Landin, “Implantable materials for local drug delivery in bone regeneration”, *Advanced Materials Interfaces*, pp. 325–378, 2016.
- [18] M. Wawrzyńska, J. Arkowski, A. Włodarczak, M. Kopaczyńska, and D. Biały, “Development of drug-eluting stents (DES)”, in *Functionalised Cardiovascular Stents*, Elsevier, 2018, pp. 45–56.
- [19] N. Bink, V. B. Mohan, and S. Fakirov, “Recent advances in plastic stents: a comprehensive review”, *International Journal of Polymeric Materials and Polymeric Biomaterials*, vol. 70, no. 1, pp. 54–74, 2021.
- [20] M. Livingston and A. Tan, “Coating techniques and release kinetics of drug-eluting stents”, *Journal of medical devices*, vol. 10, no. 1, 2016.
- [21] M. Gagliardi, D. Silvestri, C. Cristallini, M. Guadagni, G. Crifaci, and P. Giusti, “Combined drug release from biodegradable bilayer coating for endovascular stents”, *Journal of Biomedical Materials Research Part B: Applied Biomaterials*, vol. 93, no. 2, pp. 375–385, 2010.
- [22] A. Mirmohseni, J. Hosseini, M. Shojaei, and S. Davaran, “Design and evaluation of mixed self-assembled monolayers for a potential use in everolimus eluting coronary stents”, *Colloids and Surfaces B: Biointerfaces*, vol. 112, pp. 330–336, 2013.
- [23] J.-k. Park, D.-G. Kim, I. H. Bae, K. S. Lim, M. H. Jeong, C. Choi, S.-K. Choi, S. C. Kim, and J.-W. Nah, “Blood-compatible and biodegradable polymer-coated drug-eluting stent”, *Macromolecular Research*, vol. 23, no. 3, pp. 237–244, 2015.
- [24] C. McKittrick, M. Cardona, R. Black, and C. McCormick, “Development of a bioactive polymeric drug eluting coronary stent coating using electrospraying”, *Annals of biomedical engineering*, vol. 48, no. 1, pp. 271–281, 2020.
- [25] S.-J. Liu, F.-J. Chiang, C.-Y. Hsiao, Y.-C. Kau, and K.-S. Liu, “Fabrication of balloon-expandable self-lock drug-eluting polycaprolactone stents using micro-injection molding and spray coating techniques”, *Annals of biomedical engineering*, vol. 38, no. 10, pp. 3185–3194, 2010.
- [26] K. Kuraishi, H. Iwata, S. Nakano, S. Kubota, H. Tonami, M. Toda, N. Toma, S. Matsushima, K. Hamada, S. Ogawa, *et al.*, “Development of nanofiber-covered stents using electrospinning: in vitro and acute phase in vivo experiments”, *Journal of Biomedical Materials Research Part B: Applied Biomaterials*, vol. 88, no. 1, pp. 230–239, 2009.
- [27] Y. Zhu, C. Hu, B. Li, H. Yang, Y. Cheng, and W. Cui, “A highly flexible paclitaxel-loaded poly (ϵ -caprolactone) electrospun fibrous-membrane-covered stent for benign cardiac stricture”, *Acta biomaterialia*, vol. 9, no. 9, pp. 8328–8336, 2013.

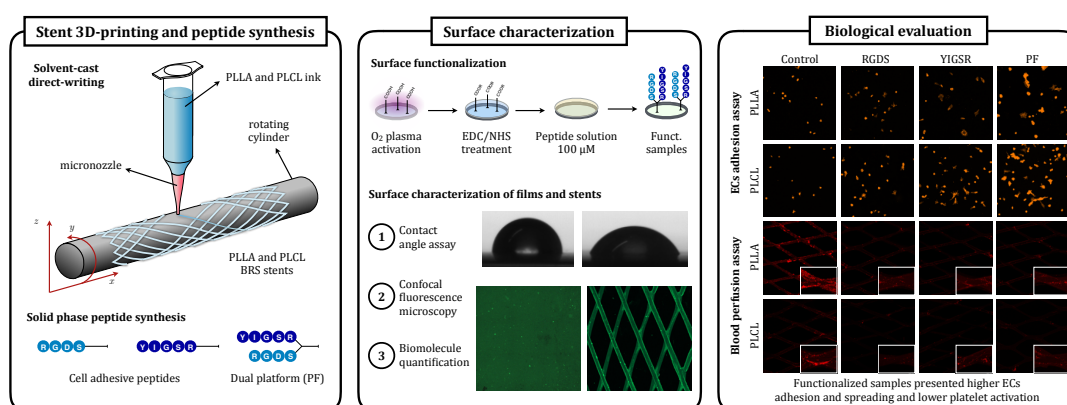
- [28] C.-H. Lee, S.-H. Chang, Y.-H. Lin, S.-J. Liu, C.-J. Wang, M.-Y. Hsu, K.-C. Hung, Y.-H. Yeh, W.-J. Chen, I.-C. Hsieh, and M.-S. Wen, “Acceleration of re-endothelialization and inhibition of neointimal formation using hybrid biodegradable nanofibrous rosuvastatin-loaded stents”, *Biomaterials*, vol. 35, no. 15, pp. 4417–4427, 2014.
- [29] Y. Zhang, J. Wang, J. Xiao, T. Fang, N. Hu, M. Li, L. Deng, Y. Cheng, Y. Zhu, and W. Cui, “An electrospun fiber-covered stent with programmable dual drug release for endothelialization acceleration and lumen stenosis prevention”, *Acta biomaterialia*, vol. 94, pp. 295–305, 2019.
- [30] D. Kersani, J. Mougin, M. Lopez, S. Degoutin, N. Tabary, F. Cazaux, L. Janus, M. Matton, F. Chai, J. Sobocinski, *et al.*, “Stent coating by electrospinning with chitosan/polycyclodextrin based nanofibers loaded with simvastatin for restenosis prevention”, *European Journal of Pharmaceutics and Biopharmaceutics*, vol. 150, pp. 156–167, 2020.
- [31] Y. Cheng, X. Zhang, R. Liu, Y. Li, J. Zeng, M. Zhou, and Y. Zhao, “Bioinspired vascular stents with microfluidic electrospun multilayer coatings for preventing in-stent restenosis”, *Advanced Healthcare Materials*, p. 2200965, 2022.
- [32] A. J. Guerra, R. Tejada-Alejandre, C. A. Rodríguez, and J. Ciurana, “Electrospun tubular scaffold for stenting application: a proof of concept”, *Procedia Manufacturing*, vol. 41, pp. 312–319, 2019.
- [33] V. Chausse, R. Schieber, Y. Raymond, B. Ségry, R. Sabaté, K. Kolandaivelu, M.-P. Ginebra, and M. Pegueroles, “Solvent-cast direct-writing as a fabrication strategy for radiopaque stents”, *Additive Manufacturing*, p. 102392, 2021.
- [34] ISO 25539-2, *Cardiovascular implants. endovascular devices. part 1: vascular stents*. International Organization for Standardization, 2012.
- [35] M. Kamberi, S. Nayak, K. Myo-Min, T. P. Carter, L. Hancock, and D. Feder, “A novel accelerated in vitro release method for biodegradable coating of drug eluting stents: insight to the drug release mechanisms”, *European Journal of Pharmaceutical Sciences*, vol. 37, no. 3-4, pp. 217–222, 2009.
- [36] M. Kamberi and T.-N. Tran, “UV–visible spectroscopy as an alternative to liquid chromatography for determination of everolimus in surfactant-containing dissolution media: a useful approach based on solid-phase extraction”, *Journal of pharmaceutical and biomedical analysis*, vol. 70, pp. 94–100, 2012.
- [37] K. Marika, F. Katherine, L. Jianmin, C. G. Mike, and F. Debra, “A sensitive high-throughput HPLC assay for simultaneous determination of everolimus and clobetasol propionate”, *Journal of chromatographic science*, vol. 46, no. 1, pp. 23–29, 2008.
- [38] D. Capodanno, “Bioresorbable scaffolds in coronary intervention: unmet needs and evolution”, *Korean circulation journal*, vol. 48, no. 1, pp. 24–35, 2018.
- [39] K. Kolandaivelu, R. Swaminathan, W. J. Gibson, V. B. Kolachalama, K.-L. Nguyen-Ehrenreich, V. L. Giddings, L. Coleman, G. K. Wong, and E. R. Edelman, “Stent thrombogenicity early in high-risk interventional settings is driven by stent design and deployment and protected by polymer-drug coatings”, *Circulation*, vol. 123, no. 13, pp. 1400–1409, 2011.
- [40] Y. Sotomi, Y. Onuma, C. Collet, E. Tenekecioglu, R. Virmani, N. S. Kleiman, and P. W. Serruys, “Bioresorbable scaffold: the emerging reality and future directions”, *Circulation research*, vol. 120, no. 8, pp. 1341–1352, 2017.

- [41] E. Tenekecioglu, Y. Sotomi, R. Torii, C. Bourantas, Y. Miyazaki, C. Collet, T. Crake, S. Su, Y. Onuma, and P. W. Serruys, “Strut protrusion and shape impact on endothelial shear stress: insights from pre-clinical study comparing Mirage and Absorb bioresorbable scaffolds”, *The international journal of cardiovascular imaging*, vol. 33, no. 9, pp. 1313–1322, 2017.
- [42] S. Buccheri and D. Capodanno, “Bioabsorbable stents: only bad news?”, *European Heart Journal Supplements*, vol. 21, no. Supplement_B, B28–B30, 2019.
- [43] V. Chausse, C. Iglesias, E. Bou-Petit, M.-P. Ginebra, and M. Pegueroles, “Chemical vs thermal accelerated hydrolytic degradation of 3D-printed PLLA/PLCL bioresorbable stents: characterization and influence of sterilization”, *Polymer Testing*, p. 107 817, 2022.
- [44] X. Yuan, A. F. Mak, and K. Yao, “Comparative observation of accelerated degradation of poly (L-lactic acid) fibres in phosphate buffered saline and a dilute alkaline solution”, *Polymer degradation and stability*, vol. 75, no. 1, pp. 45–53, 2002.
- [45] H. Yuan, S. Zhao, H. Tu, B. Li, Q. Li, B. Feng, H. Peng, and Y. Zhang, “Stable jet electrospinning for easy fabrication of aligned ultrafine fibers”, *Journal of Materials Chemistry*, vol. 22, no. 37, pp. 19 634–19 638, 2012.
- [46] B. Sundaray, V. Subramanian, T. Natarajan, R.-Z. Xiang, C.-C. Chang, and W.-S. Fann, “Electrospinning of continuous aligned polymer fibers”, *Applied physics letters*, vol. 84, no. 7, pp. 1222–1224, 2004.
- [47] A. J. Robinson, A. Pérez-Nava, S. C. Ali, J. B. González-Campos, J. L. Holloway, and E. M. Cosgriff-Hernandez, “Comparative analysis of fiber alignment methods in electrospinning”, *Matter*, vol. 4, no. 3, pp. 821–844, 2021.
- [48] T. Han, D. H. Reneker, and A. L. Yarin, “Buckling of jets in electrospinning”, *Polymer*, vol. 48, no. 20, pp. 6064–6076, 2007.
- [49] B. M. Whited and M. N. Rylander, “The influence of electrospun scaffold topography on endothelial cell morphology, alignment, and adhesion in response to fluid flow”, *Biotechnology and bioengineering*, vol. 111, no. 1, pp. 184–195, 2014.
- [50] J. Meng, Z. Han, H. Kong, X. Qi, C. Wang, S. Xie, and H. Xu, “Electrospun aligned nanofibrous composite of MWCNT/polyurethane to enhance vascular endothelium cells proliferation and function”, *Journal of Biomedical Materials Research Part A*, vol. 95, no. 1, pp. 312–320, 2010.
- [51] R. Schieber, F. Lasserre, M. Hans, M. Fernández-Yagüe, M. Díaz-Ricart, G. Escolar, M.-P. Ginebra, F. Mücklich, and M. Pegueroles, “Direct laser interference patterning of CoCr alloy surfaces to control endothelial cell and platelet response for cardiovascular applications”, *Advanced healthcare materials*, vol. 6, no. 19, p. 1 700 327, 2017.
- [52] D. E. Heath, J. J. Lannutti, and S. L. Cooper, “Electrospun scaffold topography affects endothelial cell proliferation, metabolic activity, and morphology”, *Journal of Biomedical Materials Research Part A*, vol. 94, no. 4, pp. 1195–1204, 2010.
- [53] A. K. Gaharwar, M. Nikkhah, S. Sant, and A. Khademhosseini, “Anisotropic poly (glycerol sebacate)-poly (ϵ -caprolactone) electrospun fibers promote endothelial cell guidance”, *Biofabrication*, vol. 7, no. 1, p. 015 001, 2014.
- [54] A. Seidlitz, S. Nagel, B. Semmling, K. Sternberg, H. K Kroemer, and W. Weitschies, “In vitro dissolution testing of drug-eluting stents”, *Current pharmaceutical biotechnology*, vol. 14, no. 1, pp. 67–75, 2013.

- [55] A. Seidlitz, “Drug-eluting stents”, *In Vitro Drug Release Testing of Special Dosage Forms*, pp. 87–117, 2019.
- [56] A. Raval, P. Bahadur, and A. Raval, “Effect of nonionic surfactants in release media on accelerated in-vitro release profile of sirolimus eluting stents with biodegradable polymeric coating”, *Journal of pharmaceutical analysis*, vol. 8, no. 1, pp. 45–54, 2018.
- [57] C. Naseerali, P. Hari, and K. Sreenivasan, “The release kinetics of drug eluting stents containing sirolimus as coated drug: role of release media”, *Journal of Chromatography B*, vol. 878, no. 7-8, pp. 709–712, 2010.

Functionalization of 3D-printed polymeric bioresorbable stents with a dual cell-adhesive peptidic platform combining RGDS and YIGSR sequences

Biomimetic surface modification with cell-adhesive peptides is a promising approach to improve endothelialization of current bioresorbable stents (BRS). Among them, RGDS and YIGSR sequences have been reported to mediate adhesion and migration of endothelial cells (ECs) while preventing platelet activation. This work presents the functionalization of novel 3D-printed poly-L-lactic acid (PLLA) and poly(L-lactic-co- ϵ -caprolactone) (PLCL) BRS with linear RGDS and YIGSR sequences, as well as a dual platform (PF) containing both motifs within a single biomolecule. Functionalized surfaces were characterized in terms of static contact angle, biomolecule distribution under confocal fluorescence microscopy and peptide quantification via detachment from the surface, showing a biomolecule density in the range of 0.5 to 3.5 nmol/cm². Biological evaluation comprised a cell adhesion test with ECs and a blood perfusion assay to assess ECs response and device hemocompatibility, respectively. Cell adhesion assays evidenced significantly increased cell number and spreading onto functionalized films with respect to control samples. Regarding stents' hemocompatibility, platelet adhesion onto PLCL stents was severely decreased with respect to PLLA. In addition, functionalization with RGDS, YIGSR and the PF rendered BRS stents displaying even further reduced platelet adhesion. In conclusion, the combination of intrinsically less prothrombogenic materials such as PLCL and its functionalization with EC-discriminating adhesive biomolecules paves the way for a new generation of BRS based on accelerated re-endothelialization approaches.



V. Chausse, C. Mas-Moruno, H. Martín-Gómez, M. Pino, M. Díaz-Ricart, G. Escolar, M.-P. Ginebra, M. Pegueroles, *Functionalization of 3D printed polymeric bioresorbable stents with a dual cell-adhesive peptidic platform combining RGDS and YIGSR sequences* (under revision in *Biomaterials Science*).

6.1 Introduction

Stent deployment in stenosed coronary arteries allows for blood flow restoration at the expense of endothelium disruption. Although materials used for stent fabrication are globally biocompatible, their permanent presence in the artery together with the lack of a healthy protective endothelium may lead to adverse biological effects [1]. Metals surface electrical charge and wettability influence protein adsorption behavior in such a way that protein denaturation may occur, which in turn eventually leads to coagulation and thrombosis. Polymer-coated stents are mainly hydrophobic and delaminate as they degrade, leaving the underlying metal exposed [2]. Drug-eluting stents are loaded with antiproliferative drugs to avoid overproliferation of smooth muscle cells (SMCs) and potential restenosis. However, these drugs also inhibit endothelial cells (ECs) proliferation and thus have a detrimental effect on the ultimate recovery of a functional endothelium [3, 4]. Besides, newly developed bioresorbable stents (BRS) present high strut profiles associated to increased blood flow turbulence and platelet deposition, contributing to a higher risk of device thrombosis [5–7]. Therefore, stents' clinical performance may only be improved by simultaneously discriminating ECs response from that of SMCs and by ensuring device hemocompatibility.

Accordingly, surface modification of stents has been proposed with the purpose to reduce thrombogenicity, prevent denaturation of adsorbed proteins and accelerate re-endothelialization. Some designs introduce a layer of polymeric material on the stent surface in order to reduce undesirable protein adhesion such as fibrinogen, which may lead to activation of platelets [1]. These coatings can be deposited by means of nonthermal plasma, an extensively used technique for surface activation or modification [8]. For instance, antifouling coatings based on polyethylene glycol (PEG) significantly prevent platelet adhesion [9–11]. Other strategies involve the use of polydopamine and polyethylenimine as intermediates to incorporate an anti-platelet and anti-thrombotic drug [12] or an anticoagulant drug such as heparin [13, 14]. Similarly, Meng *et al.* [15] applied a layer-by-layer strategy to coat 316L stainless steel coronary stents with chitosan and heparin to accelerate re-endothelialization after coronary stent deployment. Alternatively, titanium oxide films have been reported as a suitable coating to improve endothelialization [16, 17]. Other authors have followed a different strategy by analyzing the effect of topography on platelet adhesion onto titanium [18], poly(lactic-co-glycolic acid) [19] or cobalt-chromium [20].

Another approach to achieving hemocompatibility of stents is to functionalize their surface with active biological agents such as nitric oxide (NO) donors, antibodies, growth factors or proteins [4, 21–23]. NO plays a key role in vascular biology, as it inhibits the adhesion of platelets and leukocytes, reduces SMCs proliferation and their synthesis of collagen [24–26]. Antibodies have particular potential to accelerate

re-endothelialisation by capturing circulating endothelial progenitor cells (EPCs) to immobilise them on the stent surface [27]. However, although CD34-binding antibodies capture EPCs from the circulation, no surface marker is unique for EPCs or ECs identification and capture. Lee *et al.* reported a bilayered PCL scaffold functionalized with vascular endothelial growth factor to increase ECs proliferation [28]. Regarding proteins, collagen and fibronectin are two extracellular matrix (ECM) proteins known to enhance ECs attachment and proliferation. However, despite having favourable endothelial cell interactions, both collagen and fibronectin are known to be prothrombogenic and also promote SMCs migration [2]. Conversely, tropoelastin has shown to have favourable interactions with ECs, low thrombogenicity and growth inhibition of SMCs *in vitro* [2]. Nevertheless, the use of proteins may be troublesome, as it is associated to enzymatic instability, immunogenicity, inflammation risk and high costs [29].

In this regard, the use of custom-made bioadhesive peptides, which are derived from ECM proteins but encompass only defined cell adhesive motifs, may overcome these limitations and efficiently enhance cell adhesion and improve biointegration *in vitro* and *in vivo* [29]. Bioactive cell-adhesive peptides can be covalently immobilized on polymeric substrates and other biomaterials, following a plasma treatment to activate carboxylic groups or via direct chemisorption [30, 31]. Regarding peptide sequences, RGDS (Arg-Gly-Asp-Ser) is a universal cell adhesive recognition motif from fibronectin, but REDV (Arg-Glu-Asp-Val, from fibronectin) and YIGSR (Tyr-Ile-Gly-Ser-Arg, from laminin) sequences specifically mediate adhesion and migration of ECs while preventing SMCs and platelet adhesion [9, 32]. Other sequences, such as WKYMVm (Trp-Lys-Tyr-Met-Val-D-Met), are reported to stimulate the proliferation of endothelial colony-forming cells [33]. Interestingly, it has been recently shown that the combination of RGD with REDV and YIGSR enhances endothelialization of metallic stents [34] and vascular grafts [35]. However, the optimal configuration and surface distribution of the peptides in order to obtain accelerated ECs response is yet to be elucidated. Furthermore, distinct bioactive peptides can be combined in a single biomimetic molecule to exert synergistic or complementary effects on the surface of an implant [36–38].

This work presents the functionalization of novel 3D-printed polymeric BRS fabricated by solvent-cast direct-write (SC-DW) technique with EC adhesive peptides. Stents have been manufactured with poly-L-lactic acid (PLLA) and poly(L-lactic-co- ϵ -caprolactone) (PLCL). Solid phase peptide synthesis (SPPS) was used to synthesize linear RGDS and YIGSR sequences with PEG as a spacer unit, as well as a dual-peptide platform containing both RGDS and YIGSR motifs. Biomolecule covalent anchorage on stents and solvent-cast films was achieved subsequent to O₂-plasma treatment to activate carboxylic groups. Functionalized surfaces were characterized in terms of static contact angle, biomolecule distribution under confocal fluorescence microscopy and peptide quantification via detachment from the surface. Biological evaluation included a cell

adhesion test on functionalized films with human umbilical vein endothelial cells (HUVECs) and a thrombogenicity assay on functionalized stents to assess ECs response and device hemocompatibility, respectively.

6.2 Materials and methods

6.2.1 Chemicals and materials

Medical grade PLLA (Purasorb[®] PL 65; inherent viscosity 6.5 dL/g, $M_w=1,675,000$ g/mol) and PLCL (Purasorb[®] PLC 9538, 95:5 lactic-to-caprolactone molar ratio, 3.8 dL/g, $M_w=700,000$ g/mol) were purchased from Corbion (Netherlands). Acetonitrile (ACN, Carlo Erba Reagents, Spain) and chloroform ($\geq 99.5\%$, Sigma-Aldrich, USA) were used as received. 1-ethyl-3-(3-dimethylaminopropyl) carbodiimide (EDC) and N-hydroxysuccinimide (NHS) were purchased from Sigma-Aldrich (USA). All chemicals required for the peptide synthesis, including resins, Fmoc-L-amino acids and coupling reagents, were obtained from Iris Biotech GmbH (Germany) and Sigma-Aldrich (USA).

6.2.2 Solvent casting of films

PLLA and PLCL pellets were dissolved in chloroform at 3.6% or 4.5% concentration (w/v), respectively, in a dual asymmetric centrifuge (SpeedMixer[™], DAC 150.1 FVZ, FlackTek, Germany) at 3500 rpm in 8 runs of 5 min. Resulting mixtures were poured onto a Petri dish and incubated in a chloroform saturated atmosphere at room temperature (RT) for 3 days. Obtained films underwent thermal treatment at 80 °C for 12 hours and were stored in a desiccator until further use.

6.2.3 3D Printing of stents

PLLA and PLCL stents were manufactured by means of SC-DW technique as reported elsewhere [39]. Briefly, dissolution of PLLA or PLCL pellets in chloroform at a 10% or 12.5% ratio (w/v), respectively, rendered printable inks. Tubular printing was achieved by modification of a BCN 3D+ printer (BCN 3D technologies, Spain) via substitution of its *y* axis for a 3-mm in diameter rotating mandrel. Stents were printed with a 250 μm nozzle (Optimum[®] SmoothFlow[™], Nordson, USA) following rhombic cell design, 30 mm in length, 3 mm in diameter and number of peaks equal to 10. After printing, stents were cut in half in the longitudinal direction and flattened between two glass slides, subjected to thermal treatment at 80 °C for 12 hours and stored in a desiccator until further use.

6.2.4 Solid-phase peptide synthesis

The peptidic sequences RGDS and YIGSR and the combined platform RGDS-YIGSR (PF) were manually synthesized as previously reported [30, 31, 34, 36]. Briefly, Fmoc Rink-amide MBHA resin (200 mg, 0.4 mmol g⁻¹) was used as solid support for solid-phase peptide synthesis following the Fmoc/tBu strategy [40, 41]. Deprotection steps and washings between couplings were carried out with N,N-dimethylformamide (DMF) and dichloromethane (DCM). Solvents and soluble reagents were removed using a vacuum filtration system and all reactions and treatments were performed at room temperature. Sequential coupling reactions were carried out with Fmoc-L-amino acids (3 eq.), ethyl 2-cyano-2-(hydroxyimino)acetate (OxymaPure) (3 eq.) and N,N-diisopropylcarbodiimide (DIC) (3 eq.) in DMF for 60 min and monitored using the Kaiser test. In the case of the PF, the second branch was constructed after Alloc group removal with 3 treatments of PhSiH₃ (10 eq.) and Pd(PPh₃)₄ (0.1 eq.) in DCM for 15 minutes. Prior to cleavage, the free N-terminus was either acetylated (Ac) or reacted with 5(6)-carboxyfluorescein (CF) to obtain fluorescent analogues for physicochemical characterization assays.

Reversed-phase analytical high performance liquid chromatography (RP-HPLC) was performed using Shimadzu Prominence XR (Japan) equipped with a LC-20AD pump, a SIL-20AC cooling autosampler, a CTO-10AS column oven and a SPD-M20A photodiode array detector. A reversed-phase XBridge C18 column (4.6 × 100 mm, 3.5 μm, Waters) was used. The system was run at a flow rate of 1.0 mL min⁻¹ over 8 min using water (0.045% trifluoroacetic acid (TFA), v/v) and ACN (0.036% TFA, v/v) as mobile phases. Acetylated peptides were purified by semipreparative RP-HPLC using a Waters modular HPLC System (2545 quaternary gradient module, equipped with a 2489 UV/Vis detector, a 2707 autosampler and a fraction collector III) and a reversed-phase XBridge C18 (19 × 150 mm, 5 μm, Waters) column. The system was run at a flow rate of 15 mL min⁻¹ over 40 min. The solvents used were water (0.1% TFA, v/v) and ACN (0.05% TFA, v/v). All peptides were characterized by analytical RP-HPLC and matrix-assisted laser desorption/ionization time-of-flight (MALDI-TOF) spectrometry (AB 4800 Plus MALDI TOF instrument, AB Sciex, Spain). Figure 6.1a shows the structure of the synthesized linear peptides and platform.

- ▷ **RGD**: Ac-Arg-Gly-Asp-Ser-PEG-PEG-Lys-Lys-NH₂: RP-HPLC (0–40% ACN over 15 min, t_R = 4.335 min, purity 96.2%), MALDI-TOF (m/z calcd for C₄₁H₇₆N₁₄O₁₆, 1021.13; found, 1021.58).
- ▷ **CF-RGD**: CF-Arg-Gly-Asp-Ser-PEG-PEG-Lys-Lys-NH₂: RP-HPLC (5–100% ACN over 8 min, t_R = 6.382 min, purity 86.9%), MALDI-TOF (m/z calcd for C₆₀H₈₄N₁₄O₂₁, 1337.39; found, 1338.65).

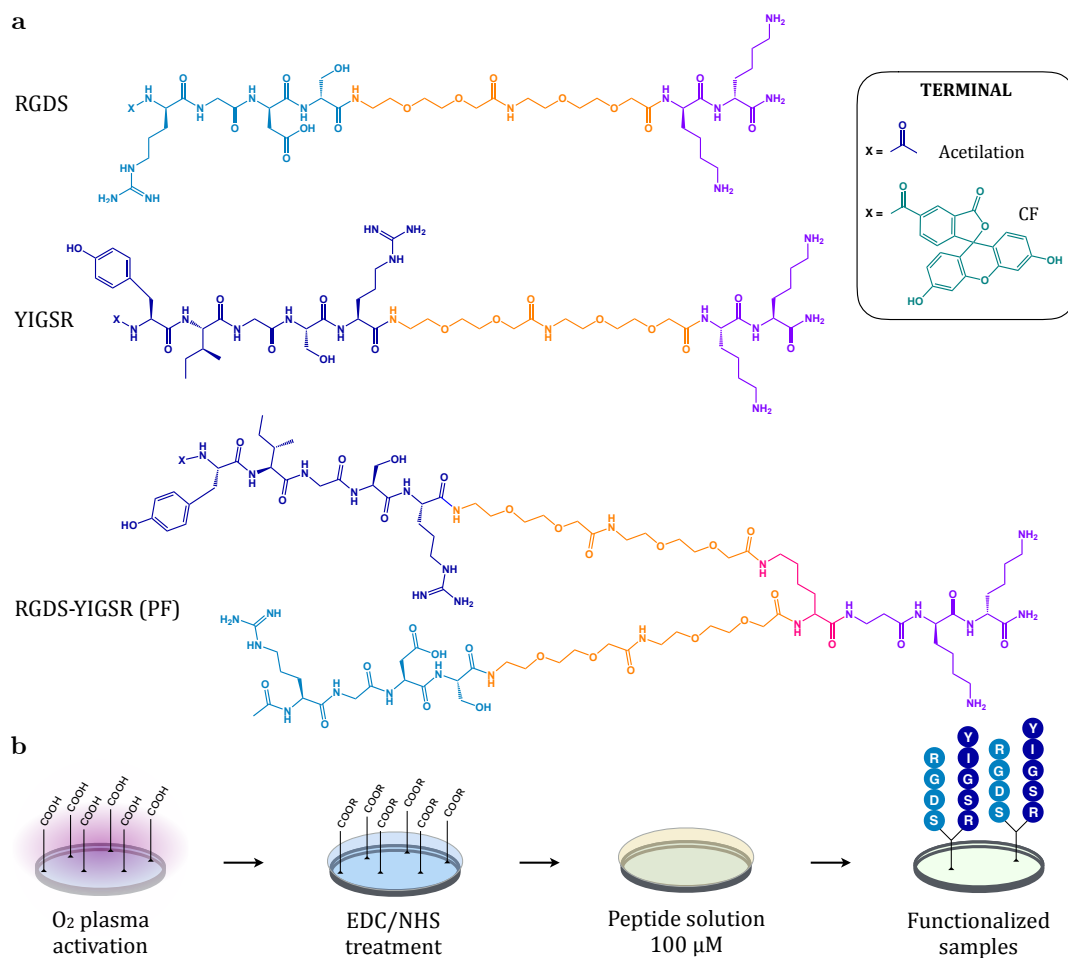


Fig. 6.1 (a) Chemical structure of the cell adhesive linear peptides and platform. All biomolecules contain the corresponding bioactive sequence (highlighted in blue), two short polyethylene glycol (PEG) chains as a spacing unit (orange) and an anchoring group with two lysine residues (purple). Additionally, the platform presents an extra lysine acting as a branching unit (rose) and a β -alanine as a spacer (black). Finally, all the molecules were either acetylated or reacted with 5(6)-carboxyfluorescein (CF) to obtain fluorescent analogues. (b) Scheme of the functionalization of the PLLA and PLCL films and stents, comprising the activation of the surface with O₂ plasma, the treatment with EDC/NHS and the covalent binding of the biomolecules onto the surface.

- ▷ **YIGSR**: Ac-Tyr-Ile-Gly-Ser-Arg-PEG-PEG-Lys-Lys-NH₂: RP-HPLC (5–100% ACN over 8 min, t_R = 5.940 min, purity 91.2%), MALDI-TOF (m/z calcd for C₅₂H₉₁N₁₅O₁₆, 1182.37; found, 1182.68).
- ▷ **CF-YIGSR**: CF-Tyr-Ile-Gly-Ser-Arg-PEG-PEG-Lys-Lys-NH₂: RP-HPLC (5–100% ACN over 8 min, t_R = 9.918 min, purity 82.5%), MALDI-TOF (m/z calcd for C₇₁H₉₉N₁₅O₂₁, 1498.63; found, 1499.69).
- ▷ **RGDS-YIGSR (PF)**: [(Ac-Arg-Gly-Asp-Ser-PEG-PEG)(Ac-Tyr-Ile-Gly-Ser-Arg-PEG-PEG)]-Lys- β Ala-Lys-Lys-NH₂: RP-HPLC (5–95% ACN over 3 min, t_R = 1.180

min, purity 93.2%), MALDI-TOF (m/z calcd for C₉₀H₁₅₇N₂₇O₃₂, 2129.37; found, 2129.16).

- ▷ **CF-RGDS-YIGSR (CF-PF)**: [(Ac-Arg-Gly-Asp-Ser-PEG-PEG)(CF-Tyr-Ile-Gly-Ser-Arg-PEG-PEG)]-Lys-βAla-Lys-Lys-NH₂: RP-HPLC (5–100% ACN over 8 min, *t_R* = 6.714 min, purity 66.3%), MALDI-TOF (m/z calcd for C₁₀₉H₁₆₅N₂₇O₃₇, 2445.64; found, 2446.14).

6.2.5 Surface functionalization

PLLA and PLCL films and stents were O₂-plasma activated for 5 min using a Standard Femto Plasma System (Diener, Germany), as shown in Figure 6.1b. Subsequently, O₂-activated samples were treated with 0.1 M EDC and 0.2 M NHS in PBS at pH 6.5 for 2 hours in order to stabilize generated carboxylic groups and render activated esters. In parallel, RGDS and YIGSR linear peptides, and the RGDS-YIGSR platform were dissolved in milliQ water at a 100 μm concentration. After rinsing with PBS, a 100 μL drop containing the peptidic molecules was deposited on each sample. The anchorage of the peptides to the surface via amide bonds was achieved after incubation overnight at room temperature. Functionalization with fluorescent peptides was performed in the dark. Finally, the excess peptide solution was removed and biofunctionalized films and stents were rinsed thrice with milliQ water and dried with N₂ gas until further use.

6.2.6 Surface physicochemical characterization

The presence and distribution of the peptides was evaluated through contact angle measurements, confocal fluoresce microscopy and biomolecule detachment. Static contact angle was measured with a Contact Angle System OCA15 plus (Dataphysics, Filderstadt, Germany) using the sessile drop method. As wetting liquids, milliQ water and diiodomethane (CH₂I₂, Acros Organics, Belgium) were used by deposition of a 1 μL drop on functionalized PLLA and PLCL films, with three measurements per sample and three samples per condition. Contact angle values were obtained by application of the Laplace-Young fitting with SCA 20 software (Dataphysics). Surface free energy with partial polar and dispersive components was derived by means of the Owens, Wendt, Rabel, and Kaelble (OWRK) method [42, 43] employing the surface tension values for water and diiodomethane determined by Ström *et al.* [44].

Furthermore, functionalized films and stents with carboxyfluorescein-labeled molecules were characterized by means of confocal fluorescence microscopy. The distribution of the peptidic molecules was evaluated in a LSM 800 confocal laser scanning microscope (Carl Zeiss, Germany). Fluorescence intensity was measured by image processing using FIJI software. Additionally, peptide surface density on films and stents was assessed

according to a modified protocol described previously [31]. Briefly, functionalized samples with fluorescent peptides were treated in 1 M NaOH solution at 70 °C for 12 minutes in order to detach the biomolecule from the surface. In parallel, a calibration curve of well-known peptidic concentrations, from 125 nM to 20 μ M, was performed for each fluorescent molecule. In a 96-well plate with black bottom, 50 μ L of the hydrolysate from the samples were added, as well as of each concentration in the standard curve. Fluorescence intensity was analyzed using a MicroPlate Reader (Synergy HTX multi-mode microplate reader, BioTek Instruments, USA), with $\lambda_{\text{excitation}} = 485$ nm and $\lambda_{\text{emission}} = 528$ nm, and converted to concentration with the corresponding calibration curve.

6.2.7 Biological characterization

Films and stents functionalized with RGDS and YIGSR linear peptides and the dual platform (PF) containing both motives (RGDS-YIGSR) were evaluated through an adhesion test with HUVECs and a thrombogenicity assay.

HUVECs adhesion test

HUVECs (PromoCell GmbH, Germany) were cultured in endothelial cell growth media (PromoCell, Germany) supplemented with 1% penicillin/streptomycin in Nunc culture flasks (ThermoFisher Scientific, USA) at 37 °C in a humidified atmosphere with 5% of CO₂. At 90% confluence, cells were detached via trypsinization (Trypsin/EDTA, Sigma-Aldrich, US) for 2 min, rinsed with PBS and resuspended in cell medium supplemented with 10% fetal bovine serum (FBS) for trypsin neutralization. Lastly, cells were centrifuged at 220g and resuspended in serum-free cell media. All experiments were conducted at passages 7 to 9. In parallel, control PLLA and PLCL films measuring 1 × 1 cm, as well as functionalized films with RGDS, YIGSR and PF, were placed in a low attachment 24 well-plate (ThermoFisher Scientific, USA) and treated with 1% bovine serum albumin (BSA) in PBS for 30 min. After rinsing three times with PBS, HUVECs were seeded at a density of 20,000 cells per film in serum-free medium. After 6 hours of incubation, non-adherent cells were removed by rinsing twice with PBS. Adhered cells were then fixed with 4% paraformaldehyde (PFA, Sigma Aldrich, USA) in PBS.

Subsequently, immunofluorescent staining was performed to assess the efficiency of the biofunctionalization of the films. After a permeabilization treatment with 0.05% Triton X-100 (Sigma-Aldrich, USA) in PBS for 20 min, cytoskeletal actin filaments (F-actin) were stained using phalloidin (1:400) (Invitrogen, USA) in Triton 0.05% for 1 h and nuclei with 4',6-diamidino-2-phenylidole (DAPI) (1:1000) (Life Technologies, USA) in PBS-Glycine for 2 min. Washing between treatments was conducted with 20 nM Glycine (Sigma-Aldrich, USA) in PBS (3 × 5 min) and both staining steps were performed in the dark. Finally, samples were mounted on microscope slides with Mowiol (Sigma-

Aldrich, USA) and observed in a LSM 800 confocal laser scanning microscope (Carl Zeiss, Germany). FIJI software was used to count the number of cells as well as to assess cell spreading by computing their area.

Blood perfusion assay

Stents' hemocompatibility was evaluated in a flat chamber perfusion system as described elsewhere [20, 45]. In short, whole blood was obtained from a healthy volunteer and minimally anticoagulated with a citrate/phosphate/dextrose solution at a final citrate concentration of 19 mM (100 mM sodium citrate, 16 mM citric acid, 18 mM sodium hydrogen phosphate, and 130 mM dextrose). Blood was circulated through the perfusion chamber at a shear rate of 800 s^{-1} during 5 min at $37 \text{ }^{\circ}\text{C}$, as shown in Figure 6.2. Control and functionalized flattened PLLA and PLCL stents were placed in the chamber aligned with the blood flow (Figure 6.2b). After perfusion, stents were rinsed in PBS and adhered platelets were fixed with 2.5% glutaraldehyde in PBS at $4 \text{ }^{\circ}\text{C}$ during 24 h. Immunofluorescent staining was performed by a blocking step with 1% BSA in PBS for 30 min, primary antibody monoclonal mouse antihuman CD36 (1:2000) (Clone 185-1G2, Lifespan, Biosciences, USA) incubation with 1% BSA in PBS for 1 h, PBS washing ($3 \times 5 \text{ min}$) and secondary antibody goat antimouse IgG-AF 568 (1:500) incubation with 1% BSA in PBS for 1 h in the dark. Finally, stents were washed with PBS and mounted on microscope slides with Mowiol (Sigma-Aldrich, USA) and observed in a LSM 800 confocal laser scanning microscope (Carl Zeiss, Germany). The percentage of the surface covered by platelets was analyzed with FIJI software.

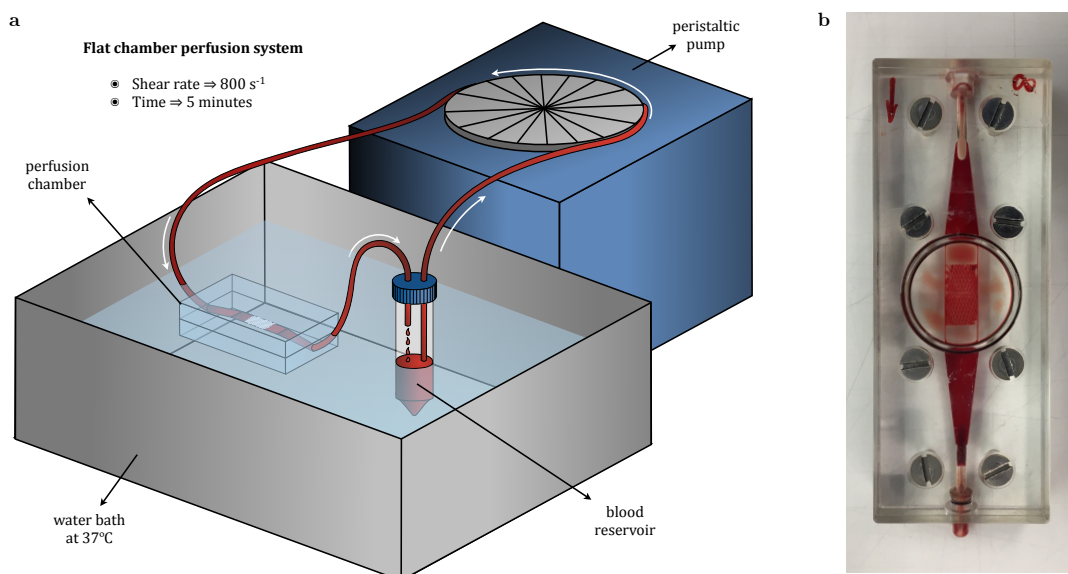


Fig. 6.2 (a) Scheme showing the experimental setup used for the thrombogenicity assay. Blood from a healthy donor was circulated through the stent in the perfusion chamber at a shear rate of 800 s^{-1} for 5 minutes using a peristaltic pump. Both the blood reservoir and the perfusion chamber were maintained in a water bath at $37 \text{ }^{\circ}\text{C}$. (b) Detail of the perfusion chamber after the assay, with the stent aligned with the blood flow.

Lastly, platelet aggregates were analyzed under scanning electron microscopy (SEM). On that account, platelets were fixed with 2.5% glutaraldehyde in PBS for 30 min and dehydrated through immersion in ethanol:water solutions with increasing ethanol content (30%, 50%, 70%, 90% and 100%) for 10 minutes each. Dehydrated samples were sputtered with platinum–palladium (80:20) and examined using JEOL JSM-7001F (Jeol, Japan) at 2 kV acceleration voltage.

6.2.8 Statistical analysis

Statistical analysis was performed using Minitab software (Minitab Inc., USA). An equality of variances test (ANOVA) with Fisher post-hoc test was used to determine statistically significant differences ($p < 0.05$ between the different groups and 95% confidence interval) for normally-distributed data. All data are represented as mean values \pm standard deviation (SD).

6.3 Results and discussion

6.3.1 Biomolecules design and synthesis

The peptidic sequences RGDS and YIGSR and the combined platform (PF) were synthesized following SPPS protocols. Figure 6.3 presents a summary of the key synthetic steps to assemble the dual platform. Starting from Fmoc Rink-amide MBHA resin as a solid support, two lysine residues (Lys, labelled purple) were introduced as an anchoring unit. Lysine was chosen for its ability to form stable amide bonds with the carboxylic groups of the polymer activated surface owing to the presence of a primary amine in its side chain. In a second step, an orthogonally protected (Fmoc/Alloc) lysine (Lys, labelled rose) was coupled to act as a branching unit. Under basic conditions, the Fmoc group protecting the α -amine may be selectively removed whereas the Alloc group remains in place, therefore permitting to assemble the next unit exclusively at the α -position. On that account, two short polyethylene glycol (PEG, labelled orange) chains and the first motif (RGDS, labelled sky blue) were coupled. PEG chains act as a spacing unit by providing the necessary separation between the surface and the bioactive sequence, therefore allowing for the optimal accessibility to cell receptors [34, 36, 46]. Furthermore, it has been shown that PEG possesses an antifouling character, such that unspecific adsorption of proteins and cells is diminished, thus limiting the aggregation of platelets and the risk of potential thrombosis [10, 11, 47, 48]. The second branch with the PEG spacer and the YIGSR motif (labelled dark blue) was introduced after removal of the Alloc group protecting the ϵ -amine in the branching lysine by means of catalytic amounts of palladium. Finally, the resulting molecule was cleaved from the solid support with concurrent removal of all protective groups in the

side chains (tBu, Boc and Pbf), purified and characterized as detailed in the Methods section.

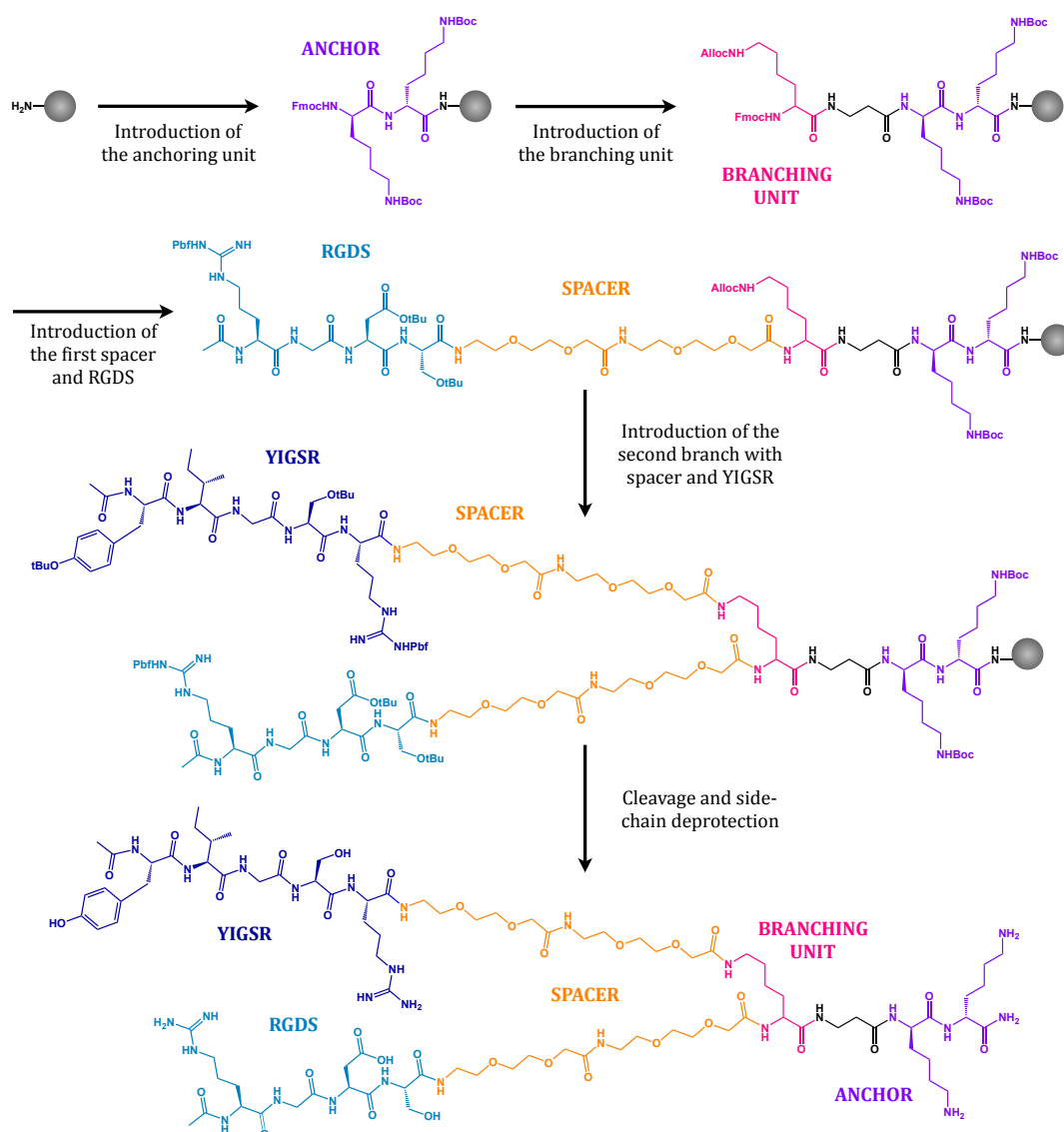


Fig. 6.3 Main steps during the synthesis of the dual platform. The major components are highlighted in color: the anchor (purple), branching (rose) and spacer (orange) units, the RGDS motif (sky blue) and the YIGSR motif (dark blue).

6.3.2 Peptide immobilization on films and stents

PLLA and PLCL films were successfully obtained through solvent casting. Subsequent to surface O_2 -plasma activation, the linear peptides RGDS and YIGSR and the dual PF were covalently anchored onto the films. Table 6.1 summarizes the data gathered from the static contact angle assay. Plain PLLA presented the highest water contact angle, $94.3^\circ \pm 3.6$, whereas plain PLCL presented a marginally more hydrophilic behavior with $83.1^\circ \pm 5.1$ ($p < 0.05$). When functionalizing the polymers with RGDS, YIGSR or the PF the contact angle decreased to around 60° independently of the

base material, with differences among biomolecules found to be statistically non-significant. A decrease in the water contact angle is widely described in the literature after application of plasma treatments to PLLA [49–51] or subsequent to grafting with RGDS and YIGSR peptides [34, 52]. Regarding surface free energy (γ), PLLA was found to present the lowest among all conditions, specially with almost negligible polar component (γ^p). Analogously to increasing hydrophilicity when functionalized, PLLA and PLCL's surface free energy also increased to around 55 mJ/m², both in terms of dispersive and polar components.

Tab. 6.1 Physicochemical characterization of PLLA and PLCL films functionalized with RGDS, YIGSR and PF with respect to control. Static contact angle for water ($\theta_{\text{H}_2\text{O}}$), diiodomethane ($\theta_{\text{CH}_2\text{I}_2}$) and total surface free energy (γ), split in dispersive component (γ^d) and polar component (γ^p). Conditions *a*, *b*, *c* and *d* are statistically different ($p < 0.05$) for each variable.

Sample		Contact angle [°]		Surface free energy [mJ/m ²]		
		$\theta_{\text{H}_2\text{O}}$	$\theta_{\text{CH}_2\text{I}_2}$	γ	γ^d	γ^p
PLLA	Control	94.3 ± 3.6 ^a	44.7 ± 4.4 ^a	37.7 ± 1.6 ^a	37.2 ± 2.0 ^a	0.6 ± 0.4 ^a
	RGDS	62.3 ± 4.1 ^d	27.6 ± 5.1 ^b	54.6 ± 2.3 ^b	45.1 ± 1.9 ^b	9.5 ± 0.6 ^c
	YIGSR	59.8 ± 6.7 ^d	22.2 ± 9.1 ^b	56.9 ± 4.3 ^b	46.7 ± 3.4 ^b	10.2 ± 1.9 ^c
	PF	67.5 ± 5.5 ^c	24.4 ± 5.0 ^b	53.1 ± 2.8 ^b	46.3 ± 1.4 ^b	6.8 ± 1.5 ^{b,c}
PLCL	Control	83.1 ± 5.1 ^b	44.9 ± 2.5 ^a	40.1 ± 2.0 ^a	37.0 ± 2.0 ^a	3.1 ± 1.2 ^{a,b}
	RGDS	59.5 ± 6.3 ^d	28.8 ± 9.6 ^b	55.5 ± 5.3 ^b	44.4 ± 3.5 ^b	11.1 ± 2.0 ^c
	YIGSR	63.2 ± 7.0 ^{c,d}	29.1 ± 6.3 ^b	53.8 ± 2.7 ^b	44.5 ± 1.3 ^b	9.3 ± 2.8 ^c
	PF	58.6 ± 2.9 ^d	29.4 ± 6.3 ^b	55.9 ± 2.4 ^b	44.3 ± 2.7 ^b	11.6 ± 1.3 ^c

In order to assess the spatial distribution of the biomolecules, PLLA and PLCL films were functionalized with their fluorescent analogues. Figure 6.4a shows overview images of the films obtained under confocal fluorescence microscopy, which evidenced the homogeneity of the grafting throughout the totality of the surface, although with the sparse presence of peptidic aggregates. A semiquantitative analysis of the fluorescence intensity displayed by the films is shown in Figure 6.4b. In general, increased fluorescence intensity was found for CF-PF when compared to CF-RGDS, with no striking differences between PLLA and PLCL conditions.

Analogously, 3D-printed PLLA and PLCL stents were functionalized with the synthesized biomolecules in their fluorescent version. Figure 6.5a presents the spatial distribution of peptides on PLLA and PLCL flattened stents, covering the entirety of the stent struts. Although the stents were successfully coated in a homogenous fashion, peptide agglomerates were detected at some strut junctions, such as for PLLA functionalized with CF-YIGSR. Regarding fluorescence intensity analysis, a similar trend to the one observed for functionalized films was found, as shown in Figure 6.5b. Stents functionalized with CF-RGDS displayed the lowest fluorescent intensity, whereas those grafted with CF-YIGSR and CF-PF presented significantly higher fluorescence. Furthermore, functionalized stents presented fluorescence intensity values higher than those observed for functionalized films.

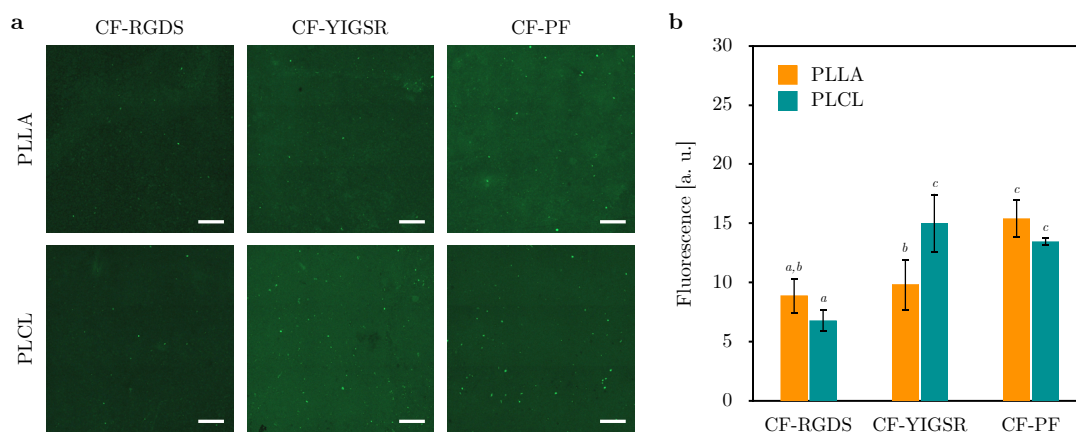


Fig. 6.4 (a) Spatial distribution of the linear sequences RGDS and YIGSR and the dual PF combining both motifs labelled with 5(6)-carboxyfluorescein (CF) onto PLLA and PLCL films under confocal fluorescence microscopy. Scale bar = 500 μm . (b) Semiquantitative analysis of the absolute fluorescence intensity onto PLLA and PLCL films measured by image processing. Conditions *a*, *b* and *c* are statistically different ($p < 0.05$).

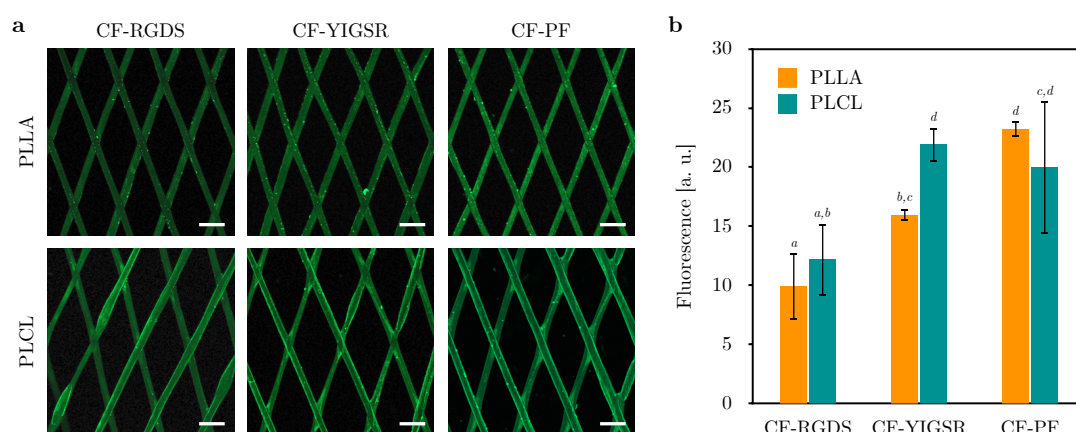


Fig. 6.5 (a) Spatial distribution of the fluorescent-labeled biomolecules CF-RGDS, CF-YIGSR and CF-PF onto PLLA and PLCL stents under confocal fluorescence microscopy. Scale bar = 500 μm . (b) Semiquantitative analysis of the absolute fluorescence intensity onto PLLA and PLCL stents measured by image processing. Conditions *a*, *b*, *c* and *d* are statistically different ($p < 0.05$).

Nevertheless, fluorescent intensity values obtained through image processing may be misleading when comparing different types of samples. For instance, films were only functionalized on one of their faces, acting as a two-dimensional object. Conversely, in the case of stents, biomolecule anchorage took place all around the stent struts as a three-dimensional object. Therefore, fluorescent intensity shown by stents may be overestimated due to the integration of the fluorescence readout coming from the different layers in which the stent was sliced.

Consequently, an alternative quantitative method was sought by means of biomolecule detachment. Quantification of the amount of peptide covalently bound to the polymeric

substrates was achieved via detachment in alkaline conditions through a calibration curve of well-known peptidic concentrations. As shown in Table 6.2, the peptidic concentration in films was found to be around 500 pmol/cm² for CF-RGDS, 1 nmol/cm² for CF-YIGSR and over 3 nmol/cm² for the dual CF-PF. No differences were found between PLLA and PLCL conditions. In the case of stents, biomolecule density ranged from 0.5 to 3.5 nmol/cm², with the CF-PF presenting the highest concentration and CF-RGDS the lowest. Again, PLLA and PLCL showed equivalent peptide density.

Tab. 6.2 Biomolecule density onto PLLA and PLCL films and stents quantified via biomolecule detachment in 1 M NaOH solution at 70 ° C for 12 minutes. Conditions *a* and *b* are statistically different (*p* < 0.05).

Biomolecule density [nmol/cm ²]	Films		Stents	
	PLLA	PLCL	PLLA	PLCL
CF-RGDS	0.58 ± 0.19 ^a	0.57 ± 0.09 ^a	0.47 ± 0.01 ^a	0.51 ± 0.05 ^a
CF-YIGSR	1.01 ± 0.17 ^a	1.10 ± 0.23 ^a	0.95 ± 0.05 ^a	1.04 ± 0.05 ^a
CF-PF	3.24 ± 0.37 ^b	3.52 ± 0.33 ^b	2.81 ± 0.52 ^b	3.53 ± 0.44 ^b

These results are according to previous works reported in the literature. Aubin *et al.* functionalized decellularized ECM with RGDS and YIGSR linear peptides through physical adsorption, and subsequent quantification of fluorescence intensity showed a slightly higher attachment rate of YIGSR compared to RGDS [35]. Similarly, Oliver *et al.* functionalized glass and titanium substrates through silanization with a dual platform containing both a cell-adhesive RGDS motif and an osteogenic DWIVA sequence (Asp-Trp-Ile-Val-Ala) [31]. Following detachment of the fluorescent peptide and quantification with a standard curve, peptide density was found to be around 40 pmol/cm² for glass and close to 80 pmol/cm² for titanium. Other studies have used quartz crystal microbalance with dissipation (QCM-D) monitoring to measure peptide density, such as RGDS, REDV and YIGSR linear peptides on CoCr, with peptide density between 30 and 180 pmol/cm² [34]. QCM-D has also been used to measure RGD peptidomimetics or a platform combining both RGD and a lactoferrin-derived antimicrobial peptide on titanium, finding molecule density between 10 and 550 pmol/cm² [53, 54]. Noel *et al.* monitored the grafting of RGDS, REDV and YIGSR with PEG on polyvinylamine-coated polyester through absorbance, and obtained peptide density between 20 and 2000 pmol/cm² [55]. Finally, Lei *et al.* estimated RGDS, REDV and YIGSR surface density onto PET via fluorescence microscopy, obtaining values as high as 25 nmol/cm² [52]. Overall, the biomolecule density values obtained for PLLA and PLCL films and stents were found to be in the range of those previously reported, albeit dissimilar anchoring strategies and quantification methods were used.

6.3.3 Cell adhesion

The biological performance of the biomolecules was assessed by means of an adhesion test with HUVECs. Figure 6.6a presents cell adhesion onto control and functionalized

PLLA and PLCL films, visually showing increased cell number and cell spreading when ECs were incubated onto functionalized samples with respect to control untreated samples. Quantification of cell number and cell area are shown in Figure 6.6b and Figure 6.6c, respectively. Biomolecule grafting significantly improved the number of adherent ECs to PLLA, in a tendency that was found to be even more pronounced for PLCL. With respect to the different biomolecules, although both RGDS and YIGSR linear sequences showed increased number of adhered cells, the platform (PF) combining both motifs presented the best results. A similar trend was found when analyzing cell spreading. While adhered to the surface, ECs in control samples presented sphere-like shape, whereas when introducing cell-adhesive peptides cells regained a more extended morphology. The condition showing the highest cell area was PLLA functionalized with YIGSR. Still, all biomolecules significantly improved cell spreading in comparison to plain PLLA and PLCL samples.

These results are in agreement with the increased hydrophilicity displayed by the functionalized films. In general, cell adhesion increases with increasing wettability. As reported by Lee *et al.*, cells adhere and spread on surfaces with moderate hydrophilicity, with maximum adhesion and growth found at water contact angles in the range of 50° to 60° [56]. Furthermore, surface free energy constitutes an indicator of potential cellular adhesion, with materials displaying surface energy above 30 mJ/m² tending to present greater bioadhesion [57]. In the case of PLLA, several authors have associated a greater wettability with improved cell adhesion following oxygen or nitrogen plasma treatments [49, 50].

Concerning the use of peptides, a wide variety of studies have reported improved adhesion, proliferation and migration of ECs on different metallic and polymeric materials functionalized with RGDS [46] and/or REDV [34, 55, 58–62] and/or YIGSR [9, 34, 52, 63–65]. Among them, Castellanos *et al.* compared the effects of CoCr surface functionalization with RGDS, REDV and YIGSR peptides [34]. Cell studies demonstrated that an equimolar combination of RGDS and YIGSR greatly enhanced ECs adhesion and proliferation without significantly enhancing SMCs adhesion. Similar results regarding the combination of RGDS and YIGSR at an equimolar ratio were described in the studies of Peng *et al.* [65] and Choi *et al.* [63]. Besides, it had previously been reported that RGDS induced more cell adhesion than YIGSR and REDV [52], in contrast to the results presented in this work. Nevertheless, this may be explained by the high densities at which the different peptides were grafted on the surface (0.5 to 1 nmol/cm²), as Noel *et al.* demonstrated that, over a certain density threshold, RGDS and YIGSR presented similar performance with regards to HUVECs cell adhesion [55]. Furthermore, it has been indicated that RGDS and YIGSR interact via distinct mechanisms with cells, the former through multiple integrins and the latter via the 67 kDa laminin receptor, thus with the potential to act synergistically [52]. The results obtained in the present work are therefore in accordance with those presented previously, showing that the inclusion

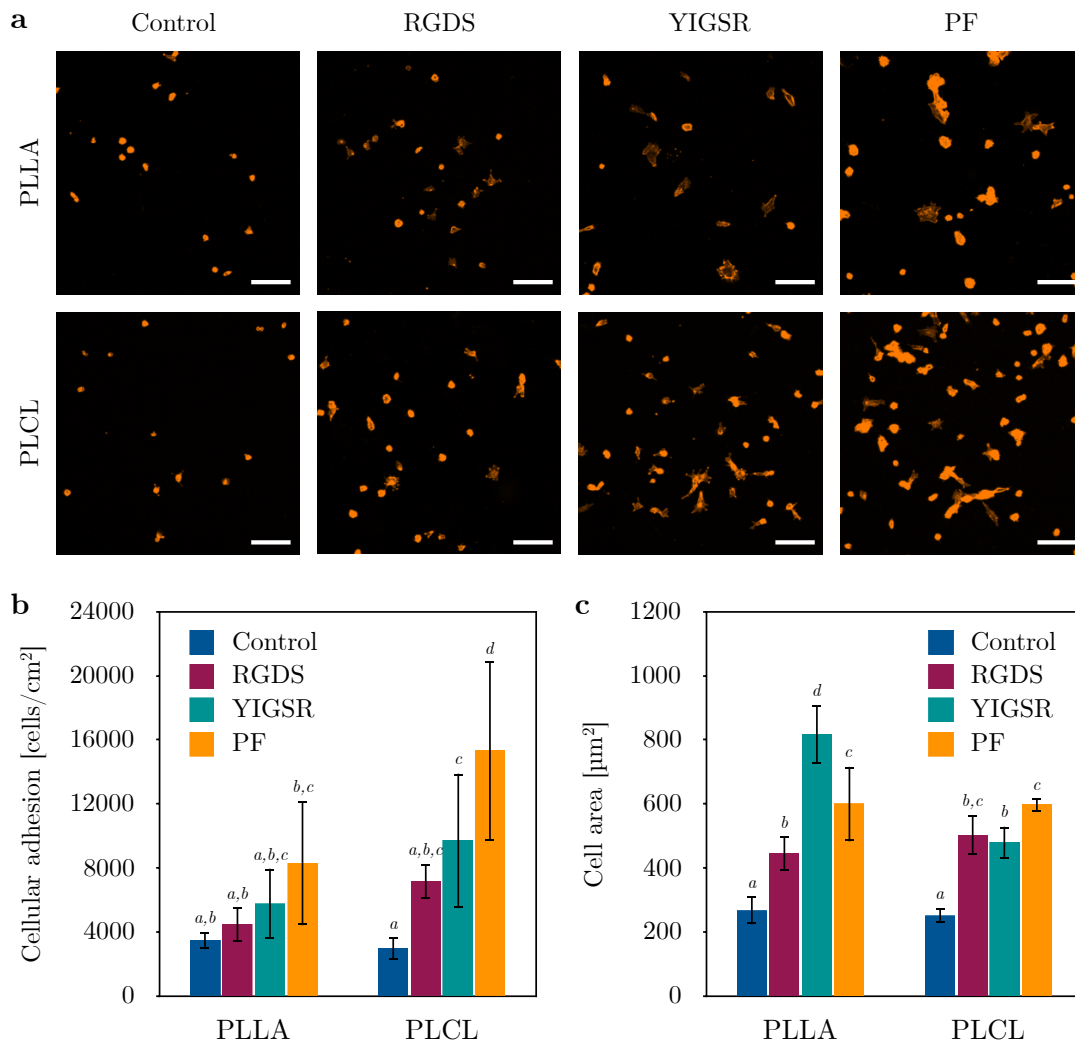


Fig. 6.6 HUVECs cell adhesion on control and functionalized PLLA and PLCL films after 6 hours of incubation. (a) Confocal fluorescence microscopy images, with actin filaments immunostained with phalloidin. Scale bar = 100 μm . (b) Cell attachment, in cells/cm², and (c) cell spreading, in μm^2 . Conditions *a*, *b*, *c* and *d* are statistically different ($p < 0.05$).

of both peptide motifs in a unique biomolecule suggests the occurrence of synergistic effects in cell adhesion.

6.3.4 Platelet adhesion

Platelet adhesion was evaluated through a blood perfusion assay by placing the stents in a flat perfusion chamber maintained at 37 °C while donor's blood was pumped at a shear rate of 800 s⁻¹ for 5 minutes. Adherent platelets' membrane was labelled with a fluorescent dye in order to visualize platelet adhesion on stent struts under confocal fluorescence microscopy (Figure 6.7a). Qualitatively, obtained overview images evidenced the dissimilarities arising among the different conditions. For PLLA, unmodified stents presented significant platelet adhesion, whereas it was found to

be much lower for stents functionalized with peptides. Image analysis with FIJI permitted to compute the percentage of stent surface occupied by platelets, showing that for plain PLLA, 28.8% of its area presented adherent platelets (Figure 6.7b). In addition, both the linear peptides RGDS and YIGSR, together with the dual PF, presented an antithrombogenic effect, as the area covered by platelets was found to be around or below 5%. Among the biomolecules, RGDS seemed to have the most powerful antithrombogenic effect, although differences with YIGSR and PF were minimal. Conversely, plain PLCL appeared to present a much lower prothrombogenic behavior than plain PLLA, as only 5.2% of its surface was covered by platelets, an equivalent percentage to functionalized PLLA stents. Furthermore, functionalization of PLCL with the biomolecules rendered stents with outstanding hemocompatibility, with platelet coverage found to be around 1% of the stent's surface. This behavior was further confirmed upon sample dehydration and visualization under SEM. As shown in Figure 6.7c, platelet aggregates were extensive in control PLLA stents, whereas functionalized samples presented only individual platelets at certain locations. Similarly, platelet adhesion was found to be infrequent for control PLCL stents, and even more sporadic for functionalized stents.

The coagulation cascade that may lead to thrombosis and potential stent failure is triggered by platelet activation, which in turn depends on protein adsorption onto the polymer surface. Activated platelets extend pseudopods and spread over the surface before releasing signals for other platelets that eventually lead to thrombi formation. Therefore, hemocompatibility is mainly driven by the biomaterial's wettability, functional chemical groups availability, charge and topography with regards to protein adsorption [66, 67]. Among the proteins present in the blood plasma, albumin is regarded as beneficial due to its capacity to generate a passivating layer, whereas adsorption of fibrinogen promotes platelet deposition [68]. Strohbach *et al.* investigated the role of biodegradable PLLA-based polymers in blood cell activation by measuring fibrinogen adsorption. Among the different polymers, PLLA presented the highest fibrinogen adsorption and platelet activation. In general, hydrophobic surfaces facilitate adsorption of proteins and thus platelet-surface activation, whereas in hydrophilic surfaces protein adsorption is impaired due to the energetic cost of displacing water [69, 70]. On that account, although PLLA is broadly regarded to be hemocompatible [71, 72], several authors have described strategies to improve its hemocompatibility through surface functionalization [22, 73]. Some authors have focused on favouring albumin adsorption over that of fibrinogen by means of PLLA fluorination or have studied the impact that surface chemistry has on adsorbed fibrinogen conformation and its influence on platelet adhesion and activation [74, 75]. Other approaches include the loading of drugs such as curcumin and paclitaxel [76], heparin [77, 78] or tantalum ions to improve hydrophilicity [79]. Hietala *et al.* analyzed platelet deposition on stainless steel and PLLA stents, with the latter showing increased platelet adhesion [13]. However, when coating the PLLA stent with a PLCL layer, platelet attachment was

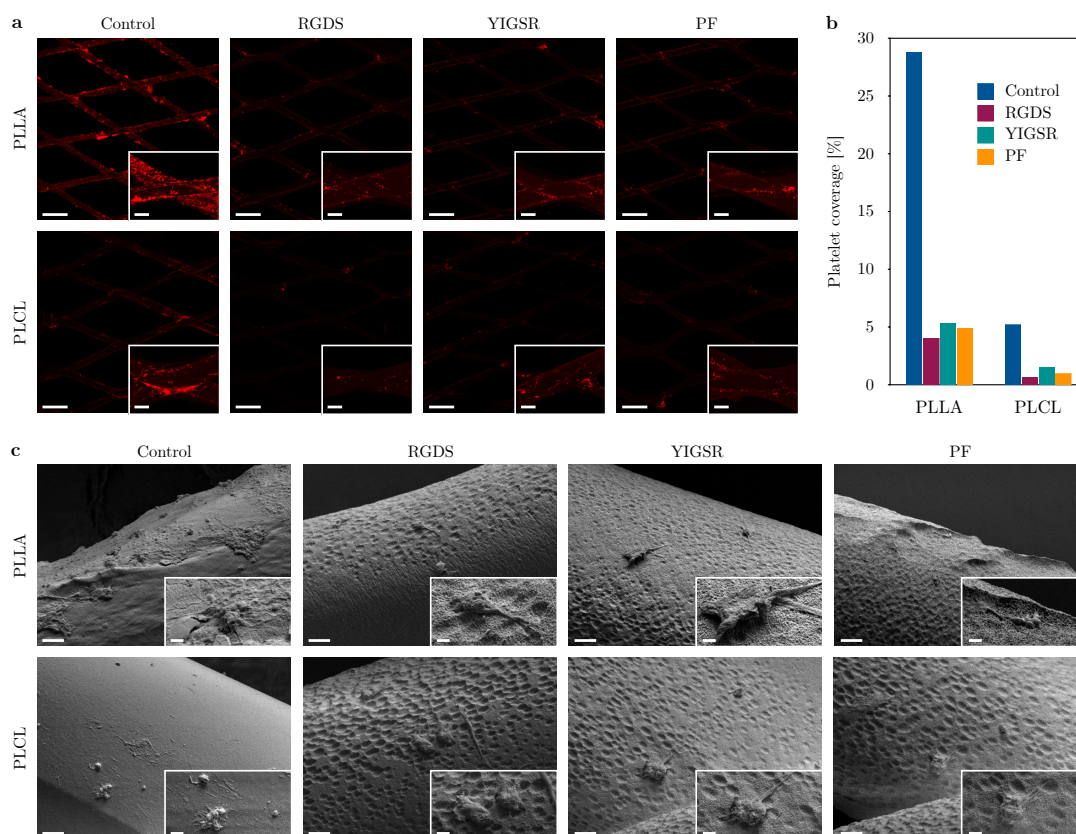


Fig. 6.7 Platelet adhesion on control and functionalized PLLA and PLCL stents following blood perfusion in a chamber for 5 minutes at a shear rate of 800 s^{-1} . (a) Fluorescence microscopy overview images of adhered platelets on control and functionalized stents (scale bar = $500 \mu\text{m}$), with focus on strut junctions (scale bar = $100 \mu\text{m}$). (b) Percentage of the stent's area occupied by platelets. (c) SEM images of adherent platelets (scale bar = $10 \mu\text{m}$), with magnified details of individual platelets or platelet aggregates (scale bar = $2 \mu\text{m}$).

effectively reduced. This behavior was also reported by Rudolph *et al.* regarding the thrombogenic potential of different polymers following a platelet activation test [80]. PLLA was shown to activate platelets in view of high levels of β -thromboglobulin, a protein exerted from platelet granules upon activation, whereas PLCL (70:30) presented β -thromboglobulin concentration within the normal range. Similarly, PLLA/PCL blends were found to induce significantly less platelet aggregation than PLLA in a blood cell activation study. Although fibrinogen concentration was comparable to that of PLLA, the authors attributed the dissimilar platelet response to the conformational state of adsorbed fibrinogen [69]. These results are in agreement with the better hemocompatibility shown by plain PLCL stents with respect to control PLLA stents (Figure 6.7a,b) and with its lower water contact angle (83.1 ± 5.1 vs 94.3 ± 3.6) and higher surface free energy, specially regarding its polar component, as shown in Table 6.1.

Furthermore, the lower thrombogenicity associated to the presence of peptides has been previously reported for REDV [58–61] and/or for YIGSR [9, 24, 55, 63, 64, 81].

Although it has been shown that the REDV sequence is recognized by $\alpha_4\beta_1$ integrin receptors, which are hardly present on the platelets surface, the mechanism in which the YIGSR sequence affects platelet adhesion and aggregation is not yet fully understood. Tandon *et al.* had reported that YIGSR supported platelet adhesion through the 67 kDa laminin receptor on platelets [82]. Conversely, Castellanos *et al.* reported that YIGSR and YIGSR+RGD peptides showed decreased platelet adhesion and aggregation, analogously to Peng *et al.*, and suggested that YIGSR might block $\alpha_{IIb}\beta_3$ integrin, that is, the most abundant platelet receptor [81, 83]. Hence platelet interaction with laminin remains ill-defined and YIGSR role is still a matter of controversy [55]. Regarding the role of RGDS, Kapp *et al.* evaluated the activity and selectivity profile of ligands for RGD-binding integrins, showing that RGD peptides were active on integrins $\alpha_v\beta_3$, $\alpha_v\beta_5$, $\alpha_5\beta_1$, and selective against $\alpha_v\beta_6$, $\alpha_v\beta_8$ and $\alpha_{IIb}\beta_3$ [84]. Therefore, RGDS affinity for platelets would be presumed to be low. Nevertheless, Peng *et al.* found that RGD significantly induced more platelet activation than REDV or YIGSR in silk fibroin scaffolds [65], whereas Castellanos *et al.* reported that the RGDS coating was the condition with a lower platelet adhesion compared to YIGSR and RGDS+YIGSR [81]. In spite of the aforementioned discrepancies, all biomolecules evaluated in this work displayed similar antithrombogenic behavior.

Altogether, the grafting of biomolecules on hydrophobic polymers such as PLLA appears as a successful strategy for cardiovascular applications. On the one hand, functionalization with peptides resulted in reduced platelet adhesion and activation. On the other hand, peptide sequences such as YIGSR, specifically targeting ECs, effectively improved cell adhesion and spreading. In addition, its combination with RGDS in a single dual molecule evinces the synergistic effects that such an engineered biomolecule may foster in the full endothelialization of a bioresorbable stent.

6.4 Conclusions

In this work we have presented the functionalization of novel 3D-printed PLLA and PLCL BRS with endothelial cell adhesive peptides to enhance ECs response and stents' hemocompatibility. Linear sequence RGDS and YIGSR peptides have been synthesized, as well as a dual platform presenting both motifs in a single biomolecule. Successful functionalization of films and stents has been confirmed upon water angle measurements and confocal fluorescence microscopy. Quantification of covalently-bond peptides has been achieved by detachment in alkaline conditions, yielding biomolecule density in the range of 0.5 to 3.5 nmol/cm². Cell adhesion assays evidenced significantly increased cell number and spreading onto functionalized films with respect to control samples. The inclusion of RGDS and YIGSR in a unique platform suggested the occurrence of synergistic effects. Stents' hemocompatibility was evaluated upon a blood perfusion assay, with PLCL showing pronouncedly diminished platelet adhesion with reference to

PLLA. In addition, functionalization with RGDS, YIGSR and the PF rendered BRS stents displaying even further reduced platelet adhesion.

The conjunction of intrinsically less prothrombogenic materials such as PLCL and its functionalization with cell adhesive peptides constitutes an encouraging approach in the treatment of coronary heart disease. The fact that YIGSR and the dual PF simultaneously increase cell adhesion while reducing platelet activation paves the way for a new generation in BRS development. Furthermore, BRS loaded with antiproliferative drugs to avoid restenosis due to overproliferation of SMCs may be functionalized with ECs-discriminating adhesive sequences in order to guide EC proliferation until complete re-endothelialization of the scaffold.

References

- [1] A. Foerster, M. Duda, H. Kraśkiewicz, M. Wawrzyńska, H. Podbielska, and M. Kopaczyńska, “Physico-chemical stent surface modifications”, in *Functionalised Cardiovascular Stents*, Elsevier, 2018, pp. 137–148.
- [2] M. Santos, A. Waterhouse, B. Lee, A. Chan, R. Tan, P. Michael, E. Filipe, J. Hung, S. Wise, and M. Bilek, “Simple one-step covalent immobilization of bioactive agents without use of chemicals on plasma-activated low thrombogenic stent coatings”, in *Functionalised Cardiovascular Stents*, Elsevier, 2018, pp. 211–228.
- [3] T. J. Parry, R. Brosius, R. Thyagarajan, D. Carter, D. Argentieri, R. Falotico, and J. Siekierka, “Drug-eluting stents: sirolimus and paclitaxel differentially affect cultured cells and injured arteries”, *European journal of pharmacology*, vol. 524, no. 1-3, pp. 19–29, 2005.
- [4] P. Qi, S. Chen, T. Liu, J. Chen, Z. Yang, Y. Weng, J. Chen, J. Wang, M. F. Maitz, and N. Huang, “New strategies for developing cardiovascular stent surfaces with novel functions”, *Biointerphases*, vol. 9, no. 2, p. 029 017, 2014.
- [5] K. Kolandaivelu, R. Swaminathan, W. J. Gibson, V. B. Kolachalama, K.-L. Nguyen-Ehrenreich, V. L. Giddings, L. Coleman, G. K. Wong, and E. R. Edelman, “Stent thrombogenicity early in high-risk interventional settings is driven by stent design and deployment and protected by polymer-drug coatings”, *Circulation*, vol. 123, no. 13, pp. 1400–1409, 2011.
- [6] Y. Sotomi, Y. Onuma, C. Collet, E. Tenekecioglu, R. Virmani, N. S. Kleiman, and P. W. Serruys, “Bioresorbable scaffold: the emerging reality and future directions”, *Circulation research*, vol. 120, no. 8, pp. 1341–1352, 2017.
- [7] E. Tenekecioglu, Y. Sotomi, R. Torii, C. Bourantas, Y. Miyazaki, C. Collet, T. Crake, S. Su, Y. Onuma, and P. W. Serruys, “Strut protrusion and shape impact on endothelial shear stress: insights from pre-clinical study comparing Mirage and Absorb bioresorbable scaffolds”, *The international journal of cardiovascular imaging*, vol. 33, no. 9, pp. 1313–1322, 2017.
- [8] M. Ramkumar, P. Cools, A. Arunkumar, N. De Geyter, R. Morent, V. Kumar, S. Udaykumar, P. Gopinath, S. Jaganathan, and K. Pandiyaraj, “Polymer coatings for biocompatibility and reduced nonspecific adsorption”, in *Functionalised Cardiovascular Stents*, Elsevier, 2018, pp. 155–198.

- [9] H.-W. Jun and J. L. West, "Modification of polyurethaneurea with PEG and YIGSR peptide to enhance endothelialization without platelet adhesion", *Journal of Biomedical Materials Research Part B: Applied Biomaterials*, vol. 72, no. 1, pp. 131–139, 2005.
- [10] J.-k. Park, D.-G. Kim, I. H. Bae, K. S. Lim, M. H. Jeong, C. Choi, S.-K. Choi, S. C. Kim, and J.-W. Nah, "Blood-compatible and biodegradable polymer-coated drug-eluting stent", *Macromolecular Research*, vol. 23, no. 3, pp. 237–244, 2015.
- [11] A. A. Shitole, P. S. Giram, P. W. Raut, P. P. Rade, A. P. Khandwekar, N. Sharma, and B. Garnaik, "Clopidogrel eluting electrospun polyurethane/polyethylene glycol thromboresistant, hemocompatible nanofibrous scaffolds", *Journal of biomaterials applications*, vol. 33, no. 10, pp. 1327–1347, 2019.
- [12] N. Bricout, F. Chai, J. Sobocinski, A. Hertault, W. Laure, A. Ung, P. Woisel, J. Lyskawa, and N. Blanchemain, "Immobilisation of an anti-platelet adhesion and anti-thrombotic drug (EP224283) on polydopamine coated vascular stent promoting anti-thrombogenic properties", *Materials Science and Engineering: C*, vol. 113, p. 110967, 2020.
- [13] E.-M. Hietala, P. Maasilta, H. Juuti, J.-P. Nuutinen, A. L. Harjula, U.-S. Salminen, and R. Lassila, "Platelet deposition on stainless steel, spiral, and braided polylactide stents", *Thrombosis and haemostasis*, vol. 92, no. 12, pp. 1394–1401, 2004.
- [14] S. J. Lee, H. H. Jo, K. S. Lim, D. Lim, S. Lee, J. H. Lee, W. D. Kim, M. H. Jeong, J. Y. Lim, I. K. Kwon, *et al.*, "Heparin coating on 3D printed poly (l-lactic acid) biodegradable cardiovascular stent via mild surface modification approach for coronary artery implantation", *Chemical Engineering Journal*, vol. 378, p. 122116, 2019.
- [15] S. Meng, Z. Liu, L. Shen, Z. Guo, L. L. Chou, W. Zhong, Q. Du, and J. Ge, "The effect of a layer-by-layer chitosan–heparin coating on the endothelialization and coagulation properties of a coronary stent system", *Biomaterials*, vol. 30, no. 12, pp. 2276–2283, 2009.
- [16] N. Huang, P. Yang, Y. Leng, J. Chen, H. Sun, J. Wang, G. Wang, P. Ding, T. Xi, and Y. Leng, "Hemocompatibility of titanium oxide films", *Biomaterials*, vol. 24, no. 13, pp. 2177–2187, 2003.
- [17] R. Hou, L. Wu, J. Wang, Z. Yang, Q. Tu, X. Zhang, and N. Huang, "Surface-degradable drug-eluting stent with anticoagulation, antiproliferation, and endothelialization functions", *Biomolecules*, vol. 9, no. 2, p. 69, 2019.
- [18] J. Y. Park, C. H. Gemmell, and J. E. Davies, "Platelet interactions with titanium: modulation of platelet activity by surface topography", *Biomaterials*, vol. 22, no. 19, pp. 2671–2682, 2001.
- [19] L. B. Koh, I. Rodriguez, and S. S. Venkatraman, "The effect of topography of polymer surfaces on platelet adhesion", *Biomaterials*, vol. 31, no. 7, pp. 1533–1545, 2010.
- [20] R. Schieber, F. Lasserre, M. Hans, M. Fernández-Yagüe, M. Díaz-Ricart, G. Escolar, M.-P. Ginebra, F. Mücklich, and M. Pegueroles, "Direct laser interference patterning of CoCr alloy surfaces to control endothelial cell and platelet response for cardiovascular applications", *Advanced healthcare materials*, vol. 6, no. 19, p. 1700327, 2017.
- [21] K. Zhang, T. Liu, J.-A. Li, J.-Y. Chen, J. Wang, and N. Huang, "Surface modification of implanted cardiovascular metal stents: from antithrombosis and antirestenosis to endothelialization", *Journal of Biomedical Materials Research Part A*, vol. 102, no. 2, pp. 588–609, 2014.

- [22] P. Mulinti, J. Brooks, B. Lervick, J. Pullan, and A. Brooks, “Strategies to improve the hemocompatibility of biodegradable biomaterials”, in *Hemocompatibility of Biomaterials for Clinical Applications*, Elsevier, 2018, pp. 253–278.
- [23] J. Zhao and Y. Feng, “Surface engineering of cardiovascular devices for improved hemocompatibility and rapid endothelialization”, *Advanced Healthcare Materials*, vol. 9, no. 18, p. 2000920, 2020.
- [24] L. J. Taite, P. Yang, H.-W. Jun, and J. L. West, “Nitric oxide-releasing polyurethane–PEG copolymer containing the YIGSR peptide promotes endothelialization with decreased platelet adhesion”, *Journal of Biomedical Materials Research Part B: Applied Biomaterials*, vol. 84, no. 1, pp. 108–116, 2008.
- [25] S. Omar and A. de Belder, “Nitric oxide donor delivery”, in *Functionalised Cardiovascular Stents*, Elsevier, 2018, pp. 291–304.
- [26] N. Beshchasna, M. Saqib, H. Kraskiewicz, Ł. Wasyluk, O. Kuzmin, O. C. Duta, D. Ficai, Z. Ghizdavet, A. Marin, A. Ficai, *et al.*, “Recent advances in manufacturing innovative stents”, *Pharmaceutics*, vol. 12, no. 4, p. 349, 2020.
- [27] F. Boccafoschi, L. Fusaro, and M. Cannas, “Immobilization of peptides on cardiovascular stent”, in *Functionalised Cardiovascular Stents*, Elsevier, 2018, pp. 305–318.
- [28] S. J. Lee, M. E. Kim, H. Nah, J. M. Seok, M. H. Jeong, K. Park, I. K. Kwon, J. S. Lee, and S. A. Park, “Vascular endothelial growth factor immobilized on mussel-inspired three-dimensional bilayered scaffold for artificial vascular graft application: in vitro and in vivo evaluations”, *Journal of colloid and interface science*, vol. 537, pp. 333–344, 2019.
- [29] M. López-García and H. Kessler, “Stimulation of bone growth on implants by integrin ligands”, *Handbook of Biomineralization: Biological Aspects and Structure Formation*, pp. 109–126, 2007.
- [30] H. Martin-Gómez, L. Oliver-Cervelló, I. Sánchez-Campillo, V. Marchán, M.-P. Ginebra, and C. Mas-Moruno, “A versatile click chemistry-based approach for functionalizing biomaterials of diverse nature with bioactive peptides”, *Chemical Communications*, vol. 57, no. 8, pp. 982–985, 2021.
- [31] L. Oliver-Cervelló, H. Martin-Gómez, L. Reyes, F. Nouredine, E. Ada Cavalcanti-Adam, M.-P. Ginebra, and C. Mas-Moruno, “An engineered biomimetic peptide regulates cell behavior by synergistic integrin and growth factor signaling”, *Advanced healthcare materials*, vol. 10, no. 7, p. 2001757, 2021.
- [32] J. A. Hubbell, S. P. Massia, N. P. Desai, and P. D. Drumheller, “Endothelial cell-selective materials for tissue engineering in the vascular graft via a new receptor”, *Bio/technology*, vol. 9, no. 6, p. 568, 1991.
- [33] I.-H. Bae, M. H. Jeong, D. S. Park, K. S. Lim, J. W. Shim, M. K. Kim, and J.-K. Park, “Mechanical and physio-biological properties of peptide-coated stent for re-endothelialization”, *Biomaterials Research*, vol. 24, no. 1, pp. 1–9, 2020.
- [34] M. I. Castellanos, C. Mas-Moruno, A. Grau, X. Serra-Picamal, X. Trepas, F. Albericio, M. Joner, F. J. Gil, M. P. Ginebra, J. M. Manero, *et al.*, “Functionalization of CoCr surfaces with cell adhesive peptides to promote huvecs adhesion and proliferation”, *Applied Surface Science*, vol. 393, pp. 82–92, 2017.

- [35] H. Aubin, C. Mas-Moruno, M. Iijima, N. Schütterle, M. Steinbrink, A. Assmann, F. J. Gil, A. Lichtenberg, M. Pegueroles, and P. Akhyari, “Customized interface biofunctionalization of decellularized extracellular matrix: toward enhanced endothelialization”, *Tissue Engineering Part C: Methods*, vol. 22, no. 5, pp. 496–508, 2016.
- [36] C. Mas-Moruno, R. Fraioli, F. Albericio, J. M. Manero, and F. J. Gil, “Novel peptide-based platform for the dual presentation of biologically active peptide motifs on biomaterials”, *ACS applied materials & interfaces*, vol. 6, no. 9, pp. 6525–6536, 2014.
- [37] M. Hoyos-Nogués, E. Falgueras-Batlle, M.-P. Ginebra, J. M. Manero, J. Gil, and C. Mas-Moruno, “A dual molecular biointerface combining RGD and KRSR sequences improves osteoblastic functions by synergizing integrin and cell-membrane proteoglycan binding”, *International journal of molecular sciences*, vol. 20, no. 6, p. 1429, 2019.
- [38] L. Oliver-Cervelló, H. Martín-Gómez, N. Mandakhbayar, Y.-W. Jo, E. A. Cavalcanti-Adam, H.-W. Kim, M.-P. Ginebra, J.-H. Lee, and C. Mas-Moruno, “Mimicking bone extracellular matrix: from BMP-2-derived sequences to osteogenic-multifunctional coatings”, *Advanced healthcare materials*, vol. 11, no. 20, p. 2201339, 2022.
- [39] V. Chausse, R. Schieber, Y. Raymond, B. Ségry, R. Sabaté, K. Kollandavelu, M.-P. Ginebra, and M. Pegueroles, “Solvent-cast direct-writing as a fabrication strategy for radiopaque stents”, *Additive Manufacturing*, p. 102392, 2021.
- [40] M. Amblard, J.-A. Fehrentz, J. Martinez, and G. Subra, “Methods and protocols of modern solid phase peptide synthesis”, *Molecular biotechnology*, vol. 33, no. 3, pp. 239–254, 2006.
- [41] I. Coin, M. Beyermann, and M. Bienert, “Solid-phase peptide synthesis: from standard procedures to the synthesis of difficult sequences”, *Nature protocols*, vol. 2, no. 12, p. 3247, 2007.
- [42] J. Kujawa, E. Rynkowska, K. Fatyeyeva, K. Knozowska, A. Wolan, K. Dzieszowski, G. Li, and W. Kujawski, “Preparation and characterization of cellulose acetate propionate films functionalized with reactive ionic liquids”, *Polymers*, vol. 11, no. 7, p. 1217, 2019.
- [43] K.-Y. Law and H. Zhao, “Determination of solid surface tension by contact angle”, in *Surface Wetting*, Springer, 2016, pp. 135–148.
- [44] G. Ström, M. Fredriksson, and P. Stenius, “Contact angles, work of adhesion, and interfacial tensions at a dissolving hydrocarbon surface”, *Journal of colloid and interface science*, vol. 119, no. 2, pp. 352–361, 1987.
- [45] G. Arderiu, M. Díaz-Ricart, B. Buckley, G. Escolar, and A. Ordinas, “Primary arrest of circulating platelets on collagen involves phosphorylation of syk, cortactin and focal adhesion kinase: studies under flow conditions”, *Biochemical Journal*, vol. 364, no. 1, pp. 65–71, 2002.
- [46] J. He, Q. Liu, S. Zheng, R. Shen, X. Wang, J. Gao, Q. Wang, J. Huang, and J. Ding, “Enlargement, reduction, and even reversal of relative migration speeds of endothelial and smooth muscle cells on biomaterials simply by adjusting RGD nanospacing”, *ACS Applied Materials & Interfaces*, vol. 13, no. 36, pp. 42344–42356, 2021.
- [47] S. Lowe, N. M. O’Brien-Simpson, and L. A. Connal, “Antibiofouling polymer interfaces: poly (ethylene glycol) and other promising candidates”, *Polymer Chemistry*, vol. 6, no. 2, pp. 198–212, 2015.

- [48] S. Pacharra, S. McMahon, P. Duffy, P. Basnett, W. Yu, S. Seisel, U. Stervbo, N. Babel, I. Roy, R. Viebahn, *et al.*, “Cytocompatibility evaluation of a novel series of PEG-functionalized lactide-caprolactone copolymer biomaterials for cardiovascular applications”, *Frontiers in bioengineering and biotechnology*, vol. 8, p. 991, 2020.
- [49] Y. Wan, J. Yang, J. Yang, J. Bei, and S. Wang, “Cell adhesion on gaseous plasma modified poly-(l-lactide) surface under shear stress field”, *Biomaterials*, vol. 24, no. 21, pp. 3757–3764, 2003.
- [50] A. Shah, S. Shah, G. Mani, J. Wenke, and M. Agrawal, “Endothelial cell behaviour on gas-plasma-treated pla surfaces: the roles of surface chemistry and roughness”, *Journal of tissue engineering and regenerative medicine*, vol. 5, no. 4, pp. 301–312, 2011.
- [51] R. Schieber, Y. Raymond, C. Caparrós, J. Bou, E. Herrero Acero, G. M. Guebitz, C. Canal, and M. Pegueroles, “Functionalization strategies and fabrication of solvent-cast PLLA for bioresorbable stents”, *Applied Sciences*, vol. 11, no. 4, p. 1478, 2021.
- [52] Y. Lei, M. Rémy, C. Labrugère, and M.-C. Durrieu, “Peptide immobilization on polyethylene terephthalate surfaces to study specific endothelial cell adhesion, spreading and migration”, *Journal of Materials Science: Materials in Medicine*, vol. 23, no. 11, pp. 2761–2772, 2012.
- [53] R. Fraioli, S. Neubauer, F. Rechenmacher, B. Bosch, K. Dashnyam, J.-H. Kim, R. Perez, H.-W. Kim, F. Gil, M. Ginebra, *et al.*, “Control of stem cell response and bone growth on biomaterials by fully non-peptidic integrin selective ligands”, *Biomaterials science*, vol. 7, no. 4, pp. 1281–1285, 2019.
- [54] M. Hoyos-Nogues, F. Velasco, M.-P. Ginebra, J. M. Manero, F. J. Gil, and C. Mas-Moruno, “Regenerating bone via multifunctional coatings: the blending of cell integration and bacterial inhibition properties on the surface of biomaterials”, *ACS Applied Materials & Interfaces*, vol. 9, no. 26, pp. 21 618–21 630, 2017.
- [55] S. Noel, A. Hachem, Y. Merhi, and G. De Crescenzo, “Development of a polyester coating combining antithrombogenic and cell adhesive properties: influence of sequence and surface density of adhesion peptides”, *Biomacromolecules*, vol. 16, no. 6, pp. 1682–1694, 2015.
- [56] J. H. Lee, G. Khang, J. W. Lee, and H. B. Lee, “Interaction of different types of cells on polymer surfaces with wettability gradient”, *Journal of colloid and interface science*, vol. 205, no. 2, pp. 323–330, 1998.
- [57] M. Pegueroles Neyra, *Interactions between titanium surfaces and biological components*. Universitat Politècnica de Catalunya, 2009.
- [58] B. A. Butruk-Raszeja, M. S. Dresler, A. Kuźmińska, and T. Ciach, “Endothelialization of polyurethanes: surface silanization and immobilization of REDV peptide”, *Colloids and Surfaces B: Biointerfaces*, vol. 144, pp. 335–343, 2016.
- [59] M. Gabriel, K. Niederer, M. Becker, C. M. Raynaud, C.-F. Vahl, and H. Frey, “Tailoring novel PTFE surface properties: promoting cell adhesion and antifouling properties via a wet chemical approach”, *Bioconjugate chemistry*, vol. 27, no. 5, pp. 1216–1221, 2016.
- [60] C. Wen, J. Zhang, Y. Li, W. Zheng, M. Liu, Y. Zhu, X. Sui, X. Zhang, Q. Han, Y. Lin, *et al.*, “A zwitterionic hydrogel coated titanium surface with high-efficiency endothelial cell selectivity for rapid re-endothelialization”, *Biomaterials Science*, vol. 8, no. 19, pp. 5441–5451, 2020.

- [61] Y. Liu, M. C. Munisso, A. Mahara, Y. Kambe, and T. Yamaoka, “Anti-platelet adhesion and in situ capture of circulating endothelial progenitor cells on ePTFE surface modified with poly (2-methacryloyloxyethyl phosphorylcholine)(PMPC) and hemocompatible peptide 1 (HCP-1)”, *Colloids and Surfaces B: Biointerfaces*, vol. 193, p. 111–113, 2020.
- [62] R. Zhou, Y. Wu, K. Chen, D. Zhang, Q. Chen, D. Zhang, Y. She, W. Zhang, L. Liu, Y. Zhu, *et al.*, “A polymeric strategy empowering vascular cell selectivity and potential application superior to extracellular matrix peptides”, *Advanced Materials*, vol. 34, no. 42, p. 2200464, 2022.
- [63] W. S. Choi, Y. K. Joung, Y. Lee, J. W. Bae, H. K. Park, Y. H. Park, J.-C. Park, and K. D. Park, “Enhanced patency and endothelialization of small-caliber vascular grafts fabricated by coimmobilization of heparin and cell-adhesive peptides”, *ACS applied materials & interfaces*, vol. 8, no. 7, pp. 4336–4346, 2016.
- [64] D. E. Anderson, K. P. Truong, M. W. Hagen, E. K. Yim, and M. T. Hinds, “Biomimetic modification of poly (vinyl alcohol): encouraging endothelialization and preventing thrombosis with antiplatelet monotherapy”, *Acta biomaterialia*, vol. 86, pp. 291–299, 2019.
- [65] G. Peng, D. Yao, Y. Niu, H. Liu, and Y. Fan, “Surface modification of multiple bioactive peptides to improve endothelialization of vascular grafts”, *Macromolecular Bioscience*, vol. 19, no. 5, p. 1800368, 2019.
- [66] C. W. Chung, H. W. Kim, Y. B. Kim, and Y. H. Rhee, “Poly (ethylene glycol)-grafted poly (3-hydroxyundecenoate) networks for enhanced blood compatibility”, *International Journal of Biological Macromolecules*, vol. 32, no. 1-2, pp. 17–22, 2003.
- [67] A. Strohbach and R. Busch, “Predicting the in vivo performance of cardiovascular biomaterials: current approaches in vitro evaluation of blood-biomaterial interactions”, *International Journal of Molecular Sciences*, vol. 22, no. 21, p. 11390, 2021.
- [68] E. Y. Kang, S.-B. Park, B. Choi, S.-W. Baek, K.-W. Ko, W.-K. Rhim, W. Park, I.-H. Kim, and D. K. Han, “Enhanced mechanical and biological characteristics of PLLA composites through surface grafting of oligolactide on magnesium hydroxide nanoparticles”, *Biomaterials science*, vol. 8, no. 7, pp. 2018–2030, 2020.
- [69] A. Strohbach, F. Maess, K. Wulf, S. Petersen, N. Grabow, K.-P. Schmitz, S. B. Felix, and R. Busch, “The role of biodegradable poly-(L-lactide)-based polymers in blood cell activation and platelet-monocyte interaction”, *International journal of molecular sciences*, vol. 22, no. 12, p. 6340, 2021.
- [70] G. Apte, A. Lindenbauer, J. Schemberg, H. Rothe, and T.-H. Nguyen, “Controlling surface-induced platelet activation by agarose and gelatin-based hydrogel films”, *ACS omega*, vol. 6, no. 16, pp. 10963–10974, 2021.
- [71] M. Szymonowicz, Z. Rybak, W. Witkiewicz, C. Pezowicz, and J. Filipiak, “In vitro hemocompatibility studies of poly(L-lactide) and poly(L-lactide-co-glycolide) as materials for bioresorbable stents manufacture”, *Acta Bioeng. Biomech*, vol. 16, pp. 131–139, 2014.
- [72] Y. Ramot, M. Haim-Zada, A. J. Domb, and A. Nyska, “Biocompatibility and safety of PLA and its copolymers”, *Advanced drug delivery reviews*, vol. 107, pp. 153–162, 2016.
- [73] K. Bastekova, O. Gusebnikova, P. Postnikov, R. Elashnikov, M. Kunes, Z. Kolska, V. Švorčík, and O. Lyutakov, “Spatially selective modification of PLLA surface: from hydrophobic to hydrophilic or to repellent”, *Applied Surface Science*, vol. 397, pp. 226–234, 2017.

- [74] R. Khalifehzadeh, W. Ciridon, and B. D. Ratner, “Surface fluorination of polylactide as a path to improve platelet associated hemocompatibility”, *Acta Biomaterialia*, vol. 78, pp. 23–35, 2018.
- [75] L. Zhang, B. Casey, D. K. Galanakis, C. Marmorat, S. Skoog, K. Vorvolakos, M. Simon, and M. H. Rafailovich, “The influence of surface chemistry on adsorbed fibrinogen conformation, orientation, fiber formation and platelet adhesion”, *Acta biomaterialia*, vol. 54, pp. 164–174, 2017.
- [76] K. Nguyen, S.-H. Su, A. Sheng, D. Wawro, N. Schwade, C. Brouse, P. Greilich, L. Tang, and R. Eberhart, “In vitro hemocompatibility studies of drug-loaded poly-(l-lactic acid) fibers”, *Biomaterials*, vol. 24, no. 28, pp. 5191–5201, 2003.
- [77] A. Gao, F. Liu, and L. Xue, “Preparation and evaluation of heparin-immobilized poly (lactic acid)(PLA) membrane for hemodialysis”, *Journal of Membrane Science*, vol. 452, pp. 390–399, 2014.
- [78] Z. Xiong, F. Liu, H. Lin, J. Li, and Y. Wang, “Covalent bonding of heparin on the crystallized poly (lactic acid)(PLA) membrane to improve hemocompatibility via surface cross-linking and glycidyl ether reaction”, *ACS Biomaterials Science & Engineering*, vol. 2, no. 12, pp. 2207–2216, 2016.
- [79] K. Kim, S. Park, J. H. Park, W.-S. Cho, H.-E. Kim, S.-M. Lee, J. E. Kim, H.-S. Kang, and T.-S. Jang, “Improved biocompatibility of intra-arterial poly-l-lactic acid stent by tantalum ion implantation: 3-month results in a swine model”, *Journal of Korean Neurosurgical Society*, vol. 64, no. 6, pp. 853–863, 2021.
- [80] A. Rudolph, M. Teske, S. Illner, V. Kiefel, K. Sternberg, N. Grabow, A. Wree, and M. Hovakimyan, “Surface modification of biodegradable polymers towards better biocompatibility and lower thrombogenicity”, *PLoS One*, vol. 10, no. 12, e0142075, 2015.
- [81] M. I. Castellanos, J. Guillem-Marti, C. Mas-Moruno, M. Díaz-Ricart, G. Escolar, M. P. Ginebra, F. J. Gil, M. Pegueroles, and J. M. Manero, “Cell adhesive peptides functionalized on CoCr alloy stimulate endothelialization and prevent thrombogenesis and restenosis”, *Journal of Biomedical Materials Research Part A*, vol. 105, no. 4, pp. 973–983, 2017.
- [82] N. N. Tandon, E. A. Holland, U. Kralisz, H. K. Kleinman, F. Robey, and G. Jamieson, “Interaction of human platelets with laminin and identification of the 67 kDa laminin receptor on platelets”, *Biochemical journal*, vol. 274, no. 2, pp. 535–542, 1991.
- [83] B. Sivaraman and R. A. Latour, “Delineating the roles of the GPIIb/IIIa and GP-Ib-IX-V platelet receptors in mediating platelet adhesion to adsorbed fibrinogen and albumin”, *Biomaterials*, vol. 32, no. 23, pp. 5365–5370, 2011.
- [84] T. G. Kapp, F. Rechenmacher, S. Neubauer, O. V. Maltsev, E. A. Cavalcanti-Adam, R. Zarka, U. Reuning, J. Notni, H.-J. Wester, C. Mas-Moruno, *et al.*, “A comprehensive evaluation of the activity and selectivity profile of ligands for RGD-binding integrins”, *Scientific reports*, vol. 7, no. 1, p. 39 805, 2017.

Concluding remarks

7.1 General conclusions

In recent years, bioresorbable stents (BRS) have been designed as a transient support to the artery vessel wall until complete resorption. Ideally, stents would (i) retain sufficient radial strength after implantation to prevent acute vessel recoil and (ii) release the antiproliferative drug to avoid restenosis. After the healing period, they would degrade and be resorbed completely, leaving the vessel with a healthy endothelium. Nevertheless, the use of polymeric BRS has limitations of its own, such as the need for large strut thickness to achieve enough radial strength or the inherent lack of radiopacity and bioactivity of polymers.

The research developed in this PhD Thesis aimed to manufacture polymeric BRS through an additive manufacturing technique, namely solvent-cast direct-writing with reinforced mechanical properties, suitable degradation timeframe, drug release capability and enhanced biointegration. The results displayed and analyzed in the previous chapters, which are summarized and highlighted in the following conclusions, expanded our comprehension of the field in terms of 3D-printing fabrication of radiopaque BRS stents, with drug delivery capabilities or bioactivity.

Solvent-cast direct-writing as a fabrication strategy for BRS

A novel, versatile SC-DW printing system onto a rotating mandrel to manufacture bioresorbable stents has been developed. Chloroform-based PLLA or PLCL ink presented the required shear-thinning behaviour for extrusion through a micronozzle. A variety of BRS designs with different mesh patterns and densities were successfully fabricated and characterized. Expansion assays showed that stents withstood pressures of at least 16 atm and the indirect cytotoxicity test indicated that stents were biocompatible.

3D-printed radiopaque BRS

The versatility of the SC-DW approach allowed for PLLA and PLCL ink modification in order to obtain radiopaque polymeric stents with iodine, triiodobenzoic acid (TIBA) and barium sulfate (BaSO_4). The addition of radiopaque agents resulted in thicker

struts, around 200 μm , with respect to control PLLA and PLCL stents, around 130 μm . Regarding mechanical properties, some PLLA-based radiopaque stents presented strut detachment under expansion assays, whereas PLCL-based stents were able to withstand up to 16 atm without detachment. MicroCT analysis evidenced increased X-Ray attenuation for TIBA- and BaSO_4 -containing stents with respect to control PLLA or PLCL stents, showing maintained radiopacity after 3 months incubation time.

Degradation and sterilization of 3D-printed BRS

Chemical vs thermal accelerated hydrolytic degradation of 3D-printed BRS was evaluated. Under alkaline conditions (0.1 M NaOH solution), stents degraded via surface erosion given the sustained mass loss, reduced strut thickness, invariable crystallinity percentage and constant M_w . Under high temperature conditions (50 °C), stents underwent bulk degradation, due to considerable decrease in M_w and an increase in crystallinity. PLLA stents showed neither mass loss nor decreased strut thickness throughout the assay, whereas PLCL stents presented initial stages of mass loss after 3 months incubation. The autocatalyzed kinetic model described the experimental data decrease for M_n better than the uncatalyzed model. The degradation rate of PLCL was found to be 1.5 times faster than that of PLLA due to the higher availability of amorphous regions, which are hydrolyzed prior to more impervious crystalline domains. Chemical degradation of stents in alkaline media has been found unsuitable to accurately mimic *in vivo* conditions. Conversely, results obtained at elevated temperature suggest the feasibility of extrapolating the degradation rate of PLLA and PLCL stents to estimate *in vivo* degradation under operating conditions.

Regarding sterilization, γ -irradiation triggered extensive chain scission and severe polymer deterioration, whereas no significant structural alterations were found on EtO-sterilized stents. Therefore, EtO-sterilized stents are expected to reproduce the degradation displayed by unsterilized stents in terms of degradation mechanism and timeframe.

Drug-eluting 3D-printed BRS

3D-printed stents by SC-DW technique loaded with everolimus were successfully manufactured and characterized. In comparison to control PLLA or PLCL stents, everolimus-loaded stents presented significantly greater strut thickness, around 184 μm for PLLA and around 215 μm for PLCL (vs $\approx 130 \mu\text{m}$). Drug release rate from everolimus-loaded stents was found to be too modest, less than 3% of the total loaded drug in 8 weeks.

An alternative method in terms of drug loading was sought in order to obtain the desired release kinetics: a customized rotatory electrospinning (ES) system to coat PLLA stents with a membrane of PLCL electrospun fibers. A Design of Experiment (DoE) was conducted to determine the optimal ES parameters to obtain a homogeneous coating with high specific surface. Material deposition ranged from a minimum of 0.30 mg up to 1.23 mg and membrane thickness from 19.81 μm to 70.70 μm . Fiber diameter was found to be around 1 μm for all conditions, ranging from 0.84 μm to 1.16 μm . Results from the DoE permitted to select the optimal parameters in terms of flow, time and rotation speed: 0.55 mL/min, 125 s and 8 rpm. Everolimus-loaded PLCL-coated stents were fabricated, with everolimus release dramatically increased with respect to everolimus-loaded 3D-printed stents, around 50% in the first 6 hours. Everolimus release from PLCL-coated 3D-printed stents would match the dose and timeframe required for *in vivo* applications, while providing thinner struts than SC-DW drug-loaded stents.

Functionalized 3D-printed BRS with a dual cell-adhesive peptidic platform

Linear sequence RGDS and YIGSR peptides have been synthesized, as well as a dual platform presenting both motifs in a single biomolecule. Successful functionalization of films and stents has been confirmed upon water angle measurements and confocal fluorescence microscopy. Quantification of covalently-bond peptides has been achieved by detachment in alkaline conditions, yielding biomolecule density in the range of 0.5 to 3.5 nmol/cm². Endothelial cell (EC) adhesion assays evidenced significantly increased cell number and spreading onto functionalized films with respect to control samples. Stents' hemocompatibility was evaluated upon a blood perfusion assay, with PLCL showing pronouncedly diminished platelet adhesion with reference to PLLA. In addition, functionalization with RGDS, YIGSR and the PF rendered BRS stents displaying even further reduced platelet adhesion.

In summary, this PhD Thesis has contributed to the development and optimization of a novel 3D Printing technique for polymeric BRS manufacturing. Moreover, printed stents have been further modified in order to display radiopacity or release anti-proliferative drug. Additionally, biofunctionalization of stents with EC-adhesive peptides has proven to be an effective strategy to prevent platelet adhesion. Globally, it has been demonstrated that PLCL presented reinforced mechanical properties and enhanced hemocompatibility while presenting a more suitable degradation timeframe than PLLA.

7.2 Future perspectives

BRS potential in treating coronary heart disease is still to be further developed. This PhD Thesis has focused on the development and optimization of a 3D Printing technique for BRS manufacturing with tunable characteristics. Considering the obtained results, the following recommendations are proposed for further research:

- ▷ To investigate the effects of different mesh designs on the mechanical properties of printed stents, as well as to decrease the nozzle diameter in order to obtain reduced strut thickness.
- ▷ To develop *in silico* models regarding stent crimping, expansion and radial compression with the aim to gain further understanding between stent design and mechanical properties.
- ▷ To study the effects of introducing a patterning on the luminal surface of the stent in order to guide endothelial cells towards the complete colonization of the scaffold until forming a healthy endothelium.
- ▷ To investigate the effects of *in vitro* everolimus release on cell proliferation, both for ECs and SMCs.
- ▷ To perform further cell studies regarding functionalized films with the linear peptides and the dual peptidic platform with regards to cell proliferation and migration.
- ▷ To study the performance of functionalized stents under *in vitro* cell dynamic pulsatile assays that mimic arterial coronary flow to assess stent endothelialization.

Finally, although in this PhD Thesis the different features have been analyzed separately, it would be of utmost interest to combine radiopacity, drug-eluting capacity and functionalization with peptides at the same time. The integration of such features in a single BRS is expected to synergistically foster the performance of the stent by simultaneously discriminating ECs response from that of SMCs and by ensuring device hemocompatibility.

Outcomes of the Thesis

Publications

V. Chausse, R. Schieber, Y. Raymond, B. Ségry, R. Sabaté, K. Kolandaivelu, M.-P. Ginebra, M. Pegueroles, *Solvent-cast direct-writing as a fabrication strategy for radiopaque stents*, Additive Manufacturing (2021) 102392.

V. Chausse, C. Iglesias, E. Bou-Petit, M.-P. Ginebra, M. Pegueroles, *Chemical vs thermal accelerated hydrolytic degradation of 3D-printed PLLA/PLCL bioresorbable stents: Characterization and influence of sterilization*, Polymer Testing 117 (2023) 107817.

V. Chausse, E. Casanova-Batlle, C. Canal, M.-P. Ginebra, J. Ciurana, M. Pegueroles, *Solvent-cast direct-writing and electrospinning as a dual fabrication strategy for drug-eluting polymeric bioresorbable stents* (under revision in Additive Manufacturing).

V. Chausse, C. Mas-Moruno, H. Martin-Gómez, M. Pino, M. Díaz-Ricart, G. Escolar, M.-P. Ginebra, M. Pegueroles, *Functionalization of 3D printed polymeric bioresorbable stents with a dual cell-adhesive peptidic platform combining RGDS and YIGSR sequences* (under revision in Biomaterials Science).

Conference contributions

V. Chausse, T. Fox, B. Ségry, F. Mücklich, M. Pegueroles. *3D-printed PLLA/PCL bioresorbable stents with tunable characteristics by solvent-cast direct-write technique*. 11th World Biomaterials Congress. December 11th – 15th, 2020, Glasgow (United Kingdom). Virtual Conference – Oral Presentation.

V. Chausse, C. Iglesias, C. Canal, M. Pegueroles. *Development of drug-loaded, 3D printed PLLA/PLCL bioresorbable stents: characterization and influence of sterilization*. 31st Conference of the European Society for Biomaterials. September 8th, 2021, Oporto (Portugal). Virtual Conference – Poster Presentation.

V. Chausse, T. Fox, F. Mücklich, M. Pegueroles. *Micropatterned 3D-printed PLLA/PLCL bioresorbable stents: degradation and influence of sterilization*. 11th EEIGM International Conference on Advanced Materials Research. June 16th – 17th, 2022, Barcelona (Spain). Oral Presentation.

V. Chausse, E. Casanova-Batlle, C. Canal, J. Ciurana, M. Pegueroles. *Additive manufacturing and electrospinning as a dual fabrication strategy for biomimetic drug-eluting bioresorbable stents*. Tissue Engineering and Regenerative Medicine International Society (TERMIS) European Chapter Conference 2022. June 28th – July 1st, 2022, Krakow (Poland). Poster Presentation.

V. Chausse, C. Mas-Moruno, M. Pegueroles. *Functionalization of 3D printed PLLA/PLCL bioresorbable stents with endothelial cell adhesive peptides*. 32nd Conference of the European Society for Biomaterials. September 4th – 8th, 2022, Bordeaux (France). Oral Presentation.

Scholarships

Pre-doctoral grant (FPI-UPC 2018). Universitat Politècnica de Catalunya, February 2019 – March 2019.

Pre-doctoral grant (FI-AGAUR 2019). Agència de Gestió d'Ajuts Universitaris i de Recerca (AGAUR), Generalitat de Catalunya, April 2019 – August 2022.

Pre-doctoral grant (4th year). Becas Santander/UPC, September 2022 – June 2023.

